To the Graduate Council:

I am submitting herewith a thesis written by Riza C. Berkan entitled " Dynamic Modeling of EBR-II for Simulation and Control." I have examined the final copy of this thesis for form and content and recommend that it be accepted in partial fulfillment of the requirements for the degree of Master of Science, with a major in Nuclear Engineering.

B R Upadhyaya

B. R. Upadhyaya, Major Professor

We have read this thesis
and recommend its acceptence:

T. W. Kerlin

J. M. Bailey

Accepted for the Council:

Vice Provost
and Dean of The Graduate School

DYNAMIC MODELING OF EBR-II
FOR SIMULATION AND CONTROL

A Thesis
Presented for The
Master of Science
Degree

The University of Tennessee, Knoxville

Riza C. Berkan

August, 1988

ACKNOWLEDGMENT

The author wishes to thank Dr. B. R. Upadhyaya, his major professor and research advisor for his guidance and encouragement throughout the entire period of this work. His contributions to the author's education through the courses he taught as well as through personal communications are very much appreciated.

He wishes to express his gratitude to Dr. P. F. Pasqua for providing the research assistantship sponsored by the Instrumentation and Controls Division, Oak Ridge National Laboratory.

The assistance of R. A. Kisner and T. L. Wilson, members of the ACTO project in the Instrumentation and Controls Division, Oak Ridge National Laboratory, has been very helpful and is very much appreciated.

The author would like to thank Dr. T. W. Kerlin, head of the Nuclear Engineering Department for his support and interest in this work.

Many thanks go to Ms. B. Kelmers and Ms. M. McCullough for their splendid efforts in typing the equations.

ABSTRACT

Simulation and control studies of the Experimental Breeder Reactor-II have been performed using a linear model which includes the reactor, intermediate heat exchanger and the steam generator. The previously developed linear, primary system model is modified and updated with the most recent data. A steam generator model is developed including a three-element controller model. The subsystems are defined in modular form and then combined for simulation using the software **MATRIX**$_{\mathbf{X}}$. The inherent safety characteristics of the EBR-II system are verified through open-loop simulations of the subsystem models and the combined model.

The modern control theory design routines are studied and several design applications are performed using the capabilities of **MATRIX**$_{\mathbf{X}}$. The linear, quadratic Gaussian compensator (LQG) design is considered for each EBR-II subsystem. The responses of the closed-loop models to several standard step perturbations show an improvement in the system behavior compared to those for the open-loop case. An evaluation of the three-element controller and the optimal regulator results indicates that the performances are comparable. The LQG compensator

is found to be more robust with respect to the modeling errors of the open-loop system than the three-element controller. State estimator and reference tracking controller designs are also performed and the closed-loop simulation results of the EBR-II steam generator model using these controllers are obtained. The responses show that both strategies provide optimized control actions with high performance.

TABLE OF CONTENTS

LIST OF FIGURES

FIGURE PAGE

FIGURE PAGE

FIGURE PAGE

FIGURE PAGE

FIGURE PAGE

FIGURE PAGE

FIGURE PAGE

LIST OF TABLES

LIST OF ACRONYMS

ANL	Argonne National Laboratory
CAD	Computer Aided Design
EBR-II	Experimental Breeder Reactor-II
PWR	Pressurized Water Reactor
PI	Proportional-Integral
LQG	Linear Quadratic Gaussian
IHX	Intermediate Heat Exchanger
MIMO	Multiple Input Multiple Output

CHAPTER 1

INTRODUCTION

1.1 Purpose of the Study

The development of advanced liquid metal reactor technology involves various research activities related to system dynamics and control. Among the several other objectives, improving the safety characteristics of advanced reactors is of primary importance. The main concern is to make necessary design changes that would provide wide-ranging inherently safe characteristics. Dynamic modeling and simulation provide a computational environment in which such new design ideas can be developed and tested. Recovery from unanticipated transients requires safe operational maneuvers. The development of new control strategies may help solve some of these problems. Besides handling the consequences of failures of less-than-optimal control actions, better strategies may avoid redundant control efforts and may improve the system performance in daily operation. In concert with the goals of the advanced reactor development, the objectives of this study are chosen as a combination of the two tasks: dynamic modeling and control strategy development.

The Experimental Breeder Reactor-II (EBR-II) is a liquid-metal fast breeder reactor designed as an engineering test facility. The EBR-II tests and demonstrations play an important role in the development of future advanced reactors. The demonstration of the inherent capability of sodium-cooled fast reactors to sustain unprotected loss of cooling accidents have been carried out at EBR-II. The test results are also reproduced using nonlinear dynamic models of the EBR-II [20]. The codes developed and verified using EBR-II data (NATDEMO, DSNP, CSYRED) [20] are very efficient for detailed test studies; however, a linear, low-order, complete EBR-II model is not available in the literature. One of the objectives of this study is the extension to the development of a linear EBR-II model in order to improve the understanding of its dynamics. An important motivation for developing a low-order, linear model is to provide an application environment for our second objective of control design studies.

The possibility of improving the system performance using the modern control theory design methods has been a subject of extensive investigation for the last three decades. The design applications in the aerospace industry proved the high performance characteristics of the modern controllers. The question of feasibility of using modern controllers in advanced reactors is yet unanswered. One of the reasons is that the conventional controllers are efficient and reliable in controlling the nuclear systems and there is no current need for the new concepts. Another reason is related to the limitations of the computational tools. A missile dynamics may be represented by a few state variables but the simplest nuclear reactor model would include a relatively large number of state variables. The control design studies of large scale systems strictly depend on the software development. The computer aided design (CAD) package **MATRIX**$_{\mathbf{X}}$ is a good example of the latest development in this area. The second objective of this study includes investigating the modern control theory algorithms of **Matrix**$_{\mathbf{X}}$, applying standard design methods using the EBR-II model as a test bed, and evaluating the controller performance. The objective is not to propose a new control strategy for the EBR-II, instead to study the capabilities of modern controllers when they are replaced with the existing controllers of the EBR-II for simple control tasks. This approach may find further applications in the control strategy design of advanced modular reactors.

1.2 Development and Application

1.2.1 Dynamic modeling of the EBR-II

The EBR-II plant consists of three subsystems, namely, the primary system, the steam generator system and the turbine-condenser system. In this study, the dynamic modeling of the EBR-II includes the primary and the steam generator subsystems (the primary system includes the reactor core, sodium tank and the intermediate heat exchanger). A previously developed primary system model [Greene 1] is modified and updated with the most recent available data. The modified primary model is a linear, lumped-parameter model with 37 state variables. The formulation is made using the point reactor kinetics equation, Mann's heat transfer model and the first order transport-lag approximation [1]. The six-group precursor equations of the Greene model are replaced with one "averaged" precursor equation which is a well known physical model reduction technique [4]. Another modification is made in the intermediate heat exchanger (IHX) side of the Greene model. The five-lump configuration is converted to a ten-lump model. Mann's five-lump model is valid only if the ratio of total heat capacity to overall heat transfer coefficient is smaller than about 2 sec [10]. The IHX data of the EBR-II is such that the ratios for the primary and the secondary sides both exceed the 2 seconds limit when the IHX is divided into five lumps. Using ten-lump model the 2 seconds limit is not exceeded. The open-loop simulation results verify that the physical consistency and the computational accuracy are retained with these modifications. Seven important reactivity feedback mechanisms namely, Doppler, steel expansion, core sodium expansion, inner and outer reflector expansion, and fuel expansion effects are included in the model. The core bowing and the control rod reactivity feedback effects are not taken into consideration since their contribution to the steady-state operation is not significant.

The development of the steam generator model is accomplished using the energy and mass balance equations for 13 different regions. The system includes seven shell-and-tube type evaporators, two shell-and-tube type superheaters and a steam drum. The evaporator dynamics is represented using a moving boundary approach [7]. This technique is used in several previous studies and gives accurate results. The moving boundary approach uses the height of the subcooled region as a state variable which is a function of the saturation pressure and temperature. In the boiling region, a homogeneous flow model is considered [6]. This is the assumption of homogeneous steam water mixture with an average enthalpy, quality and density. An alternative approach using Zuber-Findlay relationship between the boiling density and void fraction [3] is found to be difficult to implement due to nonlinearities and complicated representation of the boiling region dynamics. The downcomer and the evaporator flows are represented by the momentum equations. The friction multiplier for the boiling region is an integral average taken over the boiling region [3]. The lumped-parameter steam generator model uses 20 state variables including the three-element controller dynamics. A proportional-integral (PI) controller is designed for drum level control [14] using three signals, namely, feedwater flow, steam flow and drum water level. The actuator is the feedwater flow valve which is represented as a first order system in the model. The design objective of the three-element controller is to maintain the drum level at its steady-state value of 8 inches below the centerline at 100 % power level.

The responses of the open-loop models to standard perturbations are obtained through simulations using the special features of $\mathbf{MATRIX_X}$. The combined model is also tested for the same perturbations. The inherent stability characteristics of the EBR-II subsystems are verified.

1.2.2 Modern control theory applications

The control design effort is mainly concentrated on the optimal output feedback controller design. The control design algorithms of **MATRIX$_x$** [15] are used for the design applications in this work. Using these algorithms, a linear, quadratic Gaussian compensator (LQG) design can be performed for single-input systems. An LQG compensator synthesis includes an optimal regulator and an optimal estimator designs. The optimal regulator design uses an optimization technique to minimize the corresponding quadratic cost function. In practice, the design minimizes the control input to obtain maximum performance. The state and input weights of the quadratic cost function must be properly chosen to complete the optimal regulator design. The estimator design is a linear observer design in which the performance is optimized with respect to the measurement noise and input disturbance (Kalman filter design) [17]. In case of corrupted measurements, the noise and disturbance intensity covariances are the necessary inputs to the estimator design algorithms. The nonmeasurable variables are also specified indicating which states need to be estimated. The closed-loop system is constructed appending the LQG compensator to the open-loop system in a feedback arrangement.

The application of the optimal feedback output controller design is implemented using the EBR-II subsystem models. Several applications such as Kalman filter design [17], robustness verification [19], and an optimal reference tracking controller design [13] are studied.

1.3 Organization of the Thesis

The purpose of Chap. 1 is to provide the problem definition, the objectives, and the general approach taken in this study. Chapter 2 contains a brief description of the EBR-II system. The modifications to the previously developed primary system model are described in Chap. 3. The development of a linear EBR-II steam generator model is given in Chap. 4.

The calculation procedure and the responses of the open-loop models are presented in Chap. 5. The results described in this chapter are obtained for three different cases. These are, the isolated primary system results, the isolated steam generator results, and the results of the combined model.

The modern control theory design applications are presented in Chap. 6. The designs are performed assuming an ideal measurement environment. The differences between the closed-loop system performances using a three-element controller and an LQG compensator are studied in this chapter.

Some specific control applications are presented in Chap. 7. The optimal estimator performance under the degraded conditions is studied. The optimal reference tracking controller design is included in Chap. 7. This chapter also includes the study of improving the optimal regulator performance by choosing proper state and input weights.

Conclusions and suggestions for future work are given in Chap. 8.

CHAPTER 2

A BRIEF DESCRIPTION OF THE EBR-II*

2.1 General Features

Experimental Breeder Reactor-II (EBR-II) is a liquid metal fast breeder reactor located at the National Reactor Testing Station in Idaho. The plant consists of a heterogoneous, unmoderated, sodium-cooled reactor (62.5 MWth); an intermediate sodium coolant loop; a steam plant which produces 20 MW of electrical power through a conventional turbine generator; and a fuel processing system consisting of systems for disassembly, decontamination, fabrication, and assembly of fuel elements and subassemblies. Both the reactor and the associated fuel recycle facilities were designed with the philosophy of providing a highly flexible installation that would permit the investigation and evaluation of various core configurations, types of fuel, fuel element designs, and processing techniques. The reactor, primary coolant system, and the fuel-handling system components

* The description of the EBR-II is taken from Ref [2].

are submerged in a large primary sodium tank. This concept is also sometimes referred to as the pool-type design (such as the Phoenix and Super-Phoenix liquid metal reactors in France).

The original purpose of the EBR-II facility was to demonstrate the feasibility of fast reactors for central station power plant applications. It was also intended to prove that a breeding ratio greater than unity could be obtained in a power producing reactor. The purpose of the facility was redirected to provide irradiation services for the development of fuels and structural materials. This transition required changes in several original concepts of operation including an increase in overall core size to compensate for reactivity losses to the system caused by additional irradiation experiments. Other changes made in fuel enrichment and blanket composition, and in operating philosophy from that of an engineering test facility to that of a high-priority neutron producer.

A simple functional description of the plant can be stated as follows. Heat generated by nuclear fission in the core is absorbed by the liquid sodium which circulates through the reactor. The absorbed heat is transferred in a shell-tube type intermediate heat exchanger to non-radioactive secondary sodium. The secondary sodium transfers the heat to the steam system in the steam generator which includes sodium-to-water/steam shell-and-tube type heat exchangers. The resulting superheated steam drives a turbine-generator to produce electricity, and is condensed to water in the condenser. The heat transferred to the condenser is dissipated to the atmosphere by cooling towers.

Figure 2.1 is a schematic of the primary and sodium systems, and Fig. 2.2 shows the detailed primary cooling system. A summary of the EBR-II design and operating data is reproduced in Table 2.1 (from Ref.[16]).

The secondary sodium system, an intermediate closed loop between the primary system and the steam system, absorbs heat produced in the primary system and transfers the heat to the steam system. The flow of secondary sodium is regulated manually to absorb all heat in excess of that required to maintain the primary bulk sodium at a constant temperature of 700 F.

Heat transfer between the primary and secondary sodium occurs in the intermediate heat exchanger located submerged in the primary tank bulk sodium. The heated secondary sodium then flows from the reactor building through yard piping to the sodium boiler building where it enters the steam generator. Heat transfer between the secondary system and the steam system is effected at this interface to produce superheated steam used to drive the turbine generator.

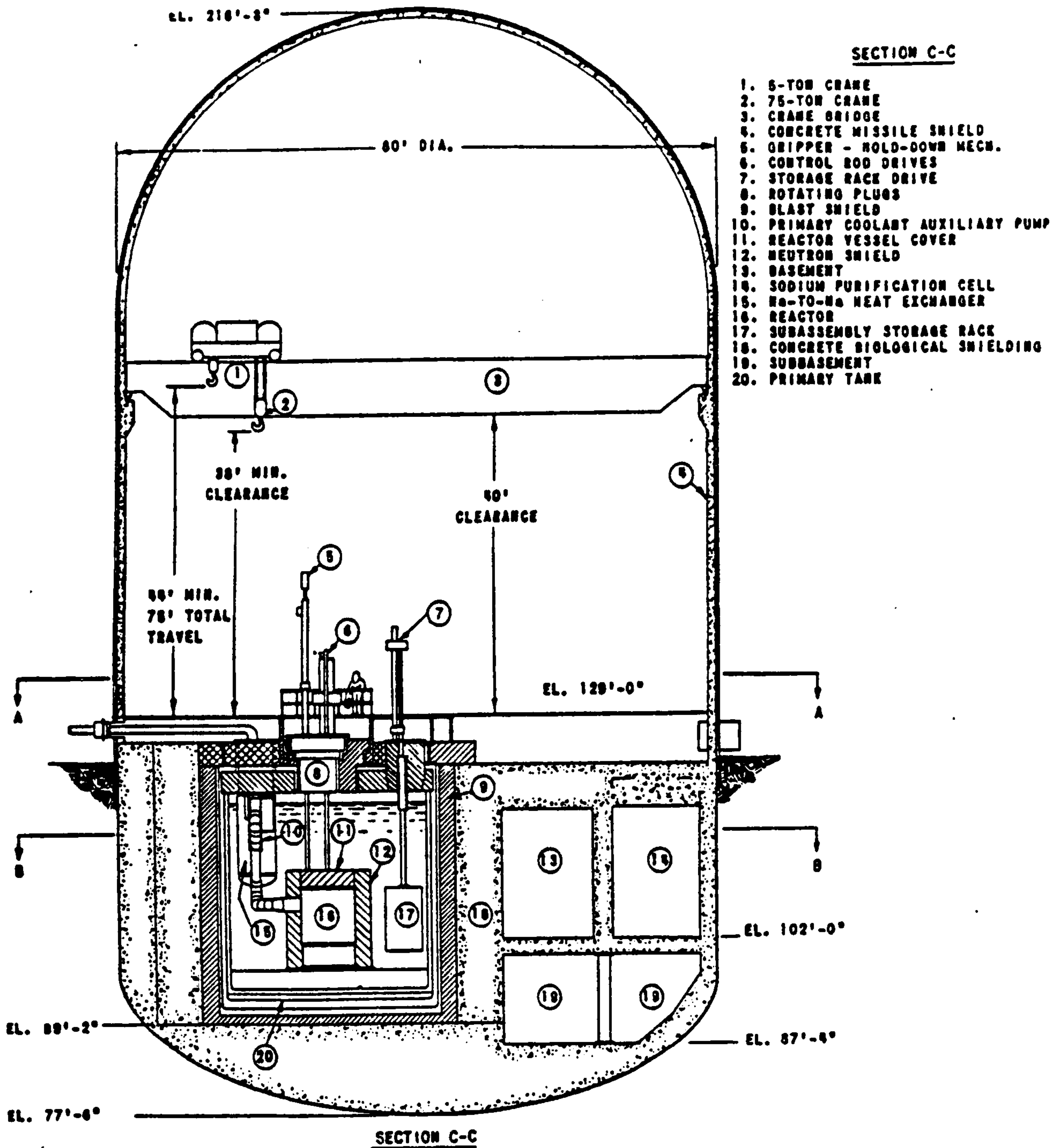

Fig. 2.1 EBR-II Primary and Secondary Sodium Systems.

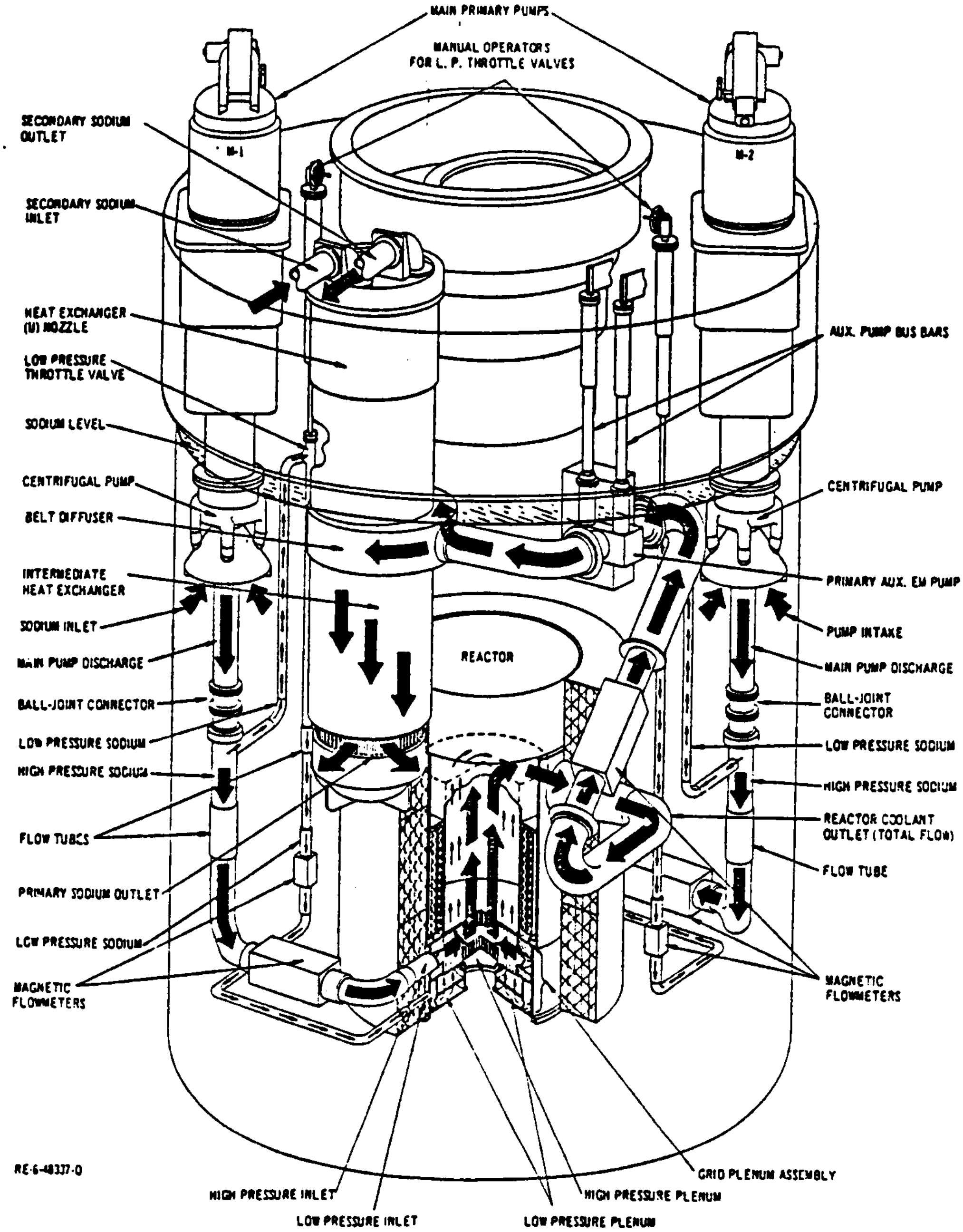

Fig. 2.2 EBR-II Primary Cooling System.

TABLE 2.1

Summary of EBR-II Design and Operating Data

Operational 100% Power	from [2]
Heat output, Mw	62.5
Gross electrical output, Mw	20
Primary sodium temperature, to reactor,F	700
Primary sodium temperature,from reactor, F	883
Sodium flow rate, through reactor, gpm	9,000
Sodium maximum velocity in core, fps	23.8
Secondary sodium flow rate, gpm	5,890
Secondary sodium temperature to IHX, F	588
Secondary sodium temperature from IHX, F	866
Core equivalent diameter, inch	19.94
Core composition, fuel alloy %	31.8
Stainless steel %	19.5
Sodium volume %	48.7
Subassemblies	
Core	53
Control (rod and thimble)	12
Safety (rod and thimble)	2
Inner Blanket	60
Outer Blanket	510
Total	637
Configuration	Hexagonal

(Table 2.1 continued)

Operational 100% power	from [2]
Fuel pin diameter, inch	0.144
Fuel pin length, inch	14.22
Fuel tube O.D., inch	0.174
Fuel tube wall thickness, inch	0.009
Fuel elements per subassembly	91
Total fission /cm^3/sec at center	3.7×10^{13}
Power density, average, Mw/liter	0.735
Power density, maximum, Mw/liter	1.23
Specific power, Mw/kg	0.311
Maximum heat flux, Btu/hr-ft^2	929,000
Average heat flux, Btu/hr-ft^2	619,000

2.2 Primary System

The primary system is housed in the reactor plant (see Fig. 2.3) and contains reactor, primary and shutdown cooling systems, neutron shield, instrumentation, control and safety drive systems, fuel handling system, primary tank and biological shield, fuel unloading and inter-building transfer, primary sodium purification system and argon blanket gas system.

The reactor contains a central core of fissionable fuel material that is completely surrounded by radial and axial blankets. The fuel and blanket materials are contained within a cylindrical reactor vessel. In the radial and upper axial direction, a neutron shield surrounds the vessel. Fuel bearing subassemblies contain upper and lower axial blanket regions in addition to the fuel material. Blanket subassemblies contain only blanket material.

2.2.1 Reactor Core

The reactor core consists of 53 fuel subassemblies, 12 control rod subassemblies and 2 safety rod assemblies. The active core height is 14.22 inches and has an equivalent diameter of 19.94 inches. Each fuel assembly consists of 91 fuel elements. The subassemblies are hexagonal in shape. Figure 2.4 shows the typical core cross section. The fuel alloy composition (called the fission) contains 95% by weight uranium (48.4% enrichment) and other elements. As shown in Fig. 2.5 the core assembly consists of upper blanket, core and lower blanket. The upper and lower blanket subassemblies consist of 19 pins each, and each 18 inches long. The core fuel elements have sodium thermal bonding between the fuel and the cladding. The total number of fissions/cm^3-sec is 4.4×10^{13} (average).

2.2.2 Inner and Outer Blankets

The reactor vessel assembly also consists of inner and outer blanket subassemblies. There are 66 inner blanket and 510 outer blanket subassemblies. Each of these consists of 19 cylindrical elements, containing 60% uranium, with sodium bonding. The total pin length for the blanket subassemblies is 50 in. Figure 2.6 shows the reactor vessel assembly with upper and lower-blanket sections, and inner and outer blanket sections.

2.2.3 Control Rods

EBR-II contains 12 control subassemblies with a fuel-pin section identical to the active core subassemblies. Figure 2.7 shows the cross section of a control rod subassembly, showing an axial void section

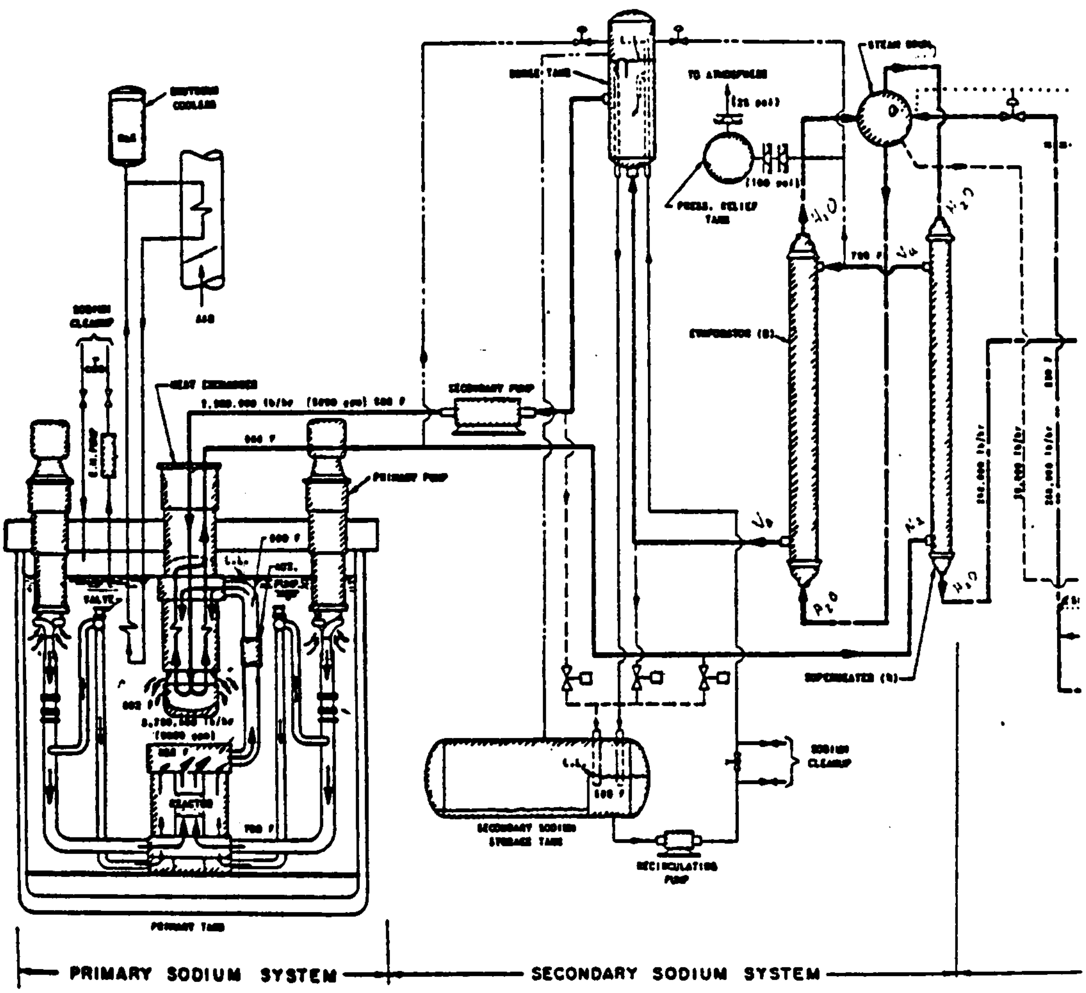

Fig. 2.3 EBR-II Plant and Primary Containment.

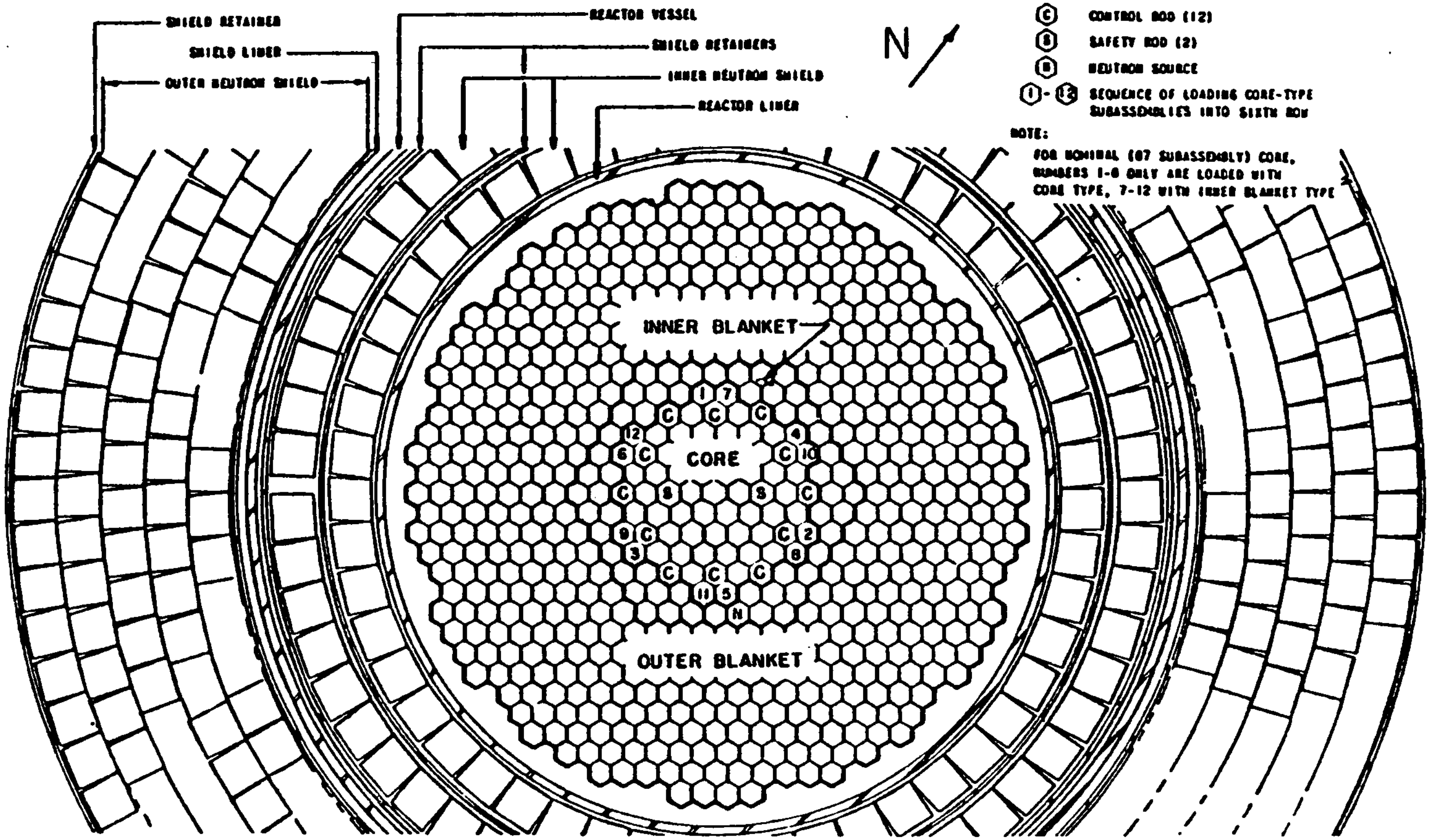

Fig. 2.4 EBR-II Core Cross Section.

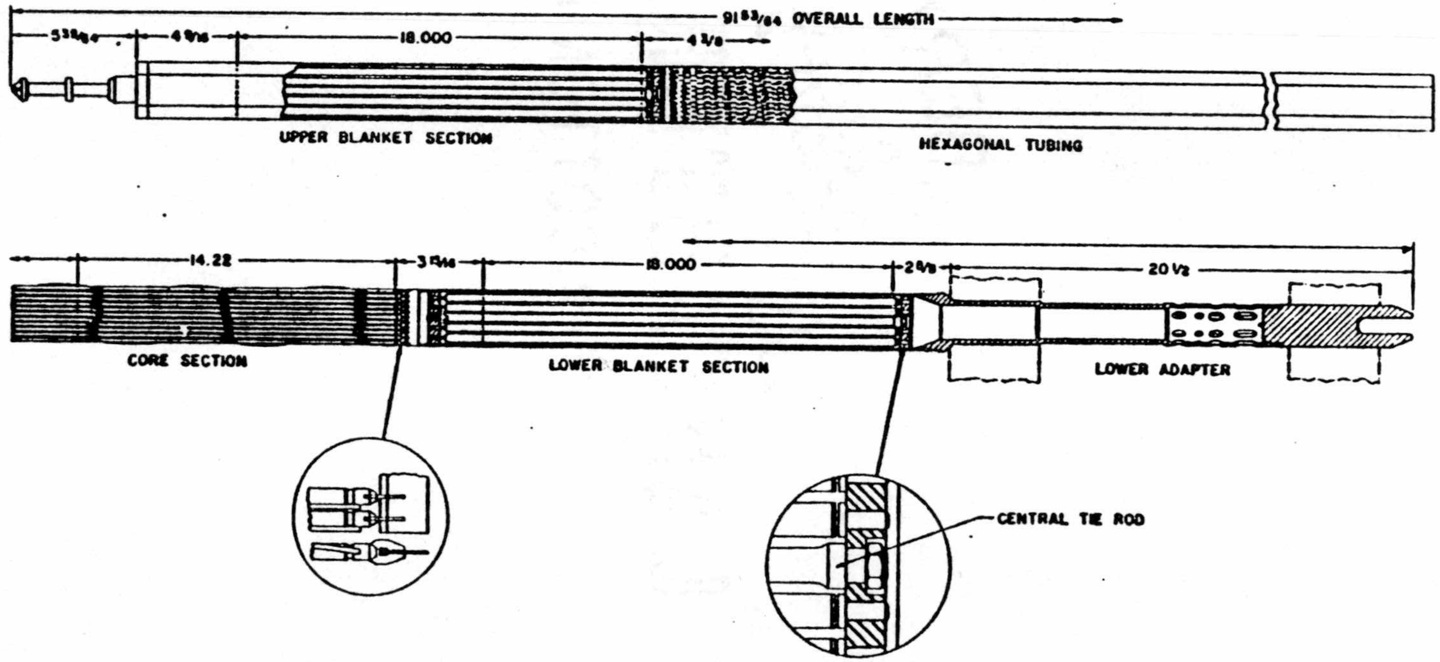

Fig. 2.5 EBR-II Core Subassembly.

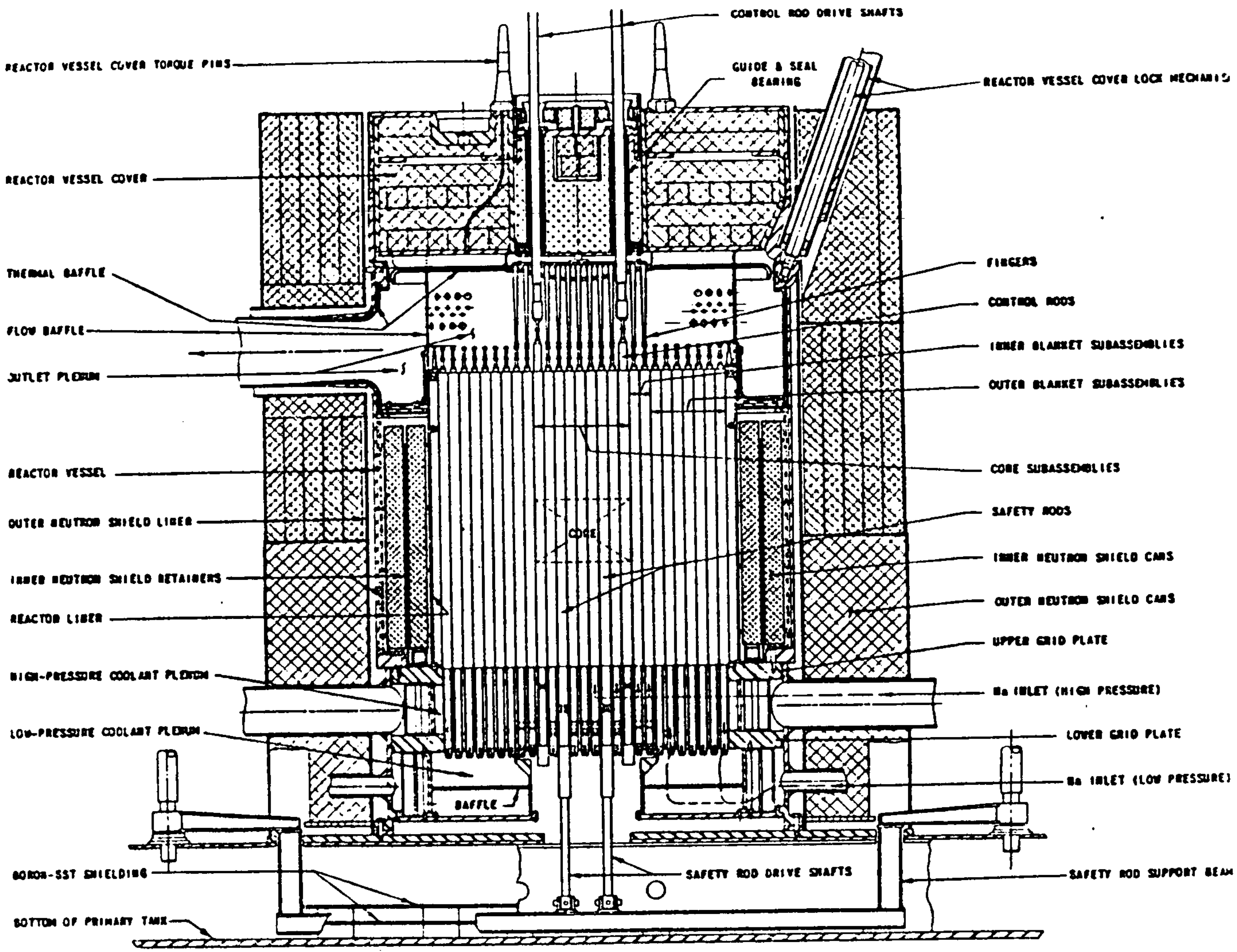

Fig. 2.6 EBR-II Reactor Vessel Assembly.

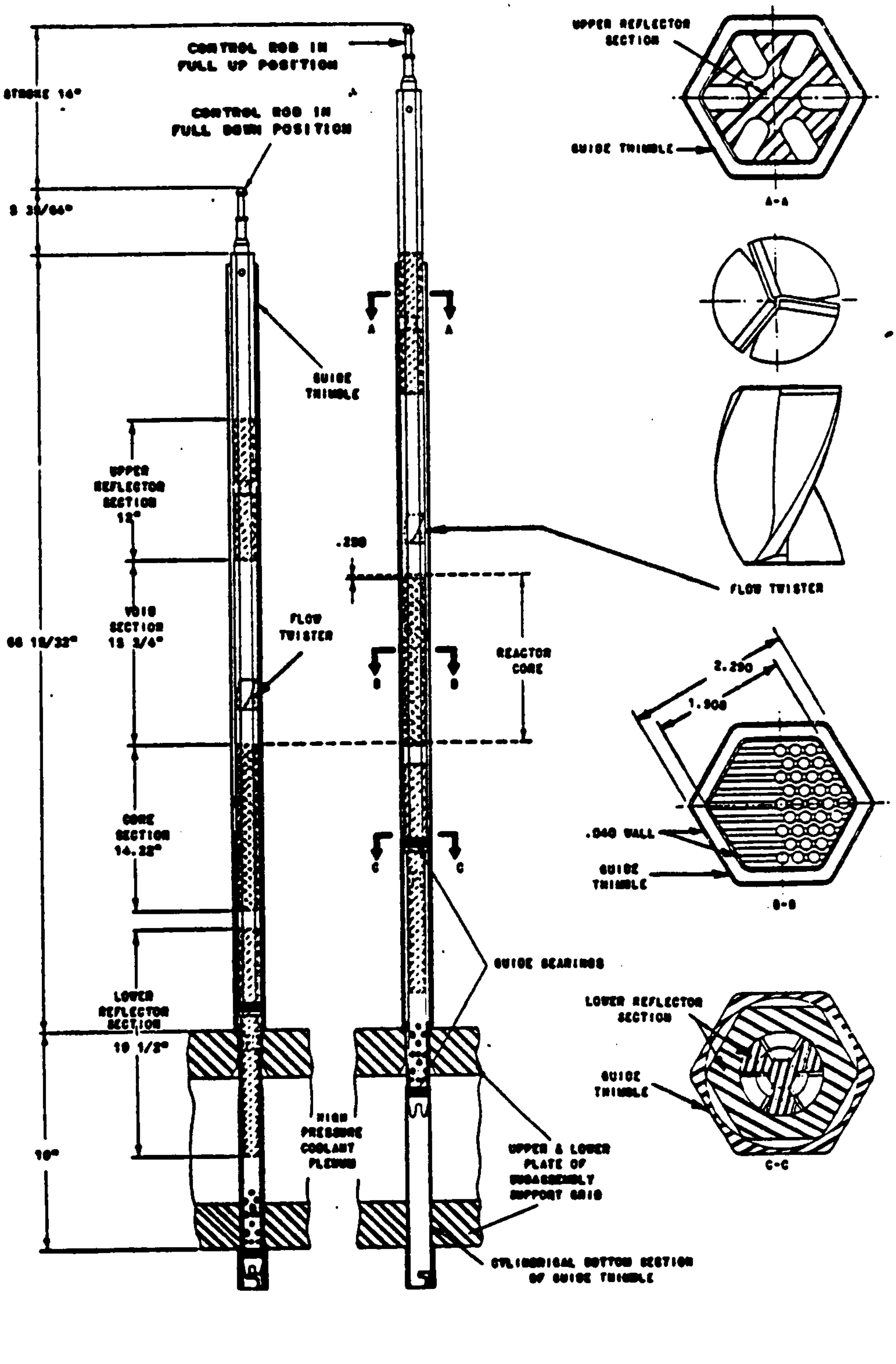

Fig. 2.7 EBR-II Control Subassembly.

above the core (normally filled with sodium). There are two safety rods to provide shutdown reactivity during reactor loading operation, and are driven from below the core.

About 85.3% of the heat is generated in the active core region, 1.9% in the upper and lower blankets, 9.8% in the inner blanket, 2.2% in the outer blanket, and the remaining (0.8%) in the neutron shield.

2.3 Primary Cooling System

Figure 2.2 shows a detailed flow path of sodium through the core, intermediate heat exchanger, primary pumps and the connecting piping. The total sodium coolant flow rate through the core is 3.81×10^6 lbm/hr. The secondary sodium flow rate is 2.5×10^6 lbm/hr. The inlet temperature of secondary sodium to the intermediate heat exchanger is about 588 F and the outlet temperature is 866 F. This is also the inlet temperature to the steam generator.

Figure 2.8 is a detailed schematic of the intermediate heat exchanger (IHX). This equipment is at an elevation above the reactor vessel. The coolant from the primary sodium tank is pumped through the core and

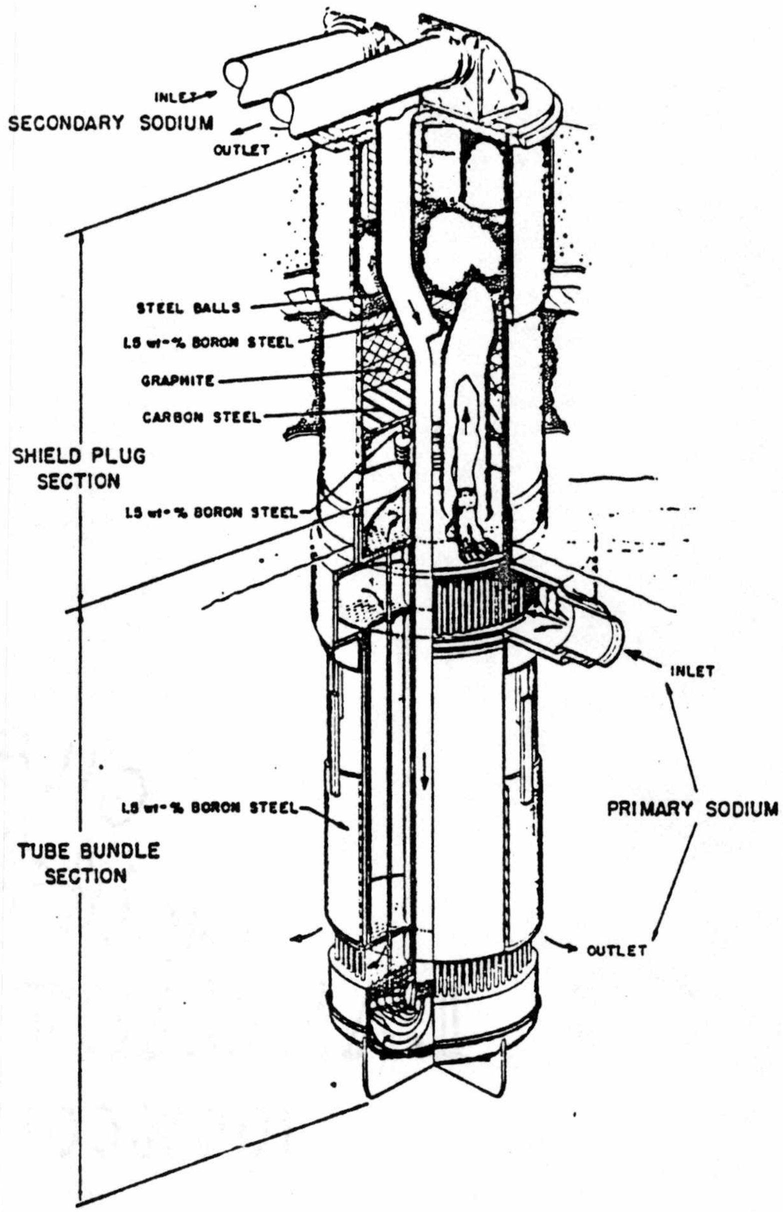

Fig. 2.8 EBR-II Intermediate Heat Exchanger.

the blanket assemblies. From the reactor vessel the primary coolant enters the shell side of IHX, flows down and discharges into the bulk sodium in the primary tank. The secondary sodium enters and leaves the IHX at the top, flowing through tubes in the IHX.

2.4 Secondary System

The steam generator and distribution system utilizes the heat delivered by the primary cooling system to produce superheated steam at 820 F, 1250 psig and delivers at a rate of 240,000 lbm/hr (when the reactor is operating at full power of 62.5 MW) to a conventionally designed turbine-generator to produce 20 MW of electrical power. Figure 2.9 shows the steam generator components. A steam drum with moisture separating components, two shell-and-tube type once-through superheaters and seven shell-and-tube type recirculating evaporators are the basic components of the EBR-II steam generator.

The feedwater flows out of the drum through the downcomer pipes to the bottom of seven parallel-connected evaporators, as shown in Figure 2.10. The feedwater rises through the duplex tubes absorbing heat from the sodium flowing in the shell, and is returned to the steam drum through the riser nozzles. The saturated steam-water

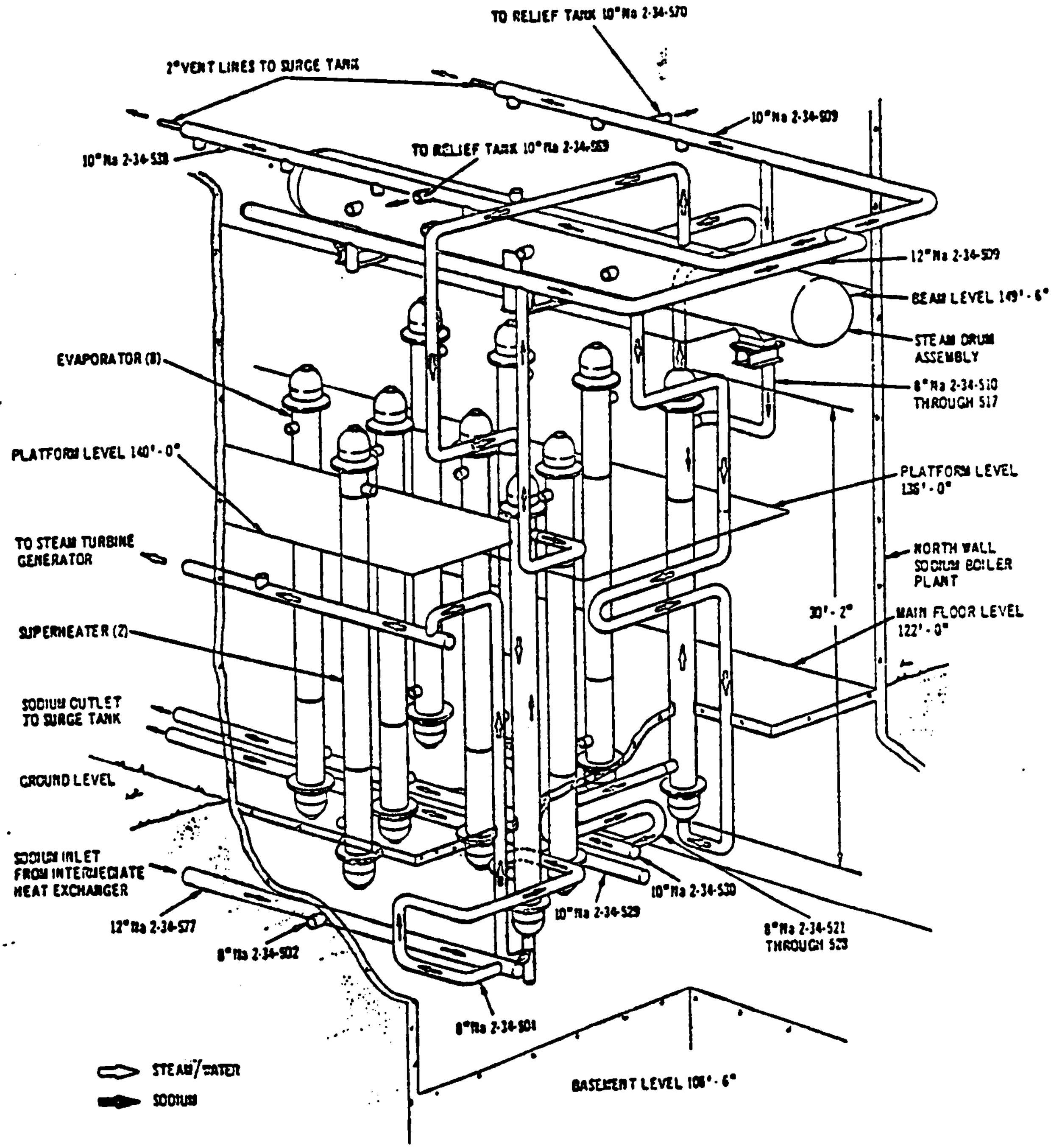

Fig. 2.9 EBR-II Steam Generator Components.

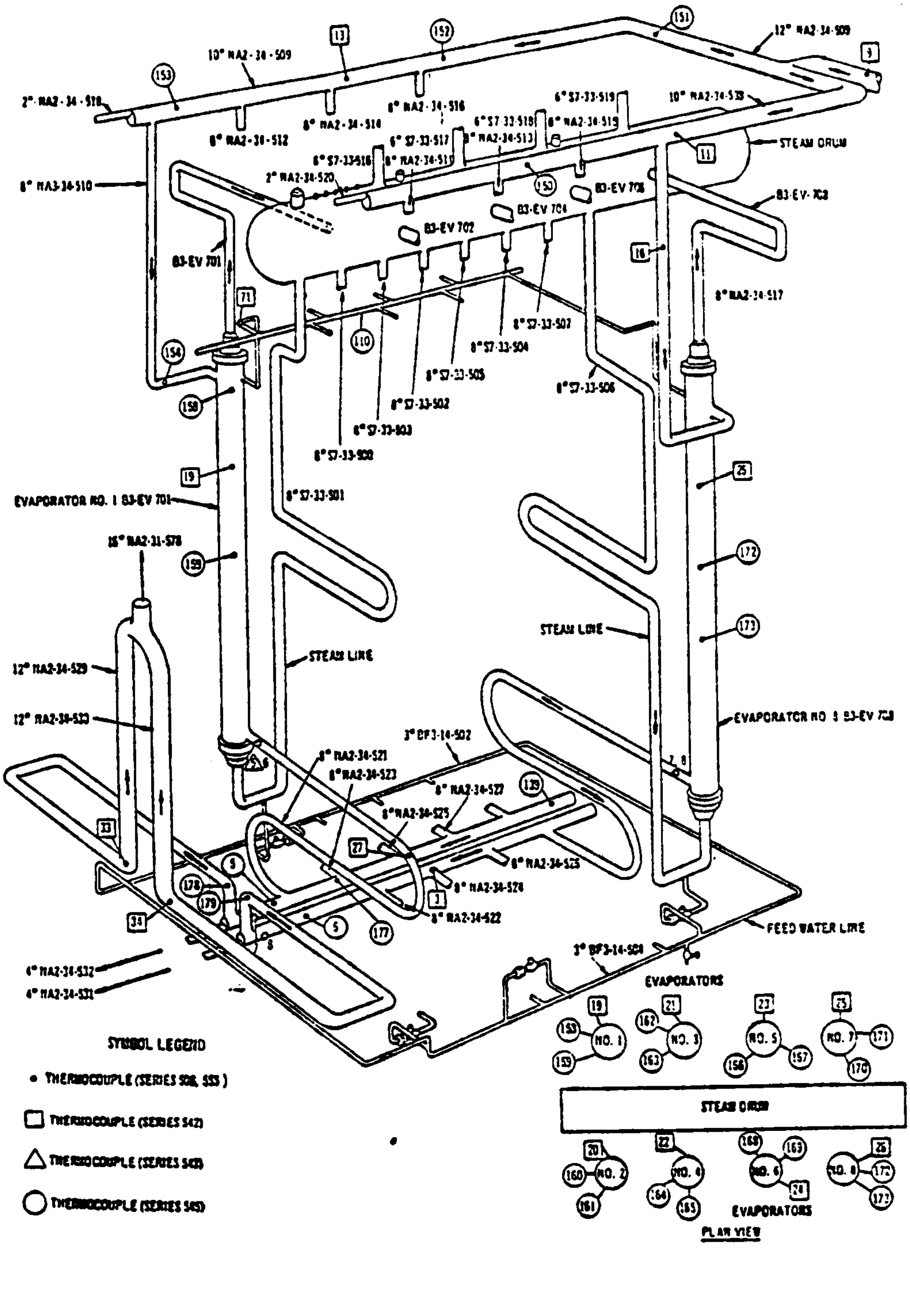

Fig. 2.10 EBR-II Evaporator Details and Sensor Locations

through the riser nozzles. The saturated steam-water mixture (a mixture of six parts water and one part steam at a temperature of 579 F at full power) hits the moisture separating components, the condensed water recirculates through the downcomer and the dry steam flows into the superheater section. The superheater details are shown in Figure 2.11.

The evaporator assembly has an overall length of 30 ft 2 inches and a maximum diameter of 56 inches. It consists of a shell assembly through which the sodium flows, and a tube assembly through which the water flows (Figure 2.12). The shell assembly consists of a schedule 20 pipe, two tee headers, a baffle nest assembly and two sodium sheets with thermal plates.

Two parallel-connected once-through superheaters are shell-and-tube type heat exchangers (Figure 2.13). The superheaters convert saturated steam at 578 F to superheated steam at 820 F by absorbing heat from the secondary sodium. The superheater assembly has exactly the same dimensions as the evaporators since it is an inverted and modified evaporator assembly. The modification is made by inserting core tubes in the duplex tubes. The core tubes decrease the cross sectional area of the duplex tubes to cause the steam velocity to be increased.

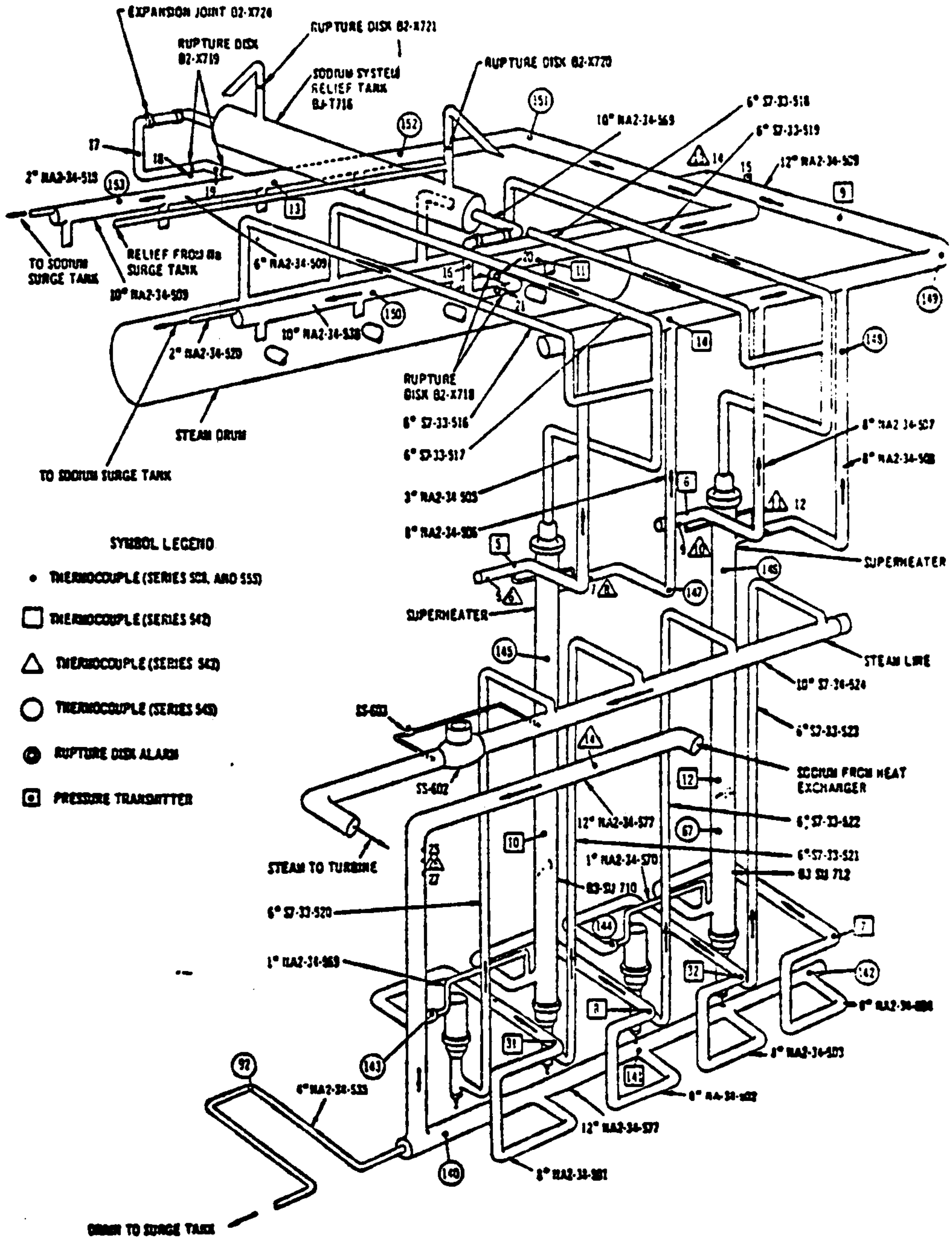

Fig. 2.11 EBR-II Superheater Details and Sensor Locations.

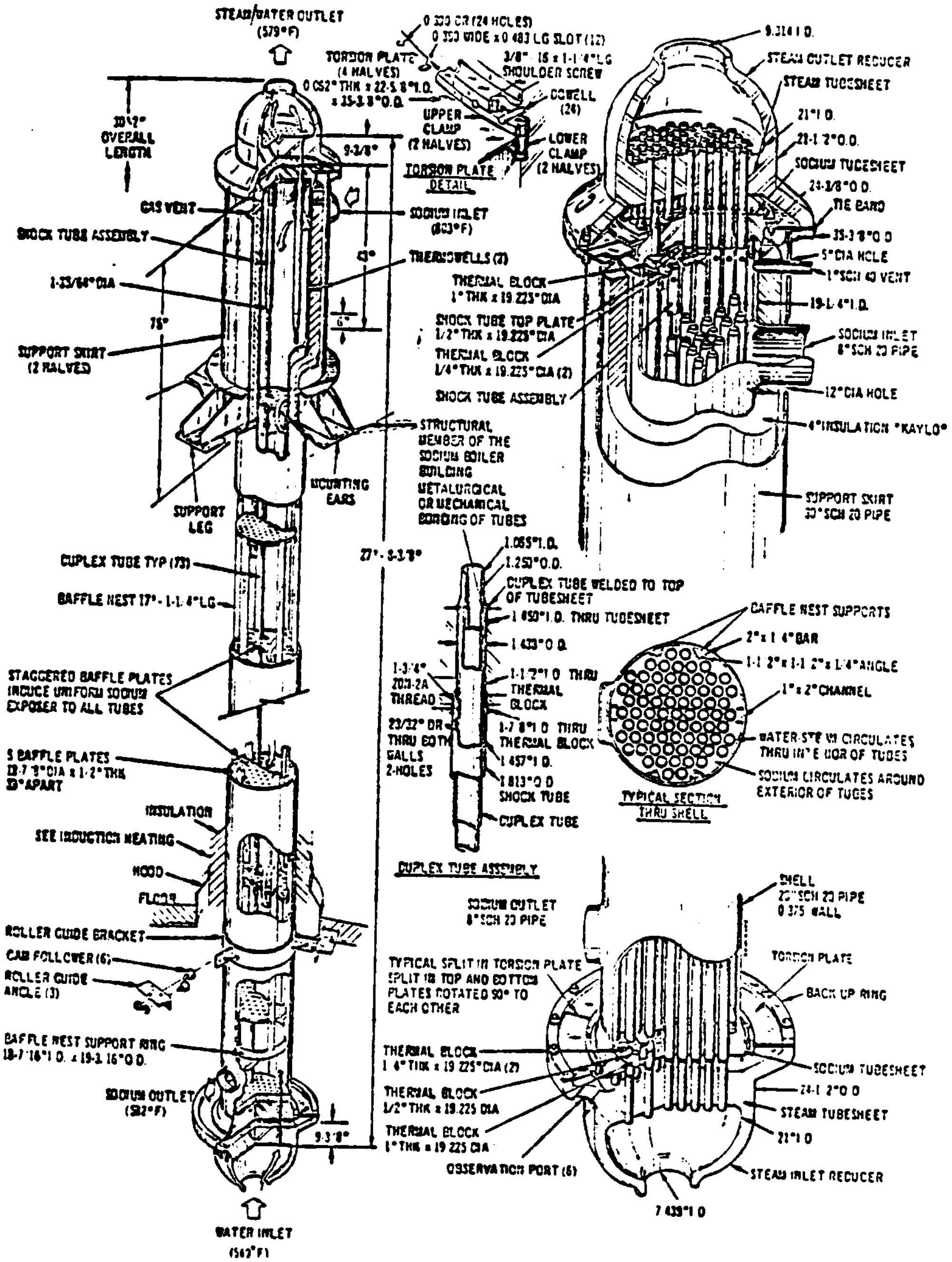

Fig. 2.12 EBR-II Evaporator Assembly.

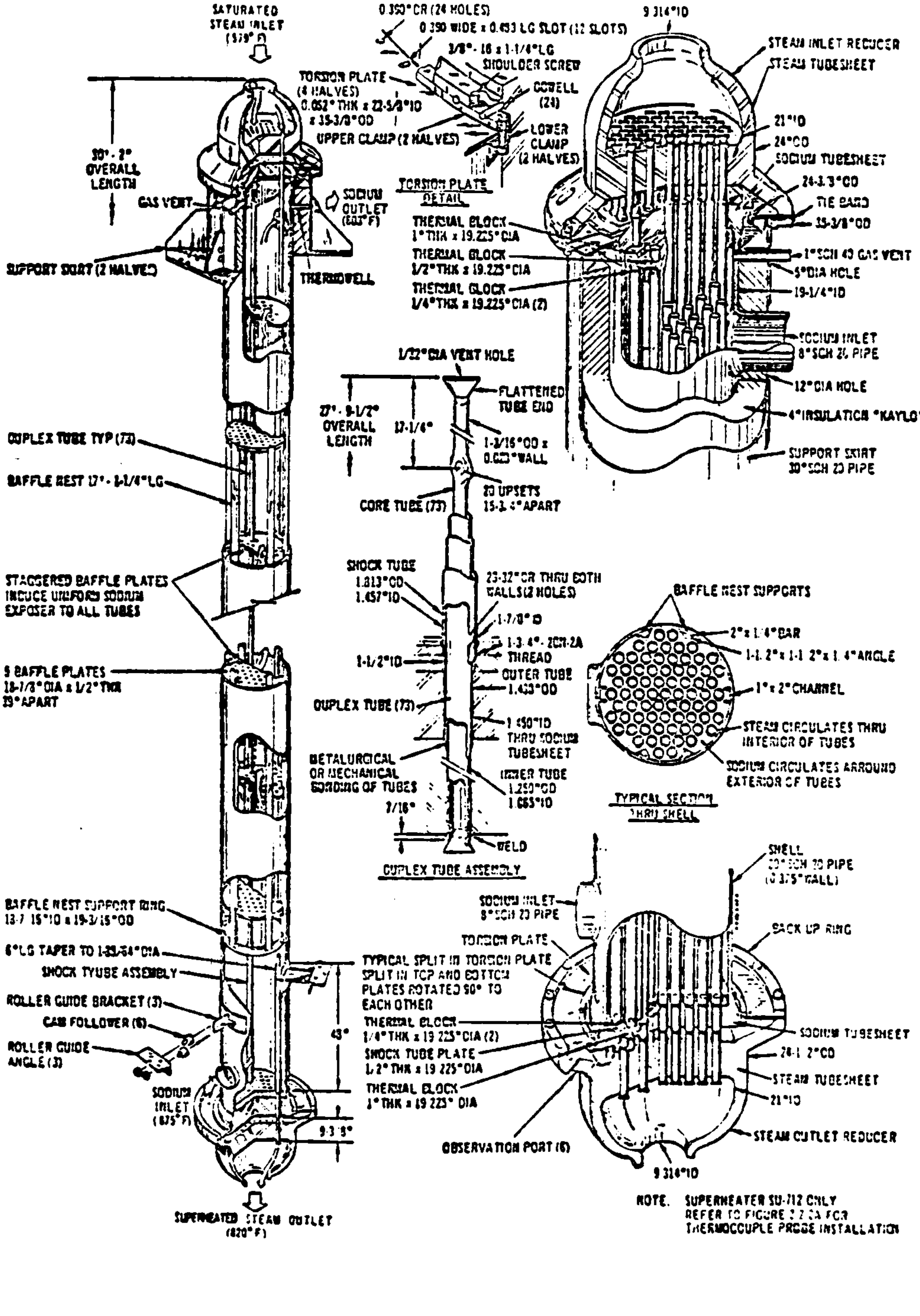

Fig. 2.13 EBR-II Superheater Assembly.

The steam drum is mounted above the evaporators with its centerline at the 154 feet elevation, and it is 48 feet long, with a 4 feet inner diameter. The water/steam mixture which enters the drum through the riser nozzles located at the centerline is deflected downward by diffuser plates anchored across each side of the drum above the riser nozzles. The diffuser plates prevent the water/steam mixture from impacting directly on the deflector and screen assembly; they also cause diffusion of the saturated steam to the side and bottom of the drum to cause initial fallout of the heaviest moisture particles. The steam passes through the primary and final screen dryer assemblies located on each side of the drum near the top, extending along the entire length of the drum.

In the EBR-II, the natural recirculation-type steam generator is selected over the once-through type because of its proven operation and inherent stability. The other design specifications, especially characteristics of the EBR-II, are designing evaporators and superheaters with sodium on the shell side and water/steam flowing through the tubes to minimize stress corrosion, and using bonded duplex tubes and double tube sheets to minimize the possibility of interaction between sodium and water/steam.

2.5 EBR-II Control Systems

EBR-II reactivity control is maintained using 12 control rod and two safety rod subassemblies as described in Sect. 2.2.3. A computer controlled rod drive system controls reactor power during steady-state and also changes reactor power. An error signal from the reactor power reading is the input to the digital computer. The permanent automatic control-rod drive system (ACRDS) provides a fast speed automatic mode plus two slow-speed modes, the manual and automatic. The technical specification limit of reactivity insertion is 0.01 $/sec (safety related). The reactor is sub-critical when the control rods are fully withdrawn. The control rod contains fuel elements in the approximate center and provides positive reactivity as it is inserted into the active core region. The two safety rods are always fully inserted for normal operations. They are automatically ejected from the core when hazardeous incidents are detected.

The primary sodium flow (loop between core and IHX) is controlled by the primary pumps where the pumping rate is variable from 0 to 100 % in a continuous stepless manner. There are no valves or other control devices in the main sodium loop. During normal operation the pump is operated at a flow rate sufficient to maintain bulk sodium temperature at 700 F at all power levels.

Secondary sodium flow is also controlled by pumps. Flow is adjustable from 0 to 100 percent of full flow capacity by varying the voltage applied to the pump windings. The control signal is adjusted manually from the sodium recirculating pump panel.

The feedwater temperature is controlled by bypassing some feedwater around the last heater, mixing a portion of 480 F feedwater with the 568 F water to maintain 550 F input. The bypass valve is manually controlled from the steam panel in the main control room.

Turbine generator is controlled by two circuits. The primary circuit controls the speed and load of the turbine where the secondary circuit controls the turbine stop valve to trip the turbine when an abnormal condition occurs.

The main control of the steam generator is performed by means of the steam drum level control. The control system is capable of single-element, four-element, or manual control. The controller accepts four analog signals: steam-drum level, feedwater flow, steam flow, and blowdown flow. The actuator is the feedwater valve.

CHAPTER 3

EBR-II PRIMARY SYSTEM MODEL DEVELOPMENT

3.1 Introduction

A nodal formulation of the reactor core and the intermediate heat exchanger is presented. The core model includes the active core, inner and outer blankets, lower and upper reflectors, and piping. The 25-node model is shown in Fig. 3.1. The formulation of the core model is partially adapted from an earlier work [Greene 1]. All the system parameters are recalculated and updated using Ref.[2]. Two changes made in the Greene model include an application of a physical model reduction method [4] and a modification in the IHX model formulation. Physical and numerical reasons for these modifications are explained in the following sections. The core bowing and control rod expansion reactivity effects have not been taken into account in the present model.

The intermediate heat exchanger (IHX) is modeled using twelve state variables which also includes the primary sodium tank as shown in Fig. 3.1. The core and IHX models are coupled into one module for the purpose of

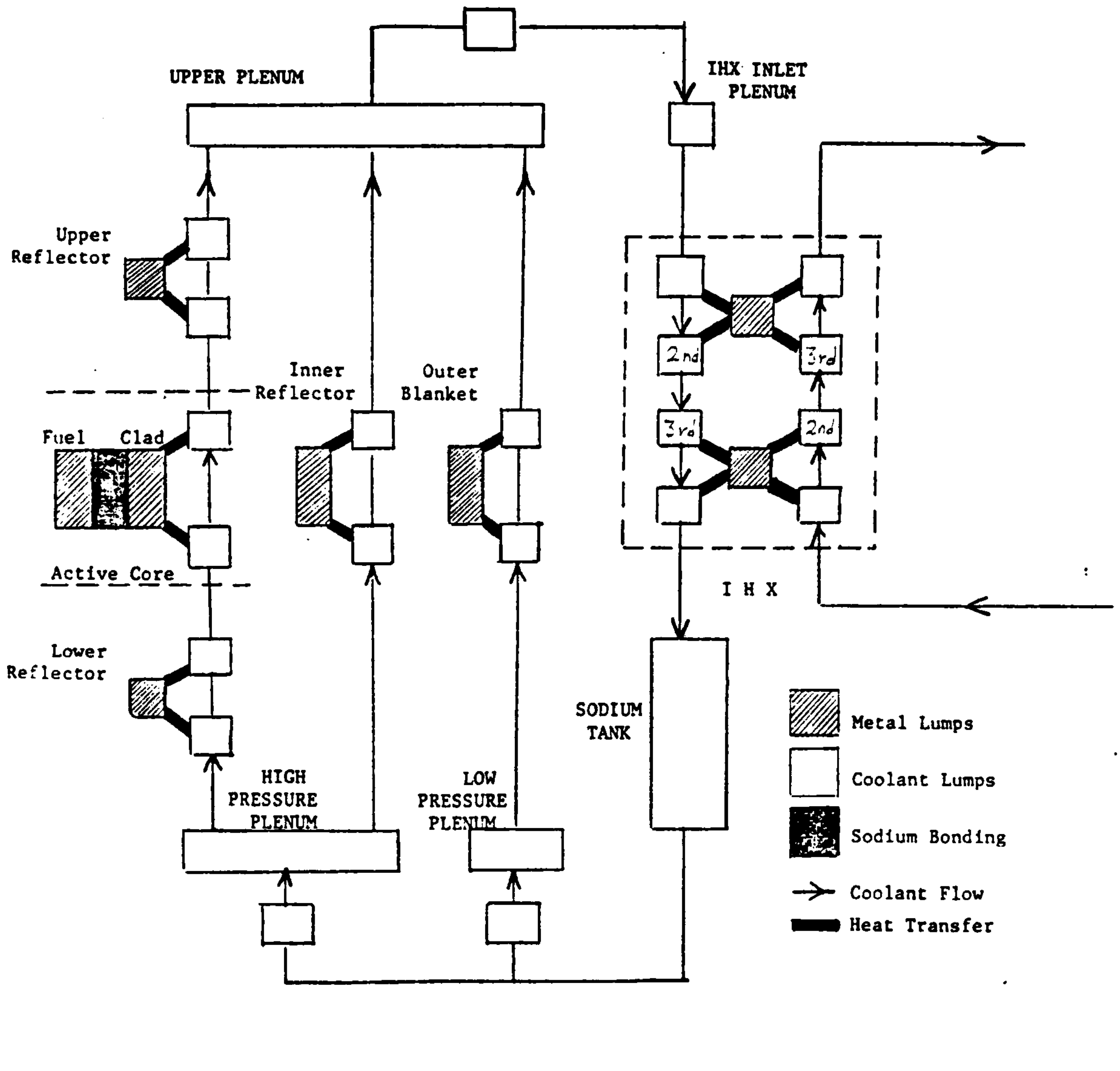

Fig. 3.1 Nodal Representation of the EBR-II Primary System Model .

simulation studies. The governing equations for each subsystem, definition of variables and the table of parameters are presented in the following sections. The corresponding nonzero elements of the system matrix A are given in Table 3.7.

3.2 Reactor Core

The active core dynamics are described by the point reactor kinetics equations [1].

3.2.1 Reactor Kinetics

$$\frac{d}{dt}\left[\frac{\delta P}{P_o}\right] = \frac{-\beta_T}{\Lambda}\frac{\delta P}{P_o} + \bar{\lambda}\frac{\delta C}{P_o} + \sum_i \frac{\alpha_i}{\Lambda}\delta T_i + \frac{\delta\rho_{ext}}{\Lambda} \qquad (3.1)$$

$$\frac{d}{dt}\left[\frac{\delta C}{P_o}\right] = \frac{\beta_T}{\Lambda}\frac{\delta P}{P_o} - \bar{\lambda}\frac{\delta C}{P_o} \qquad (3.2)$$

where

δ ≡ denotes variation from the steady-state value,

P = power,

P_o = steady-state power,

β_T = total delayed neutron fraction,

Λ = neutron generation time,

C = precursor concentration,

α_i = temperature reactivity feedback coefficient corresponding to temperature T_i,

ρ_{ext} = external reactivity,

$\bar{\lambda}$ = precursor average decay constant.

The neutronic data and the reactivity feedback coefficients are given in Tables 3.1 and 3.2, respectively. The core bowing reactivity effect becomes significant at high temperatures. The structural material inside the vessel expands radially when some critical temperature point is exceeded and results in replacing the corresponding amount of coolant volume with the structural material. The resultant effect is less heat removal since the coolant volume is reduced, and a contribution to the temperature reactivity feedback phenomena. However, compared to the other reactivity mechanisms, its behavior is complicated and not as dominant as the other feedback effects. Figure 3.2 shows its temperature dependence with respect to other

TABLE 3.1

EBR-II Neutronic Data

Precursor Decay constant (sec^{-1})	Delayed Neutron Fraction	Mean life-time (sec)
$\lambda_1 = 0.0127$	$\beta_1 = 0.000252$	$\ell_1 = 78.74$
$\lambda_2 = 0.0317$	$\beta_2 = 0.00147$	$\ell_2 = 31.5457$
$\lambda_3 = 0.1150$	$\beta_3 = 0.001344$	$\ell_3 = 8.6957$
$\lambda_4 = 0.311$	$\beta_4 = 0.002941$	$\ell_4 = 3.2154$
$\lambda_5 = 1.4$	$\beta_5 = 0.001024$	$\ell_5 = 0.7143$
$\lambda_6 = 3.78$	$\beta_6 = 0.000237$	$\ell_6 = 0.2645$

TABLE 3.1 (continued)

Total delayed neutron fraction,	$\beta_T = 0.007278$
Neutron generation time,	$\Lambda = 1.55 \times 10^{-7}$ sec
Average precursor mean-life time,	$\bar{\ell} = 12.1077$ sec
Average decay constant,	$\bar{\lambda} = \frac{1}{\bar{\ell}} = 0.08259$ sec $^{-1}$

TABLE 3.2

EBR-II Reactivity Feedback Coefficients

Coefficient	$\delta\rho$/ F	Coupled Parameter
Doppler	$+0.222 \times 10^{-6}$	Fuel temperature
Steel expansion	-0.720×10^{-5}	Clad temperature
Core Na expansion	-0.481×10^{-5}	Core Na temperature
Reflector expansion	-0.223×10^{-5}	Upper & lower reflector Na temperature
Inner reflector expansion	-0.120×10^{-5}	Inner reflector Na temperature
Fuel expansion	-0.200×10^{-5}	Fuel temperature

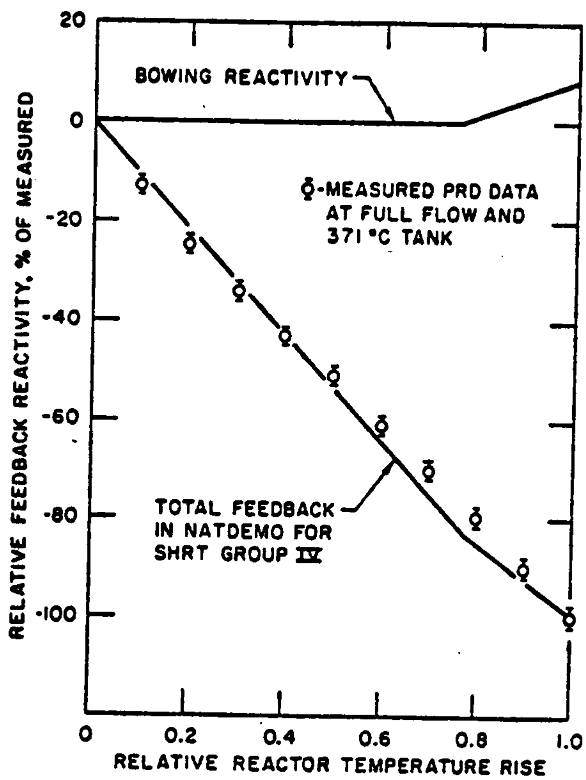

Fig. 3.2 Measured and Calculated Feedback Reactivity in EBR-II for SHRT Group IV.

reactivity effects[9]. A recent study at ANL [9] reports that the uncertainty in predicting a numerical value for thermal bowing coefficient is high (the reactivity effects have been verified by data from rod-drop, reactor oscillator, or power reactivity decrement tests). In the EBR-II core, another significant reactivity feedback effect comes from the control rod expansion at high temperatures. Expansion of a control rod introduces more neutron absorber into the core which is a negative reactivity effect and improves the safety margins.

For low-order modeling purposes these mechanisms may be ignored without losing much information about the system's behavior for small transients around the steady-state. Thermal bowing cannot be handled without increasing the order of the model by introducing some radial lumps. On the other hand, using a data representing the global effect with a high uncertainty in its prediction is not believed to yield informative results using low-order models. At steady state conditions, we assume that the control rod expansion reactivity effect is negligible.

Using the data given in Table 3.1, and averaging mean-life time over the six precursor groups, we obtain

$$\bar{\ell} = \frac{\sum_{i=1}^{6} \beta_i \ell_i}{\beta_T} \qquad (3.3)$$

Using Eq. (3.3) an average precursor equation is replaced with the six-group equations of the Greene model. This is a well known physical model reduction technique [4] and is proven to give accurate results when low-order kinetic models are concerned. Reducing the order of a model saves computational time and lowers the cost. The calculated parameters are listed in Table 3.1.

3.2.2 Core Heat Transfer

The heat transfer in active core region is modeled using five differential equations corresponding to five lumps as shown in Fig. 3.3. These nodes represent the fuel, sodium bond, cladding, inlet coolant and outlet coolant regions. The heat transfer dynamics between cladding and coolant regions is represented using Mann's model [10]. In Mann's model, the lower coolant lump outlet temperature is assumed to represent the average lump temperature which is a coupling parameter for the heat transfer driving force between the metal and the coolant regions.

Table 3.3 shows the core heat transfer parameters. The perturbation form of the state equations are given below [1].

$$\frac{d}{dt}\,\delta T = \frac{P_F P_o}{(MC_p)_F}\,\frac{\delta P}{P_o} - \frac{1}{R_1(MC_p)_F}\,(\delta T_F - \delta T_B) \tag{3.4}$$

$$\frac{d}{dt}\,\delta T_B = \frac{1}{R_1(MC_p)_B}\,(\delta T_F - \delta T_B) - \frac{1}{R_2(MC_p)_B}\,(\delta T_B - \delta T_C) \tag{3.5}$$

$$\frac{d}{dt}\,\delta T_C = \frac{1}{R_2(MC_p)_B}\,(\delta T_B - \delta T_C) - \frac{1}{R_3(MC_p)_\theta}\,(\delta T_B - \delta\theta_1) \tag{3.6}$$

$$\frac{d}{dt}\,\delta\theta_1 = \frac{1}{R_3(MC_p)_\theta}\,(\delta T_C - \delta\theta_1) + \frac{2}{\tau}(\delta\gamma_2 - \delta\theta_1) \tag{3.7}$$

$$\frac{d}{dt}\,\delta\theta_2 = \frac{1}{R_3(MC_p)_\theta}\,(\delta T_C - \delta\theta_1) + \frac{2}{\tau}(\delta\theta_1 - \delta\theta_2) \tag{3.8}$$

where

T_F	= fuel temperature,
T_B	= sodium-bond temperature,
T_C	= fuel cladding temperature,
θ_i	= temperature of the i-th coolant node,
R_1, R_2, R_3	= heat transfer resistances,
γ_2	= lower axial-reflector coolant outlet temperature,
τ	= resident time of the coolant in the active core region,
P_F	= fraction of power deposited in the fuel,
$(Cp)_B$	= specific heat capacity of the blanket material,
$(Cp)_\theta$	= specific heat capacity of the coolant,
M_B	= mass of the blanket material,
M_θ	= mass of the coolant.

TABLE 3.3

Core Heat Transfer Parameters

Power	Heat Capacity	Heat Resistance
P_o = 59267 BTU/sec	MC_f = 34.8 BTU/F	R_1 = 6.585 sec F/BTU
P_f = 49547.1 BTU/sec	MC_c = 13.33 BTU/F	R_3 = 12.5879 sec F/BTU
	MC_B = 2.03 BTU/F	R_2 = 7.0973 sec F/BTU
	MC_O = 16.69 BTU/F	τ = 0.075 sec

3.2.3 Reflector and Blanket Models

The active core in the EBR-II is surrounded by reflector and blanket materials as explained in Chap. 2. The complete core model includes twelve additional nodes representing the axial and the radial reflector zones and radial blanket region. The same heat transfer principle is carried out in developing the state equations as in the core heat transfer model. The general equations for reflector and blanket regions are described by a set of three equations for each. The parameter values are listed in Table 3.4 [1].

$$\frac{d\delta T_M}{dt} = \frac{P_i}{(MCp)_M}\frac{\delta P}{P_o} - \frac{U.A}{(MCp)_M}(\delta T_M-\delta T_1) \tag{3.9}$$

$$\frac{d\delta T_1}{dt} = \frac{U.A}{(MCp)_T}(\delta T_M-\delta T_1) + \frac{2}{\tau}(\delta\theta_{in}-\delta T_1) \tag{3.10}$$

$$\frac{d\delta T_2}{dt} = \frac{U.A}{(MCp)_T}(\delta T_M-\delta T_1) + \frac{2}{\tau}(\delta T_1-\delta T_2) \tag{3.11}$$

TABLE 3.4

Reflector and Blanket Region Data

Upper and Lower Reflector	Inner Reflector	Outer Blanket
P_f = 711.2025 BTU/sec	P_f = 5808.15 BTU/sec	P_f = 1303.87 Btu/sec
$(MC_p)_m$ = 54.70 BTU/F	$(MC_p)_m$ = 378.18 BTU/F	$(MC_p)_m$ = 1797.85 BTU/F
$(MC_p)_T$ = 27.10 Btu/F	$(MC_p)_T$ = 14.26 BTU/F	$(MC_p)_T$ = 217.36 BTU/F
UA_L = 71.08 BTU/sec-F	Resident time = 0.27 sec	Resident time = 1.09 sec
UA_U = 4.62 BTU/sec-F	UA = 32.03 BTU/sec-F	UA = 14.89 BTU/sec-F
Resident = 0.106 sec		

where

T_M = temperature of the metal node,

T_1 = temperature of the first region coolant node,

T_2 = temperature of the second region coolant node,

A = total heat transfer area,

τ = residence time of the coolant in reflector or blanket region,

U = metal to coolant heat transfer coefficient,

θ_{in} = inlet coolant temperature,

$(Cp)_M$ = specific heat capacity of the metal,

$(Cp)_T$ = specific heat capacity of the coolant.

3.2.4 Piping and Plenum Models

The model includes six lumps representing the low pressure plenum, the high pressure plenum, the upper plenum and core inlet-outlet piping regions. A first order transport-lag has been assumed for all piping. The other assumptions are: (1) constant coolant density, (2) no axial heat conduction, and (3) no heat gain or loss in the piping. The perturbation form of the state equations are as follows. The design parameters are given in Table 3.5 [1].

$$\frac{d\delta T_U}{dt} = \frac{M_1 . Cp_1}{(MCp)_u} (\delta\gamma_4 - \delta T_U) + \frac{M_2 . Cp_2}{(MCp)_u} (\delta\gamma_6 - \delta T_U) \tag{3.12}$$

$$+ \frac{M_3 . Cp_3}{(MCp)_u} (\delta\gamma_8 - \delta T_U)$$

$$\frac{d\delta T_{out}}{dt} = \frac{1}{\tau_1} (\delta T_U - \delta T_{out}) \tag{3.13}$$

$$\frac{d\delta T_{LI}}{dt} = \frac{1}{\tau_3} (\delta\theta_p - \delta T_{LI}) \tag{3.14}$$

$$\frac{d\delta T_{HI}}{dt} = \frac{1}{\tau_4} (\delta\theta_p - \delta T_{HI}) \tag{3.15}$$

$$\frac{d\delta T_H}{dt} = \frac{1}{\tau_5} (\delta T_{HI} - \delta T_H) \tag{3.16}$$

$$\frac{d\delta T_L}{dt} = \frac{1}{\tau_6} (\delta T_{LI} - \delta T_L) \tag{3.17}$$

where

Tu = upper plenum temperature,

T_{out} = reactor outlet temperature,

θ_p = primary sodium tank temperature,

T_{LI} = low-pressure plenum inlet temperature,

T_{HI} = high-pressure plenum inlet temperature,

T_H = high-pressure plenum temperature,

γ_4 = upper-reflector outlet temperature,

γ_6 = inner-reflector outlet temperature,

γ_8 = blanket region outlet temperature,

T_L = low pressure plenum temperature,

τ_1 = resident time of sodium in reactor outlet piping,

τ_2 = resident time of sodium in the pot,

τ_3 = resident time of sodium in the pot-to-reactor low pressure piping,

τ_4 = resident time of sodium in the pot-to-reactor high pressure piping,

τ_5 = resident time of sodium in the high-pressure plenum,

τ_6 = resident time of sodium in the low-pressure plenum.

3.2.5 Intermediate Heat Exchanger (IHX) Model

The sodium tank and the IHX are represented by twelve nodes in the model as shown in Fig. 3.1. The primary inlet plenum and the sodium tank are represented by first order transport-lag approximations. The heat transfer from the primary to the secondary sodium is modeled using Mann's technique [10].

TABLE 3.5

Primary Piping and Plenum Data

Time Constants	Resident Times
$\dot{M}_1/M_1 = 0.1198\ sec^{-1}$	$\tau_1 = 1.54$ sec
$\dot{M}_2/M_2 = 0.0288\ sec^{-1}$	$\tau_2 = 552.6$ sec
$\dot{M}_3/M_3 = 0.0246\ sec^{-1}$	$\tau_3 = 1.8$ sec
	$\tau_4 = 1.78$ sec
	$\tau_5 = 1.49$ sec
	$\tau_6 = 16.28$ sec

For a low-order counterflow heat exchanger model the system may be divided into five regions each representing an average temperature (as implemented in Greene's model). The configuration of the model includes two equal lumps for both primary and secondary coolant regions and a single lump for the tube wall region as shown in Fig. 3.4. However, there are cases where the five-lump configuration becomes insufficient in representing the system behavior and some unphysical responses may be encountered. An analytical identification of the problem has already been studied [Ball 10] and it has been proven that a transfer function written for the input output pair (T_{out},T_{in}) becomes nonminimum if the corresponding time constants of the five-lump model exceed a certain limit. One approach to avoid such an unphysical behavior in system responses is to define average temperatures for smaller portions of the system by dividing the system into more lumps.

The EBR-II intermediate heat exchanger data for the ratio ($U_{pm}A_{pm}/M_pC_p$) is 0.216 sec^{-1} and the corresponding time constant is 4.62 sec, thus exceeding the acceptable value of 2 sec as stated in Ref[10]. Therefore, the IHX model is formulated using two five-lump models connected in series as suggested by Ball. The simulation results presented in Chap. 5 verify that the modification improved the overall heat exchanger behavior.

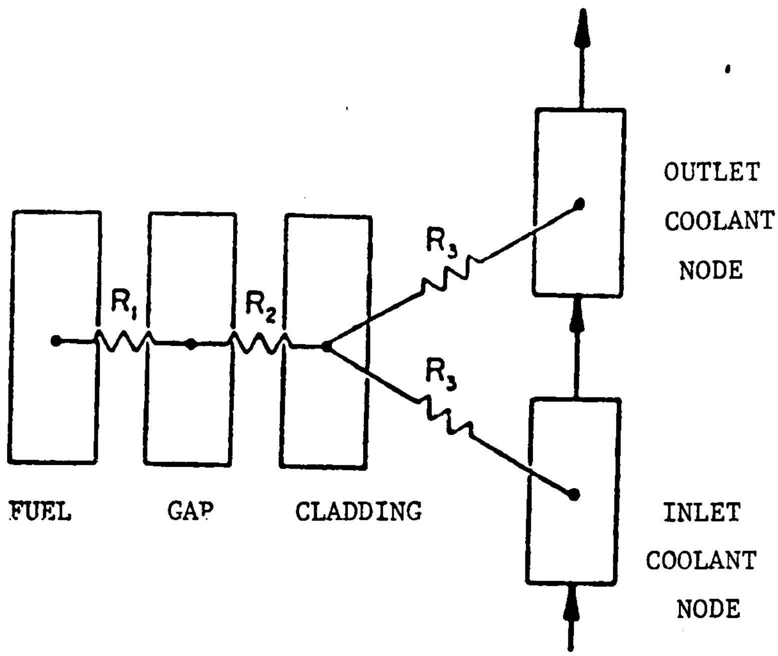

Fig. 3.3 Mann's Core Heat Transfer Model.

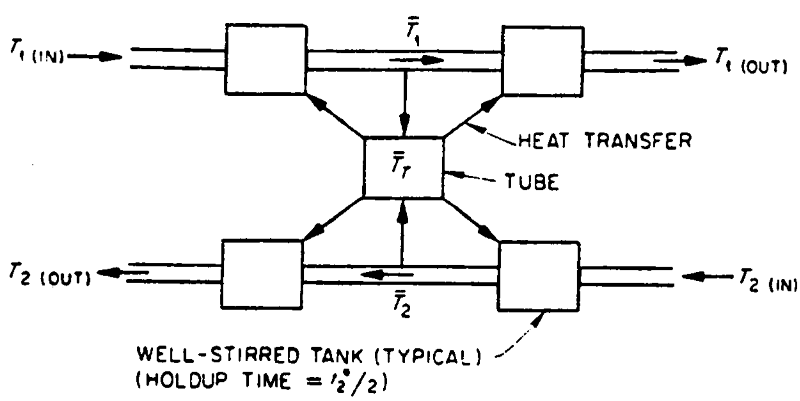

Fig. 3.4 Lumped Parameter Approximation of a Counterflow Heat Exchanger.

A five-lump model state equations are described below [1].

$$\frac{d\delta P_1}{dt} = \frac{2}{T_8}\,\delta P_{in} - \left[\,\frac{(UA)_p}{(MC_p)_p} + \frac{2}{\tau_8}\,\right]\delta P_1 + \frac{(UA)_p}{(MC_p)_p}\,\delta M \tag{3.18}$$

$$\frac{d\delta P_2}{dt} = \left[\,\frac{2}{\tau_8} - \frac{(UA)_p}{(MC_p)_p}\,\right]\delta P_1 - \frac{2}{\tau_8}\,\delta P_2 + \frac{(UA)_p}{(MC_p)_p}\,\delta M \tag{3.19}$$

$$\frac{d\delta M}{dt} = \frac{(UA)_p}{(MC_p)_M}\,\delta P_1 - \left[\,\frac{(UA)_p+(UA)_s}{(MC_p)_M}\,\right]\delta M + \frac{(UA)_s}{(MC_p)_M}\,\delta S_1 \tag{3.20}$$

$$\frac{d\delta S_1}{dt} = \frac{(UA)_s}{(MC_p)_s}\,\delta M - \left[\,\frac{(UA)_s}{(MC_p)_s} + \frac{2}{\tau_9}\,\right]\delta S_1 + \frac{2}{\tau_9}\,\delta S_{in} \tag{3.21}$$

$$\frac{d\delta S_2}{dt} = \frac{(UA)_s}{(MC_p)_s}\,\delta M - \left[\,\frac{(UA)_s}{(MC_p)_s} - \frac{2}{\tau_9}\,\right]\delta S_1 - \frac{2}{\tau_9}\,\delta S_2 \tag{3.22}$$

The primary inlet plenum and the sodium tank regions are represented by the following equations.

$$\frac{d\delta P_{in}}{dt} = \frac{1}{\tau_7}\,\delta T_{out} - \frac{1}{\tau_7}\,\delta P_{in} \tag{3.23}$$

$$\frac{d\delta\theta_p}{dt} = \frac{1}{\tau_2}\,(\delta P_2 - \delta\theta_p) \tag{3.24}$$

where

P_{in} = primary inlet plenum temperature,

T_{out} = reactor outlet temperature,

P_1 = first primary node temperature,

M = tube wall temperature,

P_2 = second primary node temperature,

S_1 = first secondary node temperature,

S_{in} = secondary sodium inlet temperature,

S_o = secondary outlet plenum temperature,

θ_p = sodium tank temperature,

τ_7 = resident time in primary outlet plenum,

τ_8 = resident time in both primary nodes,

τ_9 = resident time in both secondary nodes,

τ_{10} = sodium resident time in secondary outlet plenum.

The design parameters are given in Table 3.6.

TABLE 3.6

IHX Design Data

Heat Transfer	Heat Capacity	Resident Times
$(UA)_s$ = 598.94 BTU/sec-F	$(MC_p)_p$ = 2336.26 BTU/F	τ_7 = 1.91 sec
$(UA)_p$ = 505.03 BTU/sec-F	$(MC_p)_m$ = 841.66 BTU/F	τ_8 = 7.29 sec
		τ_9 = 2.86 sec
	$(MC_p)_s$ = 564.25 BTU/F	τ_{10} = 0.25 sec

TABLE 3.7

Nonzero Elements of System Matrix A

of the EBR-II Primary System Model

I	J	A(I,J)
1	1	-46955.
2	1	46955.
3	1	1165.7
12	1	4.59
15	1	4.59
18	1	5.32
21	1	0.107
1	2	0.0826
2	2	-0.0826
1	3	-9.8179
3	3	-24.612
4	3	422.29
3	4	24.612
4	4	-812.12
5	4	59.652
1	5	-39.763
4	5	391.82
5	5	-93.285
6	5	26.838
1	6	-13.282
5	6	33.633
6	6	-53.505
7	6	-0.171
1	7	-13.282
7	7	-26.66
16	7	18.867
8	8	-0.5555
9	8	0.614

Table 3.7. (continued)

I	J	A(I,J)
9	9	-0.614
22	9	1.834
10	10	-0.5617
11	10	0.6711
11	11	-0.6711
13	11	18.867
19	11	7.407
12	12	-1.299
13	12	2.622
14	12	2.622
1	13	-0.08632
12	13	1.299
13	13	-21.489
14	13	16.245
1	14	-0.08632
6	14	26.66
14	14	-18.867
15	15	-0.0844
16	15	0.1704
17	15	0.1714
1	16	-0.08632
15	16	0.0844
16	16	-19.038
17	16	18.696
1	17	-0.08632
17	17	-18.867
24	17	0.1198

Table 3.7 (continued)

I	J	A(I,J)
18	18	-0.0846
19	18	2.2461
20	18	2.2461
1	19	-0.3795
18	19	0.0846
19	19	-9.66
20	19	5.1611
1	20	-0.37935
20	20	-7.407
24	20	0.0288
21	21	-0.00828
22	21	0.068
23	21	0.0685
21	22	0.00828
22	22	-1.903
23	22	1.7654
23	23	-1.834
24	23	0.0246
24	24	-0.1732
25	24	0.6493
25	25	-0.6493
26	25	0.5235
26	26	-0.5235
27	26	0.549
27	27	-0.765
28	27	0.333
29	27	0.300
28	28	-0.549
32	28	0.549

Table 3.7 (continued)

I	J	A(I,J)
27	29	0.216
28	29	0.216
29	29	-0.655
30	29	1.060
31	29	1.060
30	30	-1.398
29	31	0.355
30	31	0.337
31	31	-2.458
32	32	-0.765
33	32	0.333
34	32	0.300
33	33	-0.549
37	33	0.0018
32	34	0.216
33	34	0.216
34	34	-0.655
35	34	1.060
36	34	1.060
31	35	1.398
35	35	-1.398
34	36	0.355
35	36	0.337
36	36	-2.458
8	38	0.5555
10	38	0.5617
37	37	-0.0018

CHAPTER 4

EBR-II STEAM GENERATOR MODEL DEVELOPMENT

4.1 Introduction

EBR-II steam generator is a natural circulation, recirculation steam drum/evaporator system, extracting heat from the sodium to produce superheated steam at 820 F at full power. The entire system is divided into thirteen lumps each representing average physical quantities. The nodal representation is shown in Fig.4.1. On the evaporator side, the primary tube wall and the secondary lumps are divided with a moving boundary determined by the subcooled height. The primary phenomena included in the model are the homogeneous flow in the boiling region, the mass and energy dynamics for both primary and secondary regions, the distribution of mass between downcomer, subcooled, boiling and the drum regions on the secondary side, and the momentum equation for the flow from downcomer to subcooled regions and flow leaving the boiling region. The system dynamics is assumed to be a function of two pressures: drum pressure and pressure inside the tubes of the evaporator.

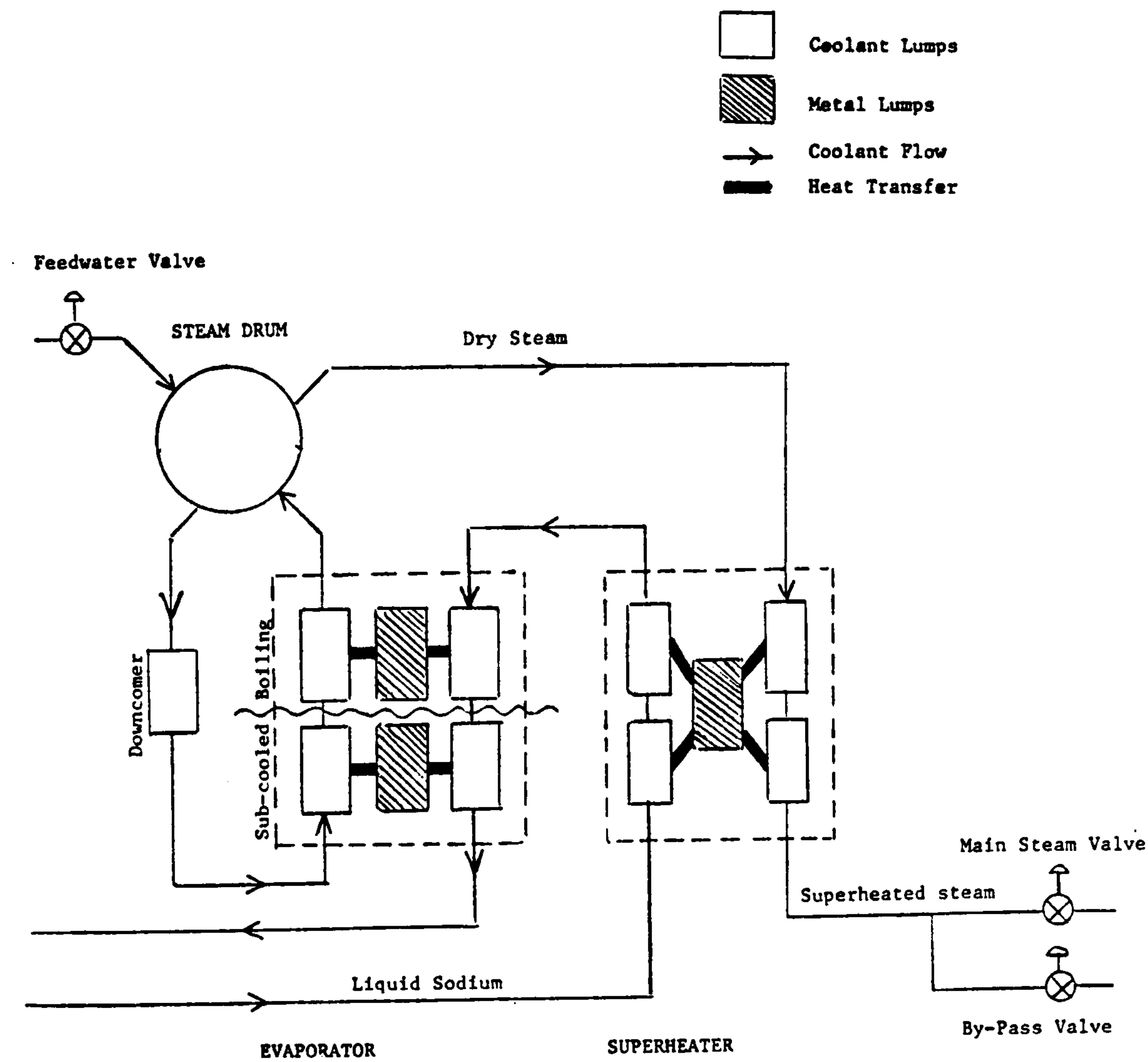

Fig. 4.1 Nodal Representation of the EBR-II Steam Generator Model.

Thermodynamic properties are determined at these two pressures. Phase equilibrium, no superheating in the boiling region, and the separators being 100% effective are the primary assumptions used in this model. The superheater model considers a single-phase heat transfer regime. The primary sodium flow is also assumed to be constant. A summary of assumptions used in the model is listed in Table 4.1.

The steam generator is represented by twenty differential equations using the state-space technique. The evaporator side consists of thirteen state variables including the downcomer and drum water temperatures, drum and boiling region pressures, drum inlet steam quality, subcooled level and drum level, primary sodium and tube wall temperatures, and two flows for the downcomer and rising mixture in the boiling region. Five state variables of the superheater model are temperatures of the primary sodium, superheated steam and the tube wall. The two remaining state variables are the control input and feedwater flow. The design parameters are shown in Tables 4.2-4.4. The nonzero elements of the system matrix A are listed in Table 4.5.

4.2 Evaporator and Drum Balance Equations

The operation of the EBR-II evaporator is quite similar to that of U-tube type steam generators; therefore, similar problems are encountered in modeling these two steam generators. One of the recent U-tube type steam generator models [6] suggests that the unknown flow at the moving boundary between subcooled and boiling regions is a linear function of the latent heat and the heat transfer rate into the subcooled region. The assumption used here is the linear dependence between flow and enthalpy increase caused by the heat transfer into this region. Another study [7] suggests that the unknown flows can be eliminated by algebraic manipulations. Two momentum equations are used for the unknown flows such as the downcomer flow and the flow leaving the evaporators, and the boundary flow is approximated as suggested in Ref [6]. The following sections describe the derivation of the model, and the nonzero elements of the coefficient matrix.

4.2.1 Drum Liquid

All water properties in the drum and downcomer regions are evaluated at the drum pressure. The assumption of perfectly mixed liquids is applied. The energy balance equations for the water in the drum can be written as follows.

$$\frac{d}{dt}[h_{\ell d}M_{\ell d}] = W_{fw}h_{fw} - W_{dc}h_{dc} + (1-x_e)\, W_{rm}h_f \qquad (4.1)$$

The mass of the water is:

$$M_{\ell d} = L\cdot A_d\cdot \rho_{\ell d} \qquad (4.2)$$

where

$h_{\ell d}$ = enthalpy of the liquid in the drum,

$M_{\ell d}$ = total mass of the liquid inside the drum,

W_{fw} = feedwater mass flow rate,

h_{fw} = enthalpy of the feedwater,

L = level in the drum,

$\rho_{\ell d}$ = density of the liquid in the drum,

A_d = longitudinal area of the drum,

x_e = steam exit quality,

W_{dc} = downcomer flow rate,

W_{rm} = rising water/steam mixture flow rate,

h_f = saturation enthalpy of the water,

h_{dc} = downcomer water enthalpy.

The perturbation form of the final state equation:

$$C_p M_{\ell d} \frac{d\delta T_{\ell d}}{dt} + [h_{\ell d} \cdot A_d \, \rho_{fd}] \frac{d\delta L}{dt} = [C_p \cdot W_{fw}] \, \delta T_{fw}$$

$$+ [h_{fw}] \, \delta W_{fw} - W_{dc} C_p T_{dc} - h_{dc} \delta W_{dc}$$

$$+ (1 - Xe) \, W_{rm} \left(\frac{\partial h_f}{\partial P_B} \right) \delta P_B + (1 - X_e) \, h_f \, \delta W_{rm}$$

$$- W_{rm} h_f \, \delta X_e \qquad (4.3)$$

where

$T_{\ell d}$ = temperature of the liquid in the drum,

T_{dc} = downcomer temperature,

T_{fw} = feedwater temperature.

4.2.2 Drum Steam

It is assumed that the rising steam is at saturation temperature, and there is no superheating. The mass balance equation for the steam in the drum is

$$\frac{dM_{sd}}{dt} = X_e W_{rm} - W_{SO} \qquad (4.4)$$

The dry steam flow leaving the drum can be stated in terms of the drum pressure and the steam valve coefficient. The assumption behind this simplification is called the "critical flow" assumption [3]. "It is assumed that the pressure drop in the downstream or turbine pressure will not change the steam flow rate from the steam generator."

$$\delta W_{SO} = C_L \delta P_D + P_D \delta C_L \tag{4.5}$$

Neglecting the effect of steam density deviation on the drum water level, the mass of the steam can be expressed as the product of steam volume and steam density. Using the chain rule it is possible to restate the density deviation in terms of the pressure deviation in the drum. Using Eq.(4.5) in Eq.(4.4) and applying the chain rule, the following is obtained.

$$V_{SD}\left(\frac{\partial \rho_{ST}}{\partial P_D}\right) \frac{d\delta P_D}{dt} = X_e \delta W_{rm} + W_{rm} \delta X_e + C_L \delta P_D + P_D \delta C_L \tag{4.6}$$

where

V_{SD} = volume of steam drum,

P_D = pressure inside steam drum,

ρ_{ST} = density of steam,

C_L = steam valve coefficient.

4.2.3 Primary Coolant Lumps

The first primary coolant lump has the dimensions determined by the subcooled height. The mass balance is written as follows.

$$\frac{d}{dt}(M_{P1}) = W_{PE} - W_{P1} \tag{4.7}$$

As indicated above, the mass of the coolant can be restated in terms of its density and volume. Using a cross sectional area which is constant through the tube, the volume is related to the subcooled height. Then Eq.(4.7) has the following form.

$$\rho_P \cdot A_P \frac{dZ_{sc}}{dt} = W_{PE} - W_{P1} \tag{4.8}$$

The energy balance for the same lump is written as

$$C_P \frac{d}{dt}(M_{P1}T_{P1}) = W_{PE}C_PT_{PE} - W_{P1}C_PT_{P1} - \dot{Q}_{PM1} \tag{4.9}$$

where

M_{P1} = mass of primary sodium,

W_{PE} = mass flow rate at the entrance of the lump,

W_{P1} = mass flow rate at the exit of the lump,

ρ_P = density of primary sodium,

A_P = flow area of primary sodium,

Z_{SC} = subcooled height,

L_{PM} = unit heat transfer length between primary and metal nodes,

T_{M1} = average metal temperature,

T_{P1} = bulk mean temperature of the node,

Q_{PM1} = heat transfer rate between primary-1 and metal-1 regions,

T_{PE} = entrance sodium temperature.

The heat transfer rate from the first sodium lump into the first metal lump is expressed as:

$$\dot{Q}_{pm1} = U_{pm} A_{pm1} (T_{p1} - T_{m1}) \tag{4.10}$$

where

U_{PM} = overall heat transfer coefficient between the primary and metal lumps.

A_{PM1} = heat transfer area between the first metal and primary regions. ($A_{PM1} = A_{PM2}$ for this model).

The unknown flow W_{p1} can be eliminated between Eq.(4.8) and (4.9) leading to the following final state equation.

$$\frac{d}{dt} \delta T_{P1} = \frac{1}{\tau_{P1}} \delta T_{PE} - [\frac{1}{\tau_{P1}} + \frac{U_{PM} \cdot A_{PM1}}{M_{P1} \cdot C_P}] \delta T_{P1} + \frac{U_{PM} A_{PM1}}{M_{P1} C_P} \delta T_{M1}$$

$$+ \frac{U_{PM}L_{PM}}{M_{P1}C_P} (T_{P1}-T_{M}1) \ \delta Z_{SC} \qquad (4.11)$$

The second primary coolant lump is treated in a similar manner as the first primary lump. Since the total height of the evaporator is constant the following relation exists.

$$\frac{dZ_{SC}}{dt} = - \frac{dZ_B}{dt} \qquad (4.12)$$

The entrance flow for the first coolant lump is the outlet flow of the second coolant lump.

$$W_{P2} = W_{PE} \qquad (4.13)$$

The energy balance for the second lump is

$$C_P \frac{d}{dt} (M_{P2}T_{P2}) = W_{P1}C_PT_{P1} - W_{P2}C_PT_{P2} - \dot{Q}_{PM2} \qquad (4.14)$$

where

T_{P2} = bulk mean temperature of the lump,

Q_{PM2} = heat transfer rate between primary-2 and metal-2 lumps,

T_{M2} = average metal temperature.

The heat transfer rate from the second sodium lump into the second metal lump is given by

$$Q_{pm2} = U_{pm} A_{pm2} (T_{p2} - T_{m2}) \tag{4.15}$$

The perturbation form of the final state equation is given by

$$\frac{d\delta T_{P2}}{dt} + \left(\frac{T_{P2}-T_{P1}}{Z_{SC}} \right) \frac{d\delta Z_{SC}}{dt} = \frac{1}{\tau_{P2}} \delta T_{P1} - \left[\frac{1}{\tau_{P2}} + \frac{U_{PM}A_{PM2}}{M_{P2}C_P} \right] \delta T_{P2}$$

$$+ \frac{U_{PM}A_{PM2}}{M_{P2}C_P} \delta T_{M2} - \frac{U_{PM}L_{PM}}{M_{P2}\cdot C_P} (T_{P2}-T_{M2}) \ \delta Z_{SC} \tag{4.16}$$

where

A_{PM2} = heat transfer area between primary-2 and metal-2 lumps,

τ_{P2} = residence time of the sodium in primary-2 lump,

M_{P2} = mass of sodium in primary-2 lump.

4.2.4 Tube Wall Lumps

Using the moving boundary approach introduces a complexity in the metal regions. In order to write a proper energy balance equation the mass transfer caused by the moving border between the metal lumps has to be taken into consideration. In this model, it is assumed that the variation in the boundary contributes some amount of energy to the total energy balance which can be written in terms of the average metal temperature and the time derivative of the subcooled height[6]. The last term of the energy balance equation stated below emphasizes this contribution.

$$C_M \frac{d}{dt} (M_{M1} T_{M1}) = \dot{Q}_{PM1} - \dot{Q}_{MS1} + \rho_M A_M C_M \overline{T}_M \frac{dZ_B}{dt} \tag{4.17}$$

where

$$\overline{T}_M = \frac{T_{M1}+T_{M2}}{2} \tag{4.18}$$

ρ_M = density of tube metal,

A_M = cross sectional area of tube metal lump,

C_M = specific heat capacity of tube metal,

$\overline{T}_M$ = average temperature at the boundary,

M_{M1} = mass of the tube metal in lump-1,

Q_{MS1} = heat transfer rate between metal-1 and secondary-1 lumps,

T_{sat} = saturation temperature of the secondary water,

T_{M1} = bulk mean temperature of metal lump-1,

T_{M2} = bulk mean temperature of metal lump-2, The heat transfer rate from the first tube region to the boiling region is written as:

$$\dot{Q}_{ms1} = U_{ms1}\, A_{ms1}\, (T_m - T_{s1}) \;. \qquad (4.19)$$

Note that the temperature in the boiling region is at the saturation value

$$T_{s1} = T_{sat} \;. \qquad (4.20)$$

The saturation temperature is related to the pressure in the boiling region (using the chain rule),provided that it is evaluated about the steady state. In other words, the saturation temperature deviation is governed only by the boiling pressure in a linear manner.

$$\delta T_{sat} = \left(\frac{\delta T_{sat}}{\delta P_B} \right) \delta P_B. \qquad (4.21)$$

Perturbation form of the final state equation is expressed below.

$$\frac{d\delta T_{m1}}{dt} - \left(\frac{T_{M1}-T_{M2}}{2Z_{SC}} \right) \frac{d\delta Z_{SC}}{dt} = \frac{U_{PM}A_{PM1}}{M_{M1}C_M}\, \delta T_{p1}$$

$$- \left[\frac{U_{PM}A_{PM}+U_{MS1}A_{MS1}}{M_{M1}C_M} \right] \delta T_{M1}$$

$$+ \frac{U_{MS1}A_{MS1}}{M_{m1}C_M} \left(\frac{\partial T_{sat}}{\partial P_B} \right) \delta P_B. \tag{4.22}$$

where

U_{MS1} = heat transfer coefficient between metal and secondary-1 lumps,

A_{MS1} = heat transfer area between metal and secondary-1 lumps.

The second metal lump is treated in a similar manner as the first one. The energy balance equation is given below.

$$C_M \frac{d}{dt} (M_{M2}T_{M2}) = \dot{Q}_{PM2} - \dot{Q}_{MS2} + \rho_M A_M C_M \bar{T}_M \frac{dZ_{SC}}{dt} \tag{4.23}$$

The heat transfer rate into the second metal region is expressed as

$$\dot{Q}_{ms2} = U_{ms2} A_{ms2} (T_{s2} - T_{m2}) . \tag{4.24}$$

The subcooled water temperature T_{s2} is not taken as a state variable in this model, instead it is assumed to be an average temperature which can approximately be written as an arithmetic average of the inlet and outlet temperatures of the lump.

$$T_{s2} = \frac{T_{pc}+T_{sat}}{2} \tag{4.25}$$

The final state equation is written as

$$\frac{d\delta T_{M2}}{dt} - [\frac{T_M - T_{M2}}{2Z_{SC}}] = \frac{U_{PM}A_{PM2}}{M_{M2}C_M}\delta T_{P2}$$

$$+ \frac{U_{MS2}A_{MS2}}{2M_{M2}\cdot C_M}\delta T_{DC} + [\frac{U_{MS2}A_{MS2}}{2M_{m2}C_M}][\frac{\partial T_{sat}}{\partial P_B}]\delta P_B$$

$$- [\frac{U_{PM}A_{PM2}+U_{MS2}A_{MS2}}{M_{M2}C_M}]\delta T_{M2} \tag{4.26}$$

where

T_{DC} = downcomer outlet temperature,

U_{MS2} = heat transfer coefficient between metal and secondary-2 lumps,

A_{MS2} = heat transfer area between metal and secondary-2 lumps,

M_{M2} = mass of the tube metal in lump-2.

4.2.5 Subcooled Region

The total heat delivered by the primary sodium system is transferred into the steam system by three different heat transfer mechanisms. Most of the source heat is absorbed in the superheaters, and the remaining produces steam in the evaporator. Steam production starts at some elevation in the evaporator as the subcooled water at the bottom reaches the saturation temperature. Above the boundary where saturation starts, heat transfer from the primary provides increase in steam quality until the steam water mixture reaches the top of the evaporator.

The phase change in the secondary coolant can be modeled using the moving boundary approach. The relationship between several thermodynamic parameters are summarized as follows. The saturation temperature is a function of the pressure inside the tubes. The subcooled height is determined by the downcomer flow, heat transfer rate from the primary side and the inlet coolant temperature of the evaporator. There is also dependence between the heat transfer rate and the saturation pressure since the heat transfer driving force parameter T_{sat} is a function of the pressure; therefore, the saturation pressure influences the moving boundary also.

The subcooled water enters the evaporator at downcomer outlet temperature T_{dc} and leaves the moving boundary at T_{sat}. As mentioned earlier, the average temperature of the subcooled region is assumed to be equal to the arithmetic mean of the inlet and outlet temperatures. The inlet flow is equal to the downcomer flow W_{dc}. The flow at the boundary is approximated (see App. A) and assumed to be a function of the heat transfer rate and the latent heat.

The mass balance equation for the subcooled region can be written as follows.

$$\frac{d}{dt}(M_{SC}) = W_{DC} - W_2 = \frac{d}{dt}(\rho_{SC} \cdot S_{SC} \cdot Z_{SC}) \qquad (4.27)$$

The equation above is manipulated to obtain subcooled height as a state variable.

$$\frac{d\delta Z_{SC}}{dt} = \frac{1}{\rho_{SC} A_{SC}} (\delta W_{DC} - \delta W_2) \qquad (4.28)$$

The energy balance equation for the subcooled region is

$$\frac{d}{dt}(M_{SC1} C_{PW} T_{SC}) = \dot{Q}_{MS2} + W_{DC} C_{PW} T_{sat} \qquad (4.29)$$

where

M_{SC} = mass of subcooled water,

C_{PW} = specific heat capacity of subcooled water,

W_{DC} = downcomer mass flow rate,

W_2 = mass flow rate of water leaving subcooled region,

ρ_{SC} = density of subcooled water,

A_{SC} = cross sectional area of subcooled region,

$\dot{Q}_{MS2}$ = heat transfer rate between metal-2 and subcooled lumps.

The unknown flow W_2 leaving the lump is expressed by the following linear relationship (see App. A).

$$W_2 = WB1\ \delta T_{m2} + WB2\ \delta T_{DC} + WB3\ \delta P_B + WB4\ \delta Z_{SC} \qquad (4.30)$$

where

WB1,WB2,WB3,WB4 = constant coefficients.

Substituting W_2 in balance equations and using simple algebra relating the mass and energy balance equations yields the following final state equation.

$$\left[\frac{A_{SC}\ \rho_{SC} Z_{SC} C_{PW}}{2}\right] \frac{D\delta T_{DC}}{dt} + \left[\frac{A_{SC}\ \rho_{SC} Z_{SC} C_{PW}}{2} \cdot \left(\frac{\partial T_{sat}}{\partial P_B}\right)\right] \frac{d\,\delta P_B}{dt}$$

$$+ \left[A_{SC} \cdot \rho_{SC} \cdot C_{PW} \left(\frac{T_{DC} + T_{sat}}{2}\right)\right] \frac{d\,\delta Z_{SC}}{dt}$$

$$= [U_{MS1} \cdot L_{MS} \cdot Z_{SC} - C_{PW} \cdot T_{sat} \cdot WB1]\ \delta T_{M2}$$

$$- [U_{MS1} \cdot L_{MS} \cdot Z_{SC} - W_{DC} C_{PW} + C_{PW} T_{sat} \cdot WB2]\ \delta T_{DC}$$

$$- [U_{MS1} \cdot A_{MS1} \left(\frac{\delta T_{sat}}{\delta P_B} \right) + W_2 C_{PW} \left(\frac{\delta T_{sat}}{\delta P_B} \right) + C_{PW} T_{sat} \cdot WB3] \ \delta P_B$$

$$+ [U_{MS1} \cdot L_{MS} \cdot \left(T_{M1} - \frac{T_{DC} + T_{sat}}{2} \right) - C_{PW} T_{sat} \cdot WB4] \ \delta Z_{SC}$$

$$+ [C_{PW} \cdot T_{DC}] \ \delta W_{DC} \qquad (4.31)$$

4.2.6 Boiling Region

As indicated above, the two phase regime in the evaporator can be modeled using at least three thermodynamic variables,namely,the moving boundary, saturation pressure and steam quality. In order to complete the model for the evaporator dynamics we need two more state equations to handle these three unknowns.

Boiling starts at the moving boundary and ends at the end of the heat transfer region near the top of the evaporator. It is assumed that the two phase mixture is homogeneous with an average enthalpy, quality and density represented by the following equations.

$$\bar{x} = \frac{x_e}{2} \qquad (4.32)$$

$$\rho_B = \rho_f (1 - \bar{x}) + \rho_g \bar{x} \qquad (4.33)$$

$$h_B = h_f(1-\bar{x}) + h_g\,\bar{x} \tag{4.34}$$

The mass balance equation for the boiling region is

$$\frac{d}{dt}(\rho_B A_B Z_B) = W_2 - W_{rm} \tag{4.35}$$

This can be rewritten in terms of the density and the boiling height as

$$A_B \left[Z_B \frac{d\delta\rho_B}{dt} + \rho_B \frac{d\delta Z_B}{dt} \right] = \delta W_2 - \delta W_{rm} \tag{4.36}$$

The perturbation form of the average density in the boiling region is expressed by the following relationship [6].

$$\delta\rho_B = K_1 \delta P + K_2 \delta X_e \tag{4.37}$$

where

$$K_1 = \frac{-\bar{x}}{(\nu_f + \bar{x}\nu_{fg})^2} \left(\frac{\delta\nu_{fg}}{\delta P_B}\right) \tag{4.38}$$

$$K_2 = \frac{-\nu_{fg}}{2(\nu_f + \bar{x}\nu_{fg})^2} \tag{4.39}$$

Note that the time derivative of the boiling height is equal to the time derivative of the subcooled height with a negative sign. Using the chain rule for the partial derivatives, the equations above yield the following final state equation.

$$- A_B \rho_B \frac{d\delta Z_{SC}}{dt} + A_B Z_B \cdot K_1 \frac{d\delta P_B}{dt} + A_B Z_B K_2 \frac{d\delta X_e}{dt}$$

$$= WB1\ \delta T_{m2} + WB2\delta T_{DC} + WB3\delta P_B + WB4\delta Z_{SC} - \delta W_{rm} \tag{4.40}$$

where

WB1, WB2, WB3, WB4 = coefficients of approximated flow equation,

W_{rm} = mass flow rate of rising mixture,

ν_f = specific volume of the liquid phase,

ν_g = specific volume of the vapor,

$\bar{x}$ = average steam quality,

$\bar{x}_e$ = exit steam quality.

A third state equation can be generated considering the energy balance throughout the boiling region.

$$\frac{d}{dt} [\rho_B A_B Z_B h_B] = \dot{Q}_{ms1} + W_2 h_f - W_{rm} h_e \tag{4.41}$$

where the outlet enthalpy

$$h_{xe} = h_f + x_e h_{fg} \tag{4.42}$$

The algebraic manipulations yield the following final state equation.

$$[A_B \cdot \rho_B \cdot Z_B \left(\frac{\partial h_f}{\partial P_B} + x \frac{\partial h_{fg}}{\partial P_B}\right) + h_B A_B Z_B K_1] \frac{d\delta P_B}{dt}$$

$$+ [A_B \; \rho \cdot Z_B \frac{h_{fg}}{2} - h_B A_B Z_B K_2] \frac{d\delta X_e}{dt}$$

$$- [h_B \cdot A_B \cdot \rho_B] \frac{d\delta Z_{SC}}{dt} = [U_{MS1} A_{MS1}] \; \delta T_{M1}$$

$$+ [W_2 \left(\frac{\partial h_f}{\partial P_B}\right) - U_{MS1} A_{MS1} \left(\frac{\partial T_{sat}}{\partial P_B}\right) - W_{RM} X_e \left(\frac{\partial h_{fg}}{\partial P_B}\right) + WB3.h_f] \; \delta P_B$$

$$- [U_{MS1}, \; L_{MS}(T_{M1} - T_{sat}] - h_f WB4] \; \delta Z_{SC}$$

$$- [h_{xe}] \; \delta W_{rm} - [W_{RM} \cdot h_{fg}] \; \delta X_e$$

$$+ [WB1 \cdot h_f] \; \delta T_{MZ} + [h_f WB2] \; \delta T_{DC} \qquad (4.43)$$

where

Q_{MS1} = heat transfer rate between metal-1 and boiling region lumps.

L_{MS} = unit heat transfer length between metal and secondary nodes.

h_{fg} = latent heat of evaporation.

4.2.7 Downcomer Region

Unlike the U-tube type steam generators, the secondary coolant enters the evaporators through piping directly. The downcomer region, therefore, is the piping between the steam drum and the evaporators. It is assumed that there is no axial heat transport through the pipes and no radial heat loss. A transport-lag is used to formulate the dynamics. Note that the downcomer inlet temperature is the temperature of the well-mixed drum liquid T_{ld}.

$$\frac{d\delta T_{dc}}{dt} = \frac{1}{\tau_{dc}} (\delta T_{\ell d} - \delta T_{dc}) \tag{4.44}$$

where

τ_{dc} = resident time in the downcomer piping.

4.2.8 Momentum Equations

In the development of the evaporator model, inlet and outlet coolant flows are the two unknowns to be modeled. In a simple study such as using a tea-kettle model for the steam generator, these flows might be considered to be constant and equal. However, when the drum dynamics is a subject of study then the deviations in flows can not be avoided. The momentum equation for the downcomer piping is

$$\frac{Z_{dc}}{g_c \cdot A_{dc}} \cdot \frac{dW_{dc}}{dt} = \Delta P + \rho_{dc} \cdot Z_{dc} - \frac{f_{dc}}{2g_c \cdot D_{dc} A^2{}_{dc}} \cdot \frac{Z_{dc}}{\rho_{dc}} |W_{dc}| \cdot W_{dc} \qquad (4.45)$$

where

Z_{dc} = height of the downcomer pipes,

A_{dc} = cross sectional area of the downcomer pipes,

W_{dc} = mass flow rate in the downcomer,

ΔP = pressure drop across the piping,

ρ_{dc} = density of downcomer fluid,

f_{dc} = friction factor in downcomer piping,

D_{dc} = hydraulic diameter,

g_c = gravitational constant.

Linearization about the steady state yields the following final form.

$$\frac{d\delta W_{dc}}{dt} = [\frac{g_c \cdot A_{dc}}{Z_{dc}}]\ \delta P_b - [\frac{g_c \cdot A_{dc}}{Z_{dc}}]\ \delta P_d$$

$$- \left[\frac{f_{dc} W_{dc}}{D_{dc} A_{dc} \rho_{dc}}\right] \delta W_{dc} \qquad (4.46)$$

The momentum equation for the outgoing flow is somewhat more complicated because of the two-phase regime. In order to obtain an equation for the flow of the water/steam mixture, the following momentum equation is used.

$$\frac{Z_{ev}}{g_c \cdot A_t} \frac{dW_{rm}}{dt} = \Delta P - \rho_{sc} Z_{sc} - \bar{\rho}_b Z_b$$

$$- \left[\frac{f_{sc} Z_{sc}}{2 g_c D_t \rho_{sc}} - \frac{f_b Z_b}{2 g_c D_t \alpha_f}\right] \bar{\phi}^2 \cdot G^2 \qquad (4.47)$$

where

Z_{ev} = height of the evaporator,

W_{rm} = mass flow rate of rising mixture,

A_t = cross sectional area of the duplex tubes,

σP = driving pressure drop,

f_{sc} = friction factor through the subcooled region,

f_b = friction factor through the boiling region,

D_t = total hydraulic diameter,

$\bar{\phi}$ = integral average two-phase friction multiplier,

Approximated Martinelli-Nelson friction multiplier is used [3].

$$\bar{\phi}^2 = 1.0 + \pi(G,P)\ 1.2(\frac{\rho f}{\rho_g} - 1)\ x^{0.824} \tag{4.48}$$

The integral average is taken as follows:

$$\bar{\phi}^2 = \frac{1}{Z_b} \int_{Z_{sc}}^{Z_{ev}} \phi^2 dZ \tag{4.49}$$

Using the relationship between steam quality and the height

$$X(Z) = \frac{X_e}{Z_b} (Z - Z_{sc}) \tag{4.50}$$

The resultant average can be written as

$$\bar{\phi}^2 = 1.0 + \frac{1.2\pi(G,P)(\frac{\rho f}{\rho g} - 1)x_e^{0.824}}{1.824} \tag{4.51}$$

where

$\pi(G,P) = 1.36 + (5.E-4)P + (3.6\ E-4)G$

$- (2.57\ E-6)\ PG$ for $G < 194.4\ lbm/ft^2 sec$

$\pi(G,P) = 1.26 - (4.E-4)P + \frac{33.6}{G} + \frac{7.777\ E-2}{G}P$

for $G > 194.4\ lbm/ft^2-sec$

where

G = Mass flux through the evaporator.

G = 205.07 lbm/ft^2-sec (for EBR-II evaporator).

Z_b = Boiling height.

The final state equation for W_{rm}

$$\frac{d\delta W_{rm}}{dt} = C_1\delta P_d + C_2\delta P_b + C_3\delta Z_{sc} + C_4\delta W_{rm} \tag{4.52}$$

where

$$C_1 = -\frac{g_c A_t}{Z_{ev}}$$

$$C_2 = \frac{g_c A_t}{Z_{ev}} - \frac{g_c A_t}{Z_{ev}}[Z_{sc}(\frac{\partial \rho_{sc}}{\partial P_B}) + Z_b(\frac{\partial \rho_b}{\partial P_B})]$$

$$+ \frac{A_t \phi^2 f_o}{2Z_{ev}D_t}[\frac{f_{sc}Z_{sc}}{\rho^2{}_{sc}}(\frac{\partial \rho_{sc}}{\partial P_B}) + \frac{f_b Z_b}{\rho^2{}_f}(\frac{\partial \bar{\rho}_f}{\partial P_B})]$$

$$C_3 = (\bar{\rho}_b - \rho_{sc})\frac{g_c A_t}{Z_{ev}} + \frac{A_t \phi^2 f_o}{2Z_{ev}D_t}[\frac{f_b}{\rho_f} - \frac{f_{sc}}{\rho_{sc}}]$$

$$C_4 = -\frac{f_{sc}Z_{sc}W_{rm}}{A_t Z_{ev} D_t \rho_{sc}} - \frac{f_b Z_b W_{rm}}{A_t Z_{ev} D_t \rho_f}\phi^2$$

4.3 Superheater State Equations

The two superheater units in EBR-II are identical in construction to the evaporators. Their design data, therefore, are exactly the same as those for the evaporators. Entering dry steam flows through the duplex tubes and is heated by the primary sodium flowing in the shell side of the superheaters, producing superheated steam at 875 F at full power.

Since the fluids on either side do not change phase during their residence in the superheaters, the modeling becomes simple. Thus the EBR-II superheater is nothing but a counter flow single-phase heat exchanger. Using Mann's technique in five-lump configuration, the superheater dynamics is represented by the heat exchanger Eqs.(3.18-3.22). The data assures that the five-lump model is efficient in representing the system dynamics. (MC_p/UA ratios are 0.87 sec for primary and 0.67 sec for secondary, both smaller than 2 sec limit.)

4.4 Three-Element Controller

In the actual plant, the drum level controller uses four signals. These are the blowdown flow, feedwater flow, steam outlet flow and drum level signals. Since the ratios of the blowdown flow to other flows are small it is assumed to be negligible on the system performance. Using three signals, the control signal is generated by the following formula.

$$u = [K_1(L - L_{set}) - K_2 (W_{st} - W_{fw})] \left(1 + \frac{K_I}{S} \right) \qquad (4.53)$$

where

K_i = proportional gain corresponding to the ith signal,

u = control signal,

L = level signal,

L_{set} = drum level set point,

K_I = integral gain,

S = Laplace transform variable.

$$K_1 = \frac{k_1}{\Delta L_{full}}$$

$$K_2 = \frac{k_2}{W_{fw,100\%}}$$

ΔL_{full} = full range of level variations,

$W_{fw,100\%}$ = 100 percent feedwater flow,

k_i = gain for the i-th error signal.

Outlet steam flow is not a state variable in this model; therefore, the steam flow is related to the drum pressure using the critical flow assumption [6]. The final state equation can be obtained by taking the inverse Laplace transform of Eq. (4.53).

$$\frac{d\delta u}{dt} + K_1 \frac{d\delta L}{dt} - K_2^* \frac{d\delta P_d}{dt} + K_2 \frac{d\delta W_{fw}}{dt}$$

$$= -K_1 \cdot K_I \delta L + K_2^* K_I \delta P_d - K_2 K_I \delta W_{fw} \tag{4.54}$$

where

$$K_2^* = K_2 \cdot C_L$$

It can be seen from the above equation that the implementation of the controller needs two more state equations, one for the actuator (W_{fw}), and the other for the drum level variable. The actuator dynamics denoted by z is related to the control input u in the following manner.

$$\frac{dz}{dt} = \frac{1}{\tau_{pos}} (u - z) \tag{4.55}$$

The feedwater flow is a function of the actuator dynamics

$$W_{fw} = f(z) \cdot K_{cv} \cdot \sqrt{\rho_{fw} \cdot \Delta p} \tag{4.56}$$

Assuming f(z) to be a linear function of z

$$W_{fw} = K_{TOT} \cdot z \tag{4.57}$$

Substituting Eq.(4.57) into Eq.(4.55) leads to the following state equation.

$$\frac{1}{K_{TOT}} \frac{d\delta W_{fw}}{dt} = \frac{1}{\tau_{pos}} \delta u - \frac{1}{K_{TOT}\tau_{pos}} \delta W_{fw} \tag{4.58}$$

where

K_{cv} = feedwater valve coefficient,

ρ_{fw} = feedwater density,

ΔP = pressure drop across the feedwater valve,

z = intermediate variable representing the value dynamics,

τ_{pos} = time constant of the feedwater valve positioning,

C_L = steam value coefficient.

Finally, the drum level is formulated using the mass balance equation for the drum water.

$$\frac{d}{dt} M_{\ell d} = W_{fw} - W_{dc} + (1 - Xe)\, W_{rm} \tag{4.59}$$

Assuming a simple geometry for the drum, the final state equation can be stated as follows.

$$\rho_{\ell d} \cdot A_d \frac{d\delta L}{dt} = \delta W_{fw} - \delta W_{dc} + (1 - Xe)\, \delta W_{rm} - W_{rm} \delta Xe \qquad (4.60)$$

TABLE 4.1

List of Assumptions Used in EBR-II

Steam Generator Model

Assumption	Corresponding Region
Phase equilibrium	Evaporator
No superheating	Drum, Evaporator
No counter flow.	Recirculation loop
Constant thermal conductivity.	All
Constant heat transfer coefficient.	All
No axial heat transfer	All.
Linear relationship between boiling height and rising mixture steam quality.	Boiling
Linear relationship between heat transfer rate into subcooled and flow rate.	Subcooled
Linear approximation to thermodynamic variables around saturation conditions.	Drum, Evaporator
100% effective moisture separation.	Drum
First order dynamics	Feedwater valve.
Critical flow assumption	Drum steam outlet.
Single phase regime	Superheaters

TABLE 4.2

EVAPORATOR DESIGN DATA [2]

100% Power level	from[2]
Recirculation ratio	1/7
Primary sodium flow rate, lbm/sec	626
Feedwater flow rate, lbm/sec	75
Secondary flow rate, lbm/sec	525
Heat capacity of sodium, Btu/lbm-F	0.3003
Heat capacity of tube wall, Btu/lbm-F	0.1098
Heat capacity of water, Btu/lbm-F	1.012
Heat capacity of steam, Btu/lbm-F	0.639
Number of duplex tubes	72
Number of evaporator units	7
Secondary cross sectional area, ft^2	2.56
Primary cross sectional area, ft^2	5.04
Heat transfer area (sodium-metal), ft^2	6260
Heat transfer area (metal-secondary), ft^2	3338
Density of subcooled water, lbm/ft^3	45.45
Density of dry steam (at 579 F), lbm/ft^3	3.10
Density of liquid sodium, lbm/ft^3	48.88
Average density in boiling region, lbm/ft^3	40.97

Table 4.2 (continued)

100% Power level	from [2]
Saturation temperature, F	579
Temperature at downcomer outlet, F	542
Evaporator steam exit quality	0.1428
Overall heat transfer coefficient (Liquid sodium-tube wall), Btu/ft^2-hr	1241
Overall heat transfer coefficient (Tube-wall-subcooled water), Btu/ft^2-hr	988
Overall heat transfer coefficient (Tube wall-boiling region), Btu/ft^2-hr	1973
Total mass of primary sodium, lbm	6290
Total mass of tube wall, lbm	80604
Friction factor of downcomer piping	0.02
Average friction multiplier (boiling)	4.01
Height of downcomer piping, ft	35
Height of evaporator, ft	27
$\frac{\partial T_{sat}}{\partial P_B}$ (around saturation), F/psi	0.099
$\frac{\partial v_{fg}}{\partial P_B}$ (around saturation), ft^3/psi-lbm	-0.0003
$\frac{\partial h_{fg}}{\partial P_B}$ (around saturation), Btu/lbm-psi	-0.1848
$\frac{\partial \rho_{sc}}{\partial P_B}$ (around saturation), lbm/ft^3-psi	-0.0093
$\frac{\partial h_f}{\partial P_B}$ (around saturation), Btu/lbm-psi	0.1332
$\frac{\partial \rho_b}{\partial P_B}$ (around saturation), lbm/ft^3-psi	0.1400

TABLE 4.3

Superheater Design Data [2]

100% Power level	from [2]
Total height, ft	27
Number of duplex tubes	72
Number of units	2
Temperature of inlet steam, F	579
Temperature of superheated steam, F	872
Temperature of primary inlet sodium, F	883
Temperature of primary outlet sodium, F	703
Overall heat transfer coefficient (Tube wall-steam), Btu/ ft^2-hr	1973
Overall heat transfer coefficient (Sodium-tube wall), Btu/ ft^2-hr	1241
Total mass of primary sodium, lbm	6290
Total mass of tube wall, lbm	80604
Cross sectional area, (steam), ft^2	2.56
Cross sectional area, (sodium), ft^2	5.04
Total heat transfer area (Tube wall-steam), ft^2	3338
Total heat transfer area (Sodium-tube wall), ft^2	6260
Primary sodium flow, lbm/sec	626
Superheated steam flow, lbm/sec	75

TABLE 4.4

Steam Drum Design Data [2]

100% Power level	from [2]
Inlet steam quality	0.1428
Outlet steam quality	1
Total length, ft	42
Diameter, ft	4.26
Drum level (below center line), inch	8
Density of drum water, lbm/ft^3	45.45
Blowdown flow, lbm/hr	20,000
Pressure drop across feedwater valve, psi	100

TABLE 4.5

Nonzero Elements of System Matrix A

of the EBR-II Steam Generator Model

I	J	A(I,J)
1	1	-2.2898
2	1	0.10631
3	1	-0.000039615
5	1	0.89941
6	1	0.30745
7	1	0.29215
8	1	0.01635
9	1	0.56
12	1	0.00778
16	1	0.094
1	2	1.6993
2	2	-0.34648
3	2	-0.0013382
4	2	7.221
5	2	-3.6272
6	2	-0.9355
7	2	-0.9355
9	2	-0.9166
1	3	-365.22
2	3	0.41627
3	3	-0.068836
5	3	3.5217
6	3	1.1239
7	3	1.1239
10	3	468.75
12	3	-0.68753
18	3	-0.13
20	3	0.4589
4	4	-1.343
5	4	0.1992
6	4	0.243

Table 4.5 (continued)

I	J	A(I,J)
5	5	-1.343
7	5	0.243
1	6	1.0803
2	6	-0.0012313
3	6	0.00020362
4	6	1.143
5	6	-0.010417
6	6	-0.45232
7	6	-0.0033246
1	7	5.689
2	7	-0.58015
3	7	-0.0010111
5	7	-3.765
6	7	-1.5921
7	7	-1.9124
1	8	1.5386
2	8	0.0070115
3	8	-0.00006987
5	8	0.059318
6	8	0.018931
7	8	0.018931
8	8	-0.089
12	8	0.00027894
18	8	-0.00026
20	8	0.00091
1	9	-1.67474
2	9	0.0019087
3	9	0.000075753
5	9	0.016148
6	9	0.0051536
7	9	0.0051536
10	9	0.1275
12	9	0.0011131
18	9	0.00022
20	9	-0.00076894

Table 4.5 (continued)

I	J	A(I,J)
8	10	-0.01635
9	10	-0.02104
10	10	-0.053
20	10	-2.49 E-8
1	11	1.2542
2	11	-0.047415
3	11	-0.000011807
5	11	-0.40113
6	11	-0.12802
7	11	-0.13318
11	11	-0.11057
12	11	-0.068753
1	12	-0.28545
2	12	-0.0013008
3	12	0.000012963
5	12	-0.011005
6	12	-0.0035122
7	12	-0.0035122
11	12	0.11057
13	13	-4.40000
14	13	4.00000
15	13	1.00000
4	14	0.1994
14	14	-37.8000
13	15	5.3913
14	15	5.5013
15	15	-1.6504
16	15	84.5000
17	15	84.5000
15	16	0.49
16	16	-137.00
17	16	-15.90
17	17	-79.0
20	18	-0.175

Table 4.5 (continued)

I	J	A(I,J)
12	19	-0.0054872
18	19	0.000262
19	19	-0.200000
20	19	-0.00089705
19	20	14.87
20	20	-0.0019777

CHAPTER 5

TRANSIENT SIMULATIONS USING OPEN-LOOP MODELS

5.1 Calculation Procedure

The linear dynamic models are represented using matrix notation and are given by

$$\begin{aligned} \dot{\underline{X}} &= A\,\underline{X} + B\,\underline{u} \\ \underline{y} &= C\,\underline{X} + D\,\underline{u} \end{aligned} \tag{5.1}$$

where

$\underline{X}$ = vector of state variables,

$\underline{y}$ = vector of measurements,

u = vector of forcing functions,

A = coefficient matrix,

B = input matrix,

C = observation matrix,

D = disturbance matrix.

The use of a set of coupled first order differential equations in the development of system models often requires an extensive algebraic manupulation in order to achieve a compact representation as in Eq.(5.1). When the number of derivative terms per equation exceeds one, the cumbersome algebra can be avoided by representing the system in the following form.

$$M \underline{\dot{X}} = N \underline{X} + E \underline{u} \tag{5.2}$$

Then the corresponding A and B system matrices calculated as

$$\begin{aligned} A &= M^{-1}.N \\ B &= M^{-1}.E \end{aligned} \tag{5.3}$$

provided M^{-1} exsists. However, taking the inverse of a large system matrix may result in some numerical problems. The possibility of encountering "ill-behaved" matrices also exsists. Thus care must be exercised in dealing with these problems.

In the present model of the EBR-II primary and steam generator systems, the two different representations stated above are used. The system matrix A of the steam generator model listed in Chapter 4 is calculated as shown in Eqs.(5.3). All calculations in this study are performed using the commercially available software package **MATRIX**$_{\mathbf{x}}$ (see Appendix B) [11]. The default integration algorithm invoked by the **MATRIX**$_{\mathbf{x}}$ is the "variable step Kutta-Merson" method [11] which is used for transient calculations.

The set of Eqns. (5.1) is a standard mathematical form used in simulation studies. Obtaining open-loop system responses to a given step perturbation requires the definition of matrices A,B,C and D. Since the purpose of this study does not include the multiple input case, the input and disturbance matrices are single column vectors. We assume that there is no disturbance at the output for open-loop transients, hence all of the D vector elements are equal to zero. We also assume that all the outputs are available for measurement and the observation matrix C is an identity matrix of order equal to that of the system matrix A. A list of state variables of the two models is given in Table 5.1.

5.2 Primary System Dynamic Simulation

5.2.1 Reactivity Perturbation Results.

An isolated primary system model includes the reactor core, IHX and the sodium tank as explained in Chap. 3. A typical perturbation of small reactivity insertion is applied to the open-loop model. Figure 5.1 shows a comparison between the fractional power responses of the primary system model and ANL rod drop test [9] for

TABLE 5.1

List of State Variables

Primary System Model

Row # of A matrix	State Variable
1	Fractional reactor power
2	Precursor concentration
3	Fuel temperature
4	Sodium Bond temperature
5	Cladding temperature
6	Core inlet sodium temperature
7	Core outlet temperature
8	Low-pressure plenum inlet temperature
9	Low-pressure plenum temperature
10	High-pressure plenum inlet temperature
11	High-pressure plenum temperature
12	Lower reflector metal temperature
13	Lower reflector inlet sodium temperature
14	Lower reflector outlet sodium temperature
15	Upper reflector metal temperature
16	Upper reflector inlet sodium temperature
17	Upper reflector outlet sodium temperature
18	Inner reflector metal temperature
19	Inner reflector inlet sodium temperature
20	Inner reflector outlet sodium temperature
21	Outer blanket metal temperature
22	Outer blanket inlet sodium temperature
23	Outer blanket outlet sodium temperature
24	Reactor upper plenum temperature
25	Reactor outlet piping temperature
26	IHX inlet plenum temperature
27	IHX first primary node temperature
28	IHX second primary node temperature
29	IHX upper metal node temperature
30	IHX secondary outlet temperature
31	IHX third secondary node temperature
32	IHX third primary node temperature
33	IHX primary outlet temperature
34	IHX lower metal node temperature
35	IHX second secondary node temperature
36	IHX secondary inlet temperature
37	Sodium tank temperature.

(Table 5.1 continued)

Steam Generator Model

Row # of A matrix	State Variable
1	Boiling region pressure
2	Evaporator subcooled height
3	Evaporator steam exit quality
4	Evaporator sodium temperature
5	Evaporator sodium outlet temperature
6	Evaporator upper metal node temperature
7	Evaporator lower metal node temperature
8	Downcomer flow
9	Evaporator rising mixture flow
10	Steam drum pressure
11	Drum water temperature
12	Downcomer temperature
13	Superheater inlet sodium temperature
14	Superheater outlet sodium temperature
15	Superheater metal temperature
16	Superheater first steam node temperature
17	Superheated steam outlet temperature
18	Drum level
19	Feedwater flow
20	Control input (three-element controller)

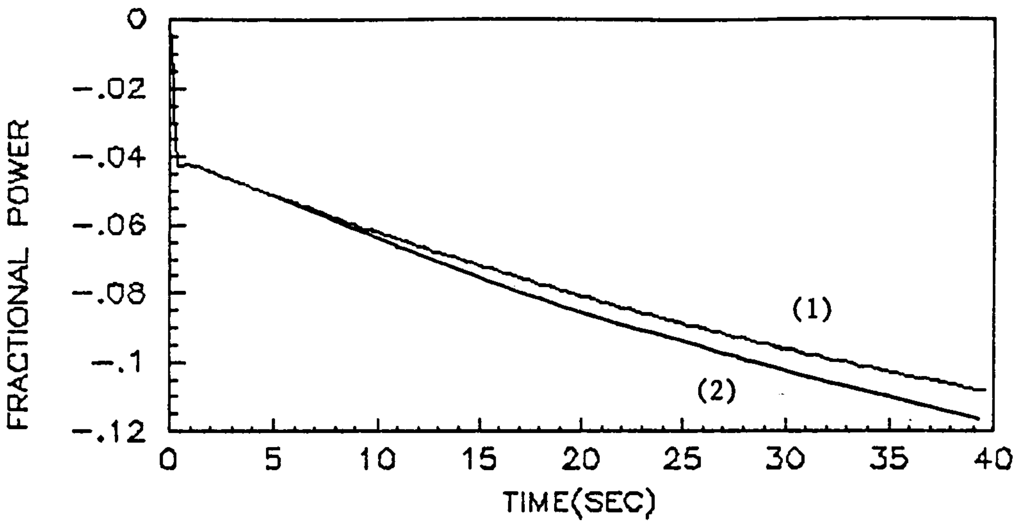

Fig. 5.1 Step Response of Fractional Reactor Power to a -5 cents Reactivity Perturbation (1) Open-loop Primary Model, (2) ANL Rod Drop Test Results[9]

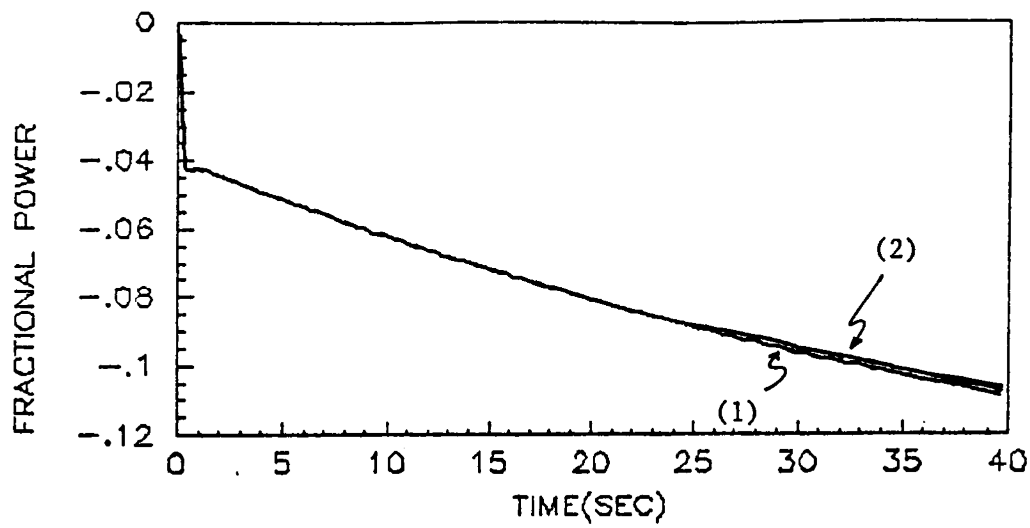

Fig. 5.2 Step Response of Fractional Power to a -5 cent Reactivity Perturbation. (1) Open-loop Primary Model, (2) Greene's Model.

a -5 cents step reactivity insertion. As it can be seen from the figure, the linear model gives a reasonable prediction of the actual power response. Figure 5.2 shows the fractional power responses of the primary model and the Greene model for a -5 cent step reactivity insertion. The difference in the responses is about 1% at 40 sec which verifies that the model reduction by replacing six precursor equations of the Greene model with one "averaged" precursor equation is a very good approximation. Using the two models, the temperature responses of the IHX coolant lumps for the same perturbation differ significantly due to " five-lump to ten-lump" modification. Figure 5.3 shows the temperature responses of the IHX model used in the Greene model. As the figure indicates, the secondary outlet sodium temperature exceeds the tube wall temperature which is a physically inconsistent result.(Note that there is no heat input to the IHX secondary inlet lump and -5 cent reactivity insertion to the core produces a heat input at the primary side of the IHX). Figure 5.4 shows the temperature responses of the modified model for the same perturbation. The dynamic behavior of the IHX model is improved using the ten-lump configuration.

The power production is distributed among the active core fuel material and several other reflector materials. The heat removal from these regions is carried out by the

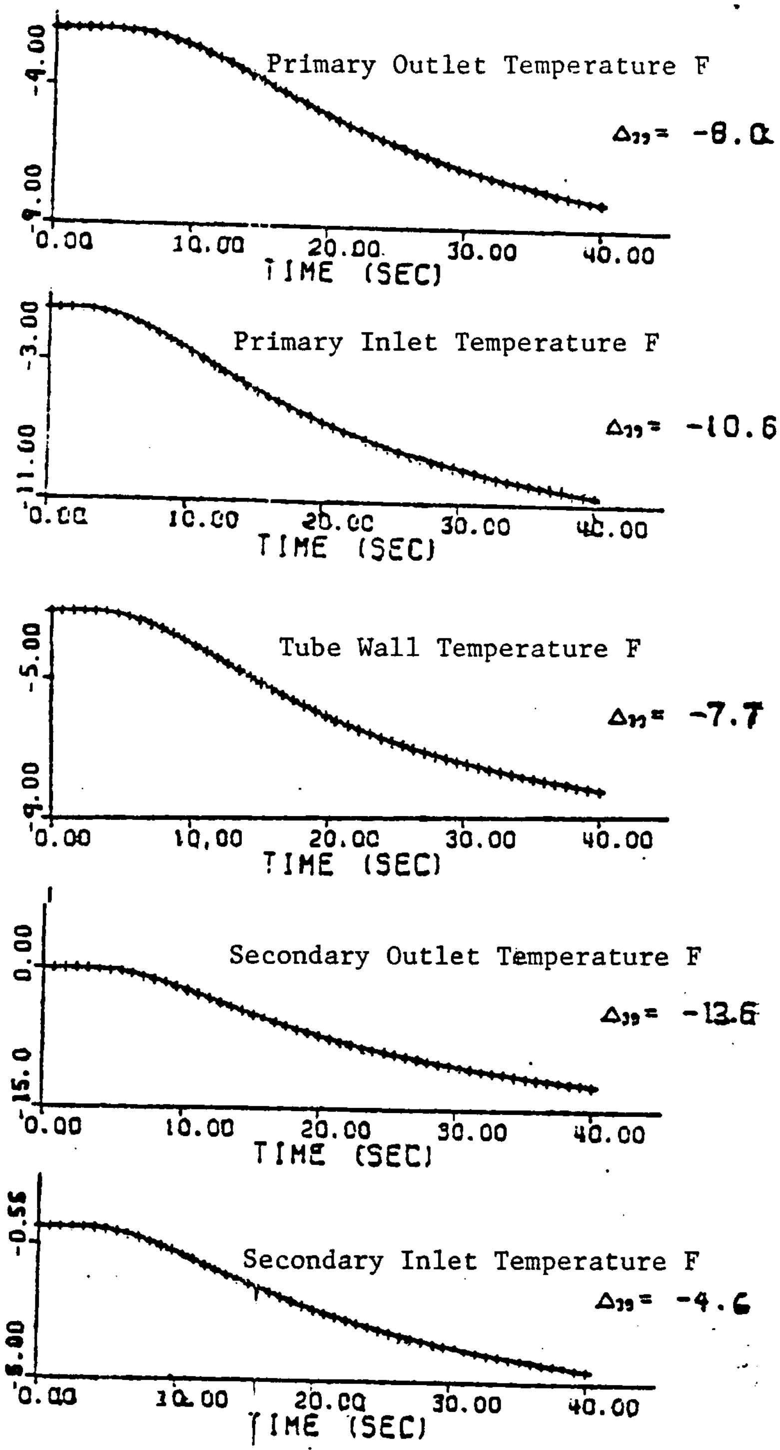

Fig. 5.3 Temperature Responses of the IHX Coolant Lumps to a -5 cent Step Reactivity Perturbation. (Greene's Model)

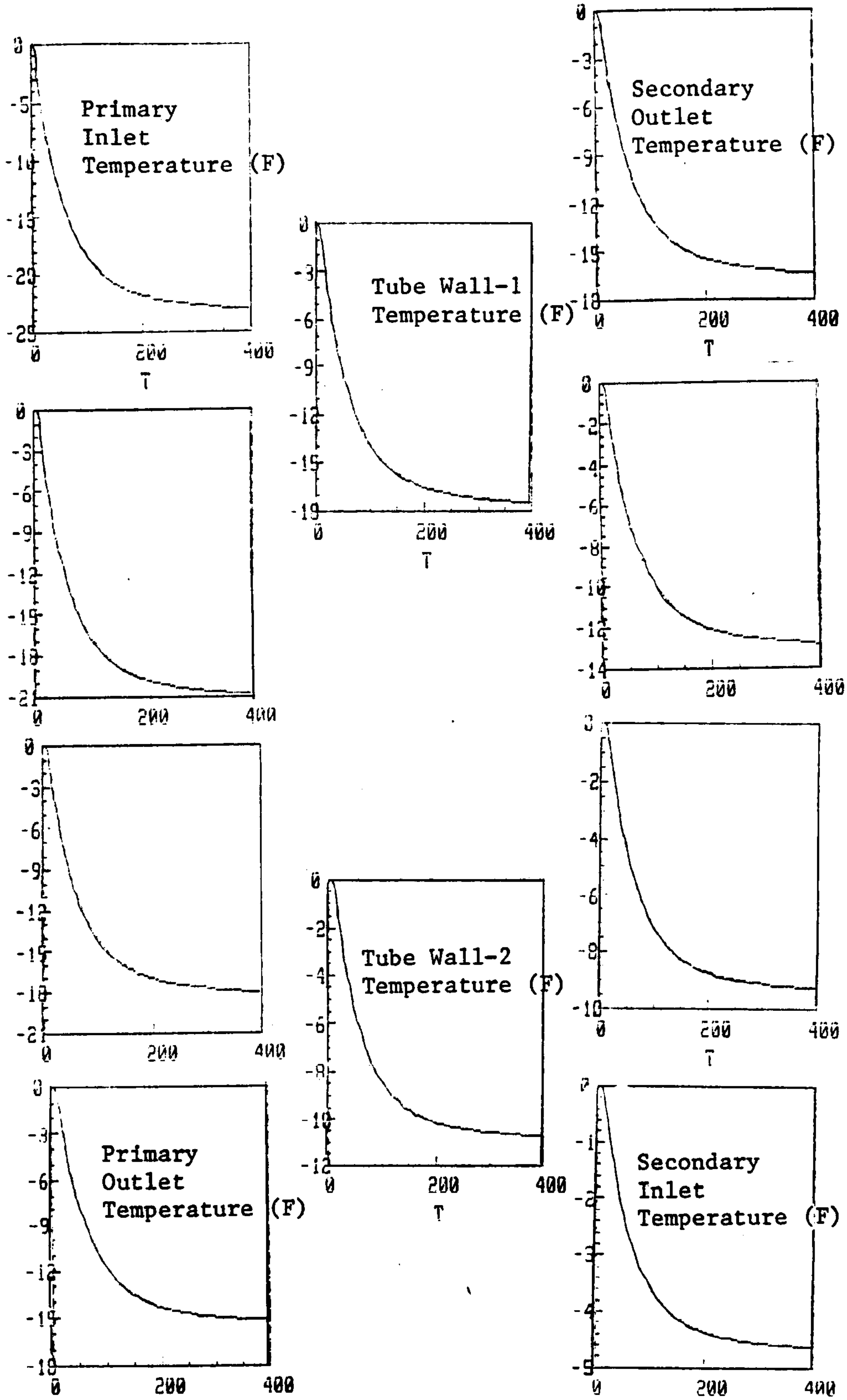

Fig. 5.4 Temperature Responses of the IHX Coolant Lumps to a -5 cent Step Reactivity Perturbation. (Open-loop Primary Model)

liquid sodium flowing upward. Any sudden temperature change in cladding is expected to be reflected in the upper coolant nodes of the corresponding lumps. The liquid sodium carrying the sudden energy increment will flow out of the core and pass through the shell side of the IHX. The excess heat will partially be removed from the primary loop as it passes through the IHX and some remaining amount of heat will return to the sodium tank. Since the dimensions of the sodium tank are large (resulting in large sodium volume), the new steady-state temperature of the sodium in the tank will be established after a long time compared with the sudden temperature change of the upper lumps. Figure 5.5 shows the temperature response of the tank sodium to a sudden flow reduction test [9]. Figure 5.5 indicates that the time constant is quite large. For the step reactivity perturbation of -5 cents, Fig. 5.6 indicates that the temperature response of the tank sodium settles down at about 2500 seconds with a large time constant resembling the time constant obtained in the flow reduction test. This delayed temperature deviation will affect the core and reflector regions as the recycling sodium temperature reaches the tank temperature. The effect of the tank sodium temperature on the reactivity can be seen in Fig. 5.7. The time response of the primary system model is observed to be in three modes: the prompt jump(0-1 sec),

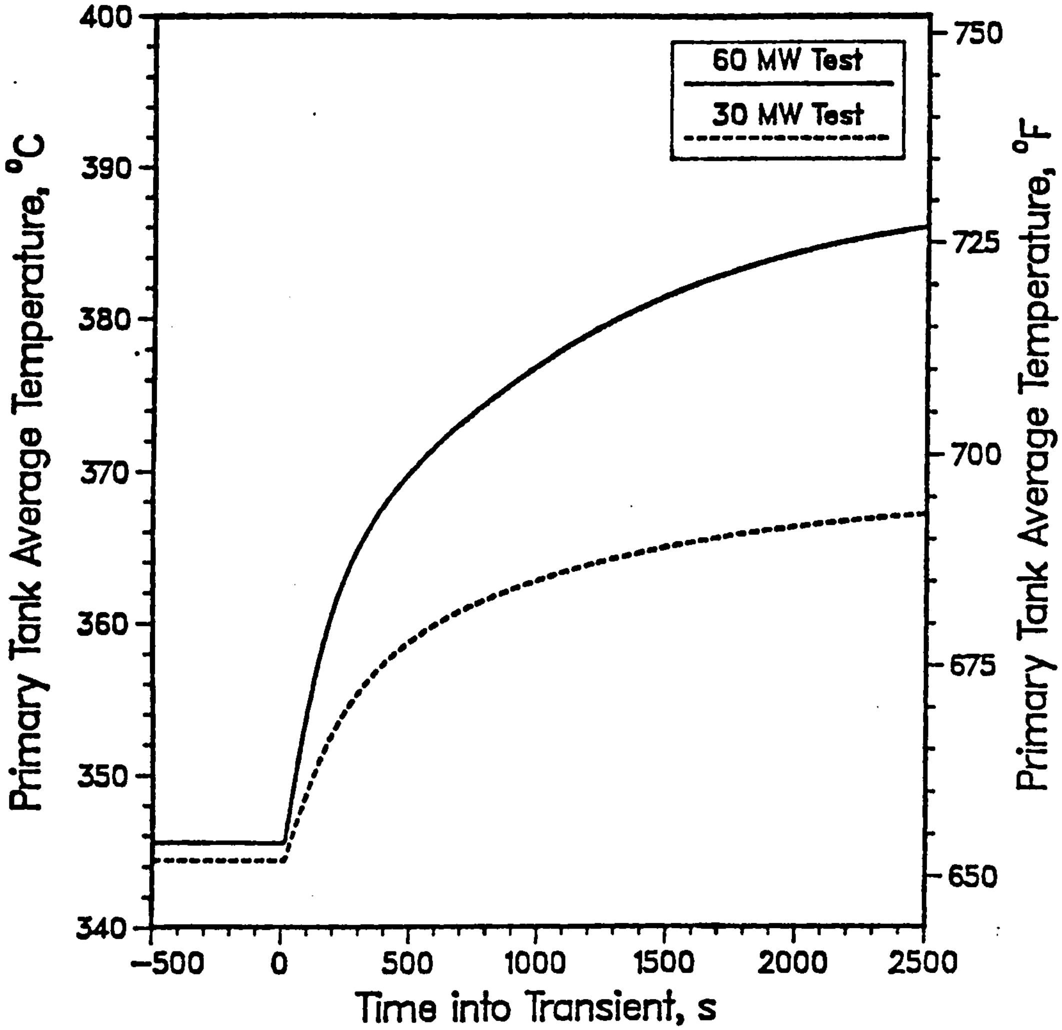

Fig. 5.5 Temperature Response of Tank Sodium to a Sudden Flow Reduction Test [9].

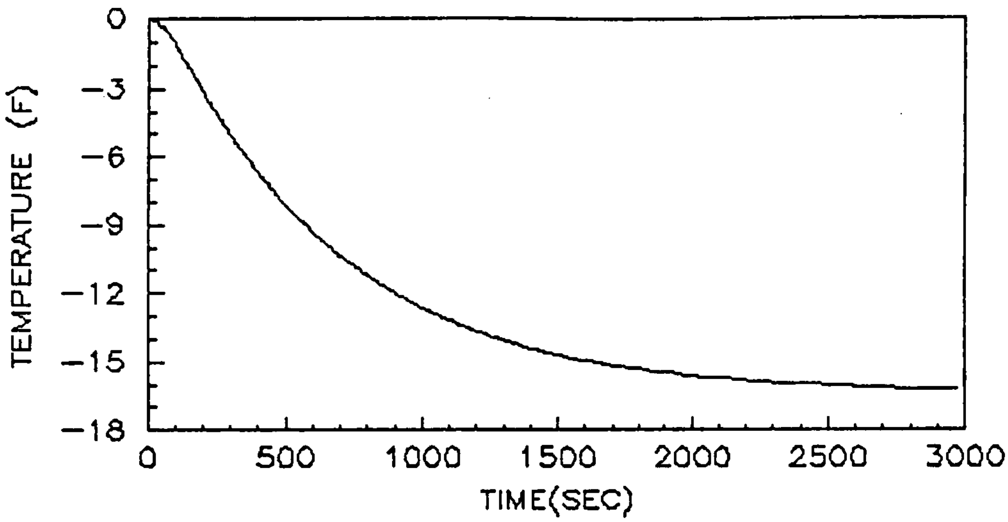

Fig. 5.6 Step response of Tank Sodium Temperature to a -5 cents Reactivity Perturbation (Open-loop Primary Model).

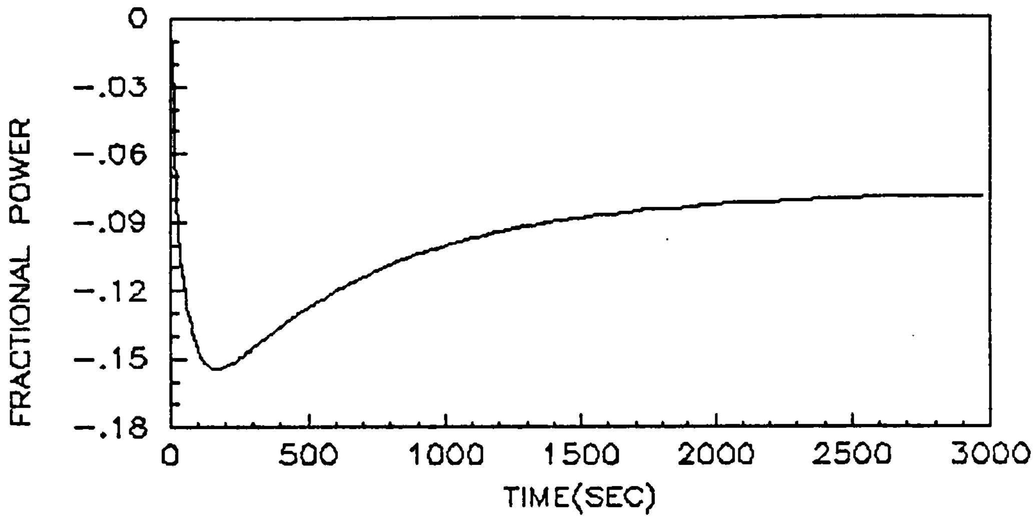

Fig. 5.7 Step Response of Fractional Reactor Power to a -5 cents Reactivity Perturbation (Open-loop Primary Model).

reactivity feedback settlement (1-200 sec) and delayed thermohydraulic effects (200-3000 sec). The temperature responses of the fuel, cladding, core coolant and the reflector wall lumps verify that the overall heat transfer mechanism is represented reasonably by the primary model. A complete set of system responses to a -5 cents step reactivity insertion is listed in Appendix. C.

5.2.2 Sodium Inlet Temperature Perturbation Results.

In order to verify that the ten-lump IHX model provides a good representation of the dynamics when the heat transfer occurs in the opposite direction (from secondary to primary), a secondary sodium loop inlet temperature perturbation is applied. This input will exist when the coupling of primary system model to the steam generator is implemented. A step perturbation of +10 F to the IHX secondary sodium inlet resulted in the system responses shown in Figs. 5.8 through 5.11. Figure 5.12 shows the temperature response of the sodium in the tank to the same input. The fractional power deviation indicates the temperature reactivity feedback effect as shown in Fig.5.13. The core outlet coolant temperature first increases as the hot sodium enters the corresponding region, then starts decreasing because of the small late power decrease caused by the reactivity feedback effect. Note that the time delay is a result of

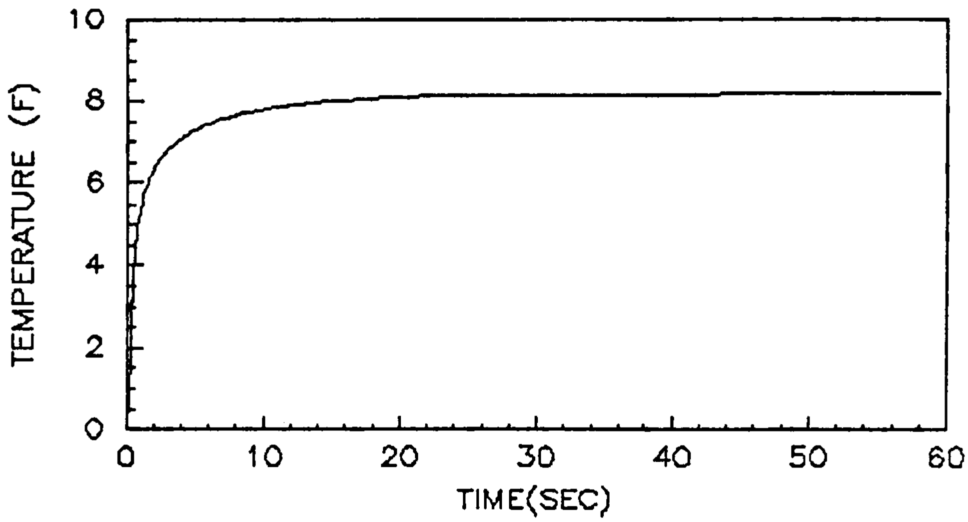

Fig. 5.8 Step Response of IHX Secondary Inlet Temperature to a +10 F IHX Secondary Inlet Temperature Perturbation (Open-loop Primary Model)

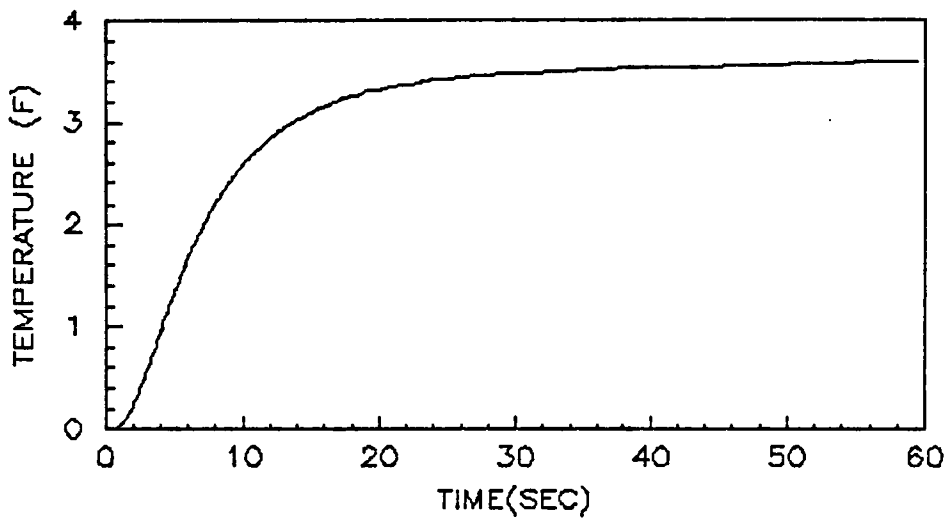

Fig. 5.9 Step Response of IHX Secondary Outlet Temperature to a +10 F IHX Secondary Inlet Temperature Perturbation (Open-loop Primary Model)

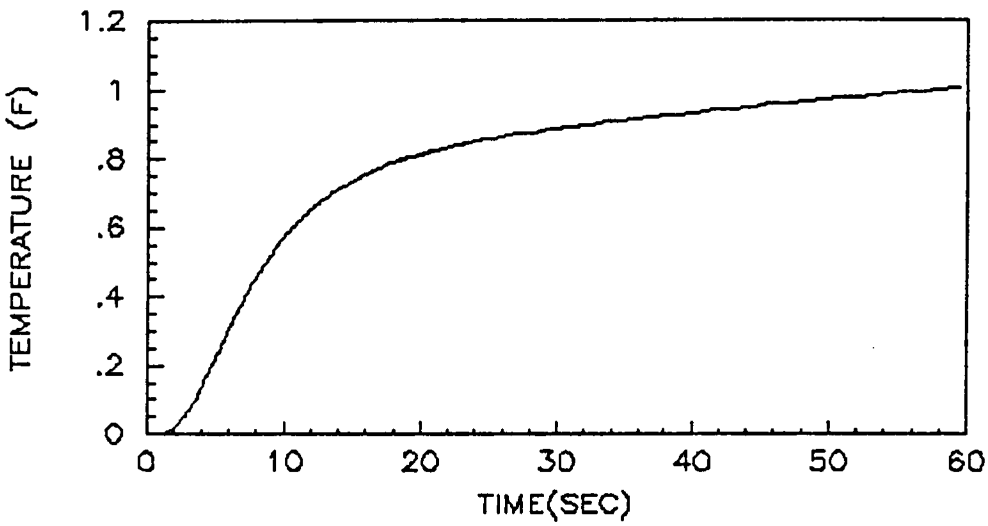

Fig. 5.10 Step Response of IHX Primary Inlet Temperature to a +10 F IHX Secondary Inlet Temperature Perturbation (Open-loop Primary Model).

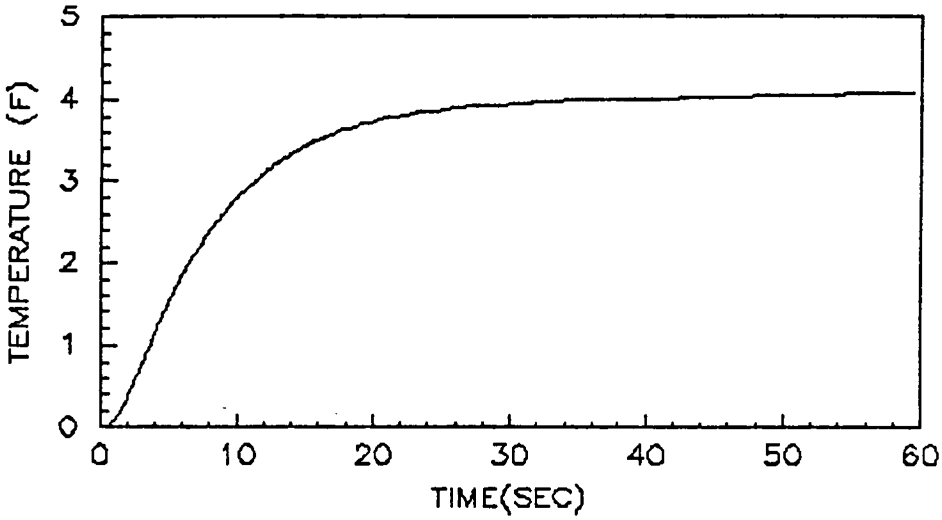

Fig. 5.11 Step Response of IHX Primary Outlet Temperature to a +10 F IHX Secondary Inlet Temperature Perturbation (Open-loop Primary Model).

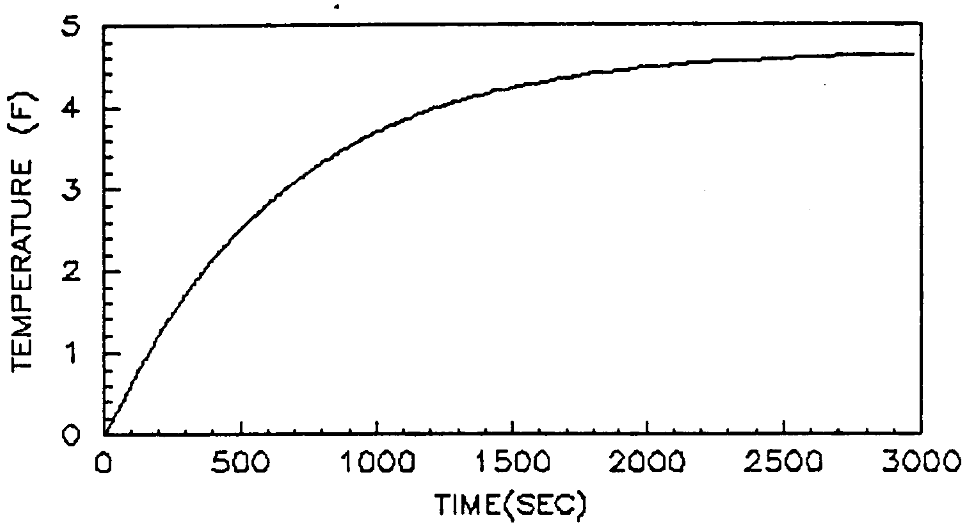

Fig. 5.12 Step Response of Sodium Tank Temperature to a +10 F IHX Secondary Inlet Temperature Perturbation (Open-loop Primary Model).

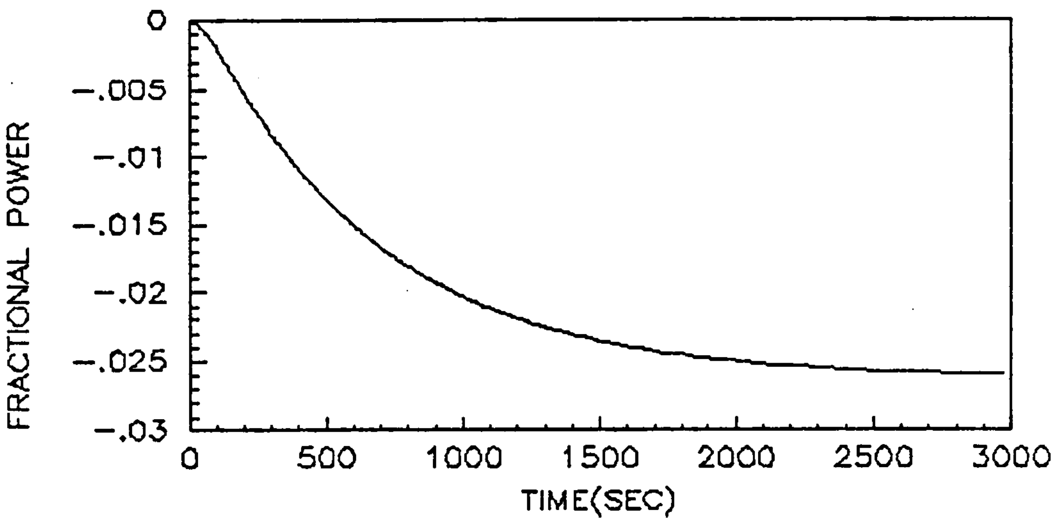

Fig. 5.13 Step Response of Fractional Reactor Power to a +10 F IHX Secondary Inlet Temperature Perturbation (Open-loop Primary Model).

large sodium mass in the tank. Figure 5.14 shows the step response of the core outlet coolant temperature to a +10 F temperature perturbation at the IHX inlet. A set of system responses for this perturbation are shown in Appendix C. Table 5.2 includes a list of numerical values corresponding to the two input vectors of -5 cents reactivity insertion and 10 F IHX secondary inlet sodium temperature perturbation.

5.3 Isolated Steam Generator Dynamic Simulation

EBR-II steam generator open-loop model contains eighteen state variables including the level dynamics. There is no control action on the drum level for open-loop simulations. The drum level is expected to diverge for any kind of disturbance to the system. Four standard step perturbations applied to the model are:

i) +10 F Feedwater temperature

ii) +10 F Inlet sodium temperature

iii) +10 lbm/sec Feedwater flow

iv) +10 % Steam valve opening

The corresponding input vectors are listed in Table 5.2.

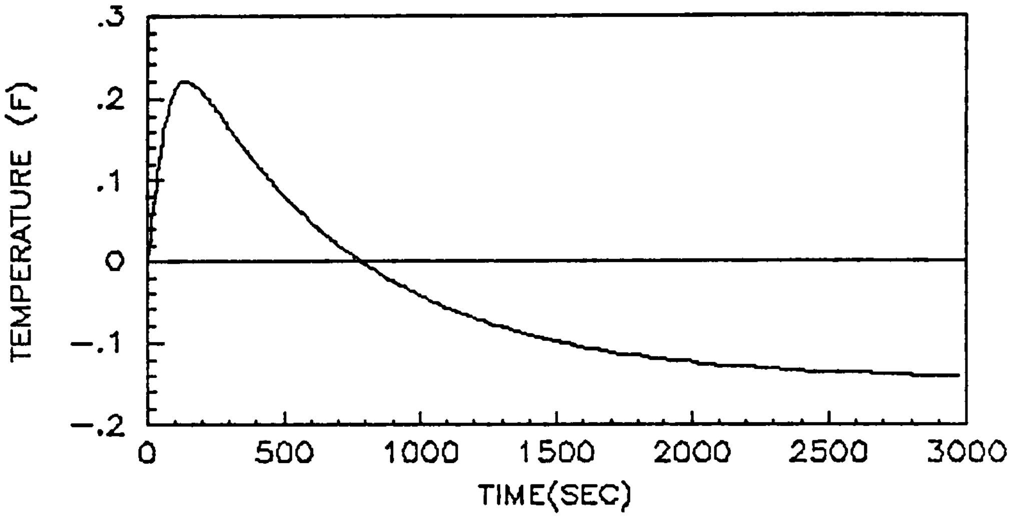

Fig. 5.14 Step Response of Core Outlet Temperature to a +10 F IHX Secondary Inlet Temperature Perturbation (Open-loop Primary Model).

5.3.1 Feedwater Temperature Perturbation Results

In the first case, an increase in the feedwater temperature increases the drum water and the downcomer temperatures as shown in Figs. 5.15 and 5.16, respectively. As the water enters the evaporator, the subcooled water temperature also increases and the bubble formation starts at lower elevations. The reason for the moving boundary to drop in level is the average temperature of the subcooled water which approaches the saturation temperature by the positive heat increment carried in by the entering downcomer water. Figure 5.17 indicates the deviation in the moving boundary. The height of the boiling region gets bigger as the subcooled height lowers; consequently, the amount of energy transfer into the boiling region increases, so does the steam quality (see Fig. 5.18). An increase in the steam quality results in more steam and an increase in the steam pressure as shown in Fig. 5.19. The step responses to a +10 F feedwater temperature are shown in Appendix C.

5.3.2 Sodium Inlet Temperature Perturbation Results

The second case of step perturbation is a 10 F sodium inlet temperature increase at the superheater inlet. The heat increment input is immediately

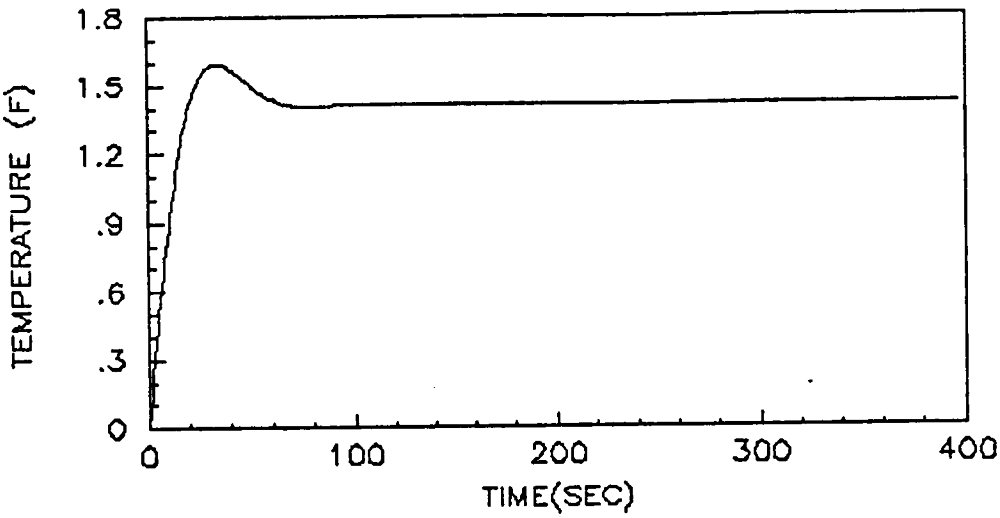

Fig. 5.15 Step Response of Drum Water Temperature to a +10 F Feedwater Temperature Perturbation (Open-loop Steam Generator Model).

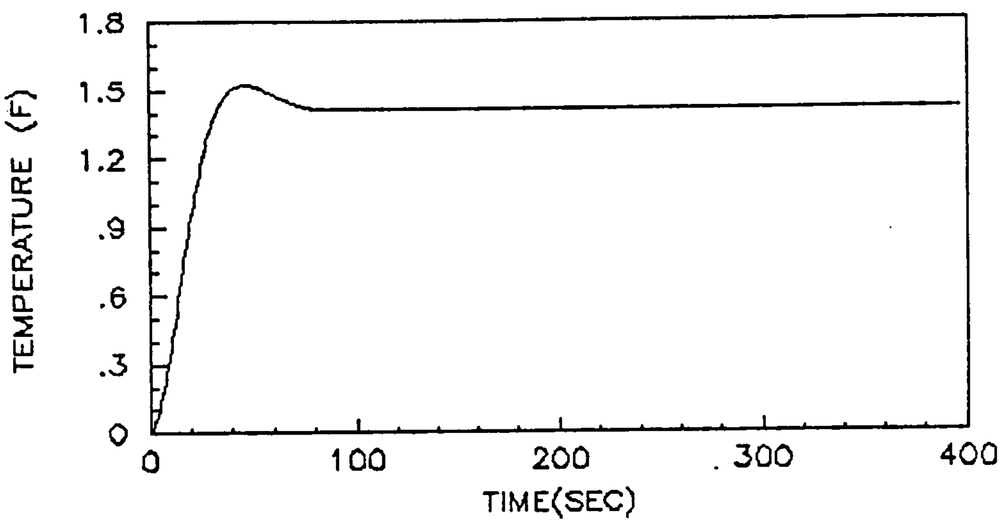

Fig. 5.16 Step Response of Downcomer Temperature to a +10 F Feedwater Temperature Perturbation (Open-loop Steam Generator Model).

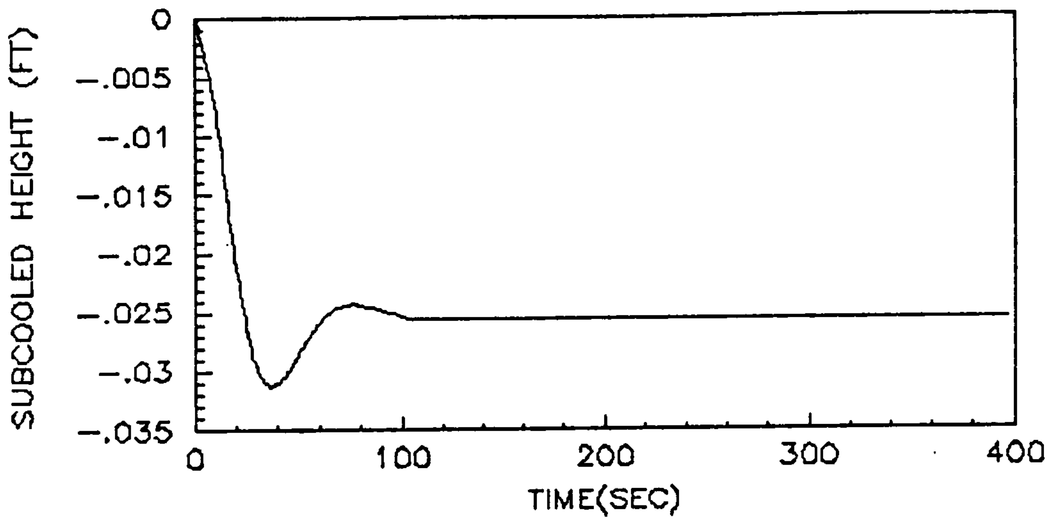

Fig. 5.17 Step Response of Subcooled Height to a + 10 F Feedwater Temperature Perturbation (Open-loop Steam Generator Model).

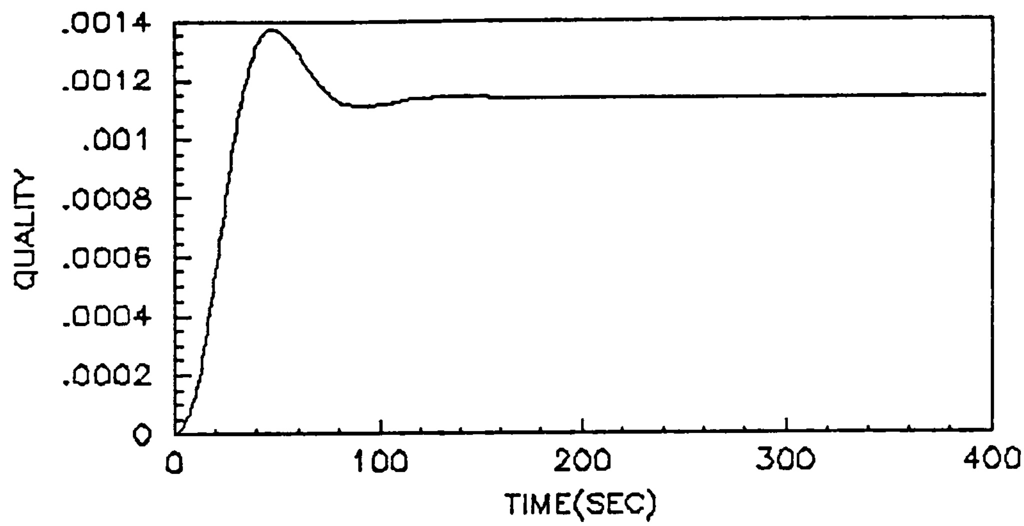

Fig. 5.18 Step Response of Steam Exit Quality to a + 10 F Feedwater Temperature Perturbation (Open-loop Steam Generator Model).

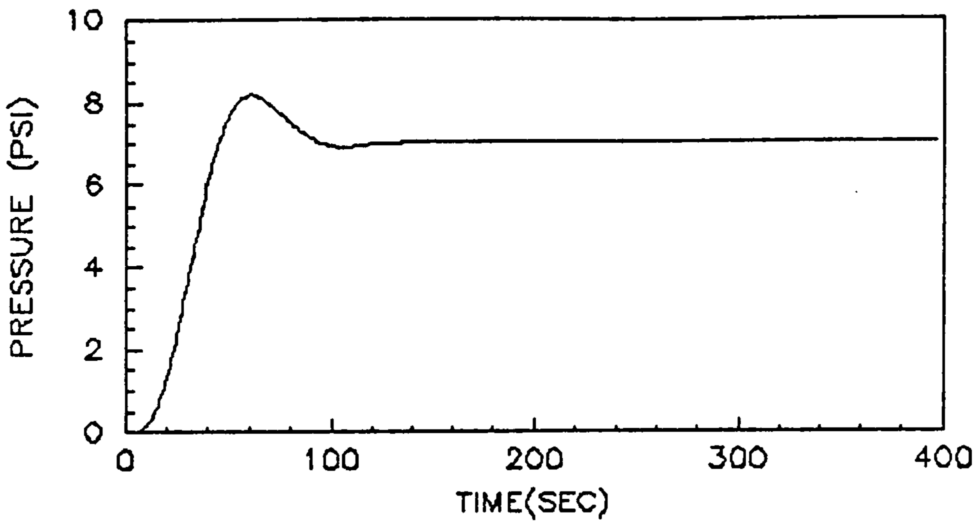

Fig. 5.19 Step Response of Drum Pressure to a +10 F Feedwater Temperature Perturbation (Open-loop Steam Generator Model).

transferred to the secondary side of the superheater as shown in Fig. 5.20. Some remaining portion of the input heat is absorbed by the evaporator which results in increasing the steam production. The steam quality and subcooled height responses are shown in Figs. 5.21 and 5.22 respectively. The evaporator sodium outlet temperature response (Fig. 5.23) indicates the amount of excess heat carried away without absorption by the steam generator. A complete set of step responses for this case is listed in Appendix C.

5.3.3 Feedwater Flow Perturbation results.

A step perturbation of +10 lbm/sec feedwater flow increase was the third input applied to the isolated steam generator model. The feedwater flow increase introduces some accumulation of additional water mass in the drum during the early stages of the transient. The addition of water mass drops the average drum water temperature as shown in Fig. 5.24. It also increases the recirculation flow, namely downcomer and rising mixture flows as shown in Figs. 5.25 and 5.26 respectively. As the secondary water inside the evaporator flows faster, the resident time decreases and the subcooled water retains its single-phase character upto some higher elevation before it reaches the saturation temperature. Figure 5.27 shows the response of the subcooled height to

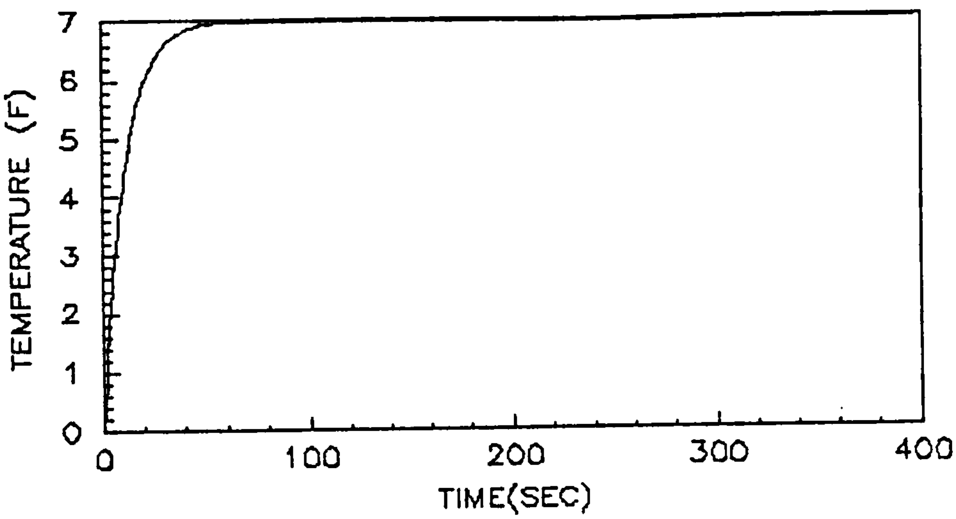

Fig. 5.20 Step Response of Superheated Steam Outlet Temperature to a +10 F Inlet Sodium Temperature Perturbation (Open-loop Steam Generator Model).

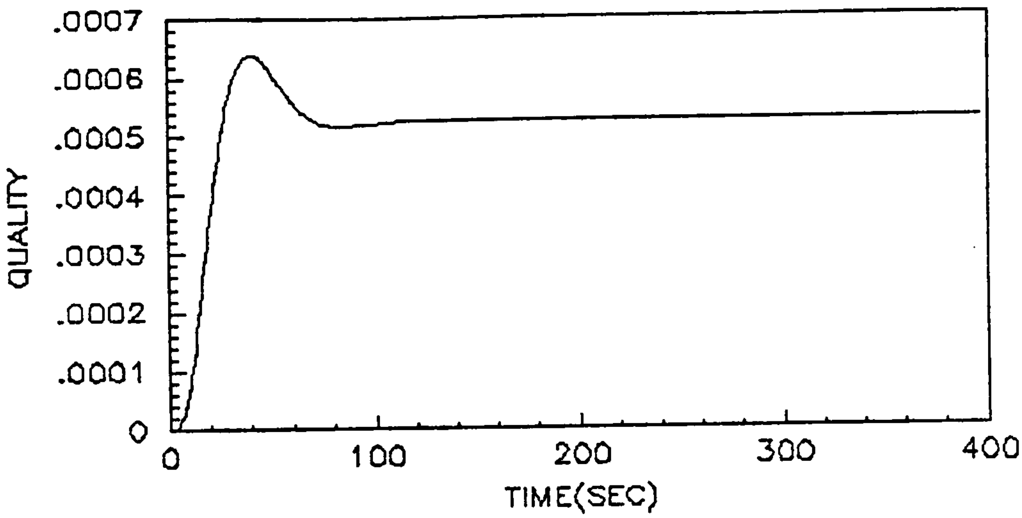

Fig. 5.21 Step Response of Steam Exit Quality to a +10 F Inlet Sodium Temperature Perturbation (Open-loop Steam Generator Model).

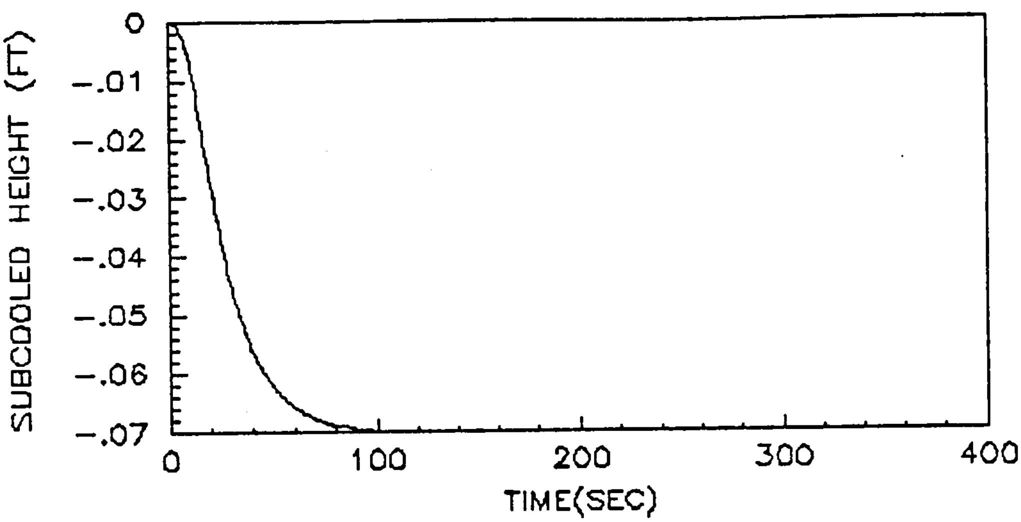

Fig. 5.22 Step Response of Subcooled Height to a +10 F Inlet Sodium Temperature Perturbation (Open-loop Steam Generator Model)

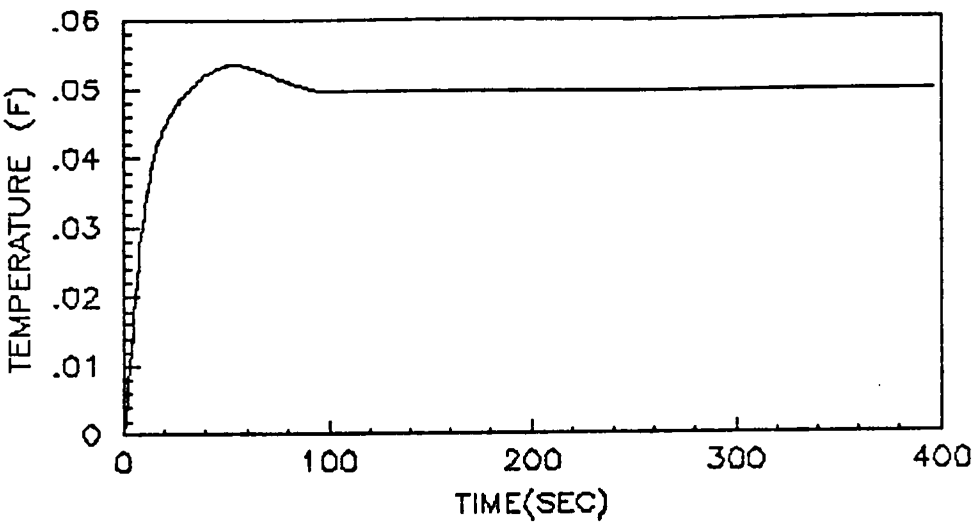

Fig. 5.23 Step Response of Evaporator Sodium Outlet Temperature to a +10 F Inlet Sodium Temperature Perturbation (Open-loop Steam Generator Model).

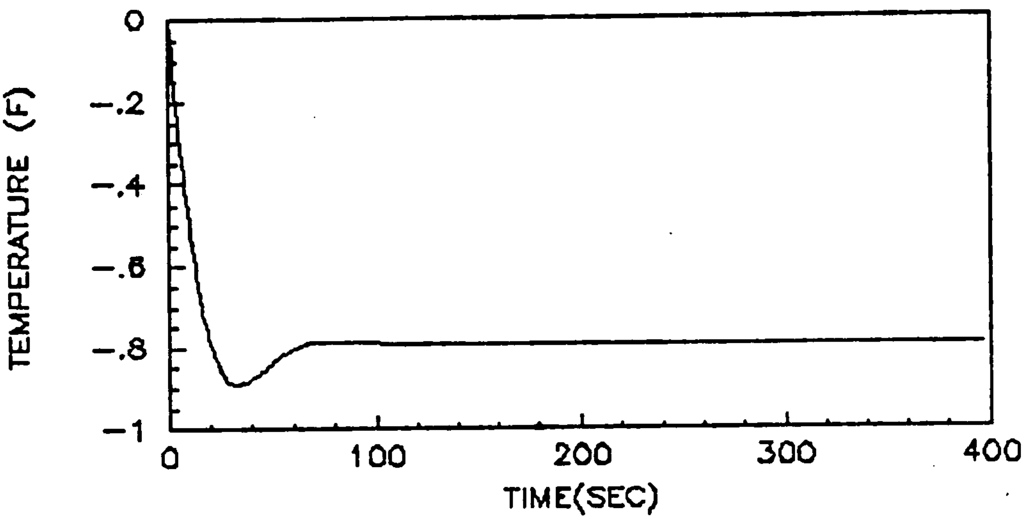

Fig. 5.24 Step Response of Drum Water Temperature to a +10 lbm/sec Feedwater Flow Perturbation (Open-loop Steam Generator Model).

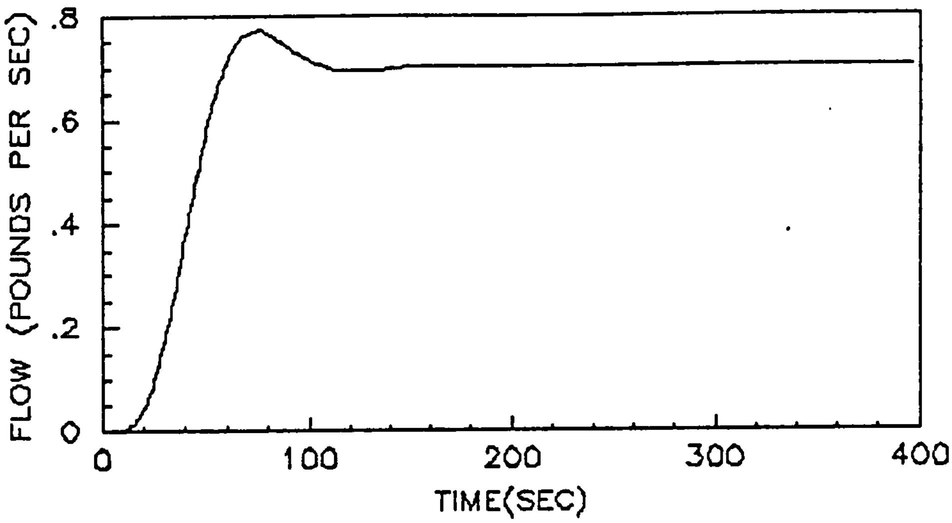

Fig. 5.25 Step Response of Downcomer Flow to a +10 lbm/sec Feedwater Flow Perturbation (Open-loop Steam Generator Model).

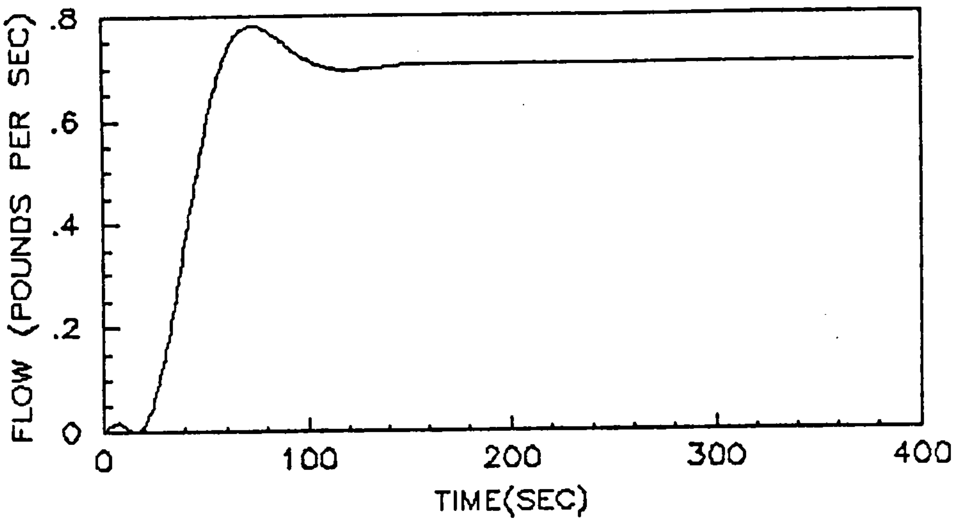

Fig. 5.26 Step Response of Evaporator Flow to a +10 lbm/sec Feedwater Flow Perturbation (Open-loop Steam Generator Model).

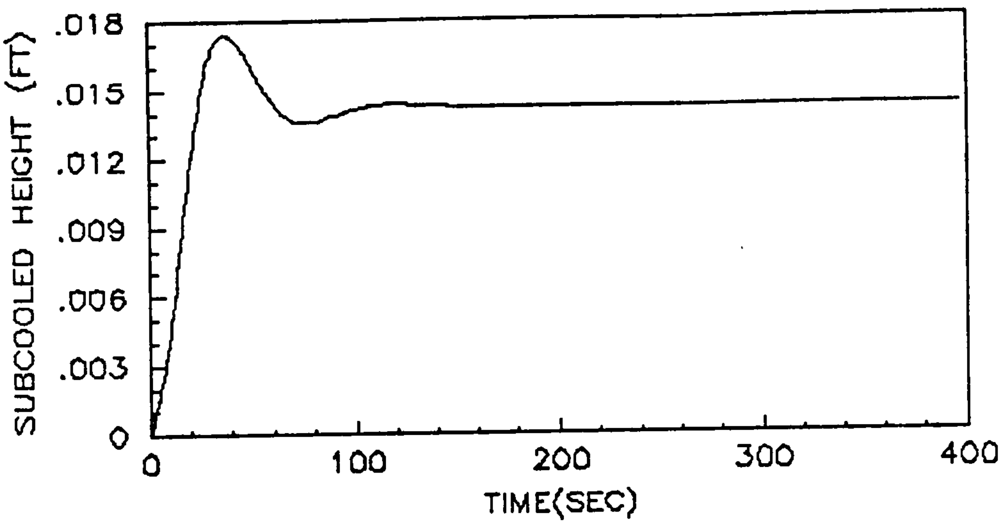

Fig. 5.27 Step Response of Subcooled Height to a +10 lbm/sec Feedwater Flow Perturbation (Open-loop Steam Generator Model).

a +10 lbm/sec feedwater flow perturbation. Accordingly, the height of the boiling section shrinks which results in less steam production and a decrease in steam quality (Fig. 5.28). The resultant steam pressure drop can be seen in Fig. 5.29. A complete set of system responses for the third input case is listed in Appendix C.

5.3.4 Steam Valve Opening Perturbation Results

The last case of +10 % steam valve opening step perturbation was modeled using the critical flow assumption defined in Chap. 4. Mathematically, this perturbation was implemented on the drum steam pressure in our model by assuming a linear relationship between the valve opening and the corresponding pressure drop in the drum. Figure 5.30 shows the steam pressure response to a +10% valve opening perturbation. In the present model, the system was assumed to be driven by the drum pressure and the pressure inside the evaporator tubes. A sudden drop in the drum pressure is followed by a pressure drop inside the evaporator tubes, and is smaller than the pressure perturbation. Consequently, the pressure difference enforces the rising mixture flow upward, increasing the recirculation flow and the downcomer flow. Note that the net pressure difference creates a driving force towards the drum since the drop in the drum pressure is larger. Figures 5.31 and 5.32

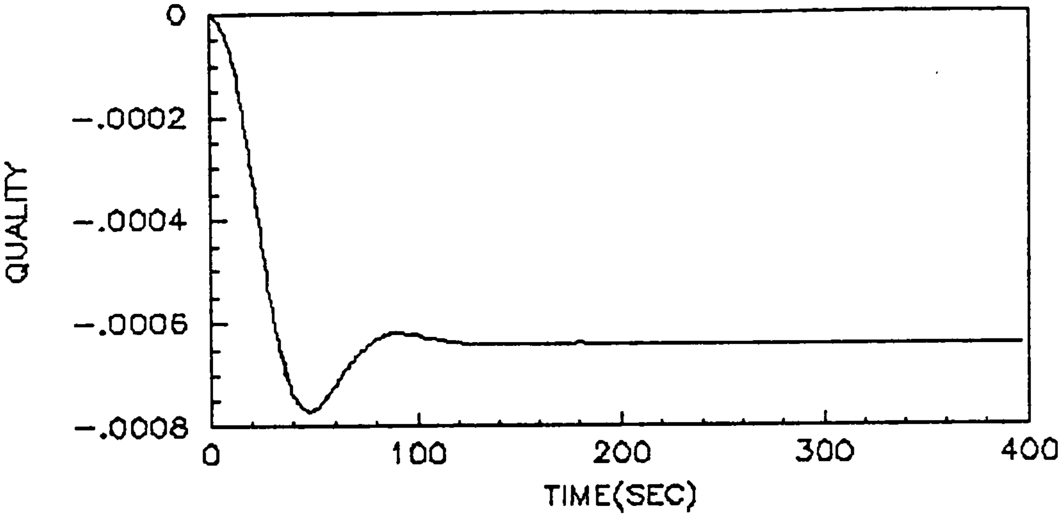

Fig. 5.28 Step Response of Steam Outlet Quality to a +10 F lbm/sec Feedwater Flow Perturbation (Open-loop Steam Generator Model).

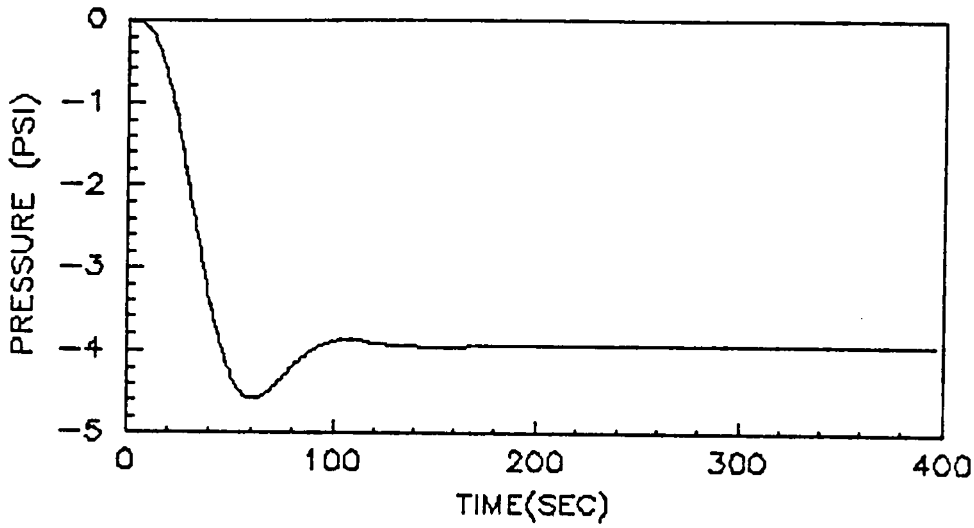

Fig. 5.29 Step Response of Drum Pressure to a +10 lbm/sec Feedwater Flow Perturbation (Open-loop Steam Generator Model).

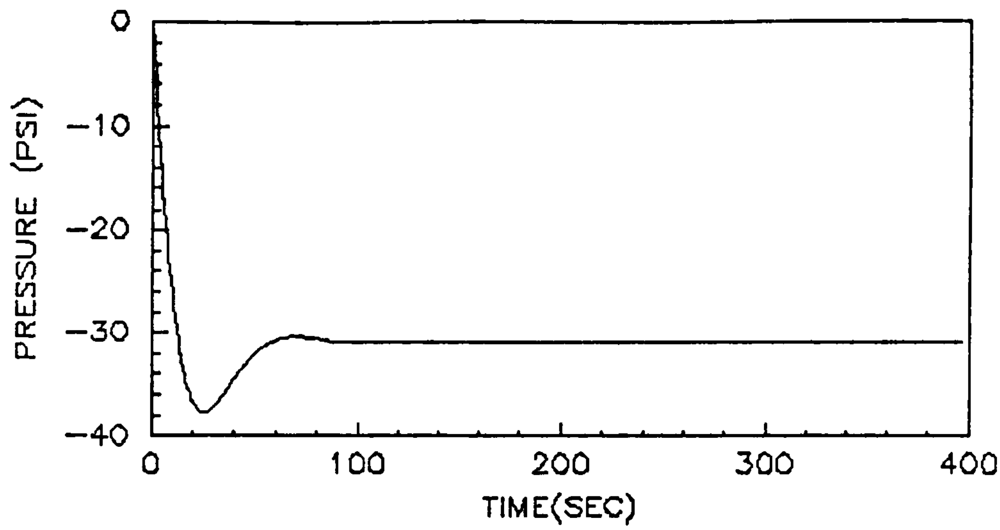

Fig. 5.30 Step Response of Drum Pressure to a +10% Steam Valve Opening Perturbation (Open-loop Steam Generator Model).

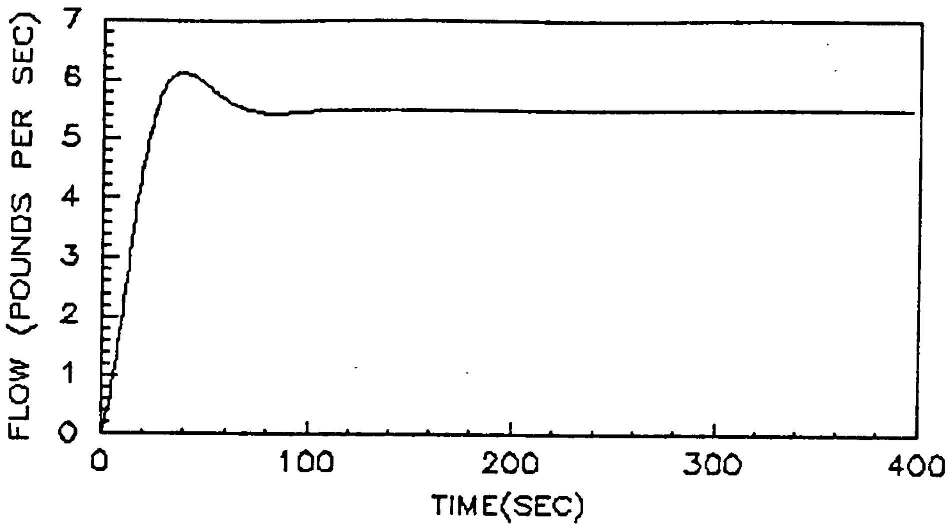

Fig. 5.31 Step Response of Downcomer Flow to a +10% Steam Valve Opening Perturbation (Open-loop Steam Generator Model).

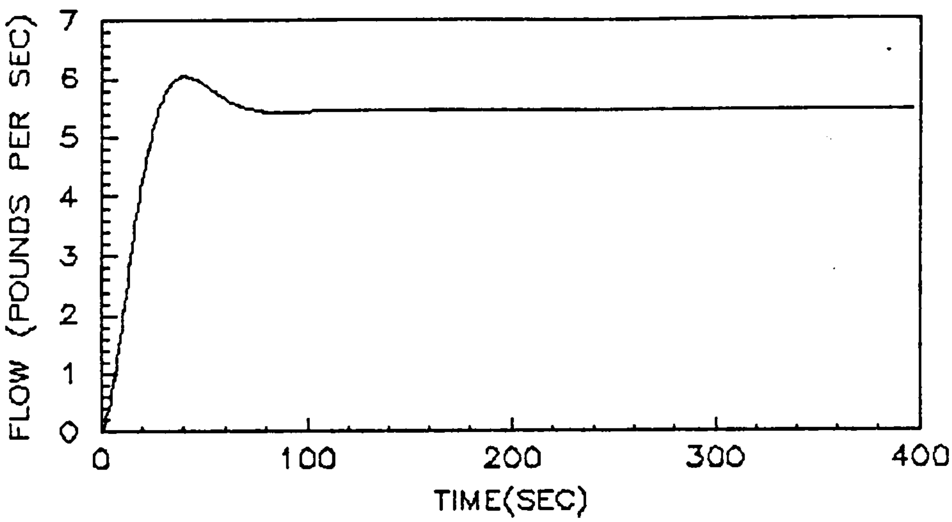

Fig. 5.32 Step Response of Evaporator Flow to a +10% Steam Valve Opening Perturbation (Open-loop Steam Generator Model).

show the downcomer and rising mixture flows respectively. The increment in the flows affects the steam production mechanism in a manner similar to the feedwater flow perturbation case,that is, steam quality decreases, subcooled height increases, etc. However, there appears another mechanism for creating a driving force for the steam production which is dominant and in the reverse direction. It is the change in the saturation conditions inside the evaporator tubes. The pressure drop lowers the required saturation temperature for the bubble formation. The subcooled height, therefore, shrinks and the steam quality tends to increase as shown in Figs. 5.33 and 5.34. A complete set of step responses is given in Appendix C.

5.3.5 Comparison of the Results With the Results of a PWR, U-Tube Steam Generator Model

The EBR-II and PWR steam generators are quite different in size, capacity, structure and range of operation. However, they are steam generating machines working with the same principles of physics. Thus, a comparison between the responses of the EBR-II steam generator model and a previously developed PWR steam generator model is considered to be worthwhile. A linear, U-Tube, recirculating type PWR steam generator model has been developed previously [Ali 6]. The Ali model uses

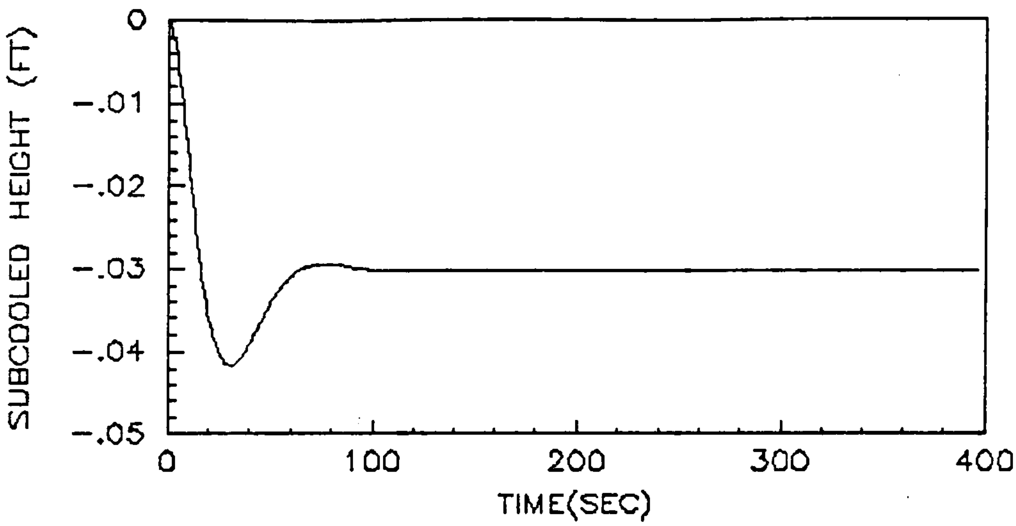

Fig. 5.33 Step Response of Subcooled Height to a +10% Steam Valve Opening Perturbation (Open-loop Steam Generator Model).

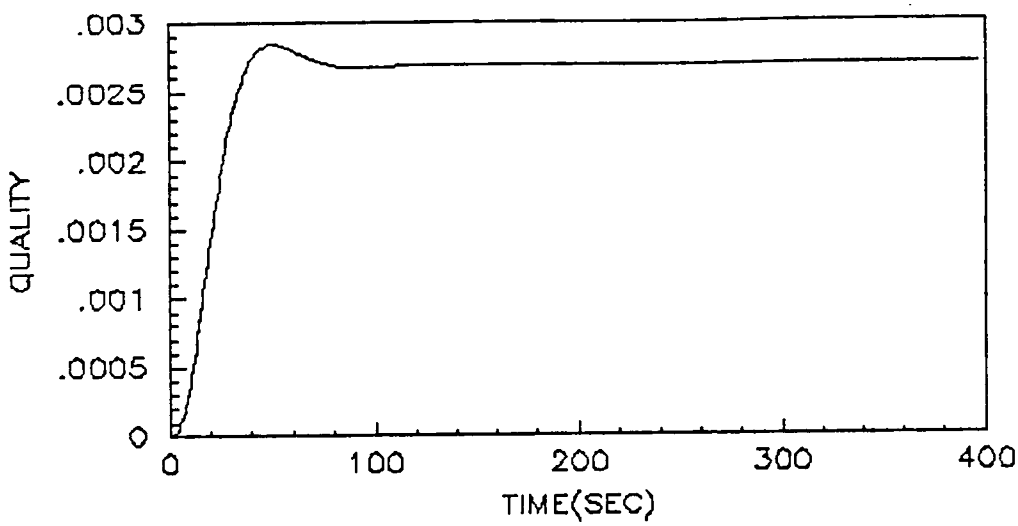

Fig. 5.34 Step Responses of Steam Exit Quality to a +10% Steam Valve Opening Perturbation (Open-loop Steam Generator Model).

typical Westinghouse data and it is validated [4]. Figure 5.35 shows the responses of several state variables to a 10 % step change in steam valve opening using the EBR-II and Ali's PWR steam generator models. Another comparison is shown in Fig. 5.36 for 10 F step change in feedwater temperature. The figures emphasize that the overall dynamic behavior of the EBR-II model is in a physical agreement with Ali's validated PWR U-Tube steam generator model.

5.3.6 Feedwater Controller Performance versus ANL Test Results

One of the important tests performed in the actual EBR-II plant is the large steam pressure reduction test (B402) at 45 MW power level. The drum pressure is reduced around 400 psi instantenously by opening the by-pass valve. During the test, the turbine is kept offline. "The purpose of the B402 test is to demonstrate that a large reduction of steam pressure is not passively safe"[23]. A nonlinear EBR-II model (NATDEMO) developed by ANL [23] includes the primary system, IHX, steam generator and the feedwater heaters. Figure 5.37 shows the drum pressure responses of the actual unit, NATDEMO code, and the linear model developed in this study. The drum level responses are shown in Fig. 5.38. These figures indicate that the linear EBR-II steam generator model including

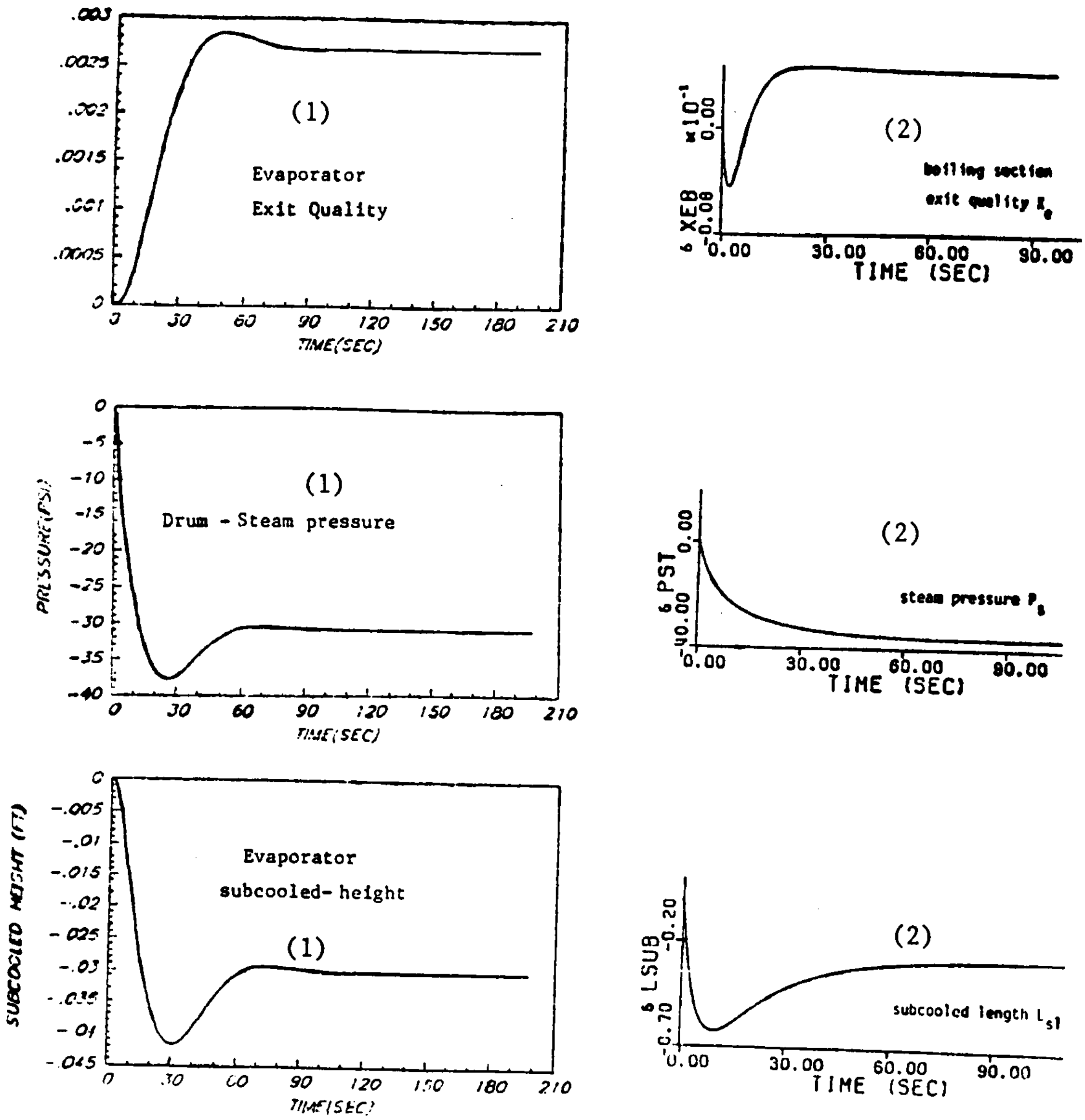

Fig. 5.35 Step Responses to a +10 % Change in Steam Valve Opening. (1) EBR-II Steam Generator Model, (2) PWR, U-Tube Steam Generator Model

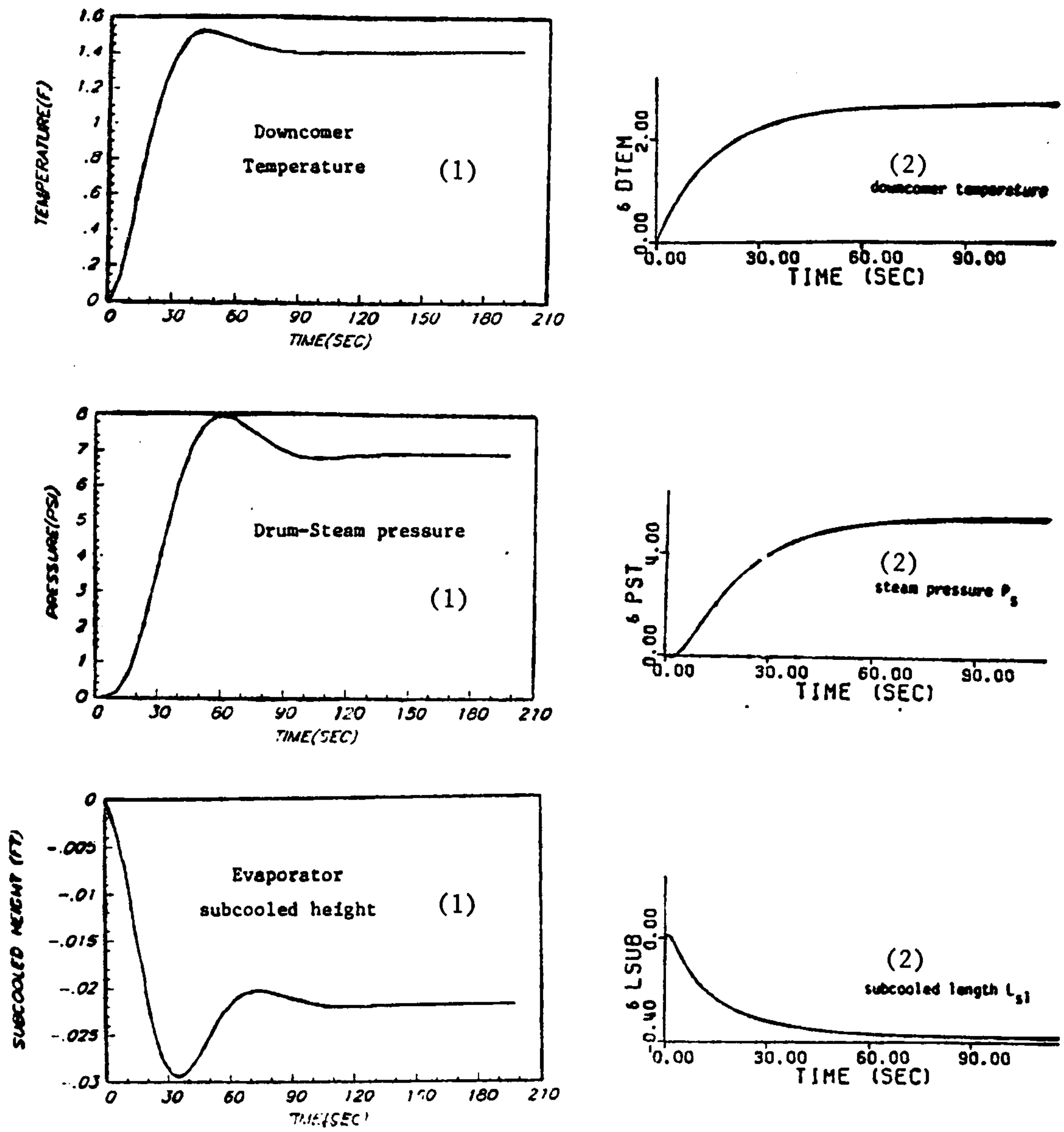

Fig. 5.36 Step Responses to a +10 F Change in Feedwater Temperature. (1) EBR-II Steam Generator Model, (2) PWR, U-Tube Steam Generator Model.

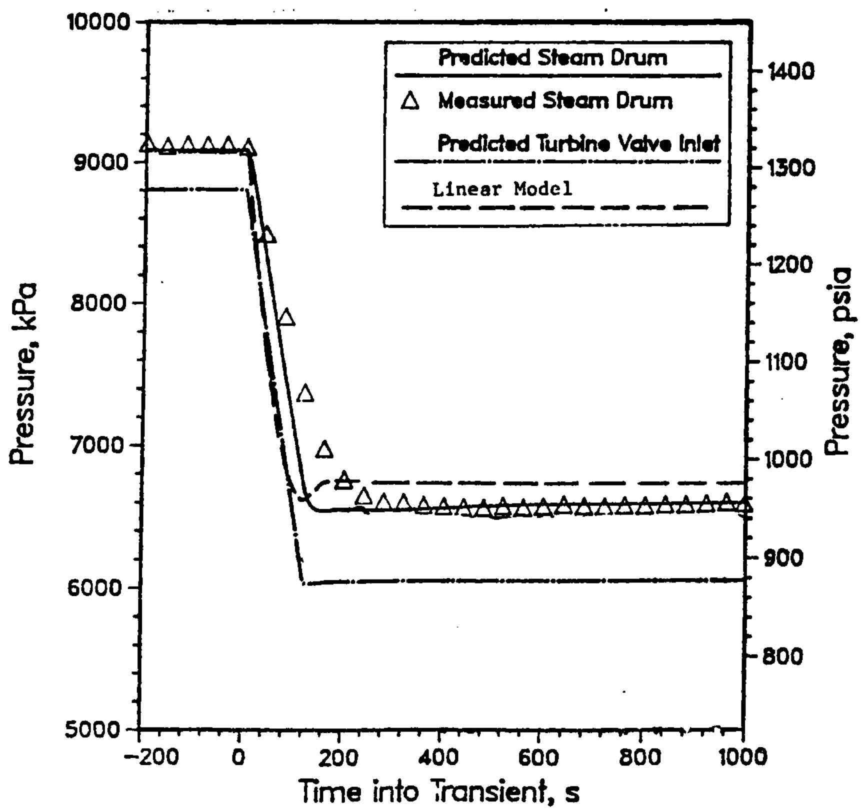

Fig. 5.37 Drum Pressure Response to a Large Steam Reduction Test B402 [ANL 23].

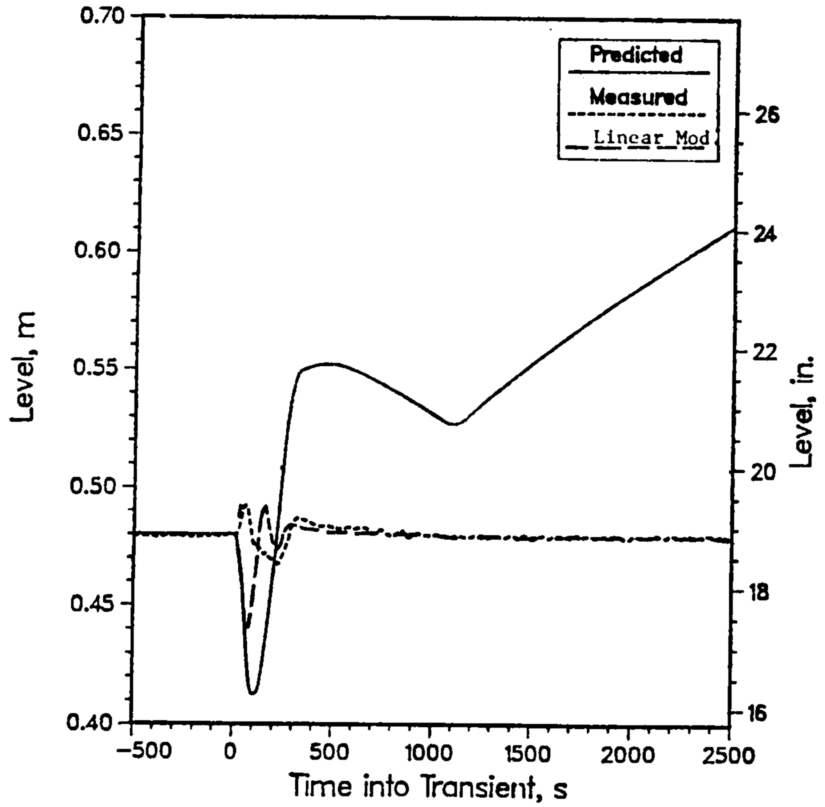

fig. 5.38 Drum Level Response to a Large Steam Reduction Test B402 [ANL 23].

the three-element controller is capable of providing good predictions. The complete validation of the model is a future work.

5.4 Simulation of the Combined System

5.4.1 Combining Subsystem Models

There are several different ways of coupling the primary system and the steam generator models using $\mathbf{MATRIX_x}$. A brief description of the methods for coupling different modules is given in Appendix B. In the present model, the coupling is implemented by creating an overall system matrix including the system matrices of primary system and steam generator models. Using the appropriate coupling terms, an overall system matrix can be formed as follows.

$$A = \begin{bmatrix} A_{pr} & CP_1 \\ CP_2 & A_{sg} \end{bmatrix} \tag{5.4}$$

where

CP_1, CP_2 = coupling matrices,

A_{pr} = system matrix of the primary model,

A_{sg} = system matrix of the steam generator model.

We can see from Fig. 3.1 that the only input to the primary system model is provided by the sodium temperature connection between the IHX secondary inlet node and evaporator outlet node. The coupling matrix CP_1, therefore, includes IHX inlet temperature forcing vector as listed in Table 5.2. Similarly, the coupling matrix CP_2 includes the transpose of the steam generator inlet temperature forcing vector as listed in Table 5.2.

5.4.2. Reactivity Perturbation Results

The application of a -5 cents step reactivity perturbation to the combined model yields similar system responses as in the simulation of the isolated primary model. Figure 5.39 shows the fractional power response to a -5 cents step reactivity insertion. The IHX outlet sodium temperature step response is shown in Fig. 5.40 which is an input to the superheater model. The temperature drop in the secondary sodium caused by the reactivity perturbation results in decreasing the superheated steam temperature as shown in Fig. 5.41. Some amount of temperature drop also appears in the shell side of the evaporators which slows down the steam production rate, that is, less steam quality, higher subcooled height. Consequently, the drum pressure decreases which is a measure of steam mass flow rate leaving the steam

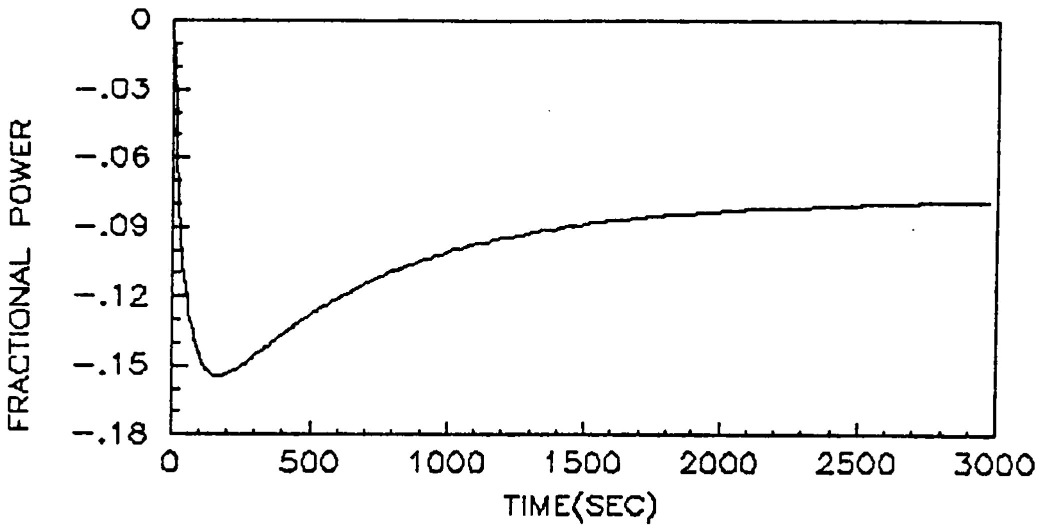

Fig. 5.39 Step Response of Fractional Reactor Power to a -5 cents Reactivity Perturbation (Open-loop Combined Model).

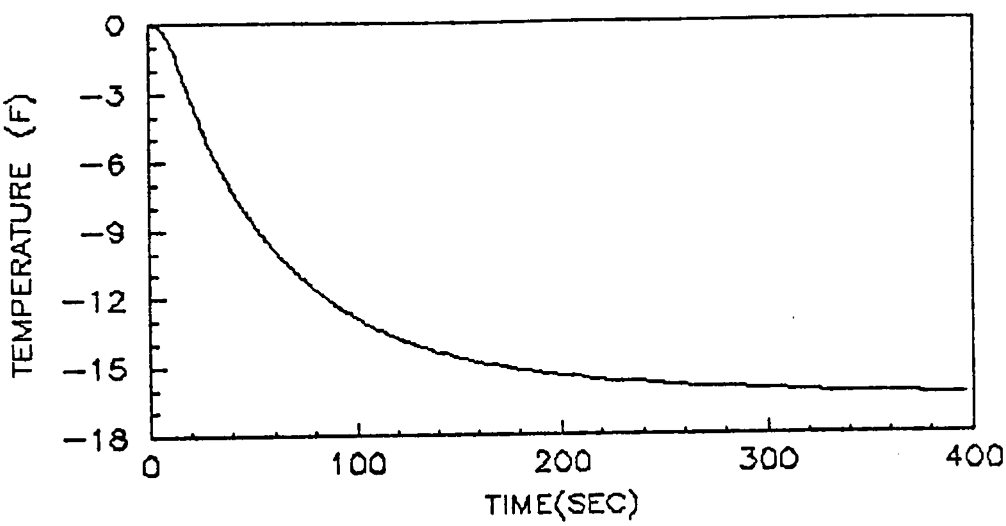

Fig. 5.40 Step Response of IHX outlet Sodium Temperature to a -5 cents Reactivity Perturbation (Open-loop Combined Model).

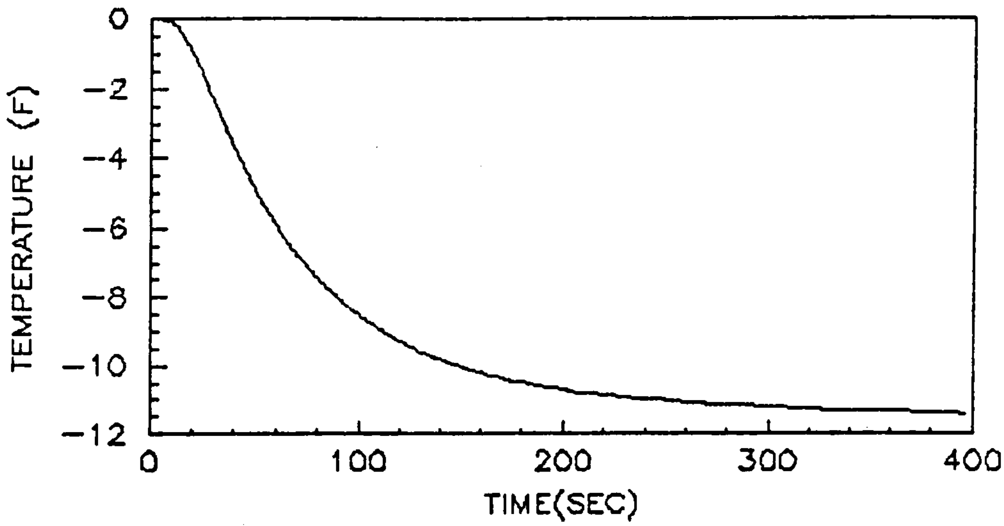

Fig. 5.41 Step Response of Superheated Steam Temperature to a -5 cents Reactivity Perturbation (Open-loop Combined Model).

generator. Figure 5.42 shows the drum pressure response to a -5 cents step reactivity perturbation.

5.4.3 Steam Valve Opening Perturbation Results.

The second input case of +10% steam valve opening step perturbation is applied to the combined system model. The steam drum pressure step response is shown in Fig. 5.43. The drop in the steam pressure affects the rest of the steam generator system in a way similar to the isolated steam generator case explained in Sect. 5.3. The fractional power response to the same perturbation is shown in Fig. 5.44. The combined EBR-II model does not include the feedwater and condenser systems. In the actual plant the superheated steam flow deviation changes the feedwater temperature since the feedwater reheaters utilize some fraction of the superheated steam. A change in the feedwater temperature causes an additional input to the evaporators which affects the secondary sodium temperature flowing through the shell side of the evaporators. This effect is carried to the primary system as the secondary sodium leaves the evaporators and enters the IHX. As a result, the primary system receives an additional heat input in reality and the reactor power is to be affected by means of the temperature reactivity feedback mechanism. The power response obtained by the present linear model, therefore, does not include this

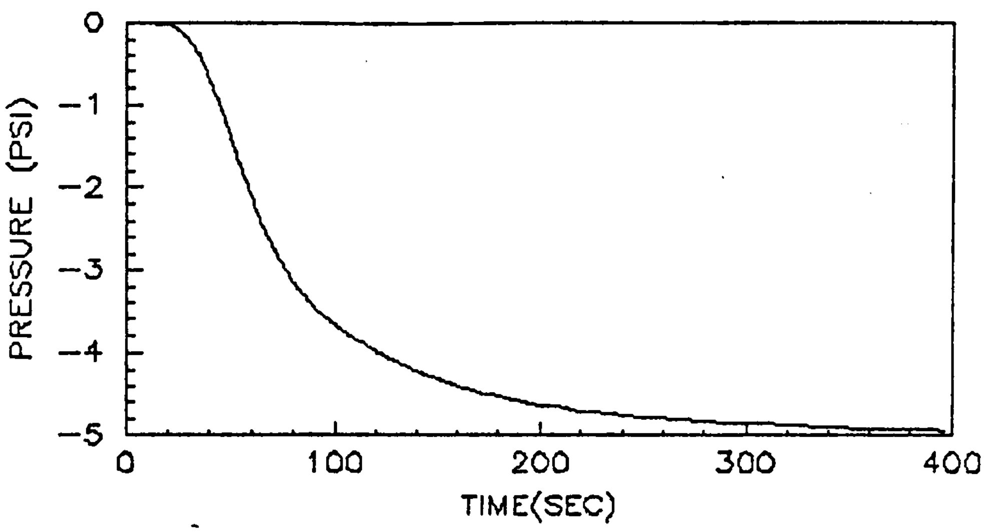

Fig. 5.42 Step Response of Drum Pressure to a -5 cents Reactivity Perturbation (Open-loop Combined Model).

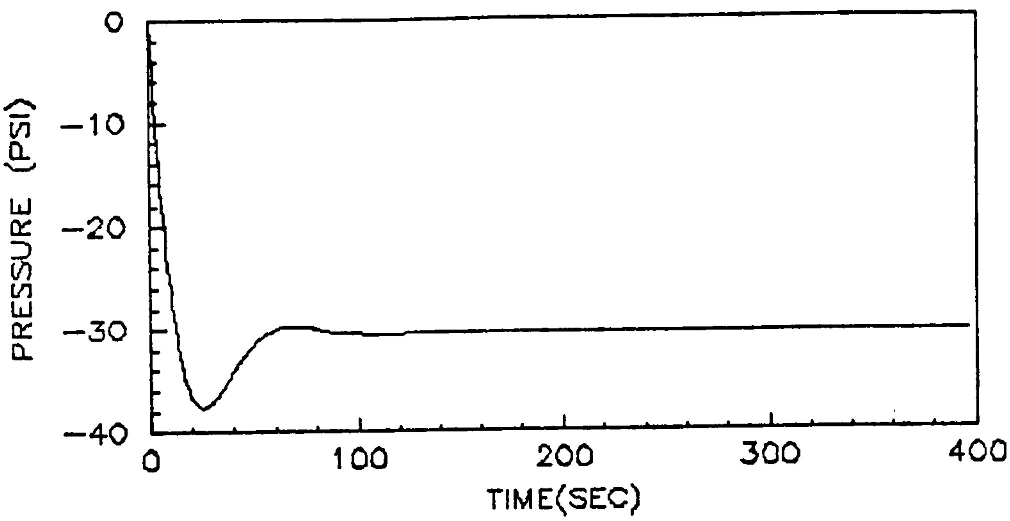

Fig. 5.43 Step Response of Drum Pressure to a +10% Steam Valve Opening Perturbation (Open-loop Combined Model).

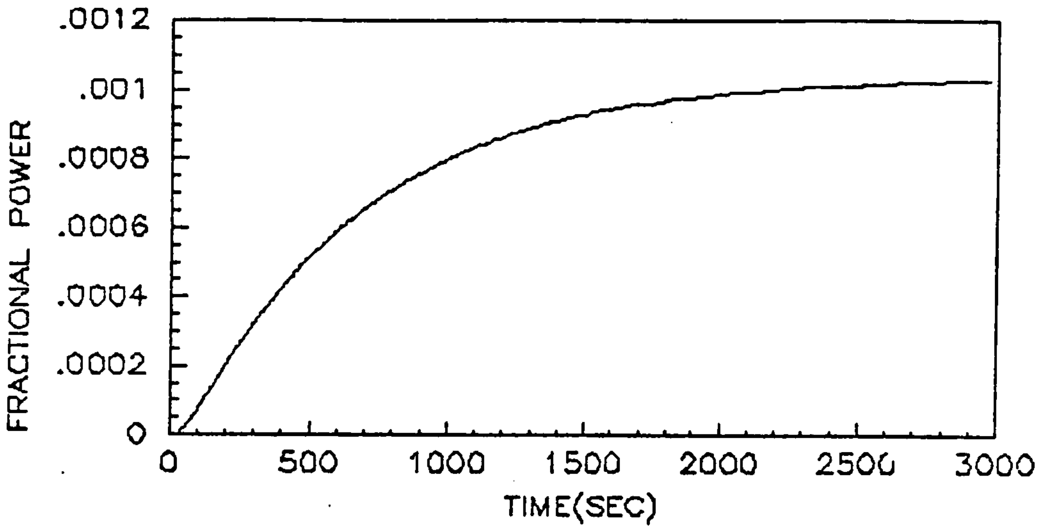

Fig. 5.44 Step Response of Fractional Power Response to a +10% Steam Valve Opening Perturbation (Open-loop Combined Model).

additional effect. A set of system responses to -5 cents reactivity and +10% steam valve opening step perturbations is given in Appendix C.

5.5 Summary

The EBR-II primary system and the steam generator models are tested using several perturbations. A standard rod-drop test of -5 cents step reactivity perturbation is applied to the isolated primary system model (includes reactor, sodium pool and IHX) and the results show reasonable agreement with earlier ANL results. Figure 5.1 shows the fractional power step responses to the same input obtained by the present linear model and from the actual plant data. The model reduction by using an average precursor equation on Greene's model along with the modified IHX formulation provided better simulation results. The results prove the overall inherent stability of the EBR-II system.

The isolated steam generator model responses to four different step perturbations agree with physical reasoning. The open-loop results indicate that the evaporator dynamics is inherently stable whereas the drum water level has to be controlled. Having a separate drum unit improves the safety characteristics of a steam generator such as reducing the effect of loss of feedwater and the shrink and swell effect. The latter phenomenon is also observed in the open-loop system responses to a +10% steam valve opening step perturbation. The overall behavior of the EBR-II steam generator is found to be such that the effect of the boiling region dynamics on the steam drum dynamics is weaker than that of a U-tube type conventional steam generator. Thus a separate drum unit improves the safety aspects. The responses of the linear EBR-II steam generator model and a validated PWR U-Tube type steam generator model are compared. The closeness of the results verifies that the linear EBR-II model provides a valid representation of the dynamics. A large steam reduction test (B402) [23] results with the predictions of the NATDEMO code [23] are compared with the currently developed linear model results. The agreement in the responses are encouraging. A complete set of step responses to +10% steam valve opening, +10 F inlet sodium temperature, +10 F feedwater temperature and +10 Lbm /sec feedwater flow perturbations is given in Appendix C.

The combined EBR-II model responses to a -5 cents step reactivity perturbation resemble the responses obtained using only the primary side model. The steam generator side of the combined model exhibits reasonable responses to the same input. The temperature drop at the reactor outlet which is an input to the superheaters, results in decreasing the temperature of the superheated steam and affects the evaporator side by reducing steam production and thus the drum pressure. A +10% steam-valve opening step perturbation to the steam generator side of the combined model produces a small primary system response due to the fact that the feedwater system model is not included. The overall results represent the steady-state dynamics of the EBR-II plant without the balance-of-plant systems.

TABLE 5.2

Forcing Functions used in the EBR-II Subsystem Model

Simulation Studies

Primary System Model		Steam Generator Model	
Reactivity (cent)	B(1,1) = -475.4	Feedwater Temperature (F)	B(12,1)= 0.009821
IHX Inlet Temperature	B(36,1)= 1.398	Feedwater Flow (lbm/sec)	B(12,1)= -0.0054872 B(18,1)= 0.000262
		Steam Valve Opening (%)	B(10,1)= -0.36
		Inlet Sodium Temperature (F)	B(13,1)= 0.4

CHAPTER 6

CONTROL DESIGN STUDIES

6.1 Introduction

This chapter describes an effort made towards designing controllers using the modern control theory routines. Modern control theory design methods are studied and several design applications are performed using the exsisting EBR-II model by utilizing the capabilities of the CAD package **MATRIX$_X$**. The design effort is mainly concentrated on the linear quadratic optimal control problem and the design performance is discussed. A conventional three-element controller which is a classical proportional-integral (PI) controller was designed for the drum level control problem of the EBR-II steam generator system as explained in Sect. 4.4. The classical approach is compared with the modern methods to study the feasibility and effectiveness of applying modern controllers to future advanced nuclear reactors.

6.2 Modern Control Theory

The development of the modern control theory began in the late nineteen fifties and has been expanding since then as new discoveries were made by control system scientists. The discovery of the state-space approach followed by the theory of Liapunov for stability analysis constituted the basis of the modern control theory. Pontryagin's contribution to the optimization of system performance using the calculus of variation technique was a remarkable achievement in the short history of the modern control theory. Over the last few decades, the modern control theory concepts have been used succesfully in a number of high-technology projects such as the U.S. space missions. Despite the fact that the modern methods can be considered revolutionary, most of the recent control system designs have been made using the classical methods, due to low cost and high performance.

One of the main interests of control engineers is to study the feasibility of using modern controllers in the nuclear industry. Some specific examples of applications of modern control theory to nuclear plants include nuclear reactor start-up, optimal nuclear reactor control, optimum maneuvers for minimum xenon buildup and fuel management issues [12].

Engineering applications of modern control strategies involve on-line computer usage as in the dynamic process control and extensive off-line usage for design purposes. Improving the capabilities of modern controllers is, therefore, dependent on the software development and building fast computers with larger memory. One of the latest CAD software development, known as **MATRIX$_x$**, provides a few modern control design routines as well as several traditional classical design tools [15].

In modern control theory, it is possible to design a compensator for any process by placing the closed-loop poles in the appropriate locations provided that the process is observable and controllable. An appropriate choice of the closed-loop poles yields satisfactory performance in general. The question of seeking an optimal solution to the design problem may seem to be a redundant effort; however, the neccessity of the optimization is important for the following reasons. In a multiple-input multiple-output (MIMO) system, the pole placement method may not completely specify the controller parameters. Fortunately attaining the desired closed-loop pole locations can be done in many different ways for MIMO systems. An n-th order system with m inputs has n x m parameters to be designed for a nondynamic compensator in a full-state feedback arrangement. This means finding the same n desired closed-loop poles in m different ways. The abundance of the adjustable parameters can be a great benefit in terms of satisfying several design requirements if an optimization technique is used. When an unfamiliar process is considered, an arbitrary choice of the closed-loop pole locations being far from the origin may require control inputs too big to be generated by the process actuators. Thus, minimization of the control input can be achieved by optimizing the performance. Another reason for the use of optimal control theory arises when uncontrollable systems are concerned. It is possible to design a control system using optimal control theory so that the overall system behavior will be acceptable, provided the uncontrollable part of the system is stable [13].

6.3 Linear Quadratic Gaussian (LQG) Optimal Control Problem

The LQG compensator design problem includes designing an optimal regulator in conjuction with an optimal observer design. The regulator problem is concerned with the design of a control policy U(t) to take a system from a nonzero state to the zero state where the zero-state is the steady state of the perturbated linear system. Consider the linear system described by a set of matrix differential equation as previously stated by Eqs. (5.3) and (5.4).

$$\dot{\underline{X}}(t) = A\,\underline{X}(t) + B\,\underline{u}$$

$$\underline{Y}(t) = C\,\underline{X}(t)$$

Define the regulator performance index

$$J[\underline{x}(t_o),\underline{u},t_o] = \int_{to}^{T} [\underline{u}^T R \underline{u} + \underline{x}^T Q \underline{x}]\, dt \qquad (6.1)$$

where

R = input weighting matrix.

Q = state weighting matrix.

The problem is to find an optimal control $u^*(t)$, $t_0<t<T$, such that J is minimized. The solution to the problem (6.1) is given by

$$\underline{u}^*\,(t) = -\,K_R\,\underline{X}(t) = -\,R^{-1}B^T\,P\,\underline{X}(t) \qquad (6.2)$$

where K_R is the regulator gain vector which includes the solution P to the matrix Riccati equation [17].

$$-\dot{P}(t) = P(t)\,A + A^T P(t) - P(t)\,B\,R^{-1}B^T P(t) + Q \qquad (6.3)$$

Equation (6.1) represents a quadratic criterion with matrices Q and R weighting appropriate state and input variables. The diagonal elements of matrix Q reflect the importance of the state variable whose steady-state error is to be minimized. It is important to note that the minimization of J does not necessarily guarantee that the error will be exactly zero. But it is always possible to attain a desired error.

The Riccati equation (6.3) is a condition obtained as a result of minimizing J and the representation of the optimal input as a linear function of the state variables (or their estimates). Very often the steady-state solution of P(t) is obtained from

$$P\,A + A^T P - P\,B\,R^{-1} B^T\,P + Q = 0 \tag{6.4}$$

The closed-loop system is given by

$$\dot{\underline{X}} = (\,A - B\,K_R\,)\,\underline{X} \tag{6.5}$$

which is asymptotically stable. The minimum cost function is given by

$$J^*(\,\underline{X}(t_0), t_0) = \underline{X}^T(t_0)\;P\;\underline{X}(t_0) \tag{6.6}$$

The compound structure of an output feedback control system can be constructed by including the state estimation features in the regulator problem. The control law can be written as

$$\underline{u} = - K_R \hat{\underline{X}}(t) \tag{6.7}$$

where $\underline{X}(t)$ is the estimate of $\underline{X}(t)$. The solution to $\underline{X}(t)$ is obtained by solving the equation

$$\dot{\hat{\underline{X}}}(t) = A \hat{\underline{X}}(t) + B \underline{u}(t) + K_E [Y(t) - C \hat{\underline{X}}(t)] \tag{6.8}$$

$$= A \hat{\underline{X}}(t) - B K_R \hat{\underline{X}}(t) + K_E [C \underline{X}(t) - C \hat{\underline{X}}(t)]$$

$$\dot{\underline{X}}(t) = [A - B K_R - K_E C] \hat{\underline{X}}(t) + K_E \underline{Y} \tag{6.9}$$

$$\underline{u}^*(t) = - K_R \hat{\underline{X}}(t) \tag{6.10}$$

where K_E is the estimator gain matrix. The design of K_E includes an optimization with respect to the process noise and observation noise, and is known as the Kalman filter design. The resulting 2n x 2n system is formed in the following manner.

$$\begin{bmatrix} \dot{\underline{X}} \\ \dot{\hat{\underline{X}}} \end{bmatrix} = \left[\begin{array}{c|c} A & -B\,K_R \\ \hline K_E\,C & A - K_E\,C - B\,K_R \end{array}\right] \begin{bmatrix} \underline{X} \\ \hat{\underline{X}} \end{bmatrix} \quad (6.11)$$

The system (6.11) represents the plant and appended output feedback compensator as shown in Fig. 6.1.

6.4 Optimal Compensator Design for EBR-II Subsystem Models

As discussed in the previous section, an optimum regulator design is to choose appropriate weights for the states and for the control input in Eq.(6.1). The relationship between the Q,R, matrices and the dynamic behavior of the closed-loop system dependent on the matrices A, B and C are quite complicated. "It is impractical to predict the effect on closed-loop behavior of a given pair of weighting matrices" [13]. The approach used in this study is to solve for the gain matrices that result from a range of weighting matrices, and simulate the corresponding closed-loop responses. The gain matrix K that produces the response closest to meeting design objectives is considered as the best choice. Despite the fact that the design proceedure is in a trial-and-error

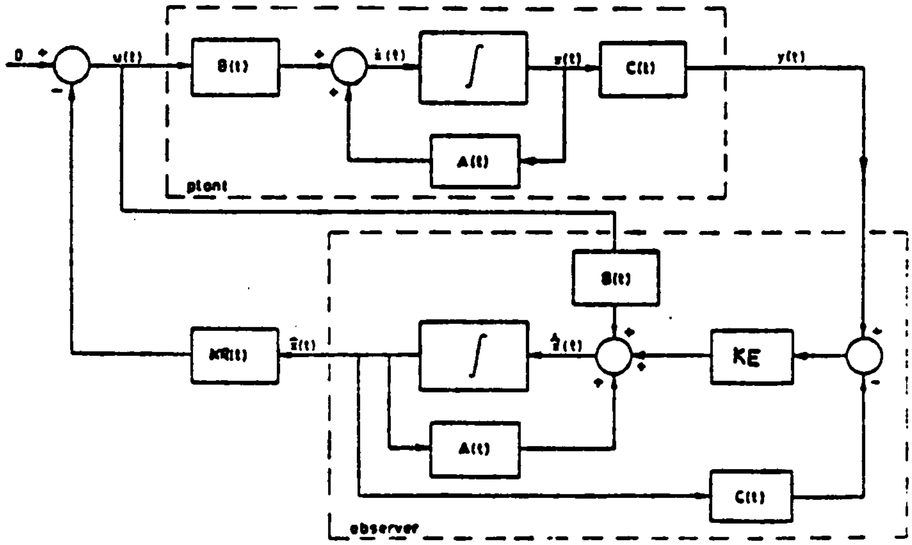

Fig. 6.1 Output Feedback Compensator.

fashion, the following background knowledge has been used as a guide.

"The weighting matrix Q specifies the importance of the various components of the state vector relative to each other. If a state variable changes unreasonably then that state has to be suppressed by increasing the corresponding weighting. However, the choice of the input weighting matrix R can not be established easily. The main idea is the following. With a desire to avoid saturation and its consequences, the control signal weighting matrix is selected large enough to avoid saturation of the control signal under normal operational conditions. As the control weights tend to infinity, the gains are such that the closed-loop poles tend to open-loop poles when the latter are stable, or to their "mirror images" when they are unstable. In a single input system the zeros of the system are defined by $C^T(sI-A)=0$. If there are r such zeros, then as the weights go to infinity r of the closed-loop poles approach these zeros and the remaining k-r closed-loop poles radiate outward to infinity in a configuration of a Butterwoth polynomial of order k-r "[13].

6.4.1 Optimal Compensator Design for EBR-II Primary System

The first modern controller design is considered for the EBR-II primary system model. The design objective is to regulate the system behavior in an allowable range, that is, not exceeding the safety limit of 2 F per minute in reactor ΔT [2]. The design uses a single control rod as the actuator. In order to avoid saturation of the actuator, the control input is designed not to exceed 0.01$/sec reactivity limit (for single speed gear train). It is assumed that all the measurements are available without any noise. The design of an optimal output feedback compensator reduces to an optimal regulator design since there is no need for an observer under the perfect measurement assumption. The state weights in the quadratic cost function are chosen to be equal to 1 for the first state (reactor power) and the remaining states are excluded (weighted zero). The input weighting is scalar and is equal to 0.0007. The compensator design is performed using the design routines in **MATRIX$_X$**. The closed-loop system responses to a -5 cent reactivity insertion show a drastic improvement over the open-loop system behavior. The fractional power response to a -5 cent reactivity step perturbation is shown in Fig. 6.2 which also includes the open-loop step response to the same input. The temperature step response of the fuel material to the same input is shown in Fig. 6.3. Figure 6.4 shows the reactor inlet and outlet temperature responses of the open-loop primary system model. Similar comparison is made for the closed-loop system model as shown in Fig. 6.5. The temperature difference between reactor outlet and inlet is changing faster than 2 F per minute for the open-loop system as shown in Fig 6.4. The closed-loop system responses shown in Fig 6.5 indicate that the variation in reactor ΔT does not exceed the allowable range which is in complete agreement with the EBR-II design specification. It can also be seen from the figures that the closed-loop responses are quite fast and the steady-state errors are very small compared to the open-loop case. Figure 6.6 shows the control input generated by the optimal control strategy. The safety limitation of 0.01$/sec is not violated and the control performance is achieved using approximately 50 % of the maximum rod speed. The nonzero steady state errors in the responses are caused by the type-0 structure of the closed-loop system [14]. One approach to drive the error to zero is to convert the type-0 system to a type-1 system by the addition of an extra state variable which represents the integration of the error corresponding to the variable of interest. In this case integration of reactor power variation.

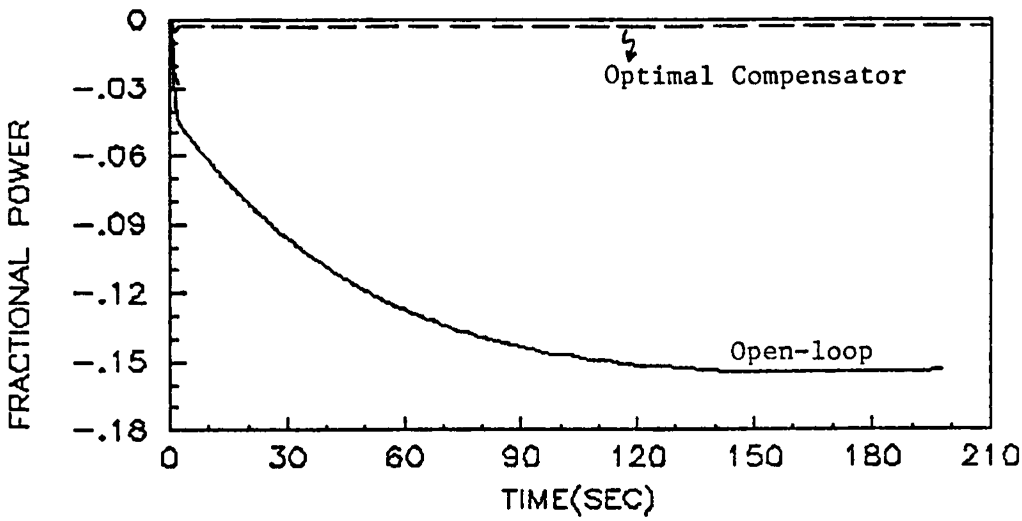

Fig. 6.2 Step Response of Fractional Reactor Power to a -5 cents Reactivity Perturbation. (Optimal Compensator and Open-loop Models).

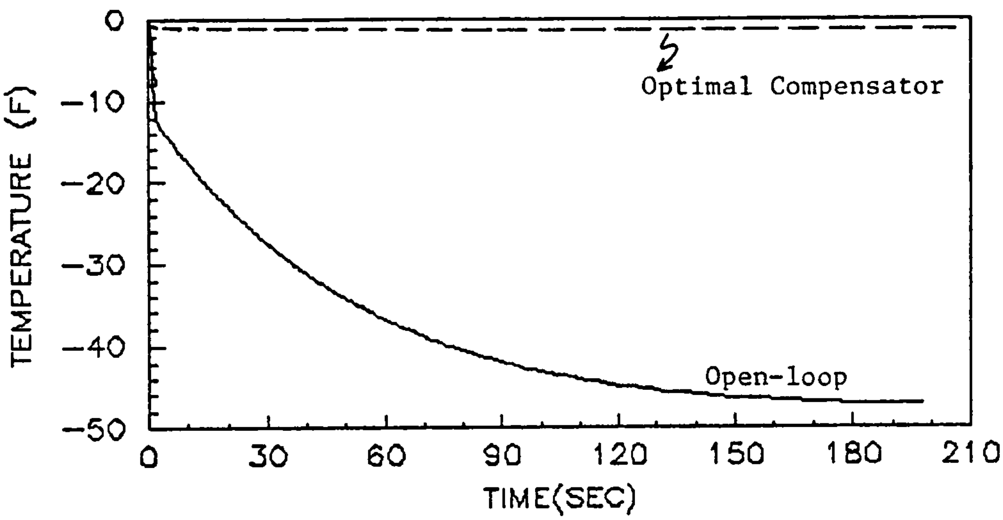

Fig. 6.3 Step Response of Fuel Temperature to a -5 cents Reactivity Perturbation (Optimal Compensator and Open-loop Models).

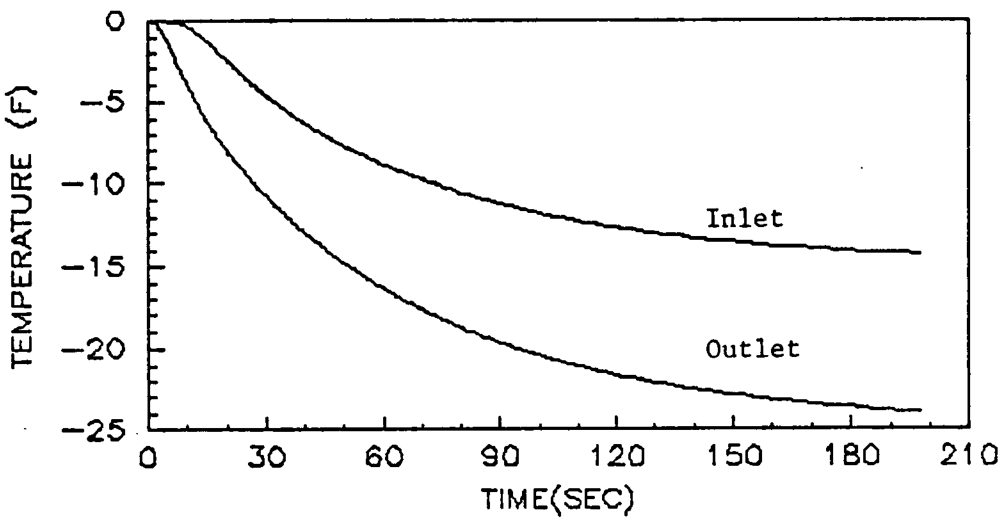

Fig. 6.4 Step Response of Reactor Inlet and Outlet Temperatures to a -5 cents Reactivity Insertion (Open-loop Model).

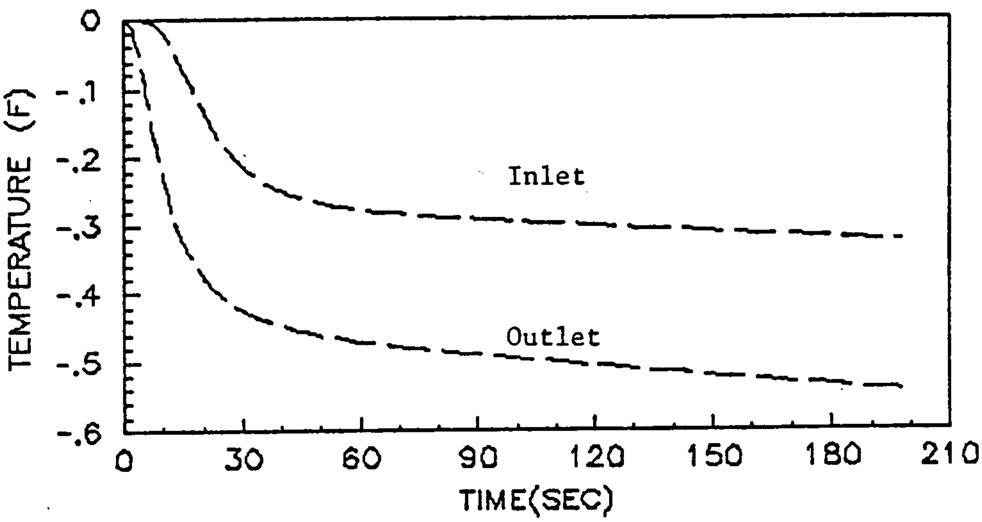

Fig. 6.5 Step Response of Reactor Inlet and Outlet Temperatures to a -5 cents Reactivity Insertion (Closed-loop Model, optimal compensator).

6.4.2 Optimal Compensator Design for EBR-II Steam Generator

The optimal regulator design for the EBR-II steam generator subsystem is performed with a similar philosophy as in the primary system. The design objective is to maintain the drum level deviation in an allowable range, that is, 4 inches above or below the steady-state level [2]. The closed-loop model includes an additional state variable (20th state variable) in the form of an integrator. Since the optimal control theory does not guarantee zero steady-state errors, the addition of an external integrator is one of the possible solutions to the nonzero steady-state error problem. The 18th and the 20th states of the model are weighted to be equal to 10, while the rest of the states are excluded (weights are zero). The input weighting is a scalar and is equal to 10^{-5} which is choosen after several trials to achieve a performance level close to the three-element controller performance. It is assumed that all the measurements were available without any noise. The detailed structure of the **MATRIX$_x$** programming is listed in App. B.5. The closed-loop responses of the steam generator model with a three-element controller, with an optimal regulator and without any control action are plotted in the same figures. The drum level response to a +10% steam valve

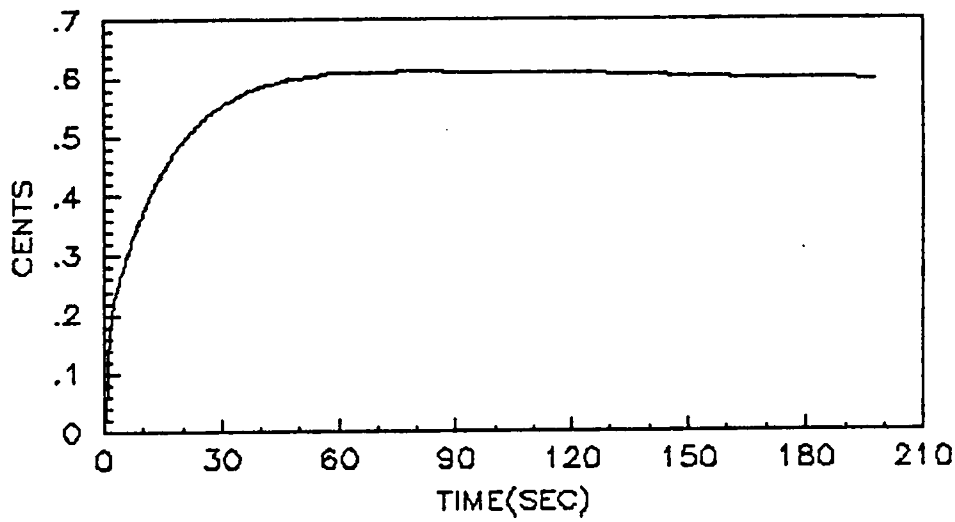

Fig. 6.6 Control Input (cents) Generated by the Optimal Compensator for a -5 cents Reactivity Perturbation.

opening step perturbation is shown in Fig. 6.7. As it can be seen from the figure, the level is controlled efficiently by both the control strategies. Figure 6.8 compares the control signals generated by the three-element controller and by the optimal regulator. Figure 6.9 shows the drum pressure response to the same perturbation. The drum level step response to a +10 F inlet sodium temperature perturbation is shown in Fig. 6.10. The control signals are compared in Fig. 6.11. Figures 6.12 and 6.13 show the drum level step response and the control signals for a +10 F feedwater temperature perturbation. The results show that the controller performances using classical and modern control design methods are very similar. A set of closed-loop responses of the EBR-II subsystem models are shown in Appendix C.

6.5 Robustness Testing

One of the most important aspects of a feedback control system is its ability to maintain stability in the presence of any plant uncertainty [19]. "This uncertainty may arise from variations in the actual plant itself due to changes in operating conditions, or may arise from the differences between the actual plant and a control design model used to represent it at any given

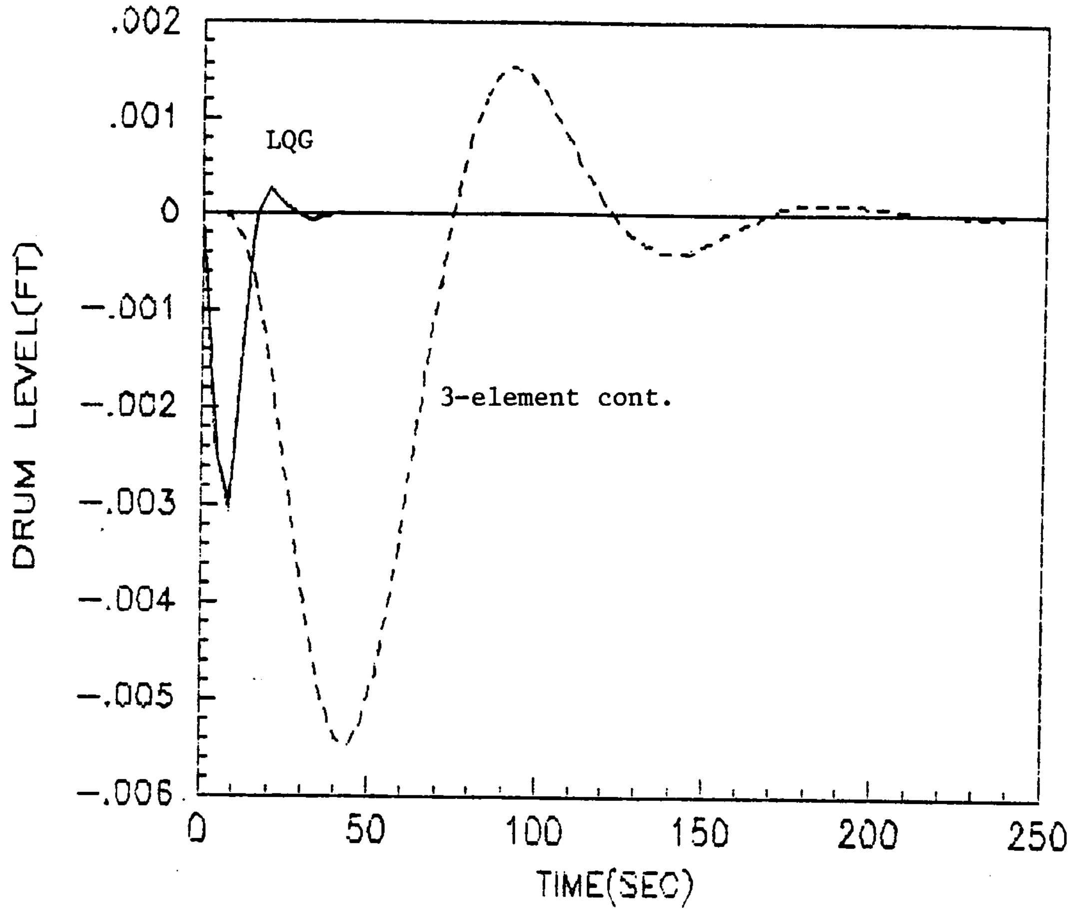

Fig. 6.7 Step Response of Drum Level to a +10% Steam Valve Opening Perturbation (Optimal Compensator, Three-element Controller and Open-loop Models).

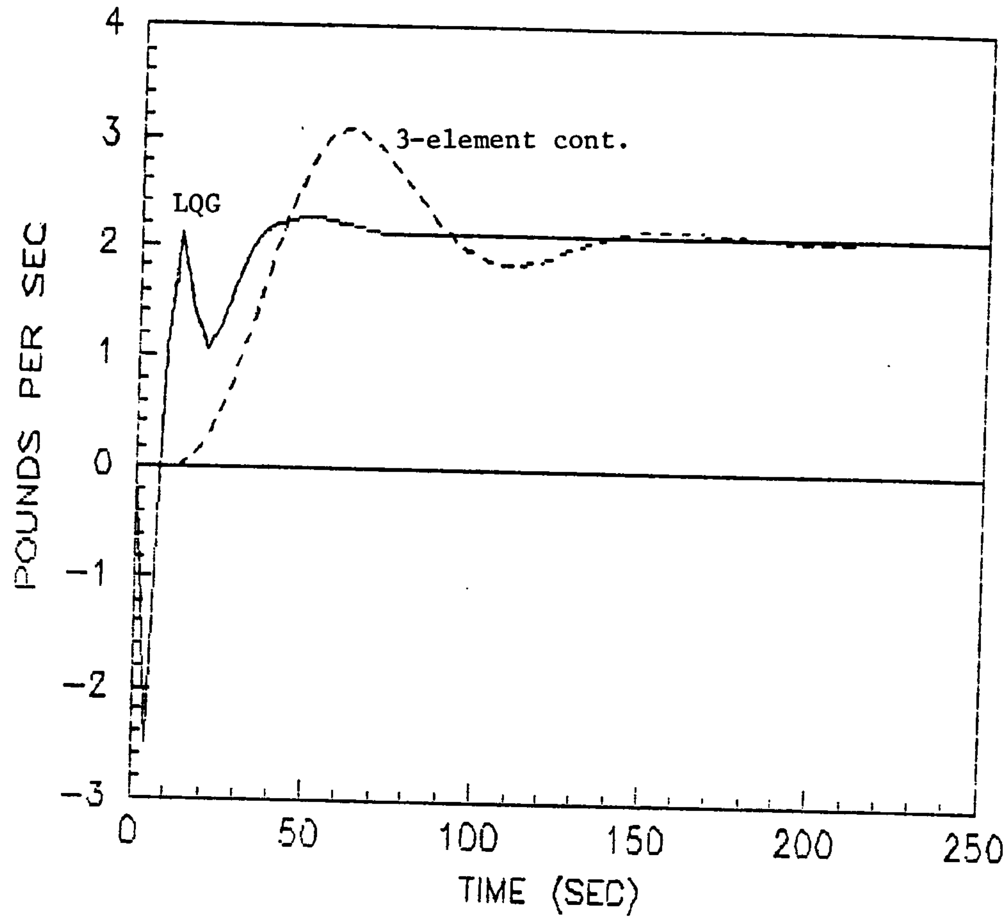

Fig. 6.8 Control Signals Generated by Three-Element Controller and Optimal Compensator for a +10% Steam Valve Perturbation.

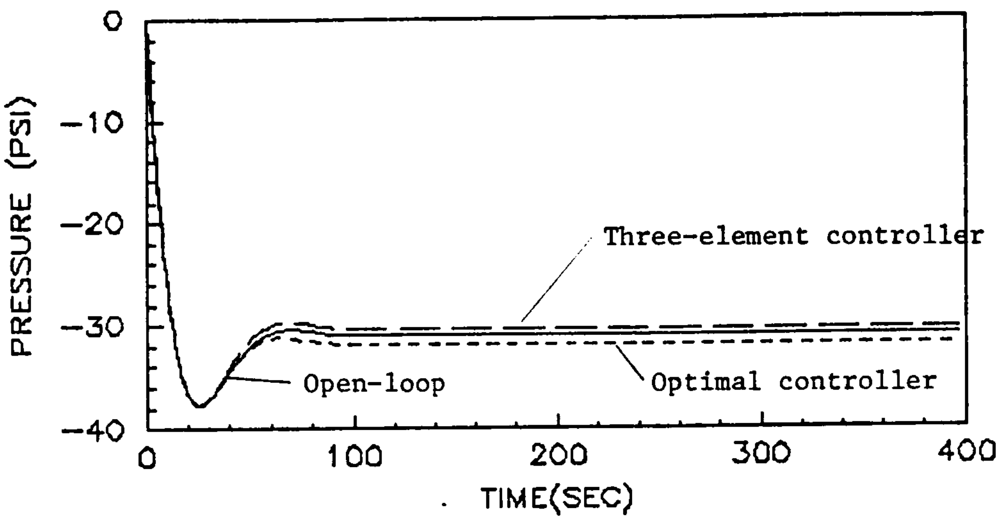

Fig. 6.9 Step Response of the Drum Pressure to a +10% Steam Valve Opening Perturbation (Optimal Comp., Three-element Controller and Open-loop Models).

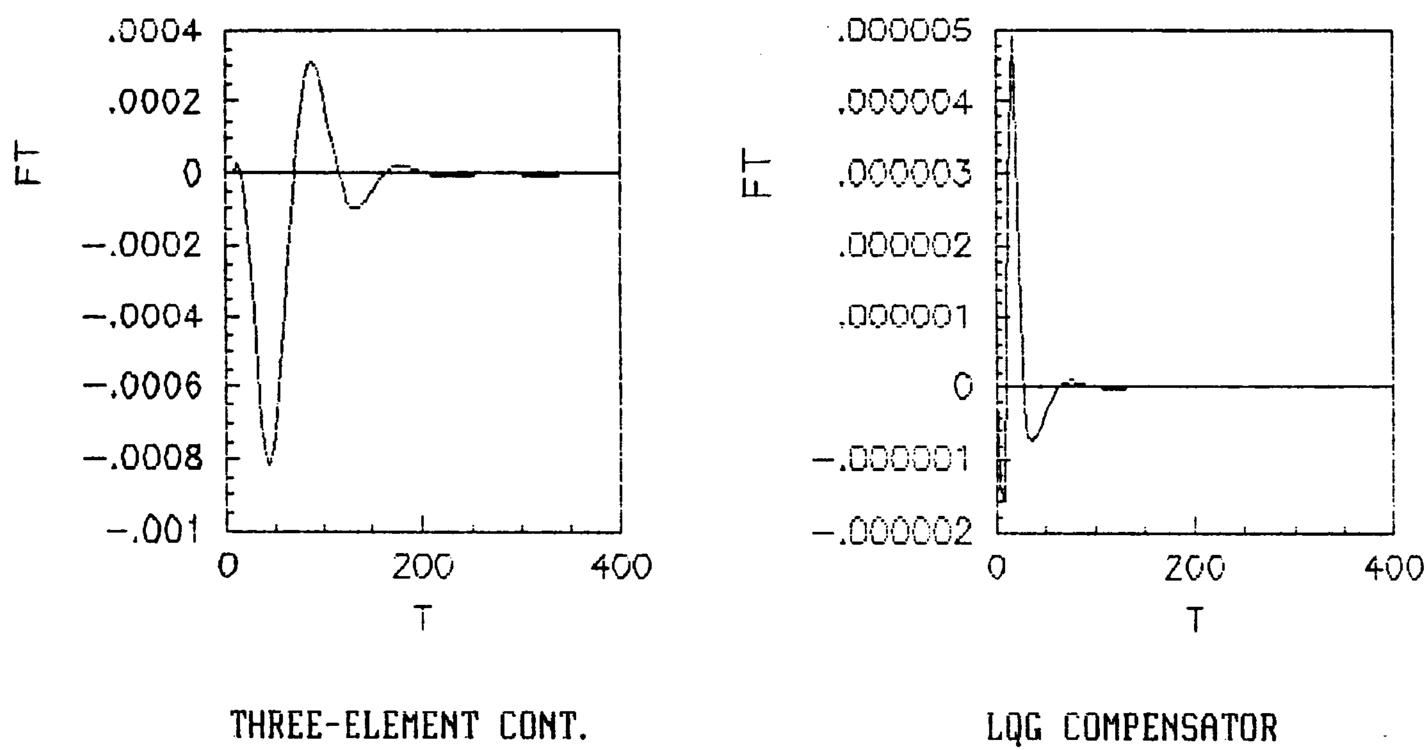

Fig. 6.10 **Step Response of Drum Level to a +10 F Inlet Sodium Temperature Perturbation (Optimal Compensator, Three-element Controller and Open-loop Models).**

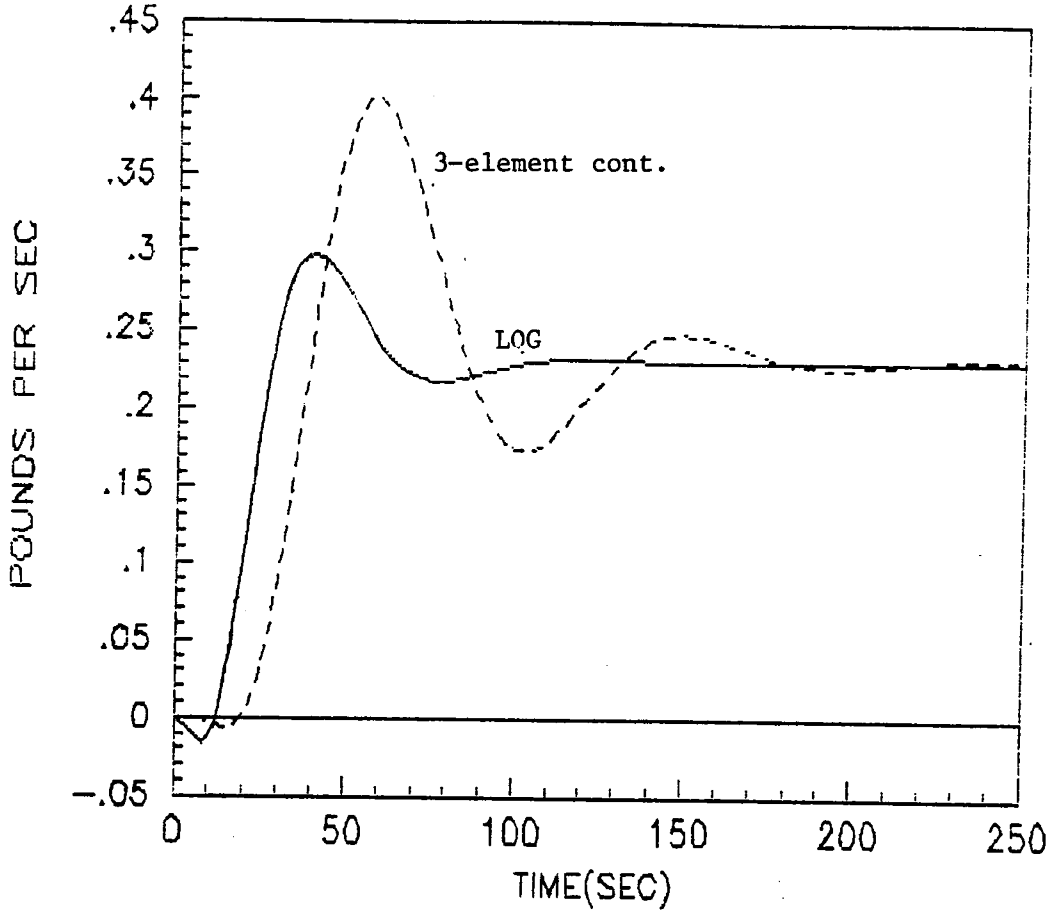

Fig. 6.11 Control Signals Generated by Three-element Controller and Optimal Compensator for a +10 F Inlet Sodium Temperature Perturbation.

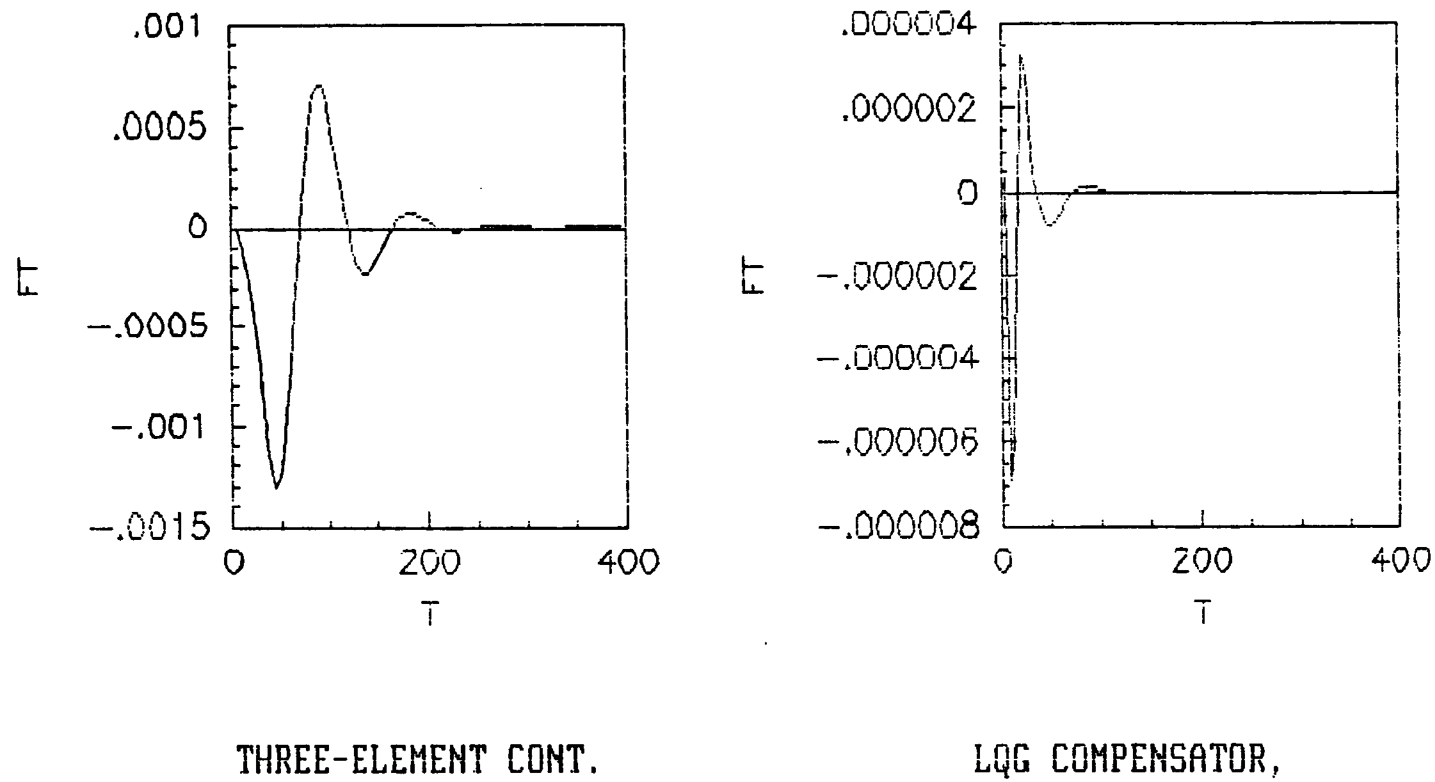

Fig. 6.12 Step Response of Drum Level to a +10 F Feedwater Temperature Perturbation (Optimal Compensator, Three-element Controller and Open-loop Models).

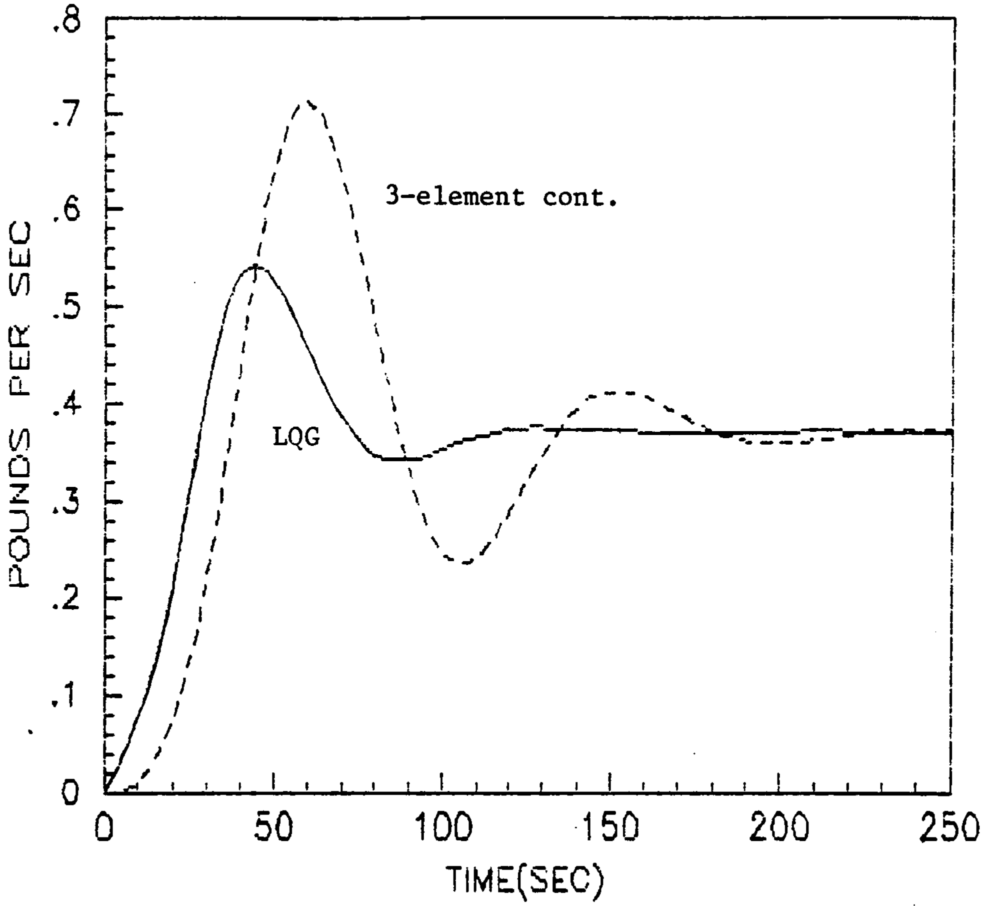

Fig. 6.13 Control Signals Generated by Three-element Controller and Optimal Compensator for a +10 F Feedwater Temperature Perturbation.

operating point"[19]. Mathematical methods of assessing stability robustness include matrix norms, measures and transformation techniques using only the design model.

A simple robustness test is considered for the three-element controller and optimal regulator previously designed for the EBR-II steam generator subsystem. The test includes simulation of the closed-loop system for a predefined plant uncertainty. Initially, the three-element controller and the optimal regulator designs are performed using the exsisting EBR-II steam generator model. The controllers are then appended to a new open-loop model which includes 5% deviation in the drum geometry calculations. We assume that the latter represents the actual plant. The step responses of both closed-loop system models to a +10% steam valve opening perturbation are shown in Figs. 6.14 and 6.15. Figure 6.14 shows the drum level step responses of the three-element controller model appended (1) to the original open-loop model and (2) to the model with uncertainty. Figure 6.15 shows the drum level step responses of the optimal regulator appended as (1) and (2) above. The closed-loop results indicate that the three-element controller is more sensitive to a plant uncertainty than the optimal regulator. Note that a steady-state error is encountered in the three-element controller case when an uncertainty is present. The drum level behavior is less

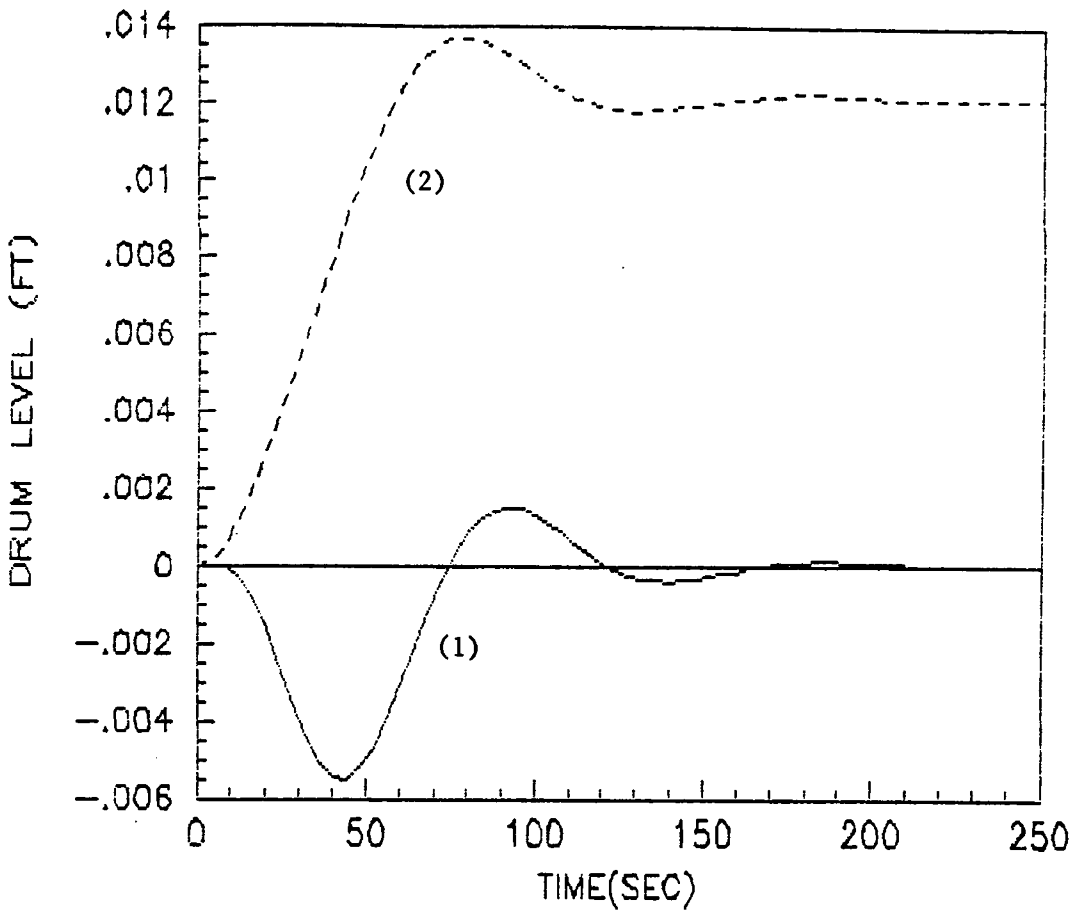

Fig. 6.14 Step Response of Drum Level to a +10% Steam Valve Opening Perturbation (Three-element Controller Appended to (1) Original Model, (2) Model With Uncertainity).

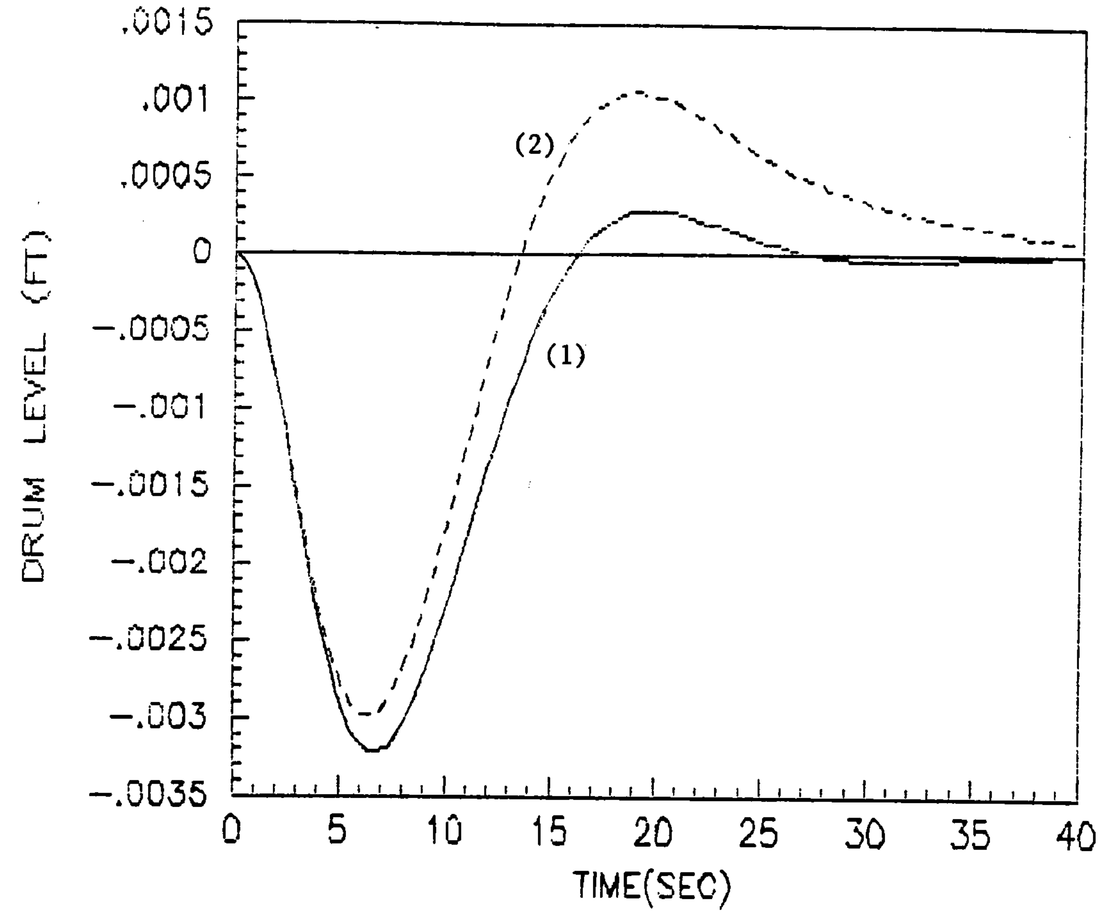

Fig. 6.15 **Step Response of Drum Level to a +10% Steam Valve Opening Perturbation (Optimal Compensator Appended to (1) Original Model, (2)Model With Uncertainity).**

affected in the optimal regulator case. The three-element controller is a local controller and its performance is affected more by a local parameter uncertainity than the full-state feedback optimal regulator which has a global type control behavior. This is one example of robustness testing. Further study is necessary to establish this for all important parameter uncertainties.

6.6 Summary

The modern control theory design methods are studied. Several optimal regulator designs are performed on the EBR-II subsystem models using **$\mathbf{MATRIX_X}$**. The output-feedback optimal controllers are fed with the full state measurements. It is assumed that all the measurements are available without any noise or disturbance. The design objective is to satisfy operational requirements using a simple optimal controller design.

A previously developed EBR-II primary system model is appended to an optimal regulator in a feedback arrangement. The closed-loop step responses to a -5 cent reactivity perturbation show a reasonable improvement in the system behavior without violating the 2 F per minute reactor ΔT increase limitation. The steady-state errors observed in the closed-loop responses are negligible. The states reach the steady-state values in 5 seconds.

An optimal regulator is designed and appended to a previously developed EBR-II steam generator model. The closed-loop responses to several standard step perturbations show that the drum level is controlled safely within the operational limits of 3 inches above and 4 inches below the center line. The results are compared with the three-element controller results, and the controller performances obtained using both strategies are found to be quite similar. The speed of the closed-loop responses using both controllers are also comparable.

A simple robustness test is performed on the EBR-II steam generator controller models. Instead of using the analytical methods of assessing robustness stability, the closed-loop systems reconstructed using the original models and the models with an uncertainty are simulated. The optimal regulator and three-element controller designs are performed using the original open-loop EBR-II steam generator model. These controllers are appended to the same model in which a 5% uncertainty is introduced to the drum geometry calculations. We assume that the model with an uncertainty represents the actual plant. The step responses of the both closed-loop models to a +10% steam valve opening perturbation show that the stability is retained; however, a steady-state error is encountered in the three-element controller case. The optimal regulator appended to the "actual plant" is capable of retaining the zero steady-state error obtained using the original model.

CHAPTER 7

SPECIAL CONTROL APPLICATIONS

7.1 Improvements in Optimal Regulator Design

As previously stated, an optimal regulator design includes assessing an appropriate combination of weightings in the corresponding quadratic cost function. A simple approach to the problem of finding the best combination requires some knowledge about the open-loop system dynamics. The problem becomes even more complicated for partially uncontrollable or unobservable systems. A basic practical method of choosing the state weightings is examining the open-loop system behavior and determining the "penalties" for those states in which the deviations from the steady-state exceed some predefined limits. A criteria can be defined using the standard performance features such as overshoot, steady-state error, bandwidth or gain/phase margins. For example, the gain margins of a controllable linear system can be calculated for each input-output pair and the state weightings can be choosen according to the corresponding gain margins. Once the starting combination is predicted then a finer tuning can be accomplished through several closed-loop simulations in a trial-and-error fashion. This method would obviously be far from being practical for large order MIMO systems. If the open-loop system has unstable poles then the unstable states have greater importance compared to others. In such cases, a change in the weights of the stable states may not affect the performance significantly since the weights of the unstable states would necessarily be chosen much higher than that of the stable states. Improving the optimal regulator design also includes selecting the control input weights. Since we are only interested in single-input systems the control input weighting selection becomes less complicated. However, an appropriate choice can not be made easily unless the actuator dynamics is completely known. It is very important to design a control input such that the process actuators are not saturated.

In light of the above discussion, the optimal controllers previously developed for the EBR-II subsystem models are reconsidered. The primary system model has eigenvalues widely spaced (stiff system). The reactor power changes very rapidly for reactivity perturbations compared with the changes in the other state variables. This fact implies that the state weight for the reactor power must be dominant. However, several optimal regulator design applications indicated that different combinations of state weights do not improve the system behavior as much as the simple design (using single weight for the reactor power). An improvement in the optimal regulator design without violating the safety limitations is made by adjusting the control-input weight. Figure 7.1 shows the step responses of fractional reactor power to a -5 cent reactivity insertion using three different optimal regulators. The designs only differ in the input weights (0.007, 0.002, 0.0007). The single state weight (reactor power) is equal to 1. As shown in Fig. 7.1, the reactor power is regulated most powerfully when the input weight is 0.0007 which generates the fastest control input among the others. Figure 7.2 shows the control inputs corresponding to the three cases of input weights. Note that when the reactor power is controlled using the fastest control input, 1 cent per second safety limitation is not violated and the rod speed is around 50% of its maximum value.

The EBR-II open-loop steam generator model includes the level dynamics. The previously developed optimal regulator model for controlling the EBR-II steam generator uses a weight only on the 18th state which is the drum level. The design uses main steam valve position as the control input with a scalar weight of 10^{-5}. A set of different combinations of state weights are tested to improve the optimal regulator performance. The new design uses the steam valve as the actuator. The primary task of stabilizing the drum level requires a relatively large weight on the drum level (unstable state) when all the state weights are used. The list of state weighs given in Table 7.1 is found to be the best combination after several trials. The overshoot ratios of each state are used for the distribution of weights. Despite the fact that 17 of the state weights are close to each other and exhibiting a big contrast ($x10^6$) compared to the level weighting, the controller performance is affected by a small change in one of the weights of 17 states. The step responses of the drum level to a +10% steam bypass valve opening perturbation using two different optimal controllers (1) single weight on drum level, (2) the combination of state weights of Table 7.1 , are shown in Fig. 7.3. The improvement in the drum level response can be seen in Fig. 7.3. A similar comparison is made for the drum pressure response to the same perturbation and is shown in Fig. 7.4.

TABLE 7.1

State Weights of the Quadratic Cost Function.

LQG Design for the EBR-II Drum Level Control

Q(I,J)	Weight
1,1	1.3
2,2	2.0
3,3	1.0
4,4	1.4
5,5	1.3
6,6	1.4
7,7	1.3
8,8	1.0
9,9	1.0
10,10	3.0
11,11	1.0
12,12	1.0
13,13	1.0
14,14	1.0
15,15	1.0
16,16	1.0
17,17	1.0
18,18	1.0D +06

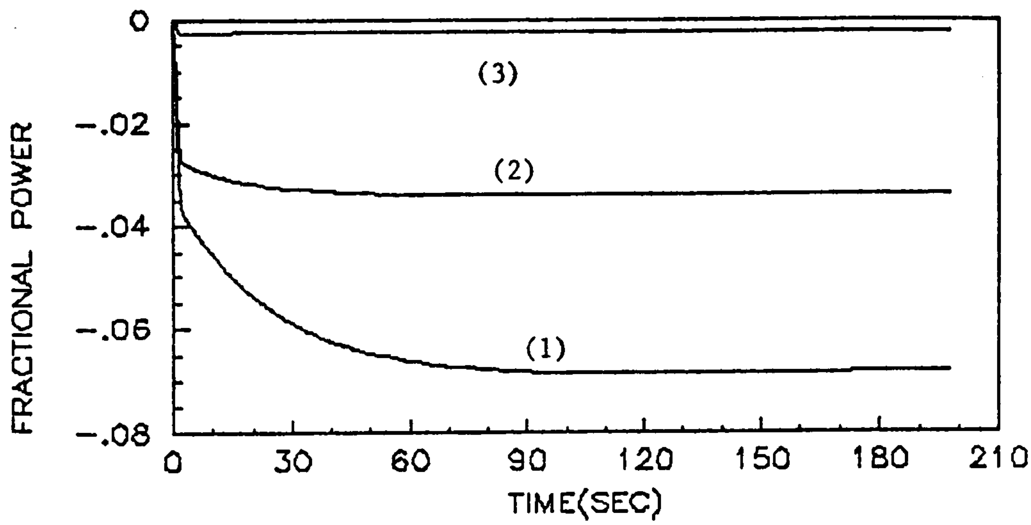

Fig 7.1 Step Responses of Fractional Reactor Power to a -5 cents Reactivity Perturbation (Closed-loop Primary system with an Optimal Compensator using (1) 5%, (2) 10%, (3) 50% of the Maximum Control Rod Speed.).

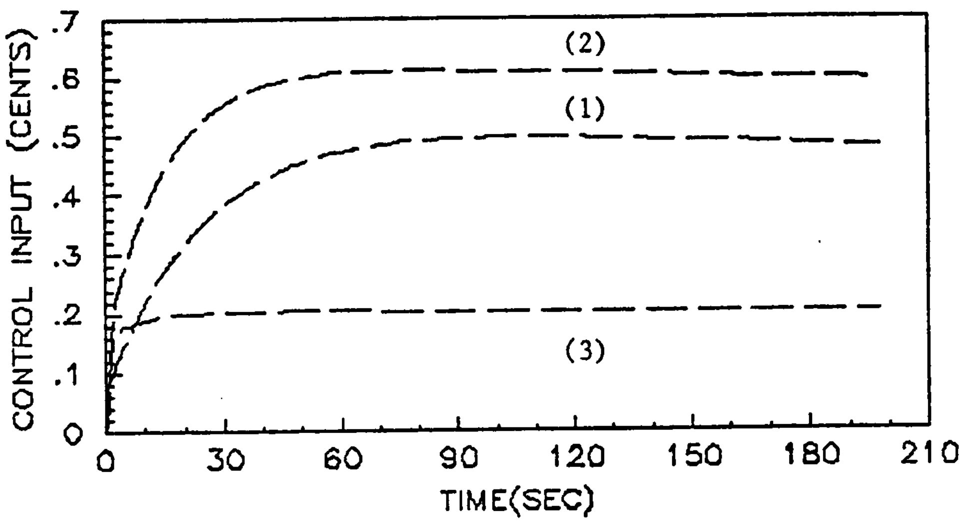

Fig. 7.2 Control Signals Generated by the Optimal Compensator Appended to the Primary Model. Step Perturbation is a -5 cents Reactivity Insertion. (1) 5%, (2) 10%, (3) 50% of the Maximum Rod Speed.

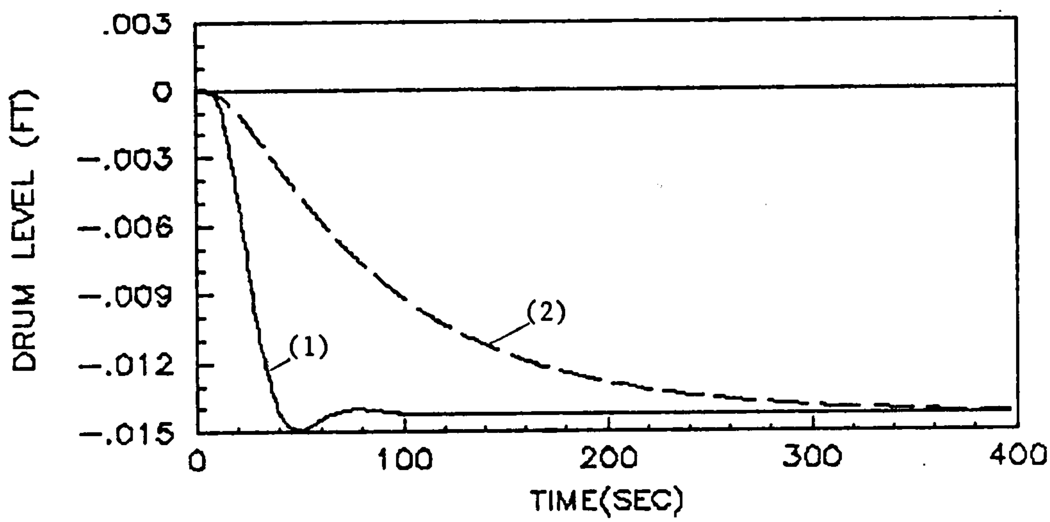

Fig. 7.3 Step Response of Drum Level to a +10% Steam By-pass Valve Opening Perturbation (Optimal Compensator (1) Simple Design (2) Improved Design).

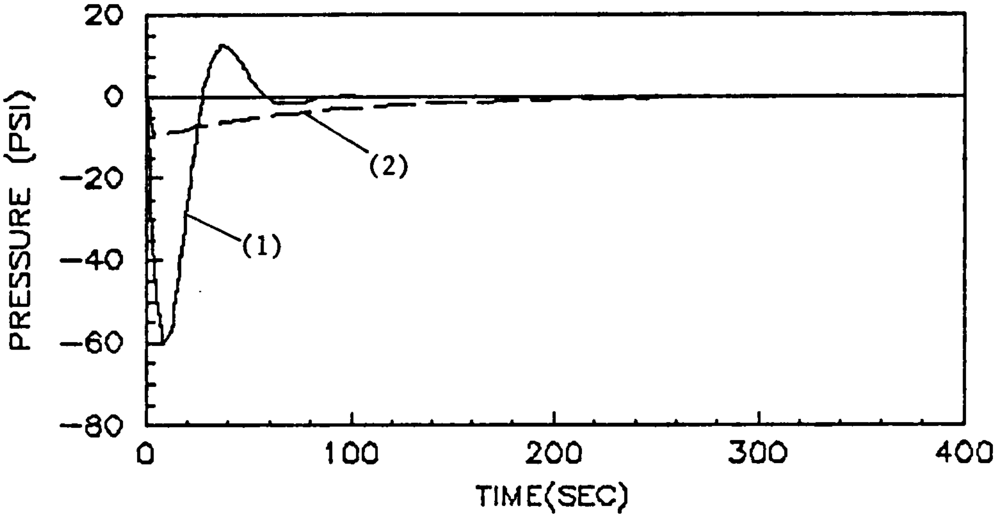

Fig. 7.4 Step Response of Drum Pressure to a +10% Steam By-pass Valve Opening Perturbation (Optimal Compensator (1) Simple Design (2) Improved Design.

7.2 LQG Compensator Design For Degraded Conditions

In a real process all of the measurements will not be available. The available measurements may also contain noise. Under these conditions an optimal output feedback controller design requires the estimation of those states which are missing in the measurement. Constant, optimal state-estimator gain matrices can be calculated using the Kalman filter design routines in **MATRIX**$_{\mathbf{x}}$(see Appendix B). A Kalman filter design optimizes the estimator performance with respect to the measurement noise and input disturbance. An LQG compensator design can be completed by designing an optimal regulator and appending it to the optimal estimator in an arrangement as shown in Fig. 6.1.

The EBR-II steam generator model is used to study the LQG compensator design under degraded conditions. It is assumed that some temperature measurements are not available. These are the superheater and evaporator tube wall temperatures and the evaporator primary sodium temperatures (states 4,5,6,7,15). It is also assumed that the noise intensities on the available measurements are about 10% of the steady state values. A small input disturbance of 10^{-3} is assumed to be exsisting on each state. An optimal estimator for the steam generator model is designed with the specifications stated above. The optimal regulator designed in Sec. 7.1 is used to complete the LQG compensator design. The step responses of the closed-loop model to a 10% steam bypass valve opening perturbation show that the controller performance is satisfactory. The drum level step responses of the two closed-loop system models (one designed for degraded condition, and the other with a perfect measurement assumption) are shown in Fig. 7.5. The drum steam pressure step responses of the two same closed-loop system models are shown in Fig. 7.6. It can be seen from these figures that the differences between the two cases are negligible under the assumptions stated above.

7.3 Set-Point Tracking Controller Design

One of the main objectives of the control design studies is to design an optimal controller for which the closed-loop behavior can be directed from one set point to another. Such a controller can be used to change the steady-state value of the reactor power. The controller's task is to adjust the closed-loop behavior in an optimized manner so that a chosen output reaches the desired steady-state with a negligible error.

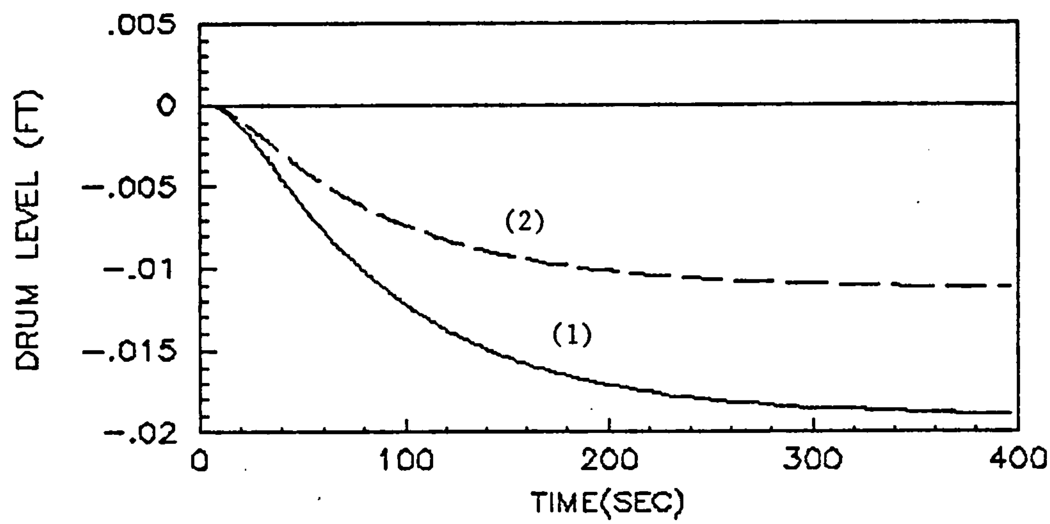

Fig. 7.5 Step Response of Drum Level to a +10% Steam Valve Opening Perturbation (LQG Compensator (1) Degraded Conditions (2) Full-state Feedback, Ideal Case.

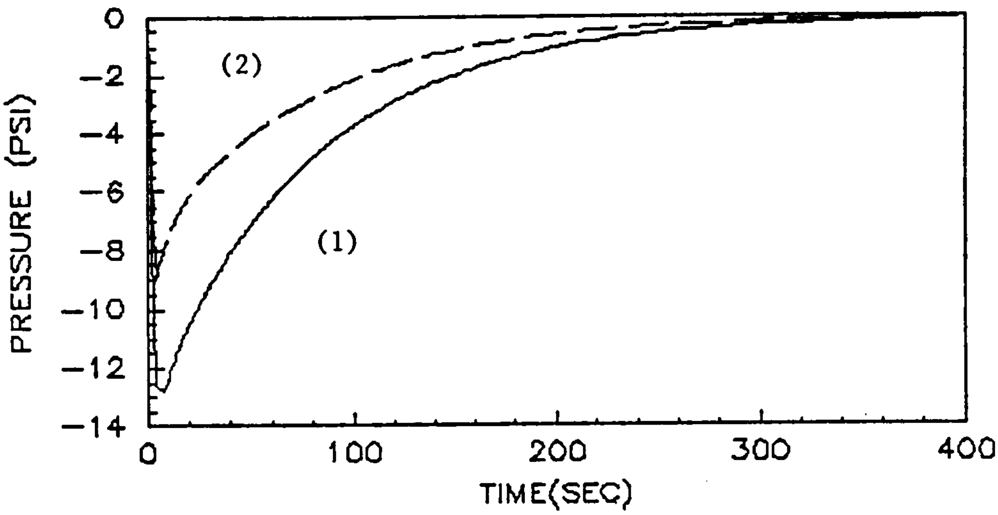

Fig. 7.6 Step Response of Drum Pressure to a +10% Steam Valve Opening Perturbation (LQG Compensator (1) Degraded Conditions (2) Full-state Feedback, Ideal Case).

A tracking optimal controller can be designed using the following formulation which is based on the meta-state representation of the system [13]. Consider a dynamic system

$$\dot{\underline{X}} = A\ \underline{X} + B\ u \tag{7.1}$$

Assume that the reference state is known.

$$\dot{\underline{X}}_r = A_r\ \underline{X}_r \tag{7.2}$$

Define an error vector

$$\underline{e} = \underline{X} - \underline{X}_r \tag{7.3}$$

$$\dot{\underline{e}} = A\ \underline{e} + E\ \underline{X}_r + B\ u \tag{7.4}$$

where

$$E = [\ A - A_r]$$

The meta-state representation is given by

$$\dot{\underline{\mathbf{X}}} = \mathbf{A}\ \underline{\mathbf{X}} + \mathbf{B}\ u \tag{7.5}$$

$$y = \mathbf{C}\ \underline{\mathbf{X}} \tag{7.6}$$

where

$$\underline{\mathbf{X}} = \begin{bmatrix} e \\ \\ X_r \end{bmatrix} \qquad \mathbf{A} = \begin{bmatrix} A & E \\ \\ 0 & 0 \end{bmatrix} \qquad \mathbf{B} = \begin{bmatrix} B \\ \\ 0 \end{bmatrix} \qquad \mathbf{C} = [\ C\ C_r]$$

The formulation of the linear, quadratic optimum control problem using the meta-state representation can be carried out as follows. An appropriate performance integral for the problem is

$$V = \int_t^T (e^TQe + u^TRu)\, d\tau \qquad (7.7)$$

For the meta-state $\underline{\mathbf{X}}$, the state weighting matrix is

$$\mathbf{Q} = \begin{bmatrix} Q & 0 \\ \\ 0 & 0 \end{bmatrix} \qquad (7.8)$$

The following equation can be derived for zero steady-state error.

$$B\ u^* + E\ \underline{X}_r = 0 \qquad (7.9)$$

The total control action can be written as a combination of two components, namely, the steady-state control and the corrective control.

$$U = u^{*}+v \tag{7.10}$$

The performance integral for the corrective control can be written as

$$\bar{\nu} = \int_{t}^{\infty} (e^{T}Qe + \nu^{T}R\nu)\, d\tau \tag{7.11}$$

Let **M** be the equivalent Ricatti matrix for the meta-state system.

$$\mathbf{M} = \begin{bmatrix} M_1 & M_2 \\ M_3 & M_4 \end{bmatrix} \tag{7.12}$$

The gain matrix G for this system is given by

$$G = R^{-1} \; [\; B^{T} \;\; 0 \;] \begin{bmatrix} M_1 & M_2 \\ M_3 & M_4 \end{bmatrix}$$

$$= [\; R^{-1}\, B^{T}\, M_1 \quad R^{-1}\, B^{T}\, M_2 \;] \tag{7.13}$$

The corresponding equations for M_1 and M_2 are obtained from the following general equation.

$$-\dot{M} = M\,A + A^{T}M - M\,B\,R^{-1}B^{T}\,M + Q \tag{7.14}$$

These are:

$$- \dot{M}_1 = M_1 A + A^T M_1 - M_1 B\, R^{-1} B^T M_1 + Q \qquad (7.15)$$

$$- \dot{M}_2 = M_1 E + [\, A^T - M_1 B\, R^{-1} B^T \,]\, M_2 \qquad (7.16)$$

The isolated EBR-II steam generator is considered for the reference input tracking control problem. The design procedure using the **MATRIX$_x$** routines can be summarized in five steps.

1) The first term in Eq. 7.13 represents the regulator gains obtained using the standard regulator design method. Using the original model, this steady state control gains can be calculated with the **MATRIX$_x$**. commands.

2) The closed-loop system matrix is then calculated as follows

$$A_c = A - B\, K_r \qquad (7.17)$$

where

K_r = Regulator gain matrix calculated by **MATRIX$_x$**.

3) In order to calculate the gain matrix corresponding to the "corrective control", Eq.(7.16) is used.

$$\dot{M}_2 = 0$$

$$M_2 = - (A_c^T)^{-1} M_1 E \tag{7.18}$$

M_1 is obtained from the **MATRIX$_X$** command "REGULATOR". The corrective gain matrix is given by

$$K_c = R^{-1} B^T M_2 \tag{7.19}$$

4) The total gain matrix is constructed.

$$K = [K_r K_c] \tag{7.20}$$

5) The meta-state representation of the system is made by calculating E matrix for the desired reference state. The observation matrix has diagonal elements equal to 1 which enables us to observe error outputs. It also includes an additional entry for the reference state which is the steady-state value of the corresponding output. This is done only to observe the error in the actual output. The final stage is to form the closed-loop system using K and the estimator gain matrix K_E in the LQG compensator design steps. Note that all the outputs are measured without any disturbance or noise; therefore, there is no state estimation in the practical implementation.

An application of the reference input tracking control problem is considered using the EBR-II steam generator system as an example. The first reference input is a step change in the drum pressure (the derivation stated above is valid for constant reference inputs). It is possible to increase the power generation in nuclear reactors by extracting more steam from the steam generator (load-following property) which results in a steam pressure drop in the drum. It is assumed that a 100 psi steam pressure drop is the reference input to be tracked. The closed-loop response of the steam pressure in the drum to the reference input is shown in Fig 7.7. The remaining error outputs are found to be close to zero. It can be seen from the figure that the reference tracking optimum control is accomplished with a small steady-state error. A second application to the EBR-II steam generator model is performed using a reference input of 4 inch level increase in the drum. Figure 7.8 shows the drum level increase to the reference input. The steady-state error is practically zero as it can be seen from the figure. Other error outputs are also close to zero. Note that the optimal regulator design for the steady-state portion of the total control action uses a weight (equal to 1) only on drum level variable which is presumably the reason for a relatively smaller steady-state error compared to the pressure tracking controller case.

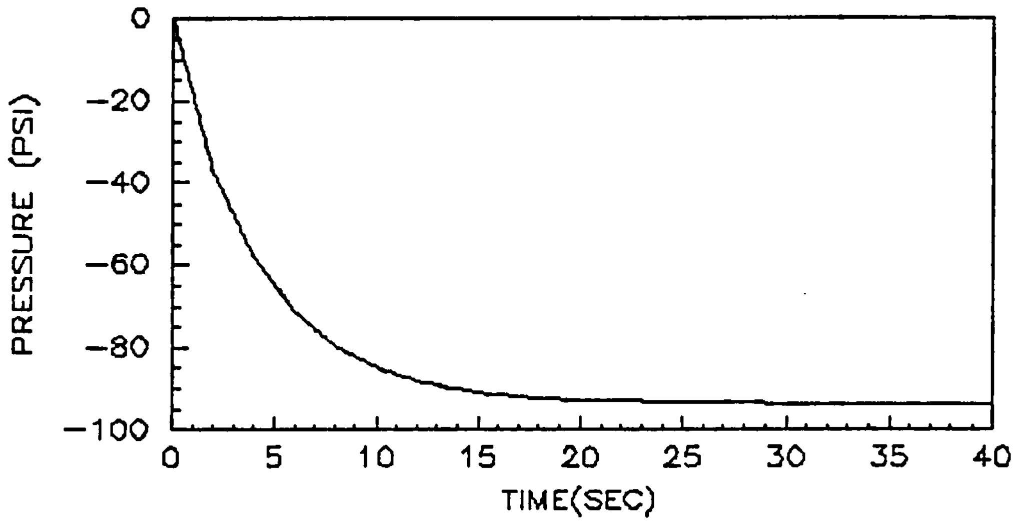

Fig. 7.7 Drum Pressure Response to a -100 psi Step Reference Input (Optimal Tracking Controller).

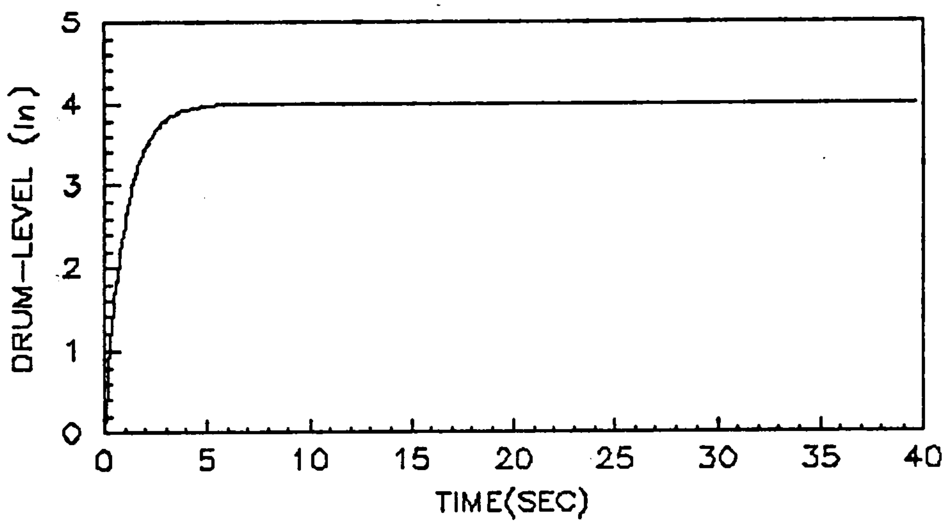

Fig. 7.8 Drum Level Response to a +4 in Step Reference Input (Optimal Tracking Controller).

7.5 Summary

Some special controller design applications to the isolated EBR-II subsystem models are considered. An attempt towards improving the optimal regulator design is made by considering all of the state weights in the corresponding quadratic cost function. After several trials a set of weights is selected as the best combination based on the closed-loop system performances. For the specific example of the EBR-II steam generator system model, the number of possible combinations of state weights is found to be limited due to the fact that an unstable pole of the open-loop model is to be weighted much larger than the other stable states to maintain stability. A similar study is performed for the EBR-II primary system model. An improvement in the optimal regulator performance is achieved by adjusting the input weights of the quadratic cost function. The results indicate that the safety limitations are not violated using the improved design.

Sensor failure or measurements with a high intensity noise are some common events in the real proceses. It is possible to design a controller using the modern control theory which can yield a reasonable performance under degraded conditions. The EBR-II steam generator system model is used to study the optimal estimator performance under such conditions. Five temperature measurements are assumed to be missing. The presence of 10% measurement noise and a small input disturbance are also assumed. A previously designed optimal regulator is appended to an optimal estimator to form the final LQG compensator. The closed-loop step responses to a steam bypass valve opening perturbation indicate that the optimal estimator performance is very close to the performance obtained using the full-state feedback optimal regulator with perfect measurements.

One of the very important applications of the optimum control theory is the reference input tracking optimal controller design. With the aid of a reference tracking controller, a desired change in the steady-state value of any system output can be made safely. A necessary formulation is studied and an optimal tracking controller is designed using the meta-state representation of the EBR-II steam generator model. The closed-loop system responses to a 100 psi pressure drop reference input show that the tracking is accomplished efficiently. The closed-loop responses to a 4 inch drum level increase reference input also assures that the performance of the optimal tracking controller is satisfactory. In both cases, the steady-state errors are negligible and the speed of the closed-loop response is reasonably high.

CHAPTER 8

CONCLUDING REMARKS

8.1 Conclusions

This study contains the development of a low-order linear EBR-II system model including the reactor, liquid sodium tank, intermediate heat exchanger, and the steam generator subsystems. The model is developed as two separate modules, namely, the primary system and the steam generator. The open-loop responses of both the modules to a few standard step perturbations are obtained and the validity of each module is discussed. The two modules are coupled and overall system behavior is evaluated. The objective of this research also includes studying the modern control theory and performing several control designs using the CAD package **MATRIX$_X$**. The modern controller performances are discussed and compared with the classical design methods. Simulations and controller designs are performed using the computer software **MATRIX$_X$** [15].

The EBR-II primary system model is taken from an earlier work [Greene 1] and modified using a physical model reduction technique [4], six precursor concentration equations replaced with one "averaged" group equation. The model includes a point reactor kinetics equation, an averaged precursor equation, Mann's heat transfer model and the first order transport-lag approximations. The core bowing and control rod expansion reactivity feedback mechanisms are not included in the model due to their negligible effects for small transients around the steady-state. The remaining seven reactivity feedback effects are taken into consideration. Another modification in the Greene model is made by using more lumps for the IHX model. The neccessity of the modification comes from the heat transfer limitations of using Greene's five-lump IHX model. The open-loop step responses to a -5 cent reactivity perturbation are physically consistent and agree with the ANL results. The results also agree with the Greene model results. The temperature responses of the IHX coolant lumps verify that increasing the number of lumps provides better results. The IHX model which is a part of the primary system model is simulated for a +10 F sodium temperature perturbation at the secondary inlet plenum. The open-loop step responses of the primary system model to the inlet sodium temperature perturbation show that the ten lump IHX model is sufficient in representing the dynamics of the heat exchanger system.

The secondary system of the EBR-II is modeled using the energy and mass balance equations for the evaporator, superheater and drum regions. Two momentum equations are used for the downcomer and evaporator flows. The phase change in the evaporator is modeled with a moving boundary approach. In the two phase region, a homogeneous flow assumption is considered [6]. The superheater dynamics is represented by a single-phase heat transfer formulation (Mann's model) [10]. A three-element controller is designed for the drum level control problem. The controller uses drum level, feedwater flow and steam flow signals. The steam leaving the drum is assumed to be completely dry and its representation is based on the critical flow assumption [4]. The open-loop step responses of the steam generator model to four different step perturbations show that the drum level is unstable unless the three-element controller is activated. It is also observed that an inherent stability exsists in the boiling region dynamics regardless of any control action on the drum level. The overall open-loop results are in physical agreement with the results obtained by previously developed PWR, U-Tube steam generator model [4]. The drum level prediction also agrees with the B402 test result [ANL 23].

The linear models of the primary system and the steam generator are coupled. The combined model step responses to a -5 cent reactivity insertion are quite similar to the results obtained using only the primary system model. On the steam generator side, the superheaters receive a sodium temperature decrease input from the primary system which is immediately absorbed by the dry steam flowing through the tube side of the superheaters. There is not much feedback from the steam generator to the primary system for small perturbations around the steady state. A + 10 % steam valve opening perturbation to the steam generator side of the combined model results in step responses that are similar to the isolated steam generator results. The primary system is not very much affected by the steam valve opening perturbation due to two reasons. The first reason is that the sodium tank in the primary system has a large time constant and a sudden temperature change in the secondary system will be slowed down on its way to the active core region; therefore, the tank-sodium temperature reactivity feedback effect on the reactor power is a slowly varying mechanism. The other reason for the weak coupling between the two modules is explained as follows. A change in the superheated steam flow affects the heat transfer rate to the feedwater through the feedwater heaters (the heaters utilize a fraction of the superheated steam). The feedwater heater system belongs to the condenser-turbine system, and the present EBR-II model does not include this. The missing information about the feedwater dynamics results in excluding the effects of the feedwater temperature variations on the evaporator dynamics.

The modern control theory design algoritms are studied. The design effort is mainly concentrated on the linear, quadratic Gaussian compensator design which includes an optimal regulator design and an optimal estimator (Kalman filter) design [15]. A full-state feedback optimal regulator is designed for the EBR-II primary system model. The measurement noise and input disturbance are assumed to be zero. The fractional reactor power is weighted in the corresponding quadratic cost function. The design uses the reactivity as the control input with a small scalar weight. The closed-loop step responses to several perturbations show improvement in the system behavior. The safety limitations of 2 F per minute reactor T change and 1 cent per second control rod speed are not violated. A similar design is performed to control the drum level in the EBR-II steam generator model. The control input for this case is the feedwater flow. The states corresponding to the drum level and the dummy variable are weighted in the quadratic cost function. The design also uses all the measurements without noise or input disturbance. The closed-loop step responses to several perturbations show consistently high performance. The comparison with the three-element controller results indicate that the both strategies are favorable. The drum level design requirement of 3 inch above, 4 inch below the center line drum level variation limit is not exceeded. When the control input and the system disturbance units are the same, the optimal regulator controller exhibits a global control behavior. This is the case when the main steam valve is used as an actuator to control the system for a steam by-pass valve opening perturbation (or using the control rods to control the primary system for small rod-drop perturbations). Note that the closed-loop system model construction in the **MATRIX$_X$** algorithms is done in a pole-placement fashion using the optimal gains where the closed-loop system with the three element-controller includes the actuator dynamics as an additional state. The nonzero steady state errors encountered in modern control design applications are related to the type-0 structure of the closed-loop systems. This observation is explicitly detailed in this study. Thus, it can not be assumed that the LQG compensator will result in a zero steady-state error. However, an error less than a specified value can be achieved by the LQG design. Theoretically the LQG design does not guarantee a zero error for a step perturbation, if the corresponding transfer function is of type-0. The problem can be solved, however, using a dummy state variable in the form of an integrator. The implementation of the LQG design for the EBR-II drum level controller includes this modification.

A simple robustness test is applied to the controllers of the EBR-II steam generator model. Instead of assessing robustness stability by analytical methods, a practical method is considered in determining the robustness levels of each controller. The test method consists of the controller models which are developed using the open-loop model and a "plant" model which includes several uncertainties in the system parameters. It is assumed that the drum geometry parameters of the open-loop model are 5 % different than the actual dimensions. The optimal regulator and the three-element controller are appended to the "plant" model (one at a time). The closed-loop step responses to a + 10 % steam by-pass valve opening perturbation show a steady-state error in the drum level using the three-element controller. The closed-loop model with an optimal regulator responds to the same input in a more favorable manner. The zero steady-state error in the drum level is practically unchanged; consequently, the optimal regulator is more robust to a plant uncertainty.

The closed-loop system performance using an optimal regulator design is related to the state and control input weights in the corresponding quadratic cost function. The best combination of the state weights is selected for the EBR-II steam generator controller in a trial-and-error fashion. A starting combination is predicted using the knowledge of the open-loop system dynamics. The drum level which is an unstable state, is suppressed by a relatively large weight where the other states are weighted based on the over-shoot ratios (open-loop case versus simple optimal regulator design case). The closed-loop step responses to a + 10 % steam by-pass valve opening perturbation show that a drastic improvement can be achieved. However, the controller performance evaluation does not include the limitations on the control signal. The actuator constraints bring certain limitations to the control input weight as well as to the state weights.

A complete LQG compensator design which includes an optimal estimator (Kalman filter) design is considered for the EBR-II steam generator system. The measurement set is assumed to be incomplete. The available measurements are assumed to contain noise. A small input disturbance on the states is also considered. An optimal estimator is designed and appended to a previously designed optimal regulator. The LQG compensator synthesis is the final form of the modern controller. The closed-loop step responses to a + 10 % steam bypass valve opening perturbation show that the linear observer design yields high performance in terms of estimating the states and regulating the closed-loop behavior in an optimal manner.

The last task presented in this study is an optimal reference-tracking controller design which has a major importance in plant operation. The analytical methods [13] are studied and an optimal tracking controller is designed using the meta-state representation of the EBR-II steam generator model. It is assumed that the measurements are complete and perfect. The closed-loop responses to the given step reference inputs such as drum level increase and drum pressure drop indicate that the optimal tracking controller is efficient in set point tracking. The steady-state errors are negligible and the response times are short.

The **$\mathbf{MATRIX_x}$** is one of the most advanced member of the **MATLAB** CAD package family. All of the simulations in this work are performed using the special features of the **$\mathbf{MATRIX_x}$** The modern control theory design algoritms such as an optimal regulator design (or the LQG design) routines are very powerful design tools. The classical methods such as root-locus or Bode plots are also available in the **$\mathbf{MATRIX_x}$** Using the menu-driven **System-Build** option, a number of modules can be coupled regardless of the complexity of input-output relationships among them. There are six integration algoritms, the default "variable Kutte-Merson" method is used in this work.

8.2 Recommendations

The development of a linear model for the EBR-II condenser-turbine system is a natural extension of the study described in this work. The combined system model with this third module can be used to predict the system behavior for the test transients. Despite the limited capabilities of linear models, it is believed that a complete EBR-II model will contribute to the development of new control strategies for advanced liquid-metal reactors.

An important suggestion is the application of model reduction techniques to the EBR-II model. The present model contains 57 state variables including the three-element controller dynamics. The software usage for the control design algorithms can be made less costly if an appropriate model reduction method is used to eliminate the redundant states.

The present model can be improved by introducing nonlinearities to the linear model. Increasing the number of lumps can give better temperature predictions for a detailed study. The core bowing and the control rod expansion reactivity feedback effects should be included in a nonlinear version of the model. The three-element controller design is a subject of further investigation and the actuator dynamics can also be represented with an improved model.

It is the author's belief that each of the control design studies presented in this work must be investigated in more detail. The selection of the best combination of weights in an optimal regulator design is one of the issues to be investigated. Despite the fact that finding the best weights can be done intuitively provided the designer is familiar with the open-loop dynamics, an analytical method based on the system matrices A and B would be very useful. The LQG compensator design applications to the EBR-II model shows that such controllers are quite efficient. A comparison between the full-state feedback compensator results and the estimator results assures that the practical implementation of the LQG compensators can handle the control problem even under degraded conditions. The applications of the optimal estimator design should be extended to more general cases of measurement degradation. The optimal tracking design problem can be incorporated with the estimator design problem. An optimal tracking controller design study under degraded conditions would be a topic for future study. When the closed-loop system structure has a type-0 form, the steady state errors can be driven to zero by appending an additional integrator to the system.

REFERENCES

REFERENCES

1. S. R. Greene, "The Design, Implementation and Cost-Benefit Analysis of a Dynamic Testing Program in the Experimental Breeder Reactor II," M.S. Thesis, The University of Tennessee (March 1979)

2. EBR-II System Description Manual, Vol.1-5, ANL (June 1972).

3. N. L. Snidow and T. L. Wilson, "U-Tube Steam Generator Modeling System," Internat. Conf. Power Plant Simulation, Cuernavaca, Mexico (Nov. 19-21, 1984).

4. T. W. Kerlin et al, "Pressurized Water Reactor Modeling for Long-Term Power System Dynamics Simulation," EPRI EL-3087, Vol. 2 (May 1983).

5. H. P. Planchon, J. I. Sackett, G. H. Golden and R. H. Sevy, "Implications of the EBR-II Inherent Safety Demonstration Test," Nucl. Eng. Design, Vol. 101, 75-90 (1987).

6. M. R. A. Ali, "Lumped Parameter, State Variable Dynamic Models For U-Tube Recirculation Type Nuclear Steam Generators, Ph.D. Dissertation, The University of Tennessee (Aug. 1976).

7. A. T. Chen, " A Digital Simulation For Nuclear Once-Through Steam Generators," Ph.D. Dissertation, The University of Tennessee (Dec. 1976).

8. M. M. El-Wakil, "Nuclear Heat Transport," The American Nuclear Society Press, La Grange Park, Illinois (May 1978).

9. Guide for Irradiation Experiments in EBR-II, ANL (March 1975).

10. S. J. Ball, "Approximate Models for Distributed-Parameter Heat-Transfer Systems," ISA Tran., Vol. 3 (Jan. 1964).

11. R. E. Crosbie and W. Heyes, "Variable-step Integration Methods for Simulation Applications," Appl. Math. Modelling, 137-140 (1976).

12. J. D. Cummins and M. H. Butterfield,"Application of Modern Control Theory in Nuclear Power," IAEA-SM-168 /B-8 (1975).

13. B. Friedland, Control System Design, McGraw-Hill, New York (1986).

14. B. C. Kuo, Automatic Control Systems, Prentice-Hall, Englewood Cliffs, N.J.(1982).

15. MATRIX$_x$ User's Guide, Integrated Systems, Inc., Version 5.0 (Oct. 1985).

16. Addendum to Hazard Summary Report on EBR-II, Argonne National Laboratory, ANL-5719. (Jan.1964) Authors: L. J. Koch, W. B. Lowenstein, H. O. Monson.

17. H. Kwakernaak and R. Sivan, Linear Optimal Control Systems, Wiley-Interscience, New York (1972).

18. Shih-Jen Wang, "Modeling And Simulation of Pressurized Water Reactor Power Plant," Ph.D. Dissertation, The University of Tennessee (June 1983).

19. J. C. Doyle, "Robustness of Multiloop Linear Feedback systems," Proceedings of the 17th IEEE Conference on Decision and Control (1978)

20. E. M. Dean, W. K. Lehto and H. A. Larson, "System Modeling And Simulation At EBR-II," Proceedings of the Sixth Power Plant Dynamics, Control & Testing Symposium, Knoxville, Tennessee (1986).

21. J. C. Cherng, "An Investigation of Feedwater Control and Nonlinear Effects for a U-Tube Steam Generator Model," M.S. Thesis, Nuclear Engineering Department, The University of Tennessee (Dec. 1978).

22. A. V. Campise, "Dynamic Simulation and Analysis of EBR-II Rod-Drop Experiments," ANL-7664, Argonne National Laboratory (March 1970).

23 Personal communication, E. E. Feldman [ANL].

APPENDICES

APPENDIX A

AUXILIARY CALCULATIONS

A.1 Boundary Flow Approximation

The development of a lumped-parameter steam generator model includes formulation of the two-phase flow phenomenon. In order to utilize the energy balance equation for the boiling region, the coolant flows (in and out) must be known in the form of state or algebraic variables. For a simple linear model such as the tea kettle model, these flows can be assumed to be constant; however, this assumption is not applicable for detailed studies due to an unacceptable comprimise in the accuracy. One of the practical methods for the treatment of the boundary flow (between boiling and subcooled regions) is to express the unknown boundary flow in terms of the available state variables such as the heat transfer rate and the latent heat of evaporation. Assuming a linear relationship, the boundary flow W_2 is written as follows.

$$W_2 = \frac{Q_{sc}}{h_f - h_{dc}} = \frac{U_{ms} \cdot A_{ms}(2T_{m2} - T_{dc} - T_f)}{2Cp(T_f - T_{dc})}$$

where

Q_{sc} = heat transfer rate into the subcooled region,

h_f = saturation enthalpy,

h_{dc} = subcooled region inlet enthalpy,

U_{ms} = heat transfer coefficient for tube metal subcooled water interface,

A_{ms} = heat transfer area,

T_{m2} = tube metal temperature.

Using the chain rule, the linearization around steady-state results in the following algebraic form.

$$W_2 = [WB1]\ T_{m2} + [WB2]\ T_{dc} + [WB3]\ P_B + [WB4]\ Z_{sc} \quad (A.1.2)$$

where
$$WB1 = \frac{\partial W_2}{\partial T_{m2}} = \frac{U_{ms} \cdot A_{ms}}{Cp(T_f - T_{dc})}$$

$$WB2 = \frac{\partial W_2}{\delta T_{dc}} = \frac{4CpU_{ms} \cdot A_{ms} \cdot (T_{m2} - T_f)}{(h_f - h_{dc})^2}$$

$$WB3 = \frac{\partial W_2}{\partial T_f} \left(\frac{\partial T_f}{\partial P_B} \right) = \frac{-\ 4CpU_{ms} \cdot A_{ms}\ (T_{m2} - T_{dc})}{(h_f - h_{dc})^2} \left(\frac{\partial T_f}{\partial P_B} \right)$$

$$WB4 = \frac{\partial W_2}{\partial Z_{sc}} = \frac{U_{ms} \cdot P_r\ (2T_m - T_{dc} - T_f)}{2(h_f - h_{dc})}$$

A.2 Heat Transfer

When the mean temperature of the tube metal lump is considered as a state variable the effective heat transfer coefficient can be expressed using the classical analogy between the flow of heat energy through thermal resistance to the flow of electrical current in an electrical resistor.

Refering to Fig. A1, the heat transfer rates are

$$\dot{Q}_{pm} = \frac{T_p - T_n}{R_o + R_m\left(\frac{A_{m2}}{A_o}\right)} = U_{pm} A_o (T_p - T_m) \qquad (A.2.1)$$

and

$$\dot{Q}_{ms} = \frac{T_n - T_s}{R_i + R_m\left(\frac{A_{m2}}{A_i}\right)} = U_{ms} A_i (T_m - T_s) \qquad (A.2.2)$$

From these equations

$$\frac{1}{U_{pm}} = \frac{1}{U_o} + \left(\frac{A_o}{A_{m2}}\right) \cdot \frac{1}{U_m} \qquad A_{m1} = \frac{A_M - A_i}{\ln\left(\frac{A_m}{A_i}\right)}$$

$$\frac{1}{U_{ms}} = \frac{1}{U_i} + \left(\frac{A_i}{A_{m1}}\right) \frac{1}{U_m} \qquad A_{m2} = \frac{A_o - A_m}{\ln\left(\frac{A_o}{A_m}\right)}$$

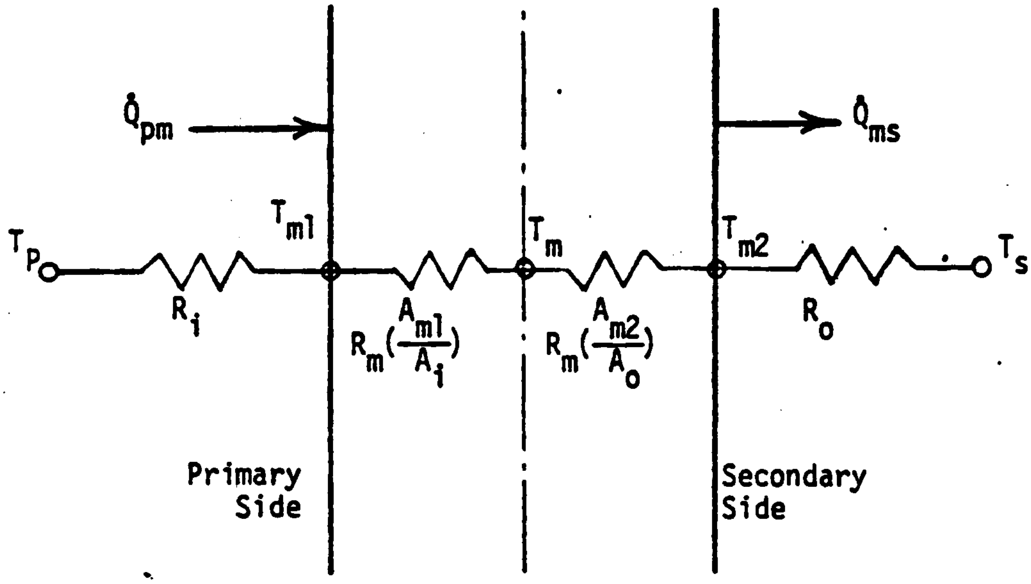

Fig. A.1 Heat Transfer .

The six different cases of heat resistances are calculated as follows.

1. No internal heat generation:

$$R = \frac{\ln r_o/r_i}{4\pi kL}$$

2. Annualar rings with same thermal conductivity, Q^{111} = constant:

$$R_{i,i+1} = \frac{(r_{i+1}^2 - r_{i-1}^2)/r_i^2}{8\pi kL}$$

3. Annular rings with different thermal conductivity, Q^{111} = constant:

$$R_{i,i+1} = \frac{1}{8\pi L}\left[\frac{r_{i+1}^2 + r_i^2}{k_{i+1} r_i^2} - \frac{r_i^2 + r_{i-1}^2}{k_i r_i^2}\right]$$

4. Annular ring closest to the surface of the cylinder, Q^{111} = constant:

$$R_{so} = \frac{(r_s^2 - r_{s-1}^2)/r_s^2}{8\pi kL}$$

5. Clad node average-to-clad surface:

$$R_{cas} = \frac{\ell u \ r_o/r_i}{r\pi kL}$$

6. Fluid film resistnce:

$$R_f = \frac{1}{h2^{\pi} r_o L}$$

where

r_o = outer diameter,

r_i = inner diameter,

k = thermal conductivity,

L = length of heat transfer area.

The overall heat transfer coefficients are calculated using the following correlations:

1- Chen's correlation [7] for the boiling region.

2- Dittus-Boelter correlation [8] for the single-phase heat transfer regimes.

3- Lyon-Martinelli correlation [8] for the liquid sodium.

APPENDIX B

CAPABILITIES OF MATRIX_X

B.1 Introduction

Matrix_X provides several tools for performing classical control analysis. These tools include commands for generating root loci, Bode plots, Nyquist diagrams, Nichols plots, and gain-phase margins. Control analysis and design of linear time-invariant state-space systems are also available in MATRIX_X. It provides capabilities for pole placement for single-input systems and linear-quadratic-Gaussian (LQG) design for continuous-time and discrete-time systems. All of the control design commands provide tools for constructing time-invariant controllers.

Most state-space control designs are based on systems that are both controllable and observable.

B.2 Design Commands

B.2.1 Stability

Stability is determined by computing the eigenvalues (poles) of the plant. For a closed-loop system matrix, SCL with NSCL states, the desired eigenvalues are computed as follows:

```
EIG(SPLIT(SCL,NSCL))
```

B.2.2 Linear Regulator Design

The REGULATOR command computes optimal constant gain, state-feedback matrices for continuous-time system under the assumption of full state feedback. Examples of the REGULATOR command are

```
[EVAL,KR]  =REGULATOR(A,B,RXX,RUU,RXU)
[EVAL,KR,P]=REGULATOR(A,B,RXX,RUU,RXU)
```

Inputs to the REGULATOR command include the A and B (plant and input) components of the continuous-time system matrix,

$$S = \begin{bmatrix} A & B \\ C & D \end{bmatrix}$$

and the design weighting matrices R_{xx}, R_{uu}, and R_{xu}, where R_{xu} is optional. The design weighting matrices provide weights on the states (x) and controls (u) as defined by the quadratic cost function. R_{uu} must be positive definite and R_{xx} must be positive semi-definite.

Outputs from the REGULATOR command are the closed-loop eigenvalues (EVAL), the optimal regulator state-feedback gain matrix (KR), and optionally, the Riccati solution matrix (P). The closed-loop eigenvalues are obtained from the closed-loop plant (A-B*KR). The matrix dimensions of the gain matrix, KR, are equal to the number of system inputs by the number of system states.

B.2.3 Kalman Filter Design

The ESTIMATOR command calculates constant, optimal state-estimator gain matrices for continuous-time systems. Examples of the ESTIMATOR command are:

```
[EVAL,KE]=ESTIMATOR(A,C,QXX,QYY,QXY)
[EVAL,KE,P]=ESTIMATOR(A,C,QXX,QYY,QXY)
```

Inputs to the ESTIMATOR command include the A and C (plant and observation) components of the continuous-time system matrix,

$$S = \begin{bmatrix} A & B \\ C & D \end{bmatrix}$$

and the noise covariance matrices Q_{xx}, Q_{yy}. Q_{xy} is optional. Q_{yy} has matrix dimensions equal to the number of plant outputs and must be positive definite, while Q_{xx} has matrix dimensions equal to the number of plant states and must be positive semi-definite. In many cases the input disturbances and output noises are uncorrelated so that $Q_{xy}=0$.

Outputs from the ESTIMATOR command are the estimator eigenvalues (EV AL), the optimal estimator gain matrix (KE), and optionally, the state estimation error covariance matrix (P). The estimator eigenvalues are obtained from (A-KE*C). The dimensions of the gain matrix KE are equal to the number of system outputs.

B.2.4 Compensator Synthesis (LQGCOMP)

The LQGCOMP command computes the system matrix for the optimal output feedback compensator. The optimal compensator is a combination of the optimal state estimator, which reconstructs the system states, and optimal regulator, which provides a linear state-feedback control law. The form of the LQGCOMP command is:

[SC,NSC]=LQGCOMP(S,NS,KR,KE)

Inputs to the LQGCOMP command are the optimal regulator and estimator gain matrices (KR and KE) and the continuous-time design system (S) with number of states (NS). The LQGCOMP assumes that both KR and KE were designed from the system matrix, S.

Output from the LQGCOMP includes the continuous-time compensator system matrix (SC) and the corresponding number of states (NSC).

$$SC = \begin{bmatrix} A_2 & B_2 \\ C_2 & D_2 \end{bmatrix}$$

$$A_2 = A_1 - K_E . C_1 - B_1 . K_R$$

$$B_2 = K_E$$

$$C_2 = K_R$$

$$D_2=0$$

where A_1, B_1 and C_1 are the open-loop system matrices.

B.2.5 Closed-Loop Performance Analysis

The closed-loop dynamic system can be constructed with the FEEDBACK or APPEND and CONNECT comands, or with the SYSTEM-BUILD graphical modeling and simulation tool . Using the FEEDBACK command, the components of the closed-loop system matrix (SCL) are as follows

$$SCL = \left[\begin{array}{cc|c} A_1 & -B_1C_2 & B_1 \\ B_2C_1 & A_2 & 0 \\ \hline C_1 & 0 & 0 \end{array}\right]$$

B.3 Simulation Commands

B.3.1 Representation of Dynamic Systems

Consider the following linear system,

$$\dot{\underline{X}} = A\underline{X} + \underline{B}u$$

$$y = C\underline{X} + \underline{D}u$$

where $\underline{X}$ is a vector of state variables, y is a vector of measurements and u is a forcing function. A, B, C and D are the constant system matrices (see Eq. 5.1). The above state-space representation of a linear dynamic system can be loaded to the computer using the following MATRIX_X syntax

```
S=[A,B;C,D]
```

where S is a matrix representing the overall system. The number of states should be specified by an arbitrary variable.

The representation of systems in the transfer function domain is also possible. Consider the following transfer function.

$$G(s) = \frac{a_1\ s^2 + a_2\ s + a_3}{b_1\ s^3 + b_2\ s^2 + b_3\ s + b_4}$$

where

a_i, i=1,..,3 = Numerator coefficients

b_i, i=1,..,4 = Denominator coefficients

G(s)= Transfer function in Laplace domain.

The $MATRIX_X$ syntax for the representation of this transfer function can be made as follows.

NUM=[0 a_1 a_2 a_3]

DEN=[b_1 b_2 b_3 b_4]

where NUM and DEN are arbitrary variable names. The order of the transfer function should be specified by an arbitrary variable.

A transformation from one type of representation to another is also possible with $MATRIX_X$ (see user's manual for details, ref.[15]).

B.3.2 Simulation Commands

Once the linear system representation in $MATRIX_X$ is completed the transient simulations can be performed using the following commands.

```
[T,Y]=STEP(S,NS,TMAX,NPTS)
```

or

```
[T,Y]=STEP(NUM,DEN,TMAX,NPTS)
```

The outputs of this command are the time vector T and the Y matrix which is the step responses of the linear system. Y matrix has a number of columns equal to the number of states and a number of rows equal to the number of time points.

The inputs of the simulation commands are the overall system representation either in state-space form or in transfer function form. TMAX specifies the length of time and NPTS specifies the number of points to be calculated. The default integration algorithm is the "variable Kutte-Merson" [15]. The variable Kutte-Merson integration is an explicit, fourth order, one-step method. The integration step is optimized to provide the largest step while remaining within the local error tolerances. The maximum step size is equal to the time increment. The choice of NPTS determines the time increment and this integration technique retains the stability of the solution regardless of any arbitrary choice of NPTS.

The linear system should be stable, otherwise the solution will diverge. In order to check the stability, user can calculate the eigenvalues of the system matrix A using the command explained in Sect. B.2.1.

B.4 System_Build Option

System_Build is a menu driven, interactive graphical environment for building, modifying and editing computer simulation models. Accessing the System_Build can be done from the $MATRIX_x$ prompt. The different dynamic models represented in $MATRIX_x$ can be appended in a hierarchical structure using the System_Build capabilities. In this section, an example of the construction of large scale dynamic models using System_Build is presented. Other capabilities of this software are explained in Ref.[15].

The two modules of the EBR-II (the primary system model and the steam generator model) are considered. Despite the fact that these models are not too large to be coupled in the $MATRIX_x$ environment, the coupling is made using the System_Build methods to provide an example for future applications. The combined structure is obtained by the following steps.

STEP	Explanation	MENU	SELECTION
1-	Edit Super Block	Top	2
2-	Name the Overall system	Name:	EBR-II
3-	Continous system	Sample Period:	0
4-	First Block definition	Describe Blocks	1
		Location:	1
5-	It is a dynamic system	Type of Block	6
6-	State-space representation	Dynamic Systems	3
7-	Name the first block	Specifications	Primary
8-	Specify the number of inputs (2)	Specifications	2
9-	Specify the number of outputs (37)	Specifications	3
10-	Specify the number of states (37)	Specifications	4
11-	Load the system matrix S_1	Specifications	5
		System Matrix:	S1
		Zero Initial states?	Y
12-	Go to the previous menu		UNDO
13-	Second Block definition	Describe Blocks	1
		Location:	3
14-	It is a dynamic system	Type of Block	6
15-	State space representation	Dynamic Systems	3

16-	Name the Second Block	Specifications	Stgen
17-	Specify the number of inputs(2)	Specifications	2
18-	Specify the number of outputs(18)	Specifications	3
19-	Specify the number of states(18)	Specifications	4
20-	Load the system matrix S_2	Specifications	5
		System Matrix:	S2
		Zero Initial states?	Y
21-	Go to the previous menu		UNDO
22-	Necessary connections	Describe Blocks	5
23-	Internal and External connections	Connect Blocks	1,2,3

(The connections are made in a graphical environment which is invoked by the connect menu)

24-	Go to the Top menu	Connect Blocks	UNDO
		Describe Blocks	TOP
25-	Analyze the structure	TOP	6
		Name:	EBR-II
		Sample Period:	0

Upon completing these steps, the overall EBR-II system model including the primary model in location 1 and the steam generator model in location 3 is ready for simulation studies. The superblock EBR-II is shown in Fig. B1. The following command can be used for simulation.

Y=SIM(T,U)

where Y is the output matrix as explained in the previous section. U is the input time vector. The dimensions of T and U must match. For a step input case U vector contains equal entries for each time step. Note that using this feature any kind of input can be applied by the user defined U vector.

The System_Build option also includes different integration algorithms. The menu contains the following selections:

1) Euler Integration
2) RK2 (Modified Euler)
3) Runga-Kutta 4th order
4) Fixed Kutta-Merson
5) Variable Kutta-Merson (Default)
6) Stiff system solver

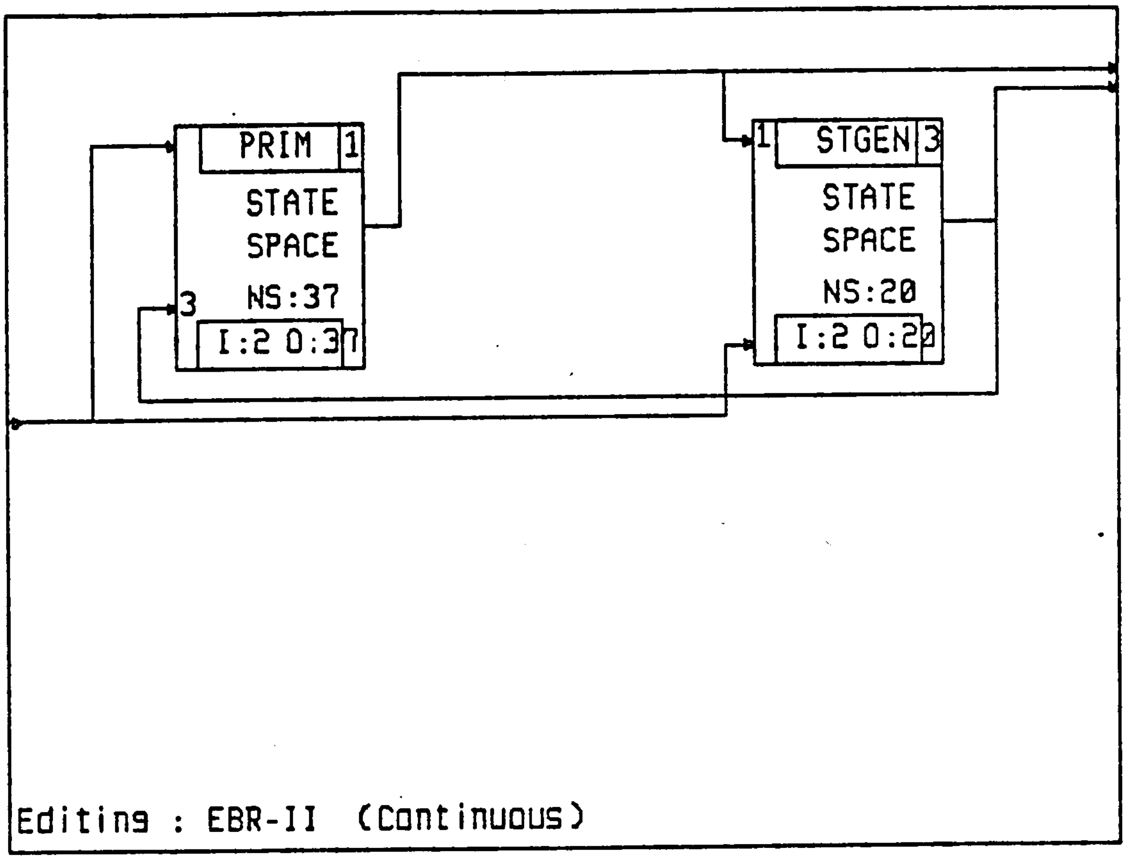

Fig. B.1 Coupling the Primary and Steam Generator Models Using System Build.

B.5 Macros Used for Design Studies

B.5.1 LQG design

```
BI=[BFPD;DD],...
[EVAL,KR]=REGULATOR(A20,B20,RXX,RUU),...
[EVAL,KE]=ESTIMATOR(A20,C20,QXX,QYY),...
[SC,NSC]=LQGCOMP(S20,20,KR,KE),...
[SCL,NSCL]=FEEDBACK(S20,20,SC,NSC],...
[AA,BB,CC,DD]=SPLIT(SCL,NSCL),...
PLANT=[AA,BI;CC,DD],...
[T,Y]=STEP(PLANT,NSCL,400),...
I=18;]MP1[,...
I=19;]MP3[,...
BI=[],...
```

```
A20= System matrix listed in Table 4.5 with one modification,...
     The last row elements are equal to zero, except the 18th column,
     which is equal to 1. (dummy state),...
B20= 20x1 vector all zeros except the 19th row equal to 1,...
BFPD= Forcing vectors of Table 5.2 extended to row number 20,...
C20 = 20x20 unity matrix,...
D20 = B20*0,...
S20 = System matrix=[A20,B20;C20,D20],...
MP1 = Graphic macro,...
MP2 = Graphic macro,...
```

B.5.2 Tuning Three-Element controller gains

```
> M(20,18)=-K1,...
  M(20,10)=-K2*0.05371,...
  M(20,19)=K2,...
  N(20,18)=KI*K1,...
  N(20,10)=K2*KI*0.05371,...
  N(20,19)=-K2*KI,...
  AFIN=INV(M)*N,...
  EIG(AFIN),...
  K1K2KI=[K1,K2,KI],...
  (if the eigenvalues have negative real parts then:),...
  SFIN=[AFIN,BF;CF,DF],...
  (testing the controller performance),...
  [T,YFIN]=STEP(SFIN,20,TMAX),...
  Y=YFIN,...
  ]MPL[,...
```

B.5.3 Optimal Tracking Design

```
<> MA=[A,E;Z1],...
   [EVAL,KR,P]=REGULATOR(A,B.RXX,RUU),...
   AC=A-B*KR,...
   AC=AC',...
   M2=-INV(AC)*P*E,...
   KR2=INV(RUU1)*B'*M2,...
   MKR=[KR,KR2],...
   MS=[MA,MB;MC,MD],...
   [EVAL,KE]=ESTIMATOR(MA,MC,MQXX,MQYY),...
   [SC,NSC]=LQGCOMP(MS,NMS,MKR,KE),...
   [SCL,NSCL]=FEEDBACK(MS,NMS,SC,NSC),...
   [T,MY]=STEP(SCL,NSCL,TMAX),...
   Y=MY,...
   ]MPL[,...
```

B.5.4 Graphics

```
<> ]MP1[,I=I+1;]MP2[,I=I+1;]MP3[,I=I+1;]MP4[,...
   (macro MP),...
   PLOT(T,Y(:,I),'UPPER LEFT/NOGRID'),...
   (macro MP2),...
   PLOT(T,Y(:,I),'LOWER LEFT/NOGRID'),...
   (macro MP3),...
   PLOT(T,Y(:,I),'UPPER RIGHT/NOGRID'),...
   (macro MP4),...
   PLOT(T,Y(:,I),'LOWER RIGHT/NOGRID'),...
```

APPENDIX C

SUMMARY OF TRANSIENT RESPONSES

The outputs of the transient simulations performed in this study are presented in this section. The organization of the figures is explained in Table C1.

TABLE C1

Organization of the Results

FIGURE	
C.1	Step Responses of Open-loop Primary Model to a -5 cents Reactivity Perturbation.
C.2	Step Responses of Open-loop Primary Model to a +10 F IHX Inlet Sodium Temperature Perturbation.
C.3	Step Responses of Open-loop Steam Generator Model to a +10 F Feedwater Temperature

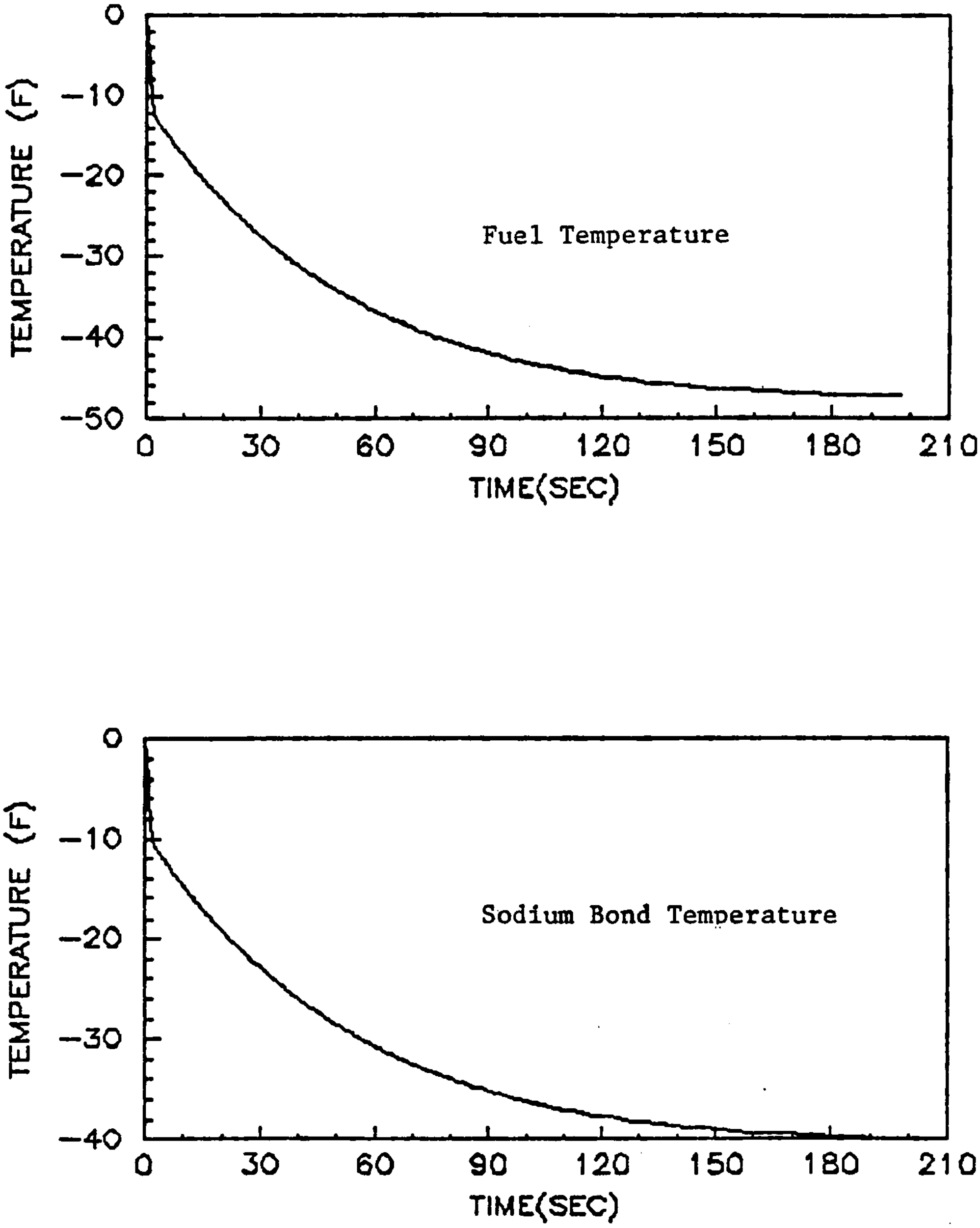

Fig. C.1 Step Responses of Open-loop Primary Model to a -5 cents Reactivity Perturbation.

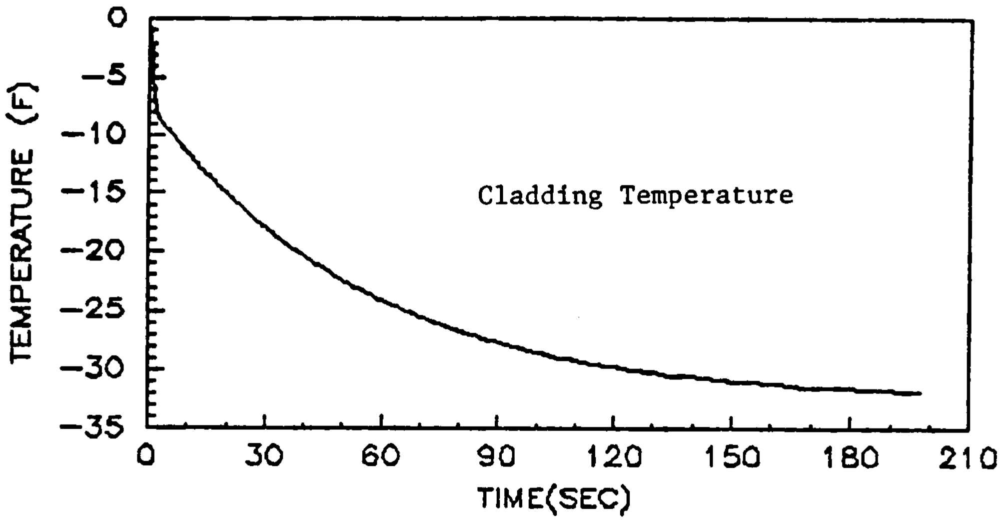

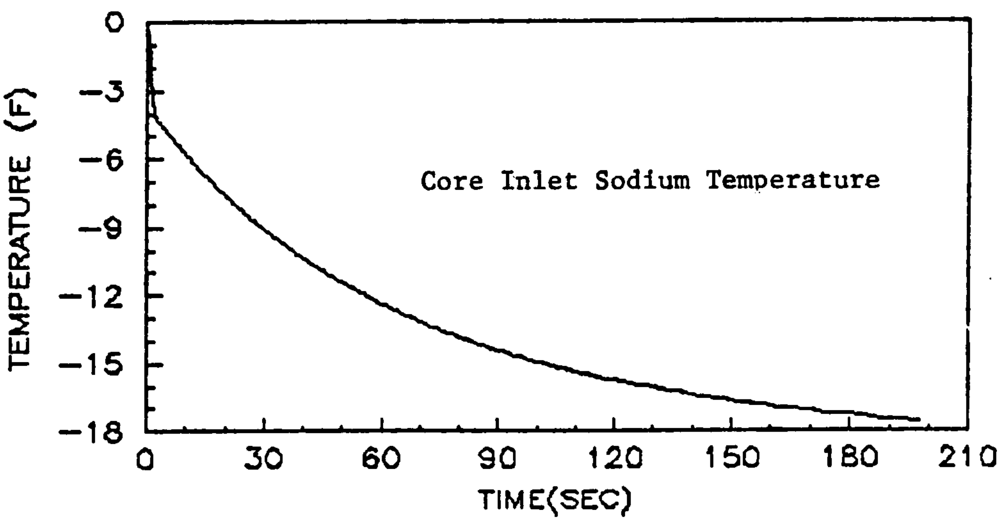

Fig. C.1 Step Responses of Open-loop Primary Model to a -5 cents Reactivity Perturbation.

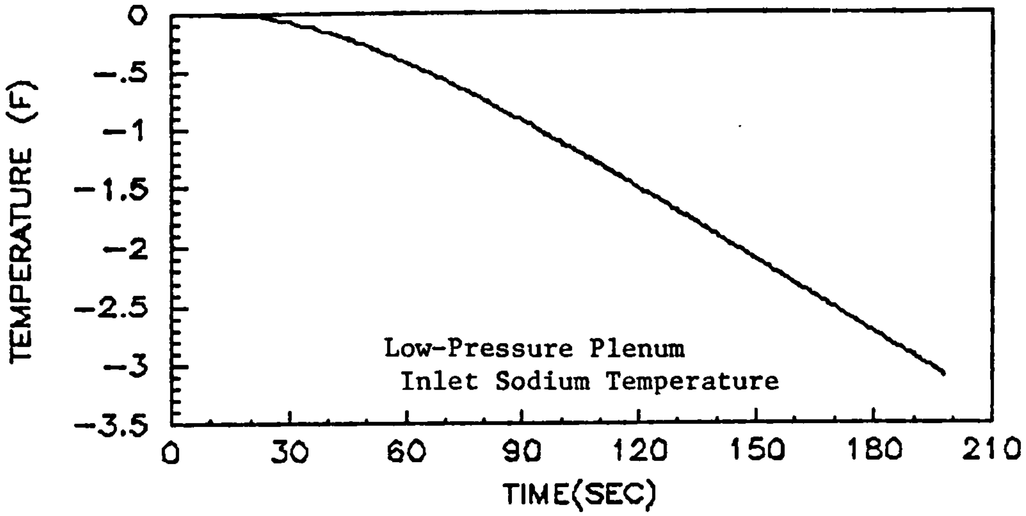

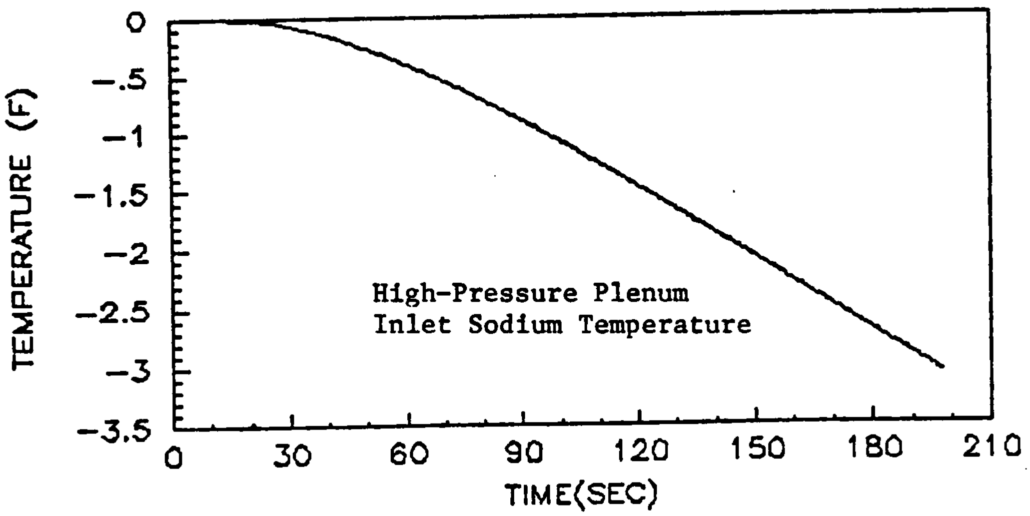

Fig. C.1 Step Responses of Open-loop Primary Model to a -5 cents Reactivity Perturbation.

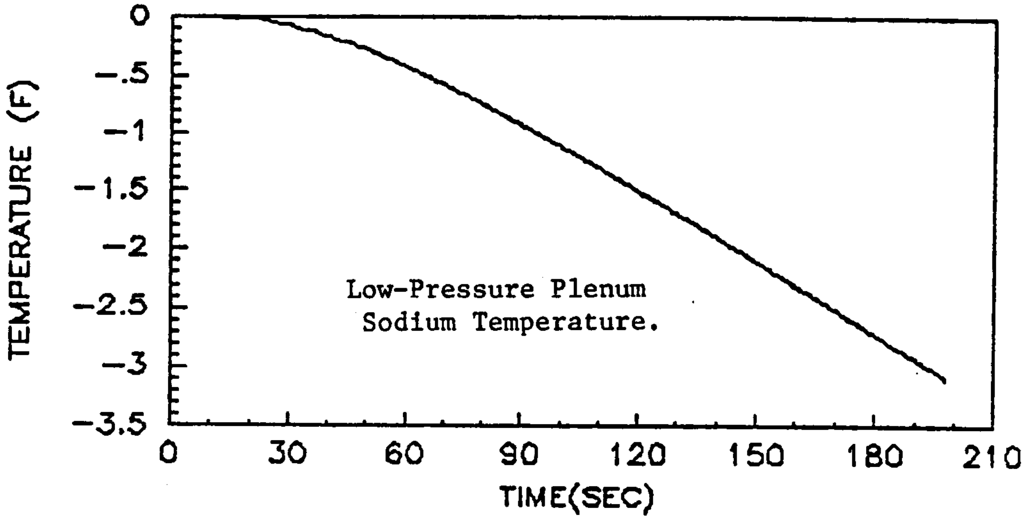

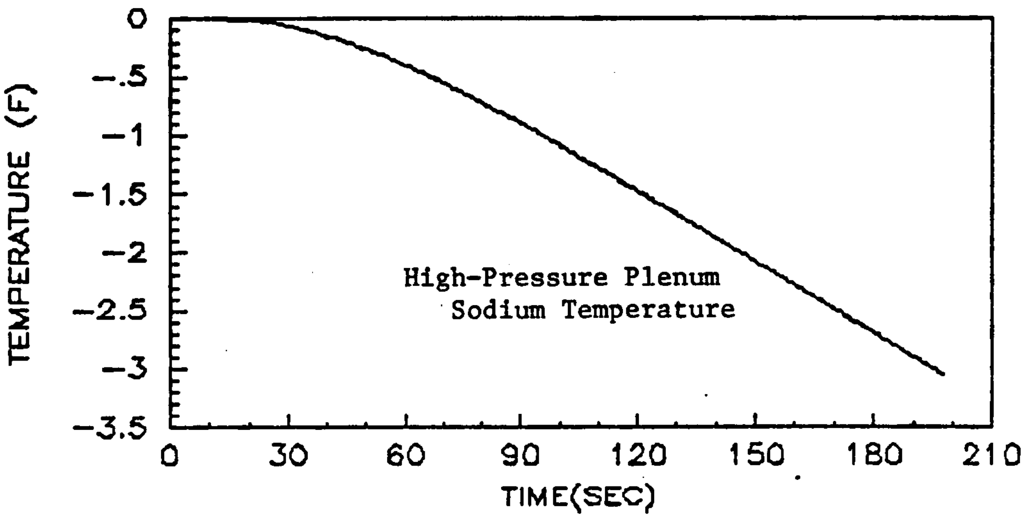

Fig. C.1 Step Responses of Open-loop Primary Model to a -5 cents Reactivity Perturbation.

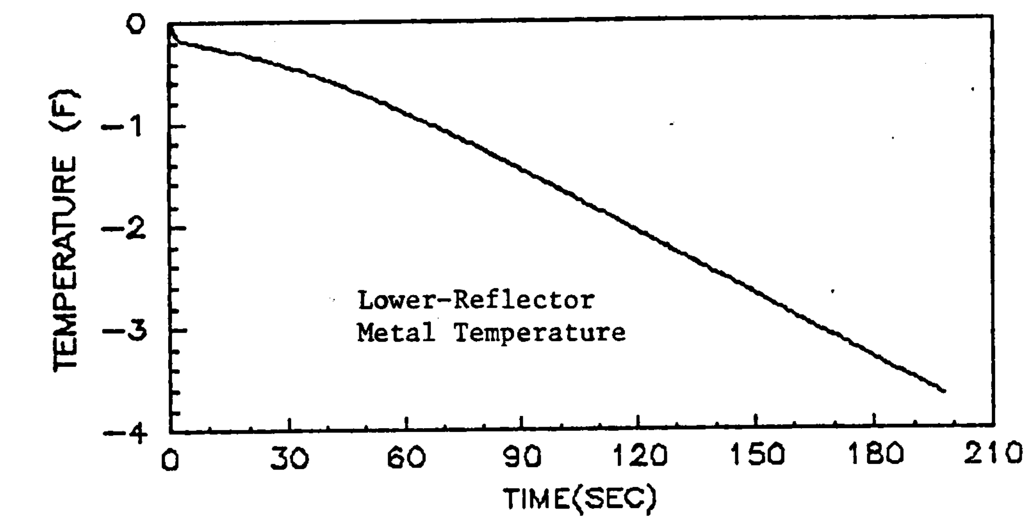

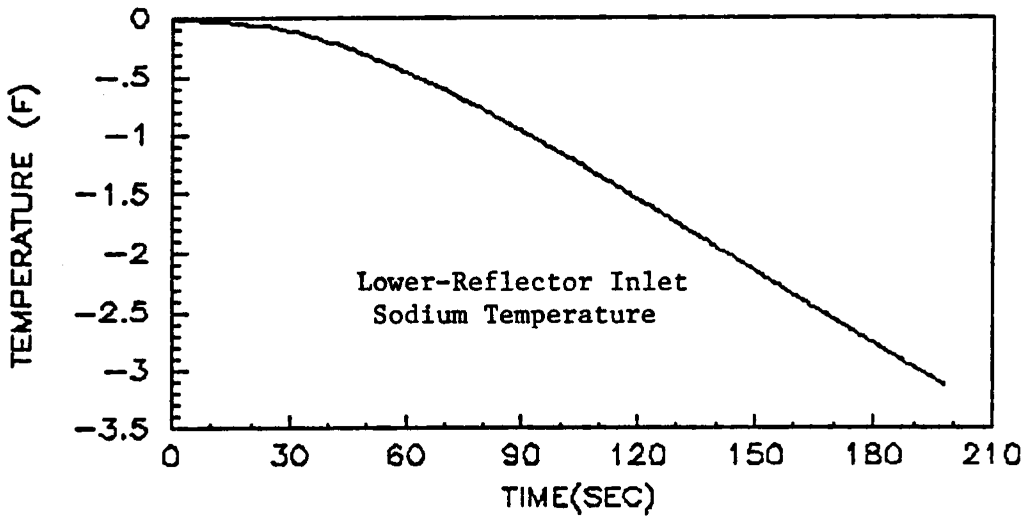

Fig. C.1 Step Responses of Open-loop Primary Model to a -5 cents Reactivity Perturbation.

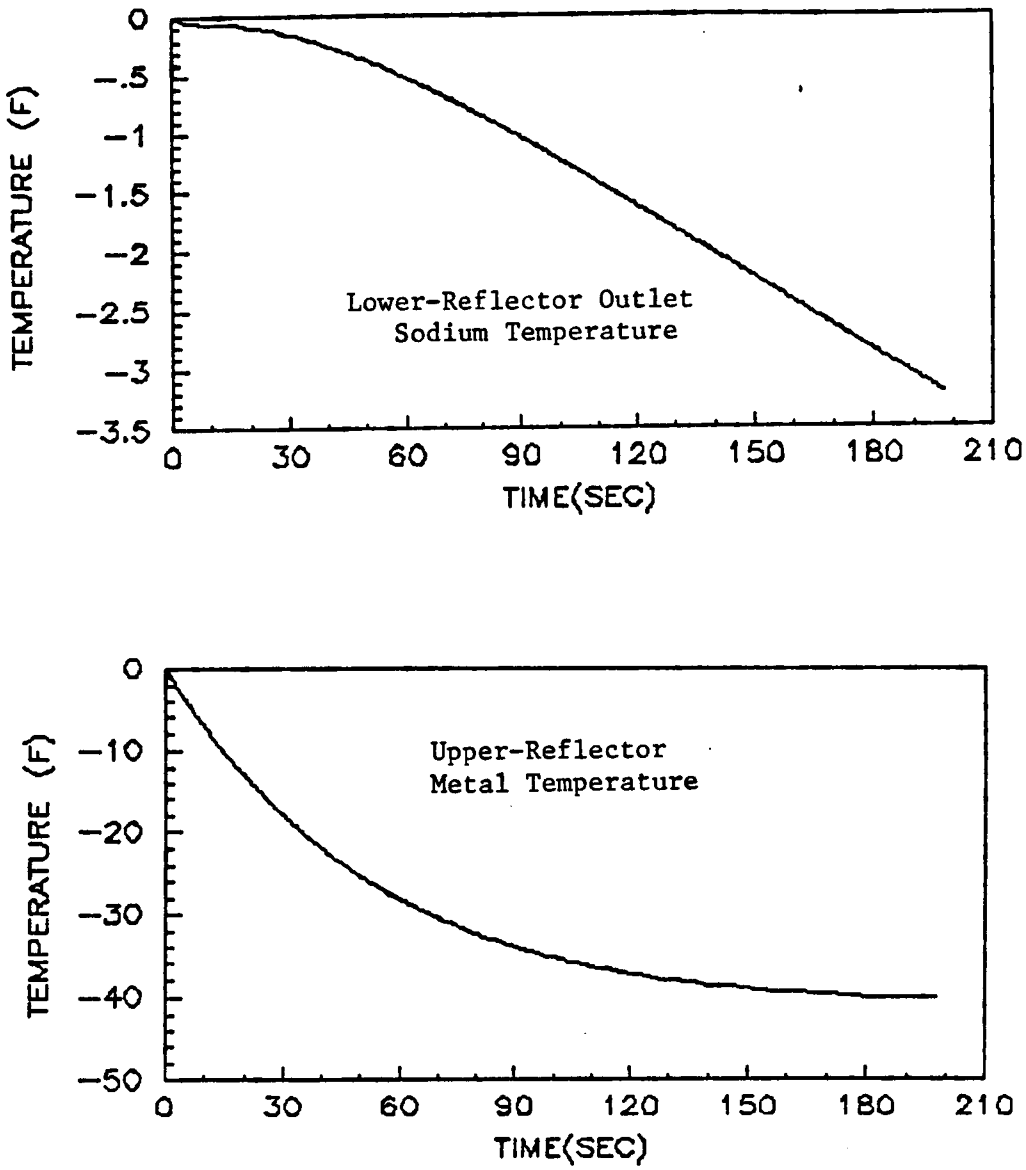

Fig. C.1 Step Responses of Open-loop Primary Model to a -5 cents Reactivity Perturbation.

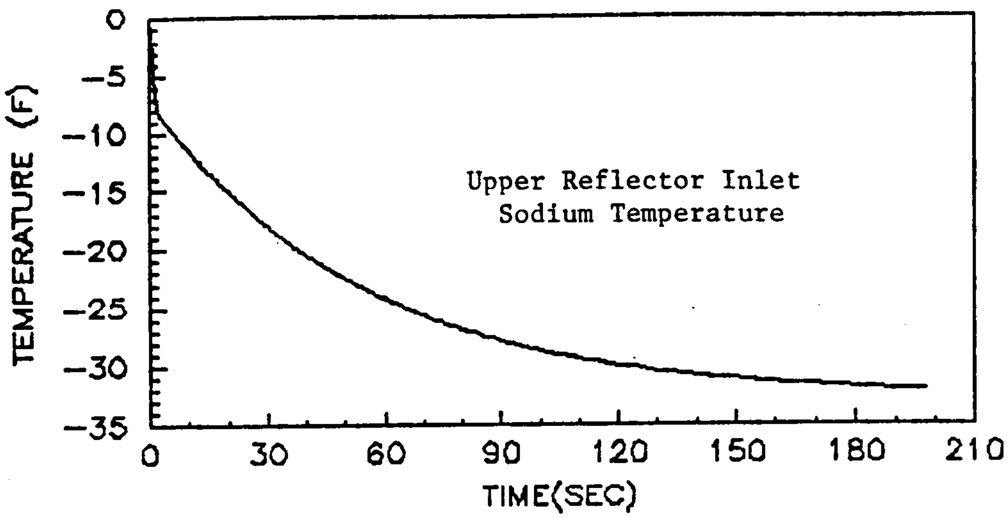

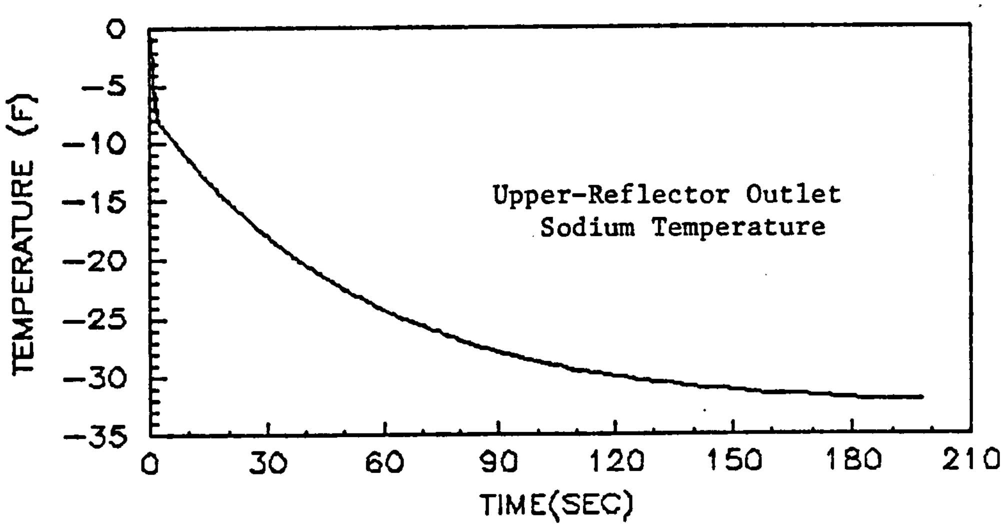

Fig. C.1 Step Responses of Open-loop Primary Model to a -5 cents Reactivity Perturbation.

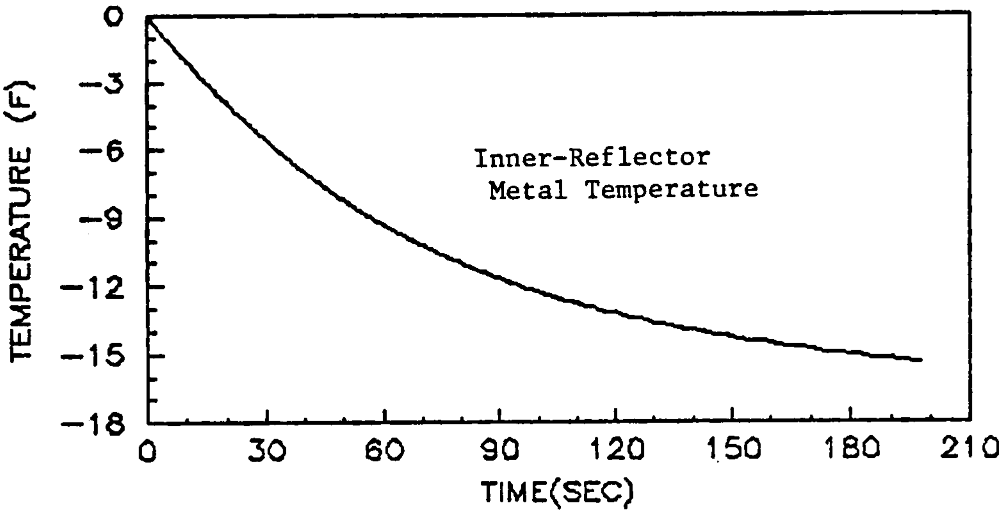

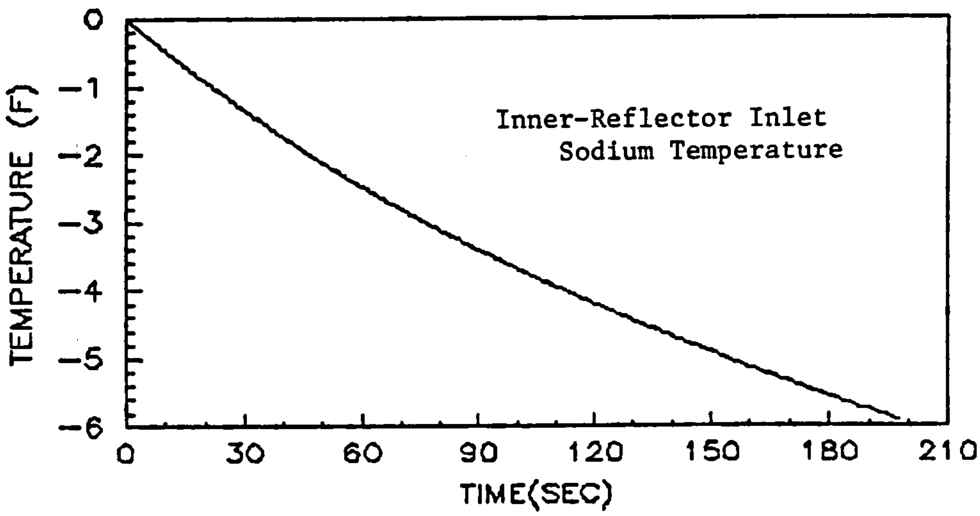

Fig. C.1 Step Responses of Open-loop Primary Model to a -5 cents Reactivity Perturbation.

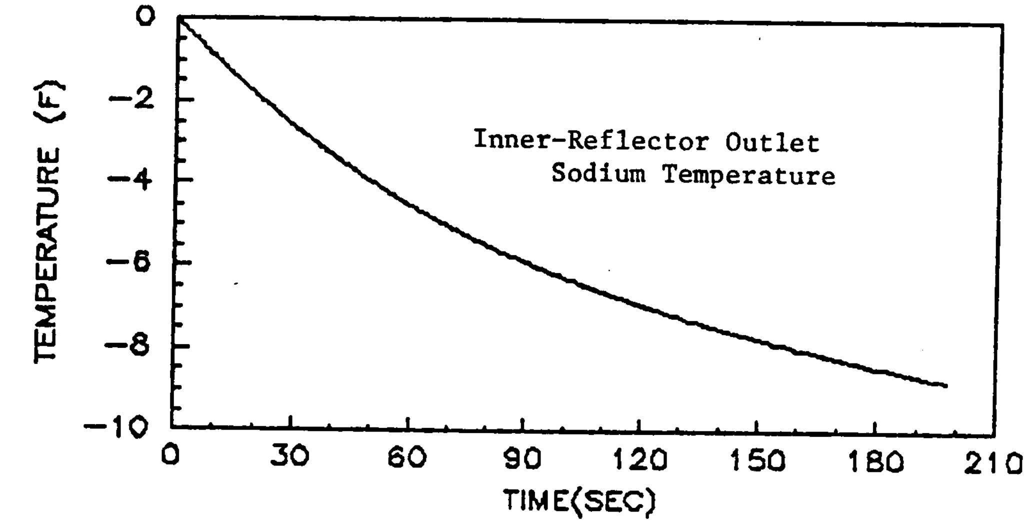

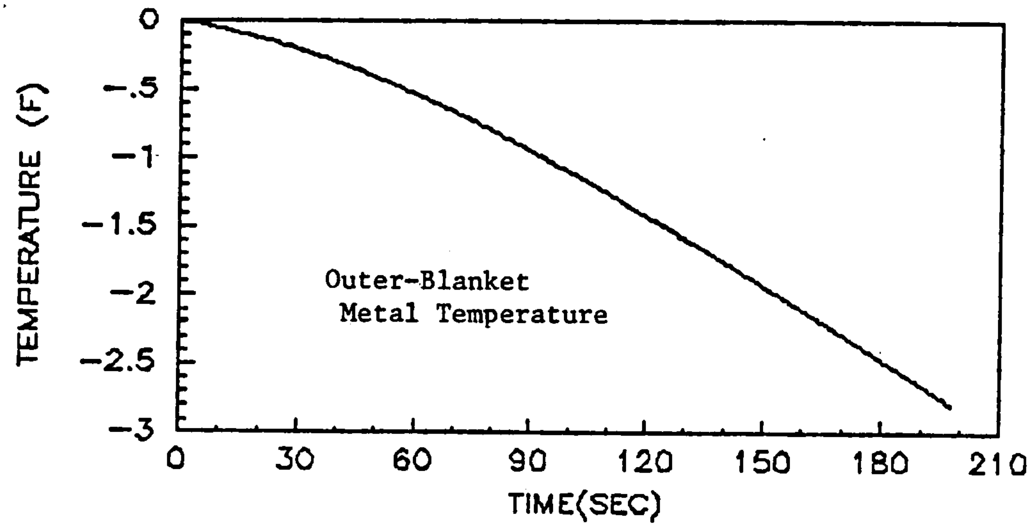

Fig. C.1 Step Responses of Open-loop Primary Model to a -5 cents Reactivity Perturbation.

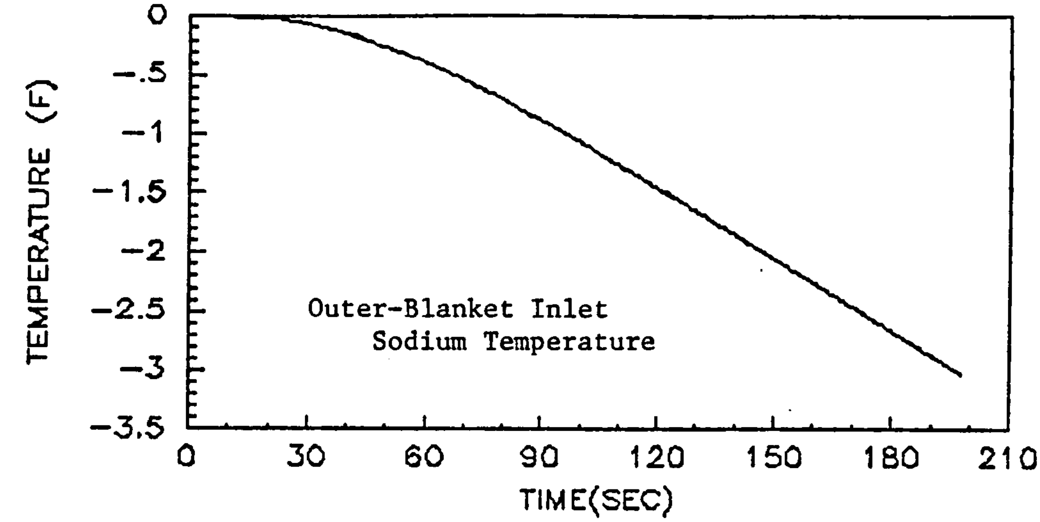

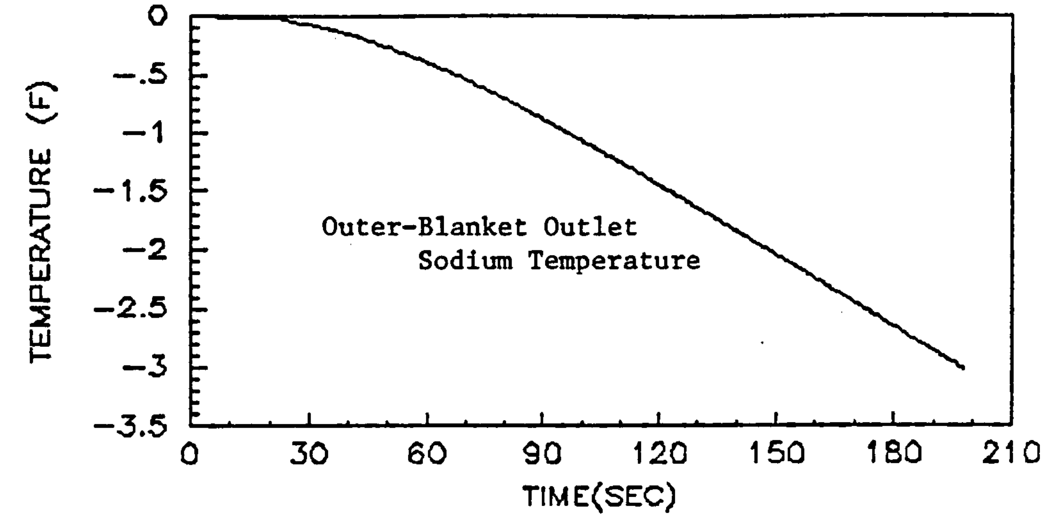

Fig. C.1 Step Responses of Open-loop Primary Model to a -5 cents Reactivity Perturbation.

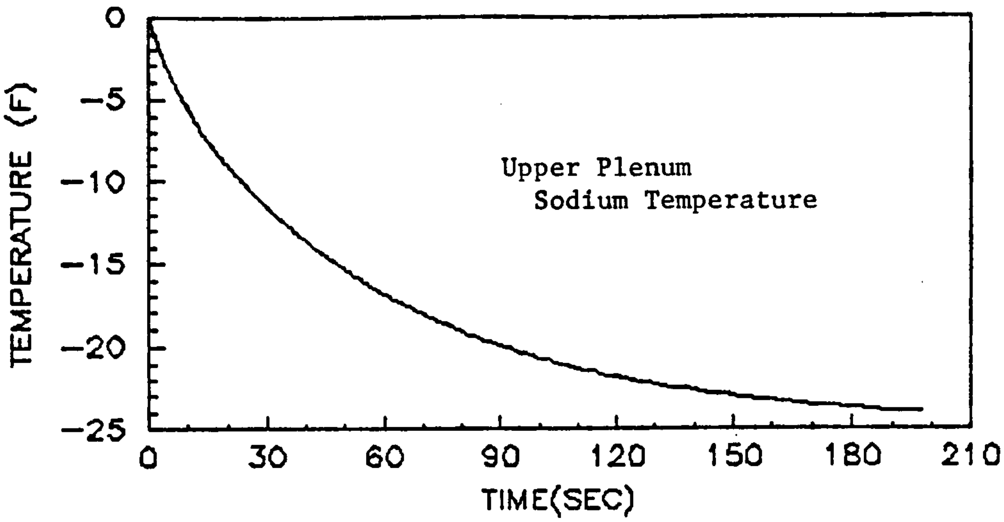

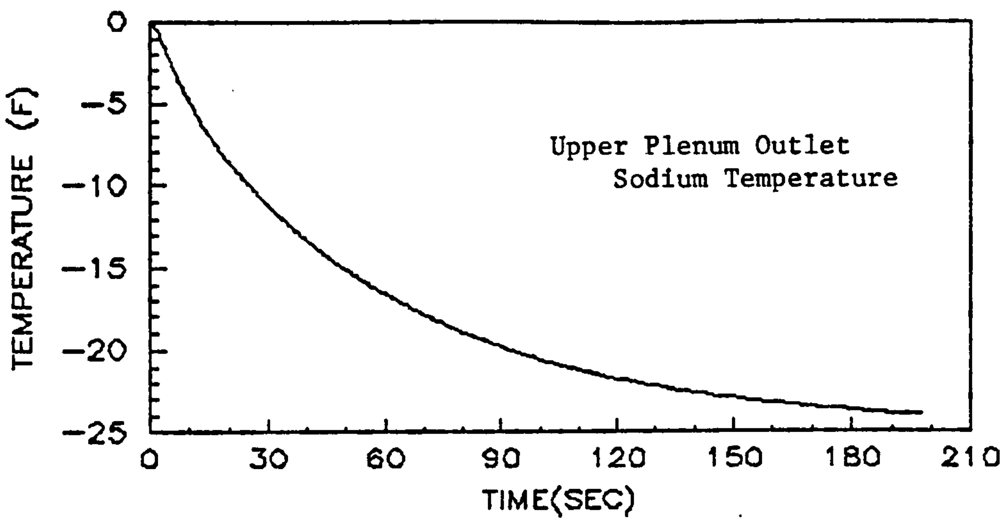

Fig. C.1 Step Responses of Open-loop Primary Model to a -5 cents Reactivity Perturbation.

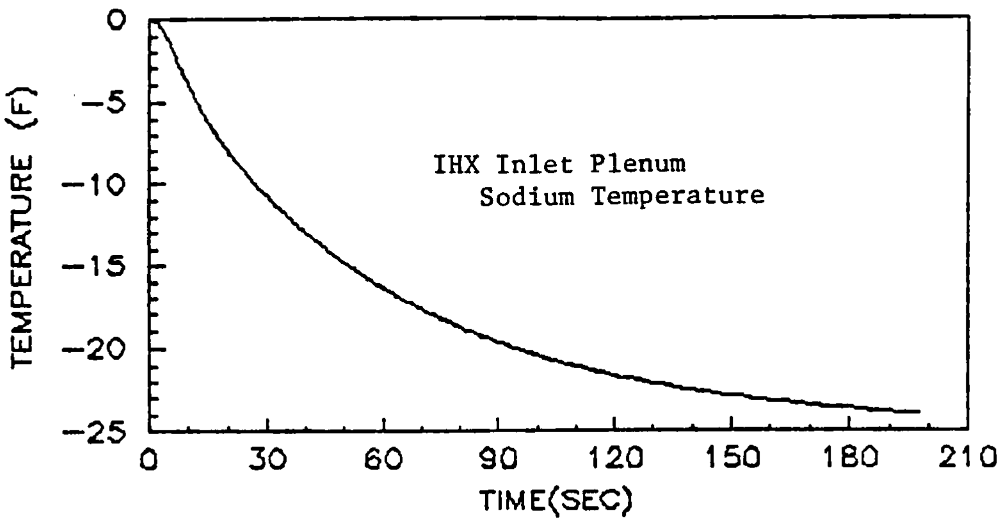

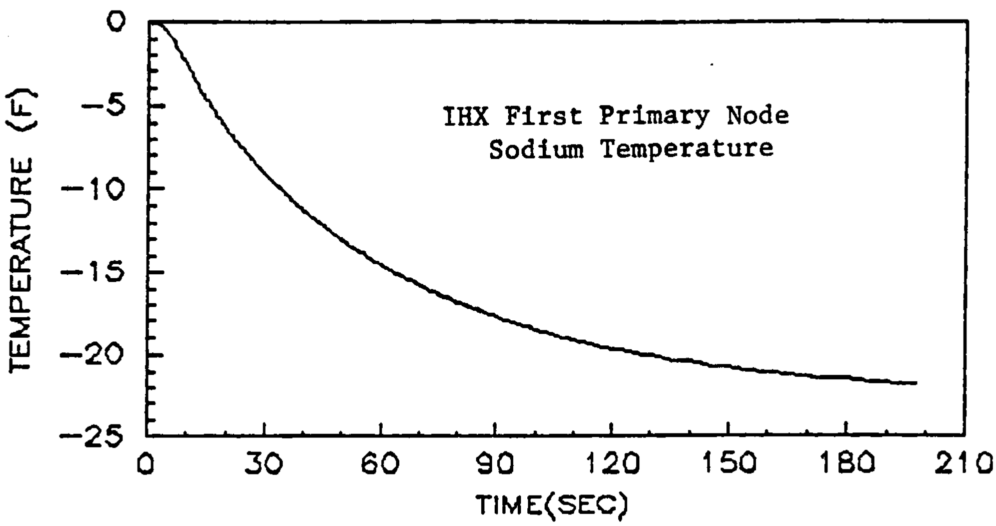

Fig. C.1 Step Responses of Open-loop Primary Model to a -5 cents Reactivity Perturbation.

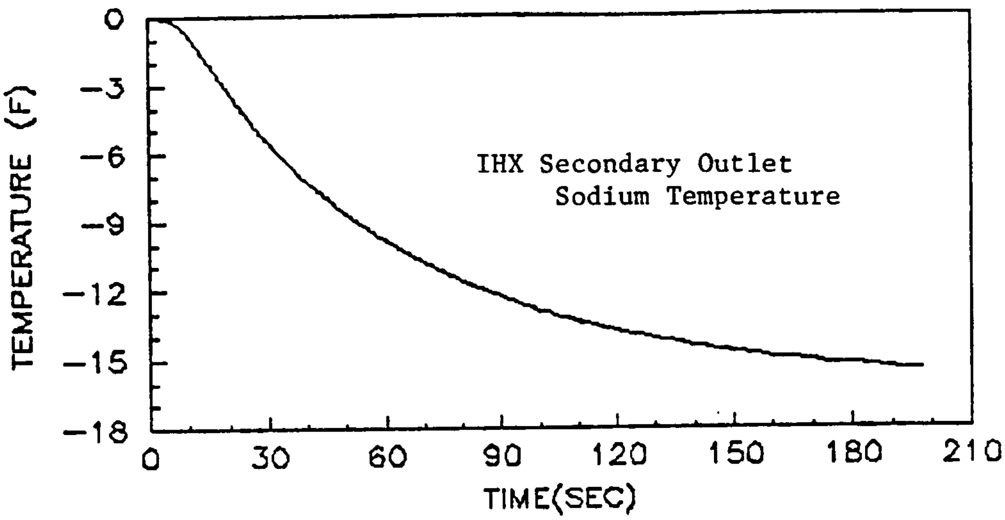

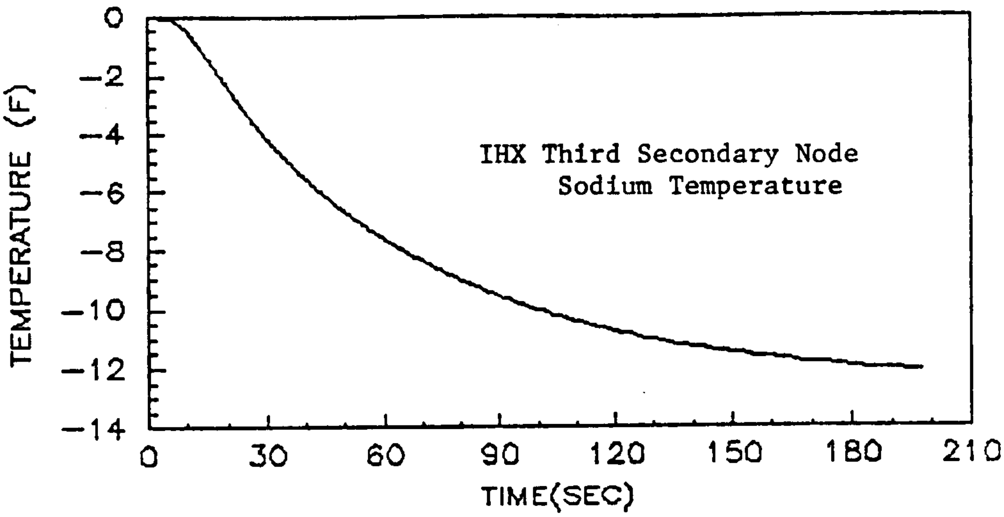

Fig. C.1 Step Responses of Open-loop Primary Model to a -5 cents Reactivity Perturbation.

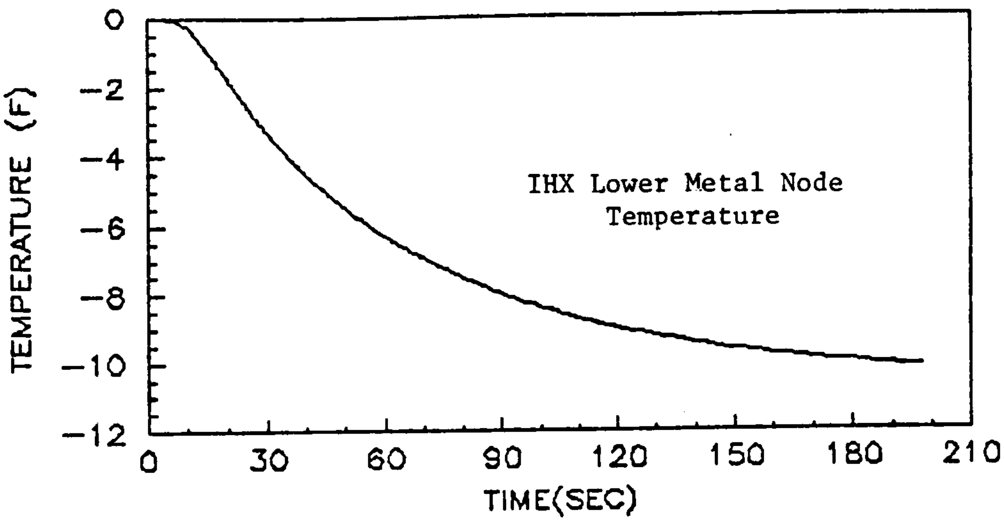

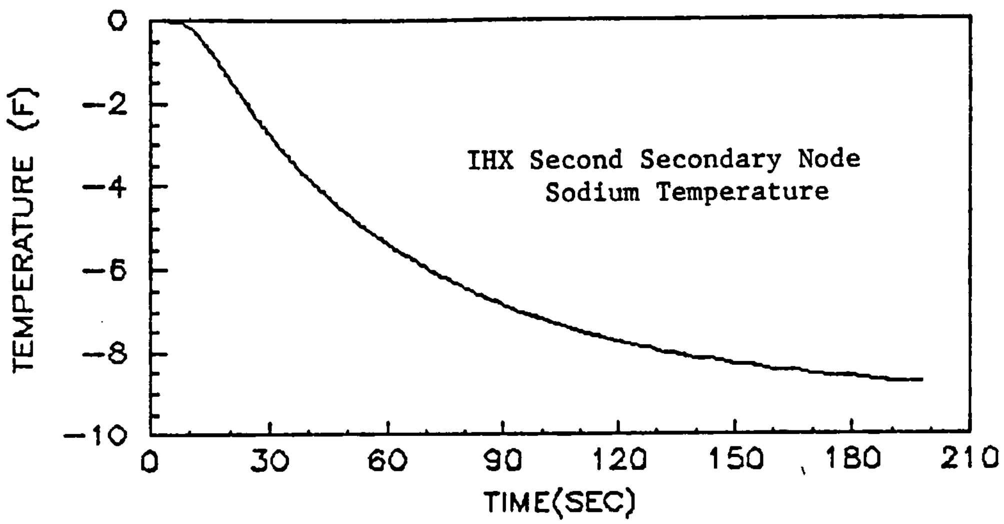

Fig. C.1 Step Responses of Open-loop Primary Model to a -5 cents Reactivity Perturbation.

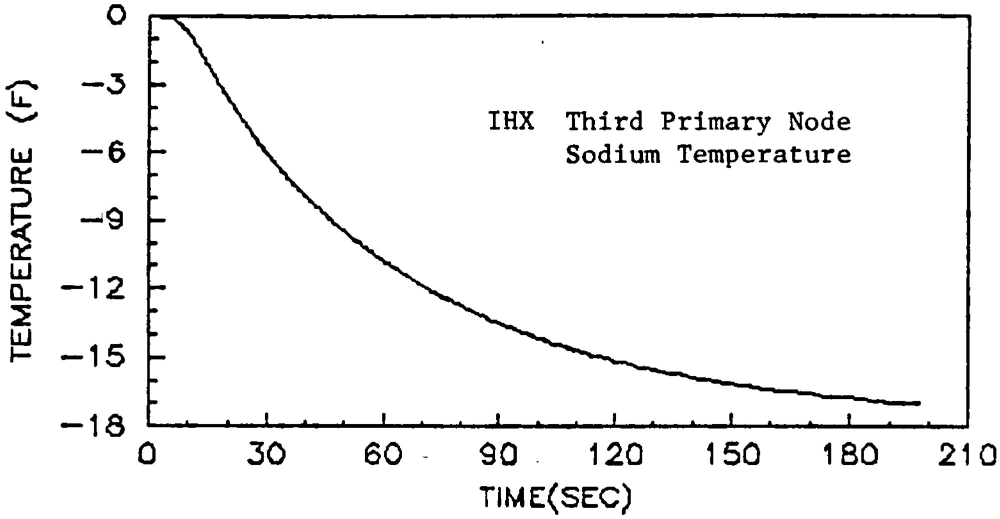

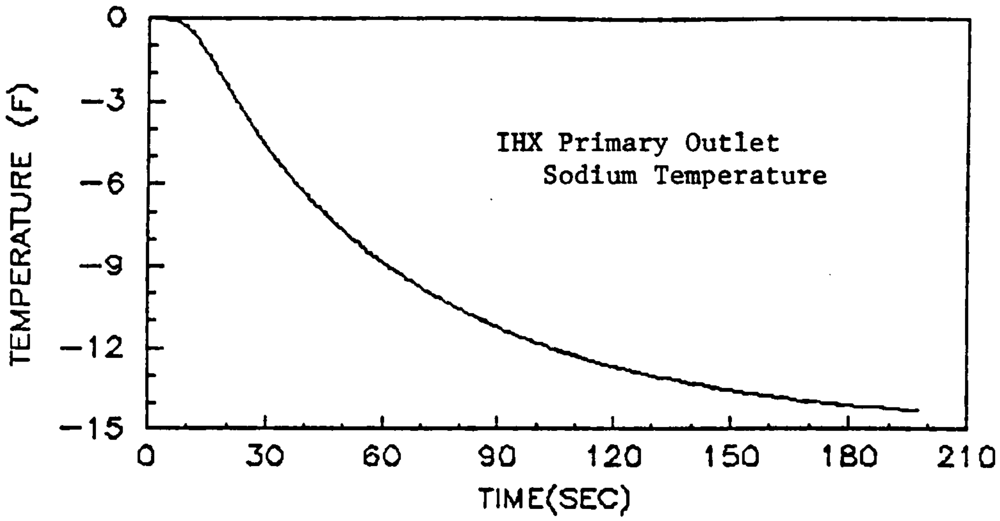

Fig. C.1 Step Responses of Open-loop Primary Model to a -5 cents Reactivity Perturbation.

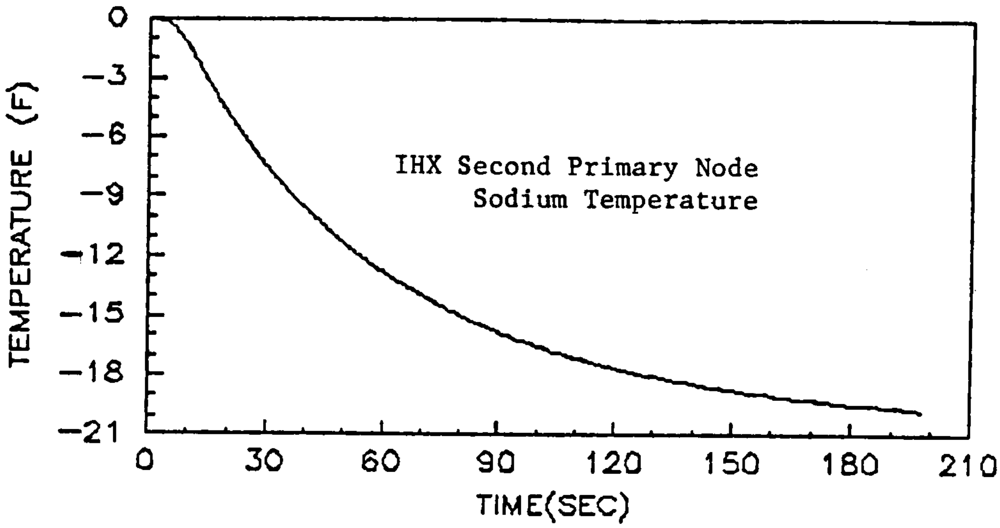

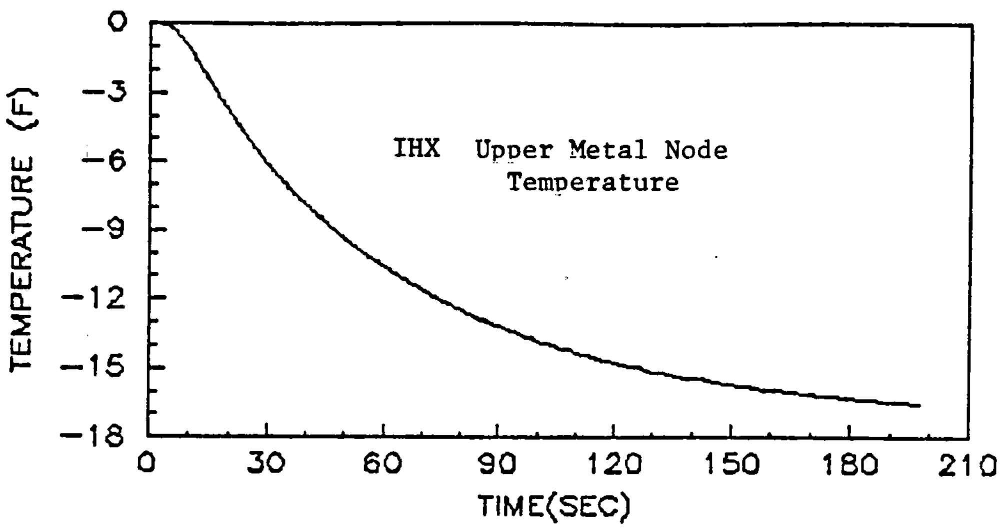

Fig. C.1 Step Responses of Open-loop Primary Model to a -5 cents Reactivity Perturbation.

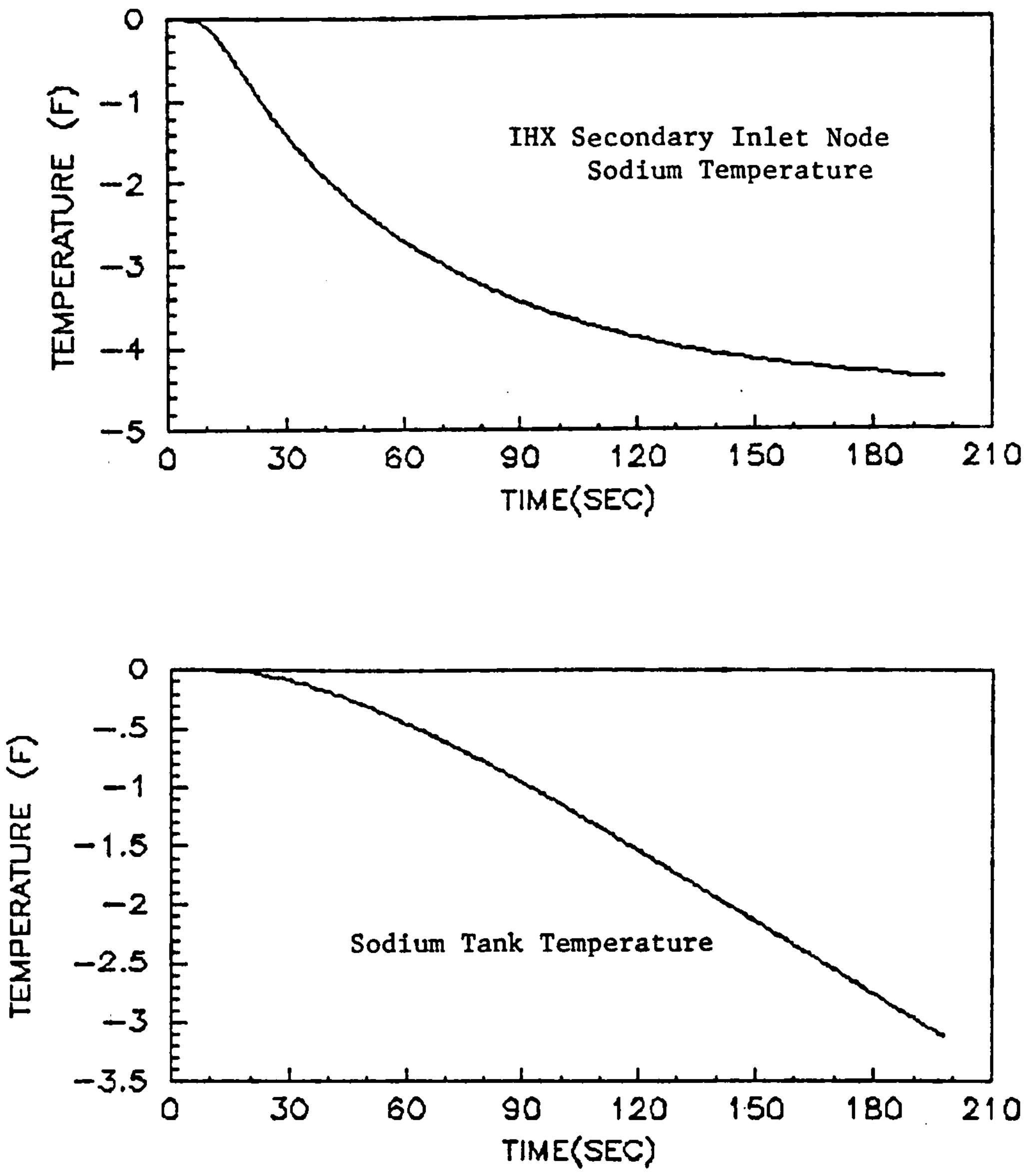

Fig. C.1 Step Responses of Open-loop Primary Model to a -5 cents Reactivity Perturbation.

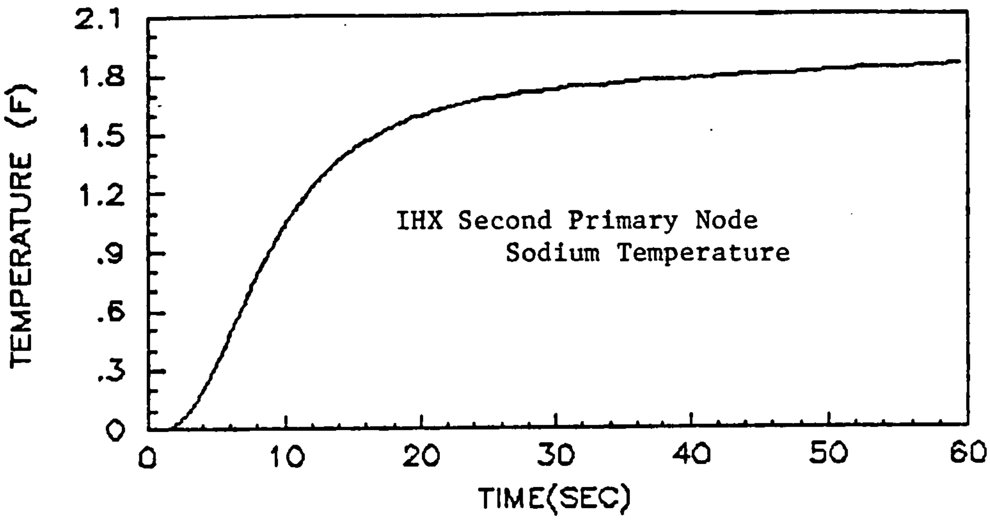

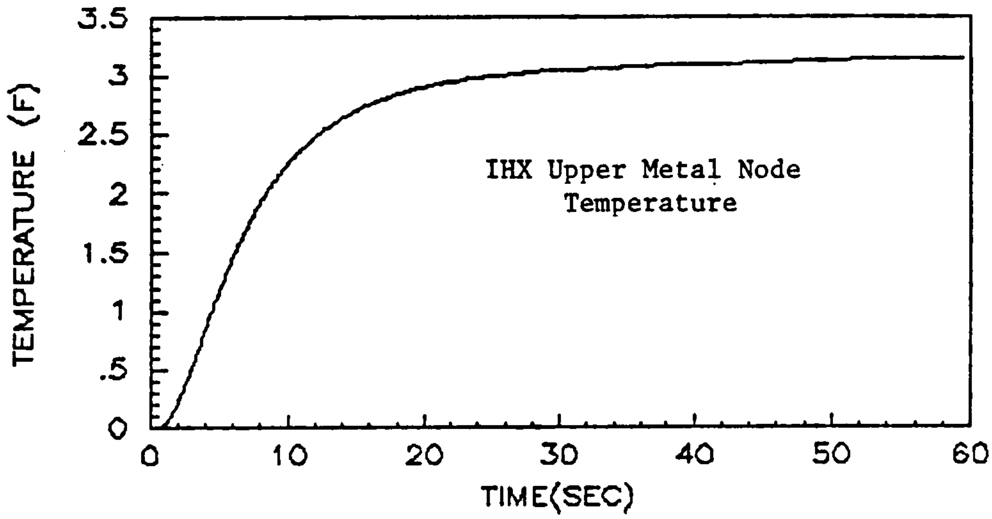

Fig. C.2 Step Responses of Open-loop Primary Model to a +10 F IHX Inlet Sodium Temperature Perturbation.

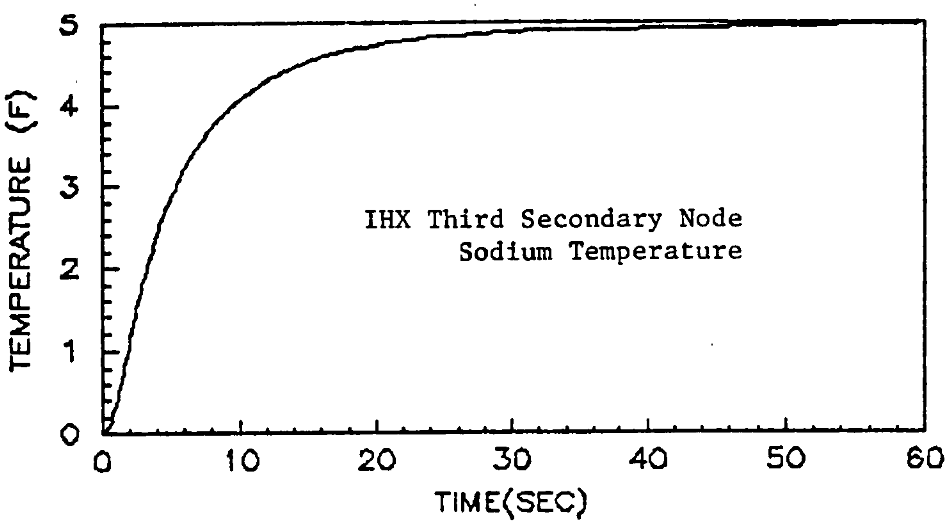

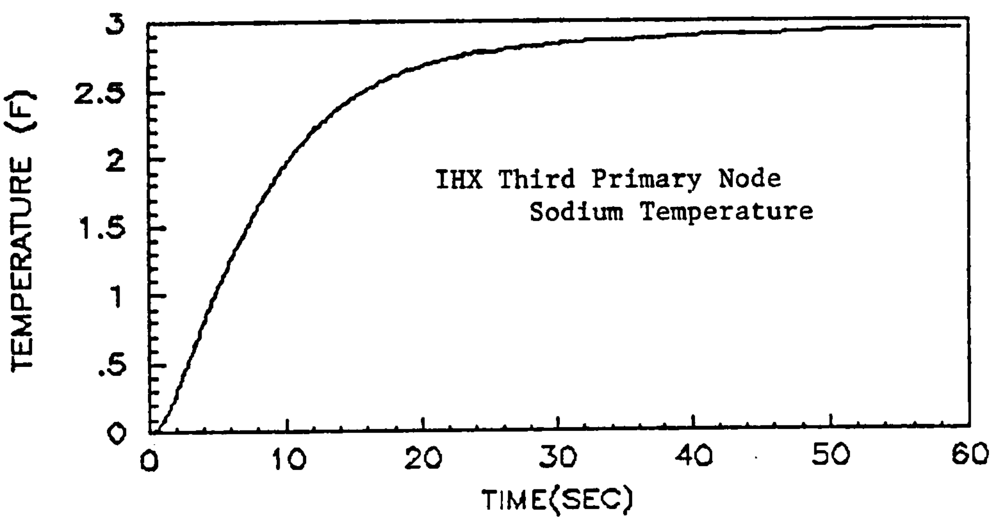

Fig. C.2 Step Responses of Open-loop Primary Model to a +10 F IHX Inlet Sodium Temperature Perturbation.

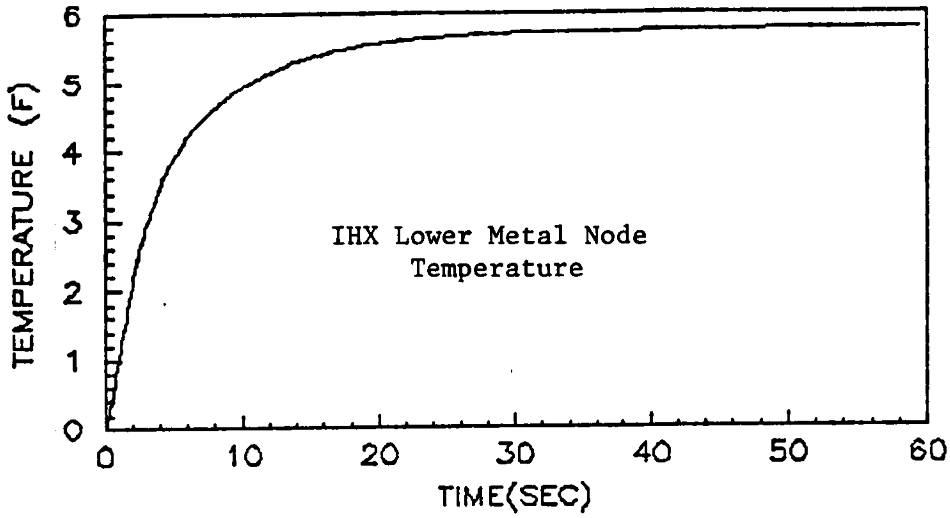

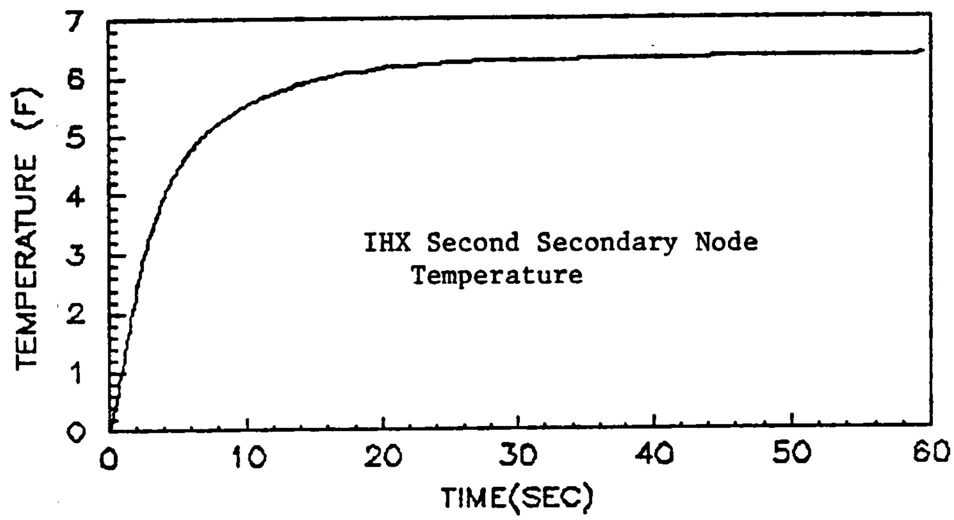

Fig. C.2 Step Responses of Open-loop Primary Model to a +10 F IHX Inlet Sodium Temperature Perturbation.

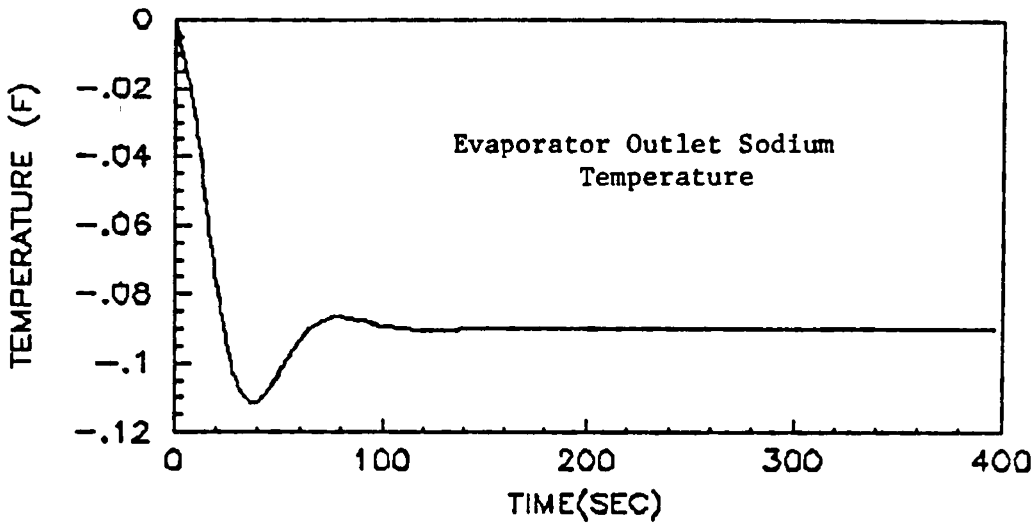

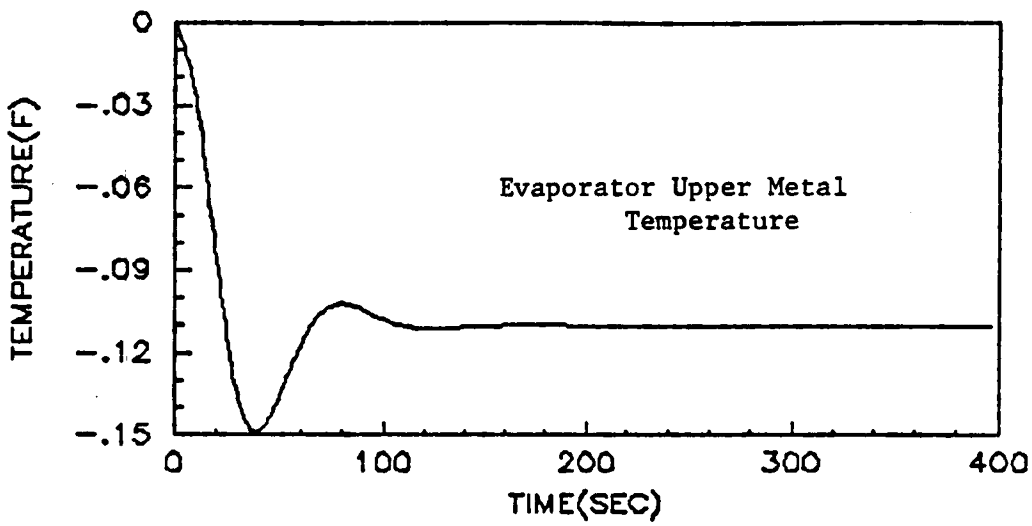

Fig. C.3 Step Responses of Open-loop Steam Generator Model to a +10 F Feedwater Temperature Perturbation.

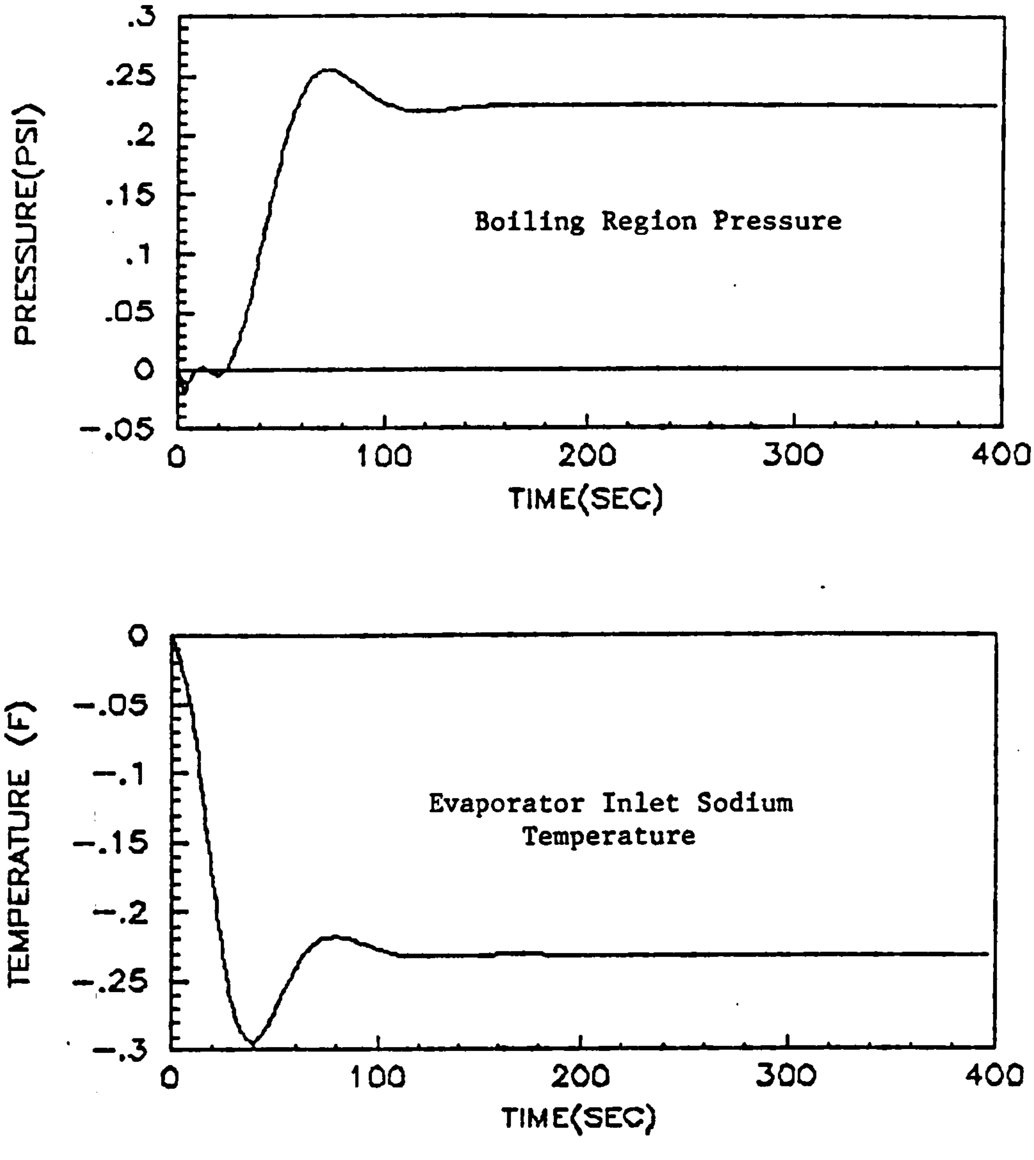

Fig. C.3 Step Responses of Open-loop Steam Generator Model to a +10 F Feedwater Temperature Perturbation.

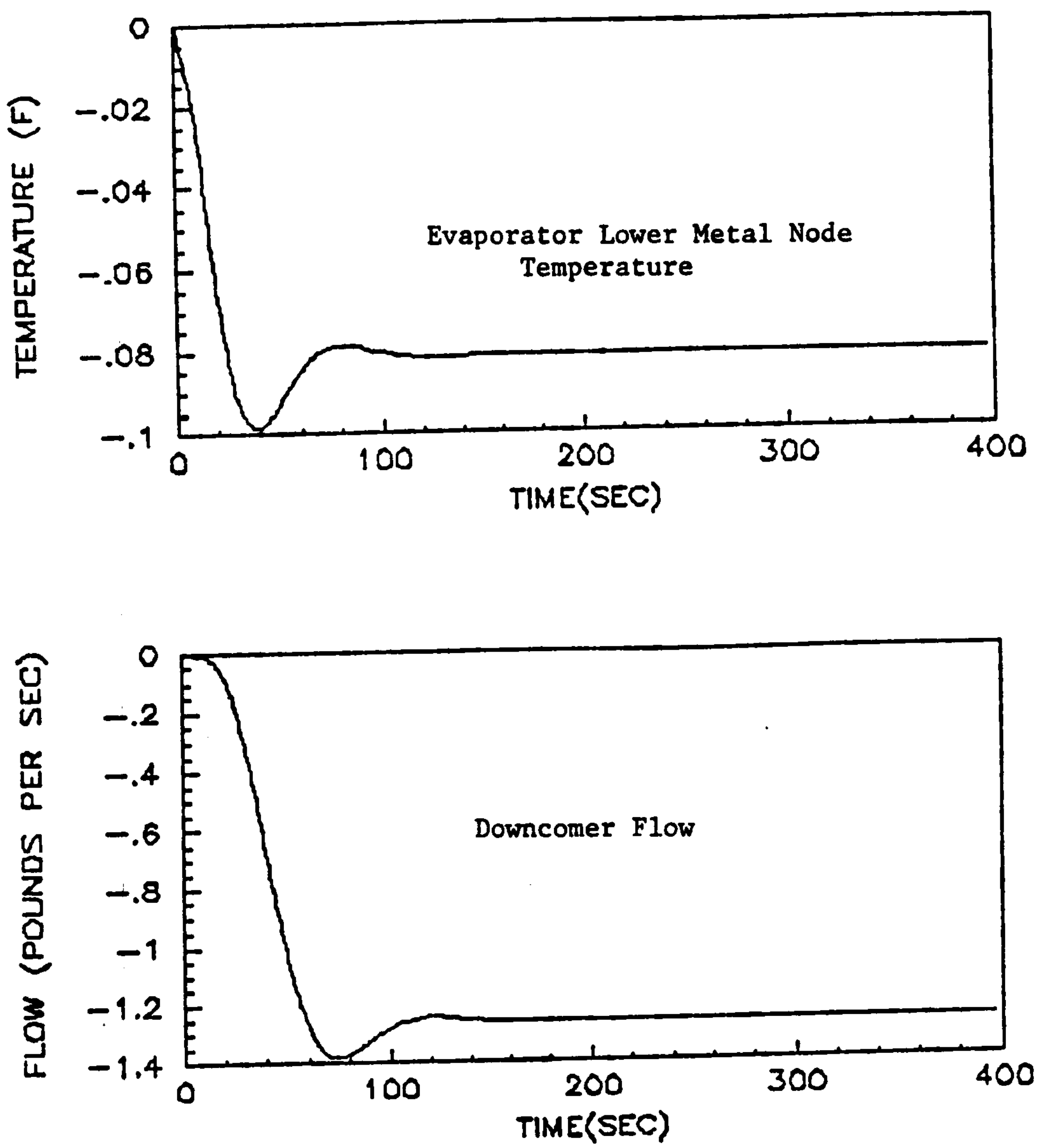

Fig. C.3 Step Responses of Open-loop Steam Generator Model to a +10 F Feedwater Temperature Perturbation..

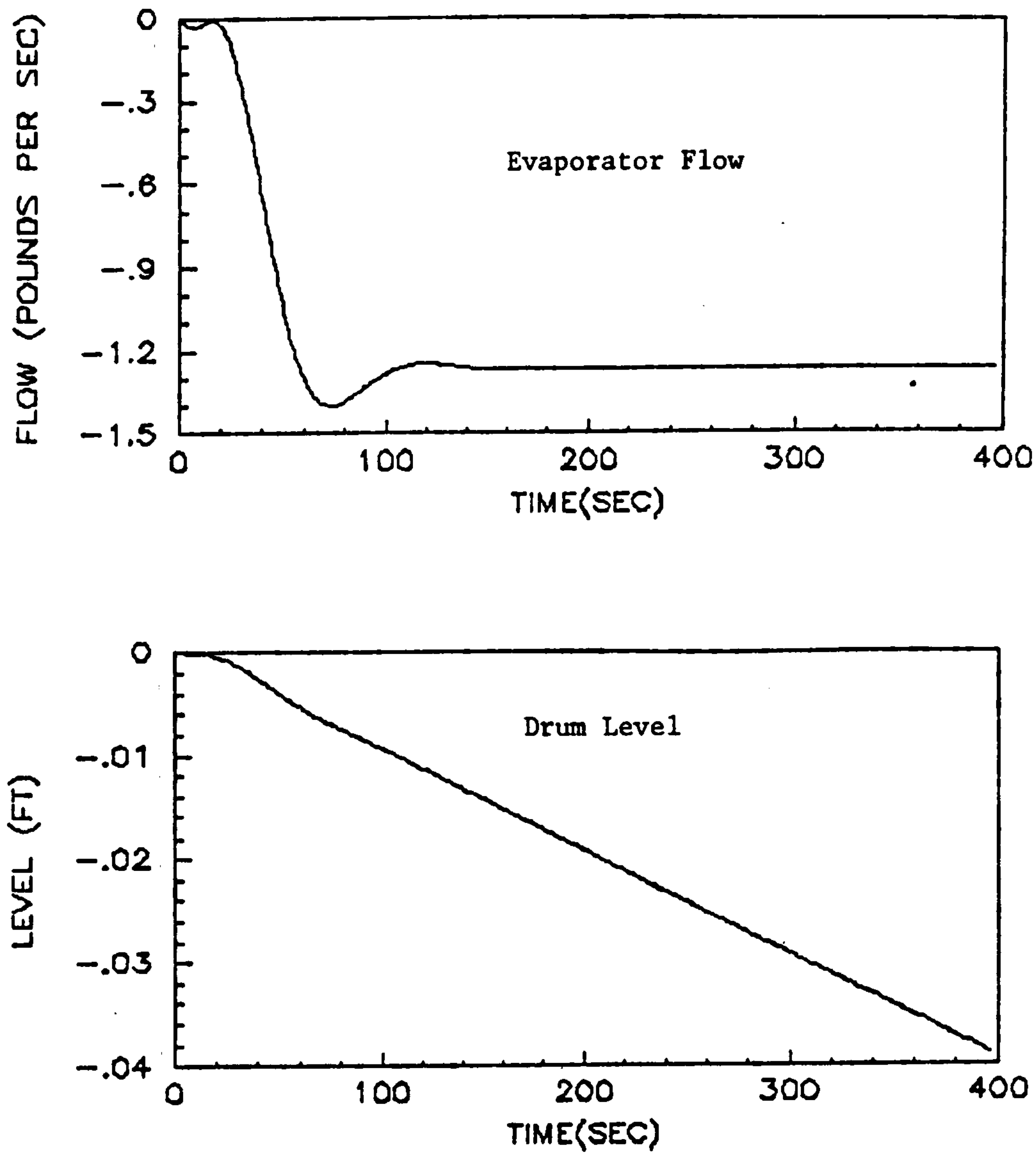

Fig. C.3 Step Responses of Open-loop Steam Generator Model to a +10 F Feedwater Temperature Perturbation.

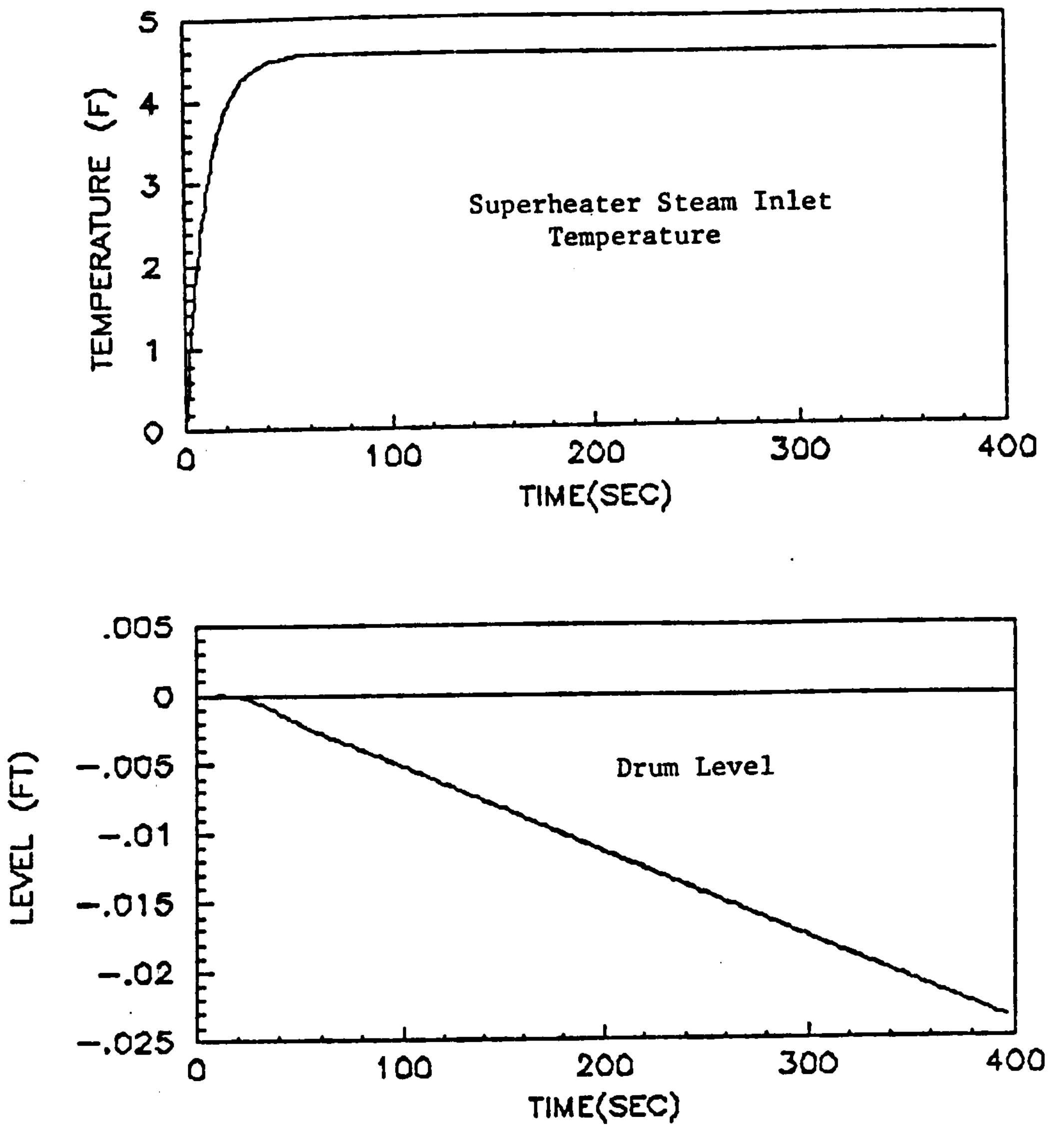

Fig. C.4 Step Responses of Open-loop Steam Generator Model to a +10 F Sodium Inlet Temperature Perturbation.

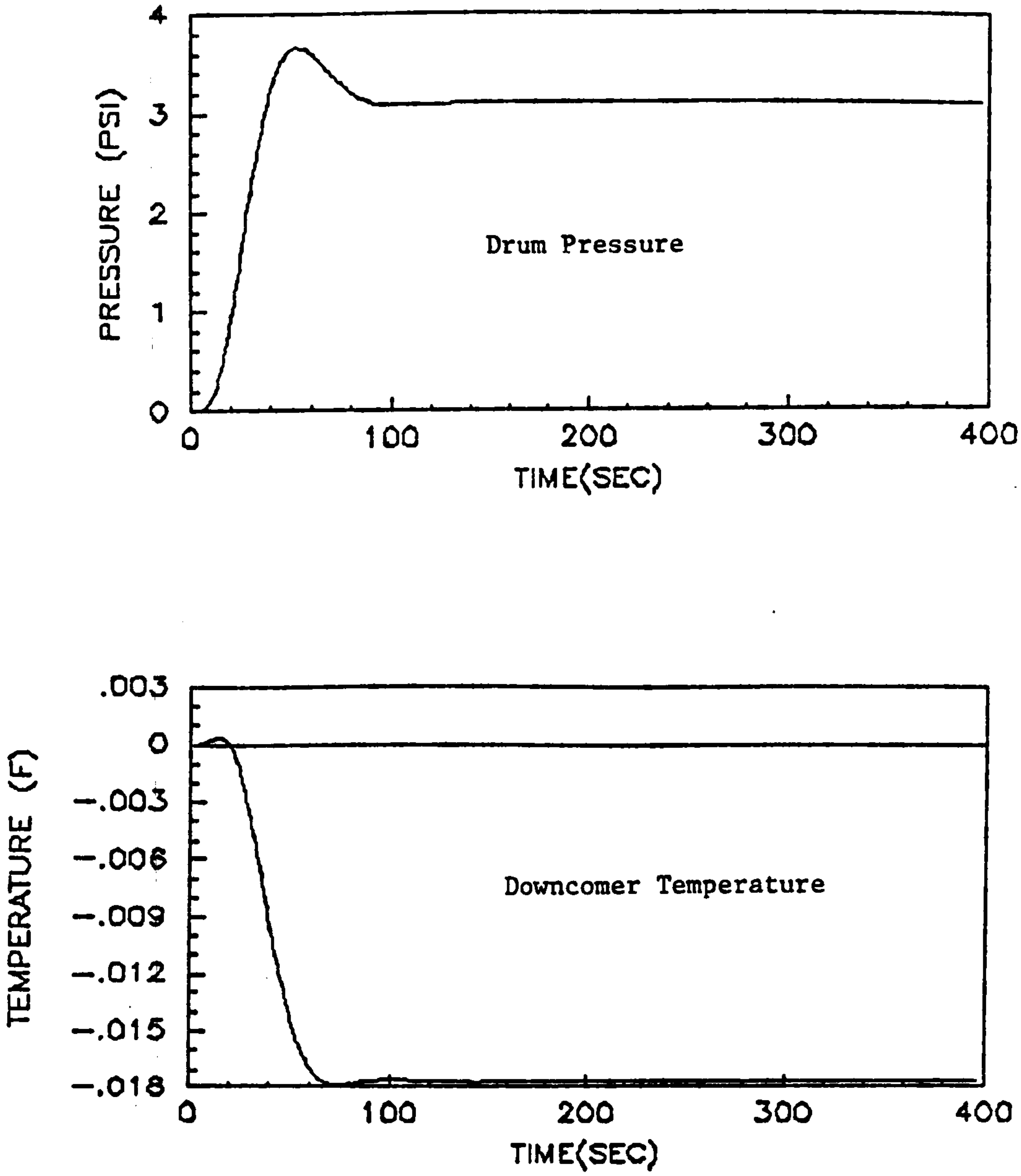

Fig. C.4 Step Responses of Open-loop Steam Generator Model to a +10 F Sodium Inlet Temperature Perturbation.

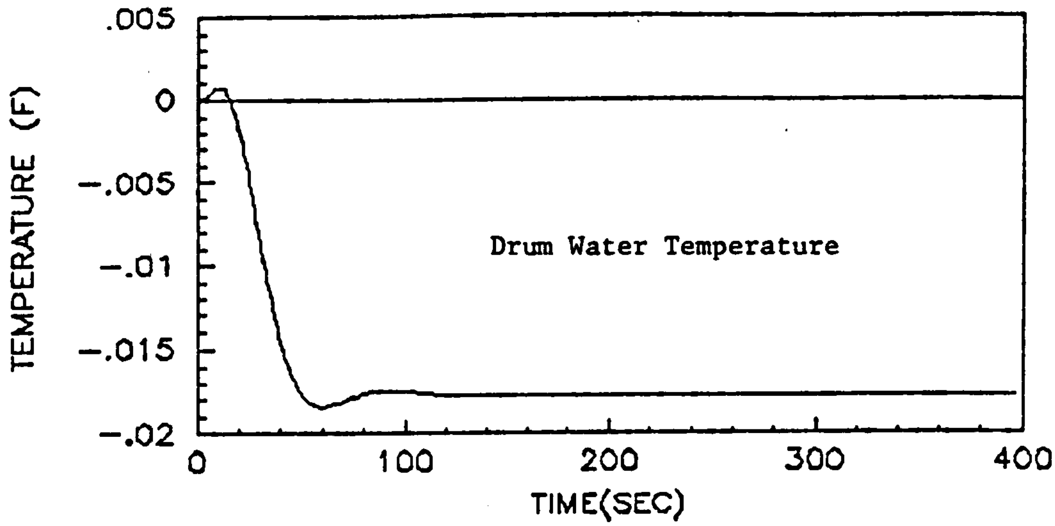

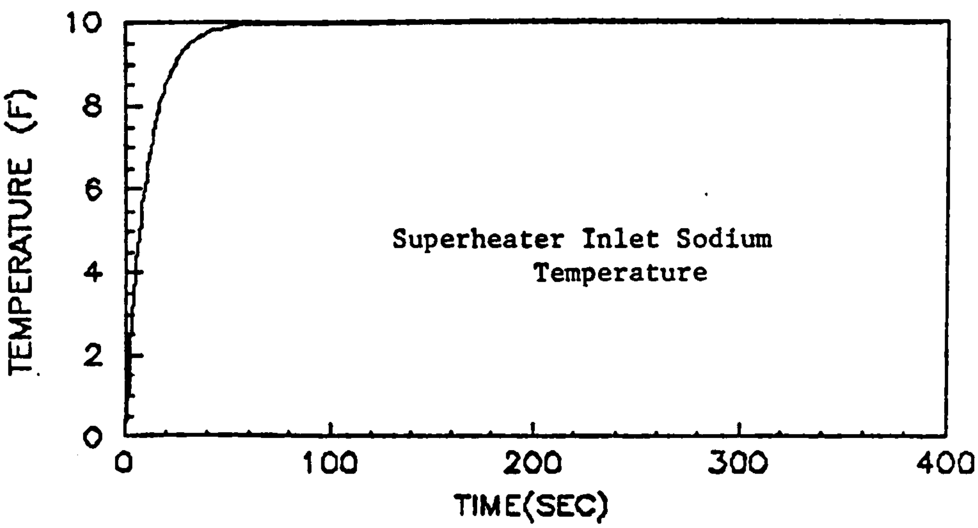

Fig. C.4 Step Responses of Open-loop Steam Generator Model to a +10 F Sodium Inlet Temperature Perturbation.

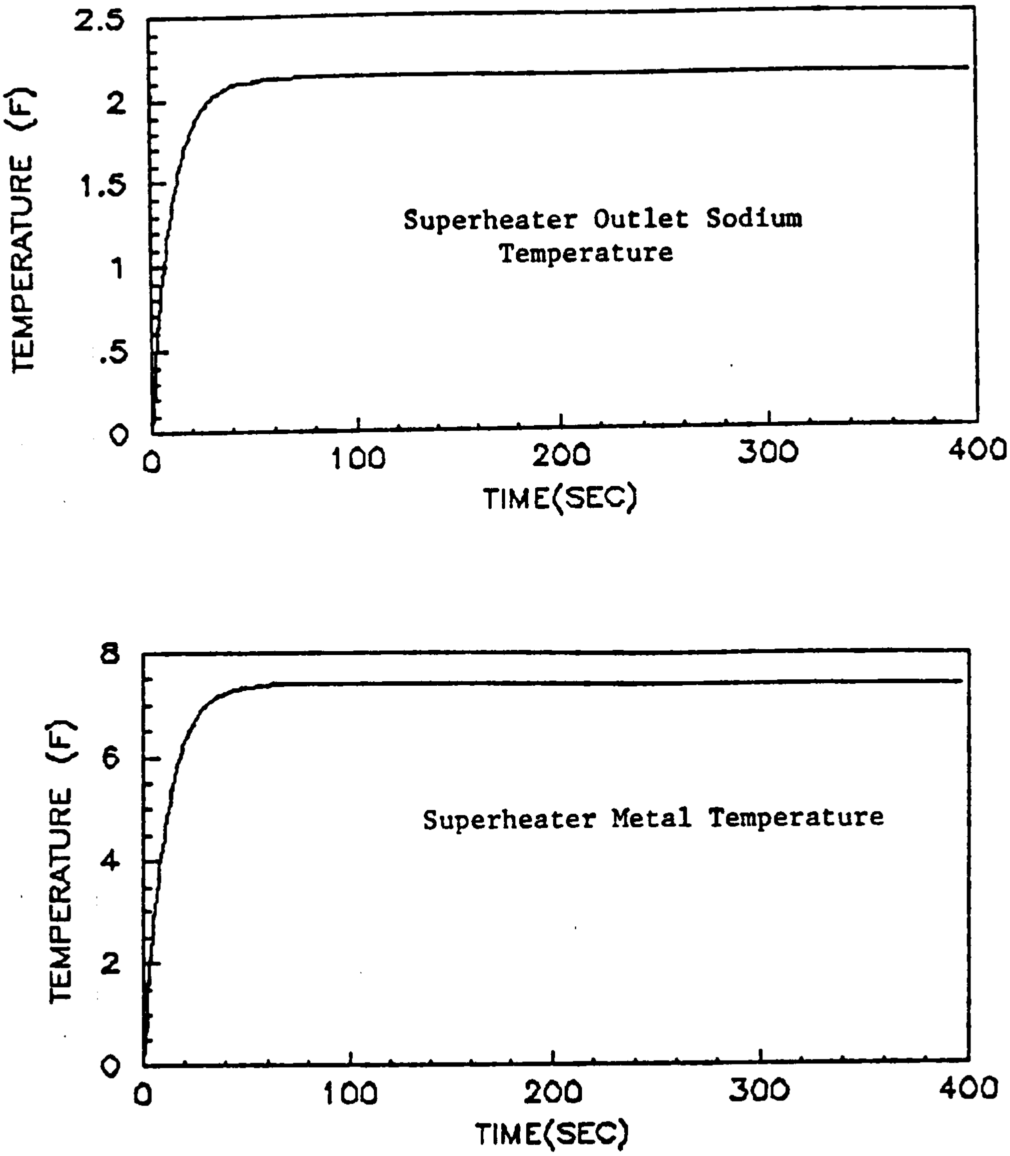

Fig. C.4 Step Responses of Open-loop Steam Generator Model to a +10 F Sodium Inlet Temperature Perturbation.

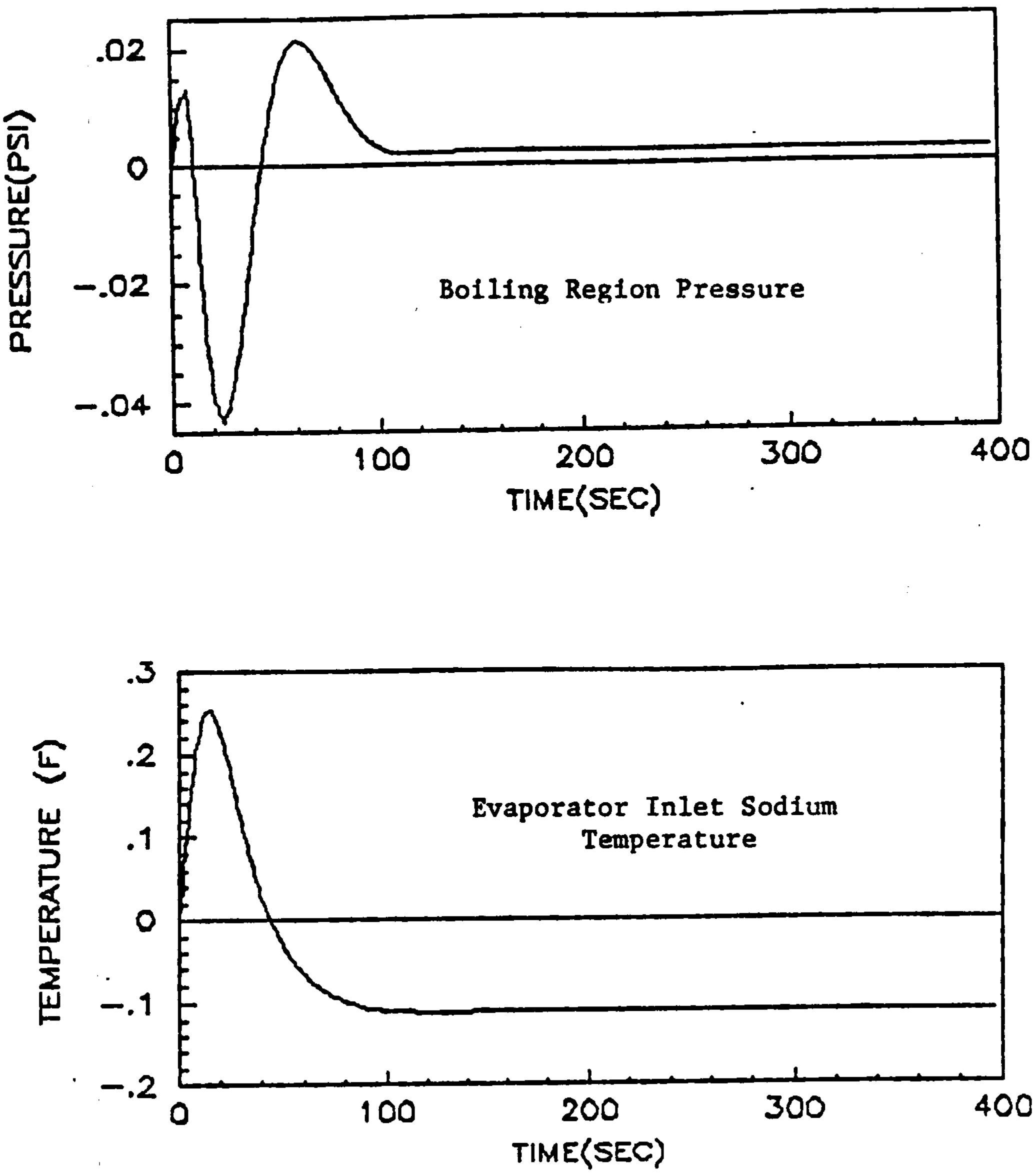

Fig. C.4 Step Responses of Open-loop Steam Generator Model to a +10 F Sodium Inlet Temperature Perturbation.

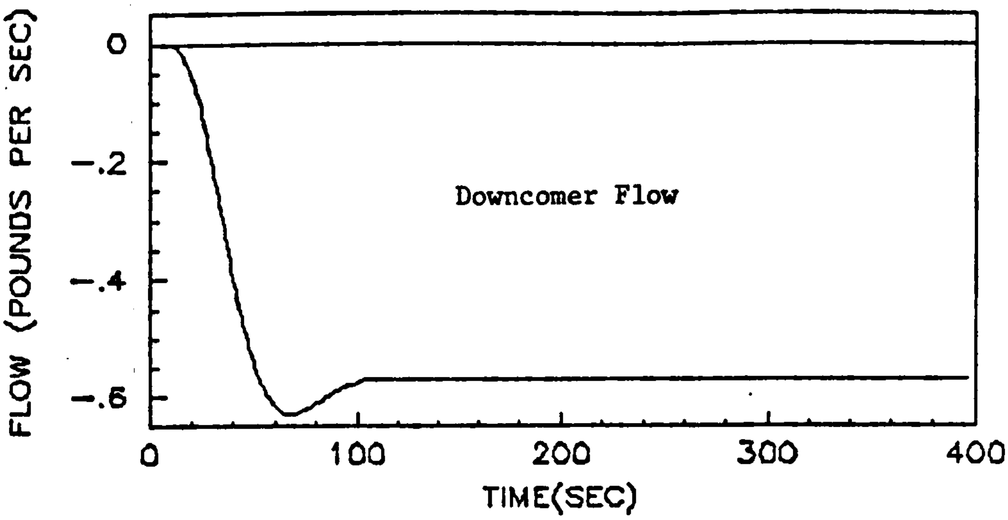

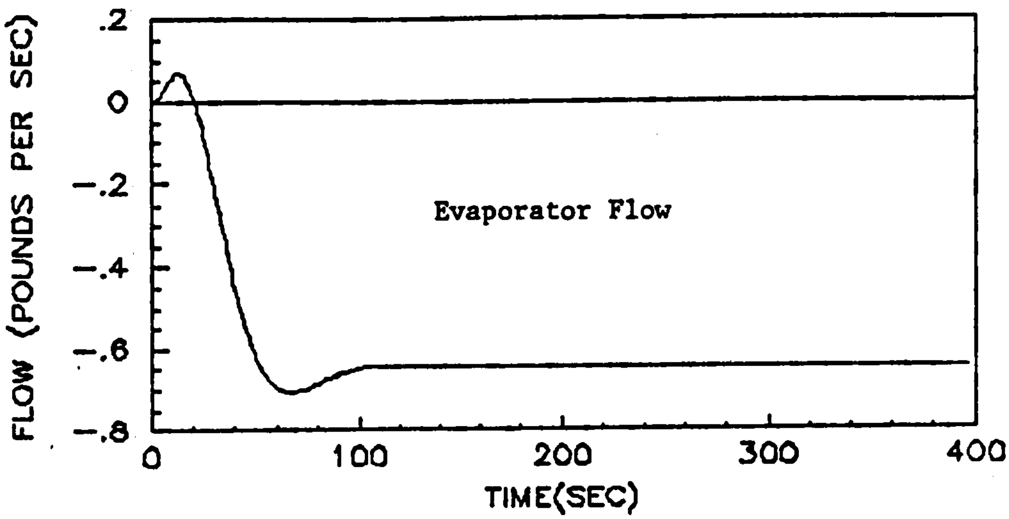

Fig. C.4 Step Responses of Open-loop Steam Generator Model to a +10 F Sodium Inlet Temperature Perturbation.

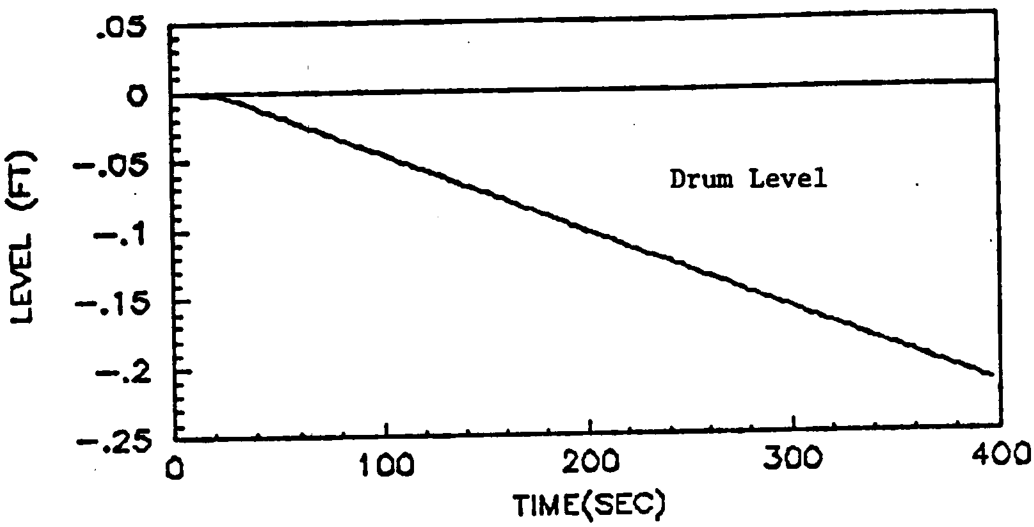

Fig. C.5 Step Responses of Open-loop Steam Generator Model to a +10% Steam Valve Opening Perturbation.

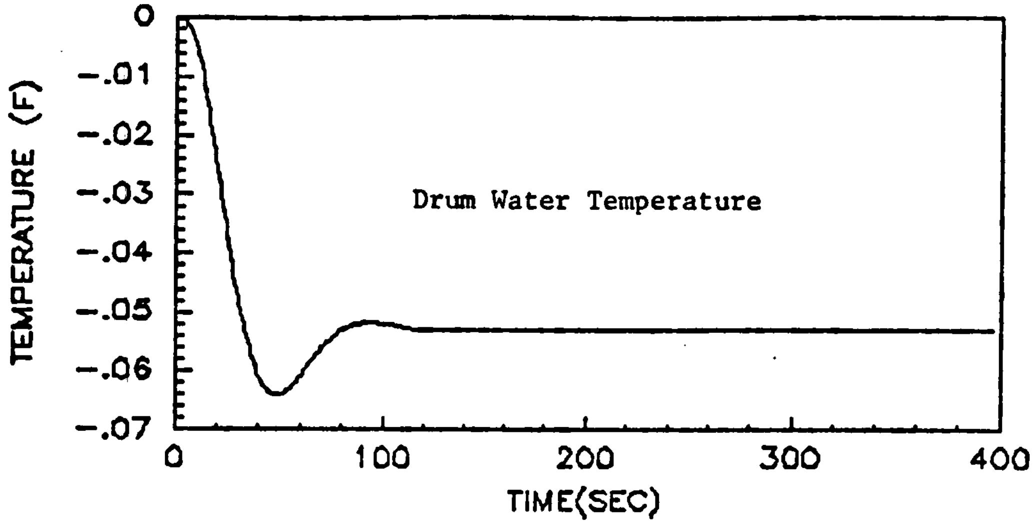

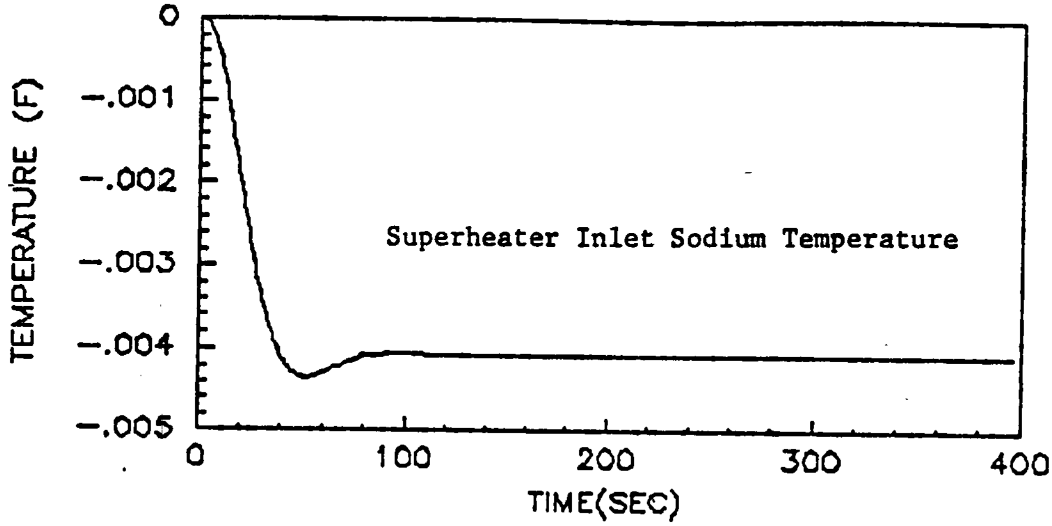

Fig. C.5 Step Responses of Open-loop Steam Generator Model to a +10% Steam Valve Opening Perturbation.

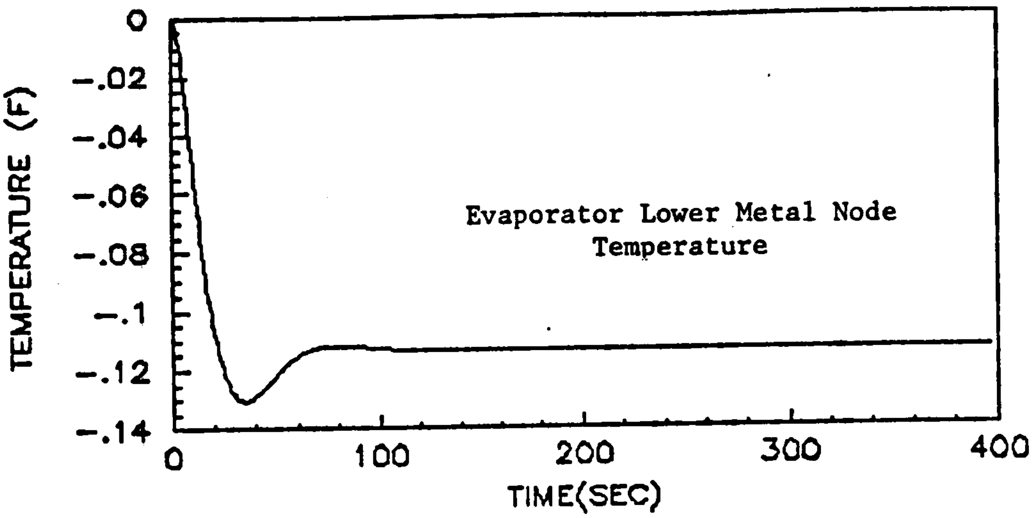

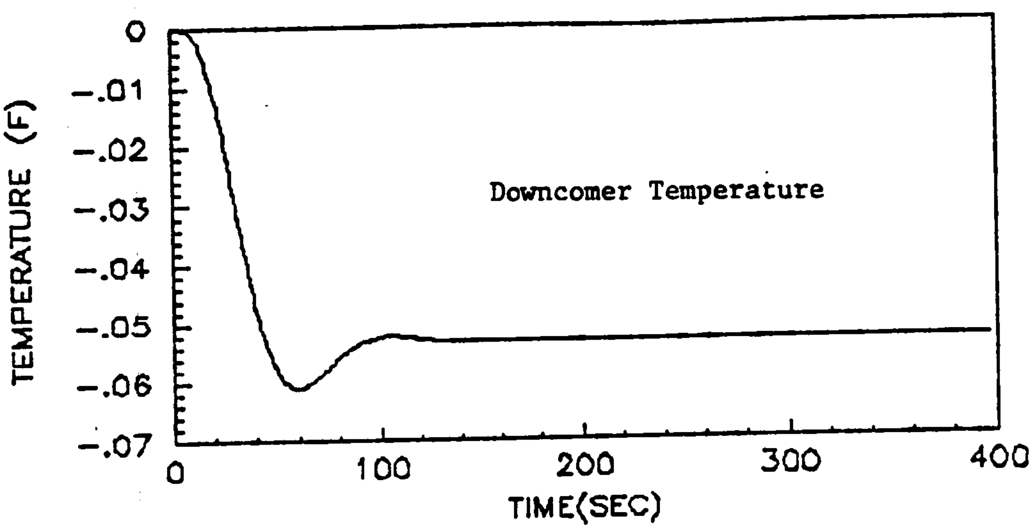

Fig. C.5 Step Responses of Open-loop Steam Generator Model to a +10% Steam Valve Opening Perturbation.

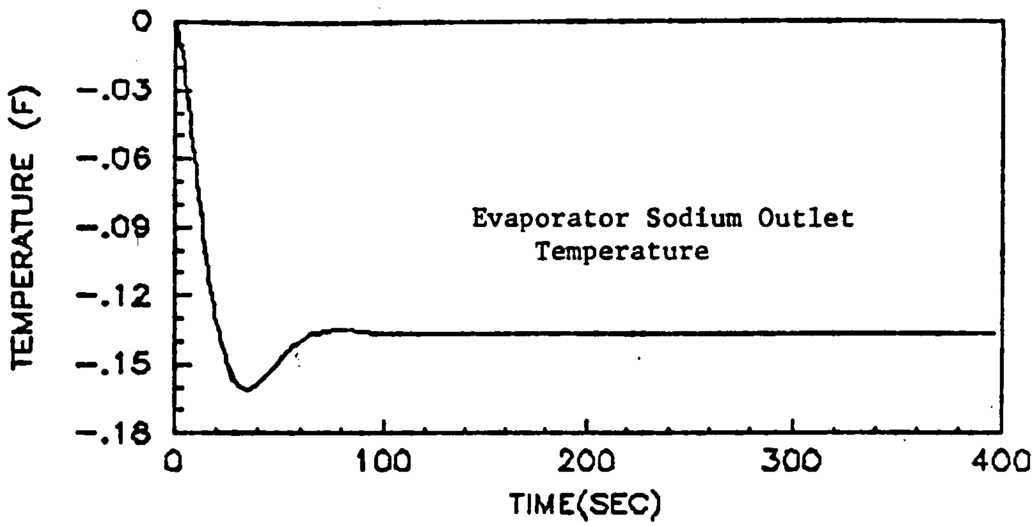

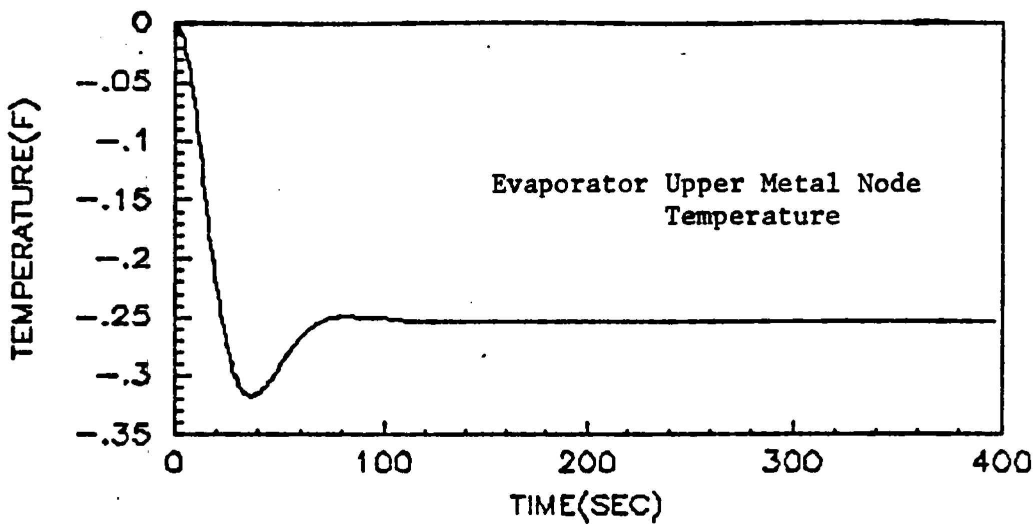

Fig. C.5 Step Responses of Open-loop Steam Generator Model to a +10% Steam Valve Opening Perturbation.

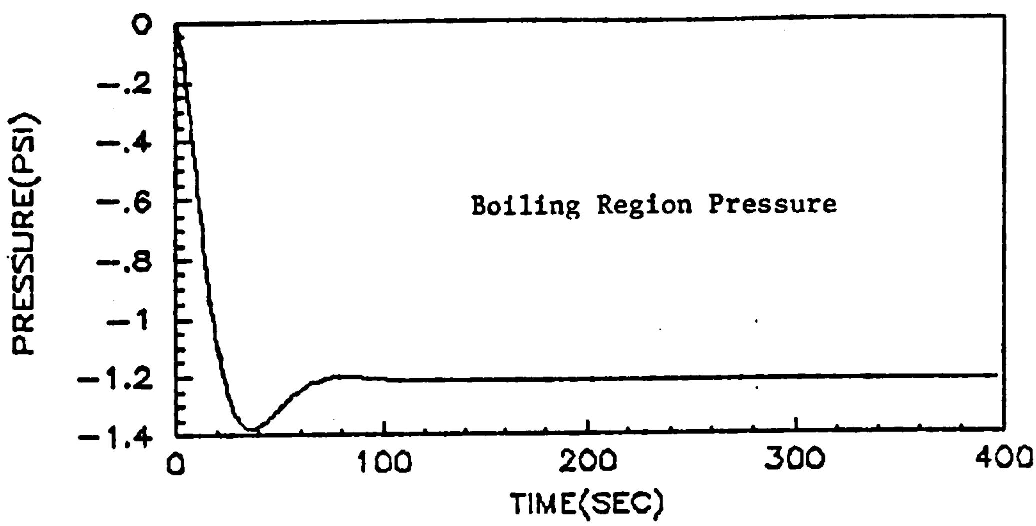

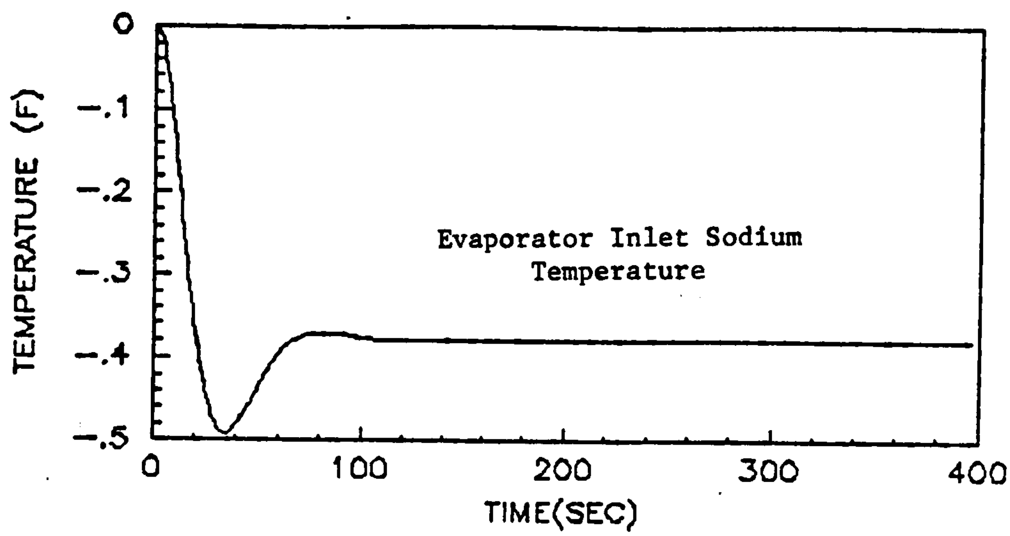

Fig. C.5 Step Responses of Open-loop Steam Generator Model to a +10% Steam Valve Opening Perturbation.

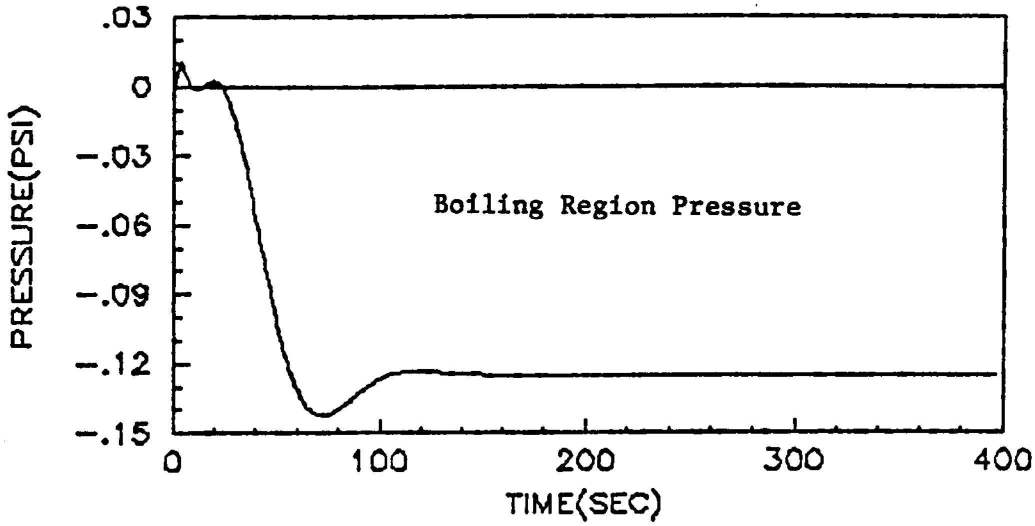

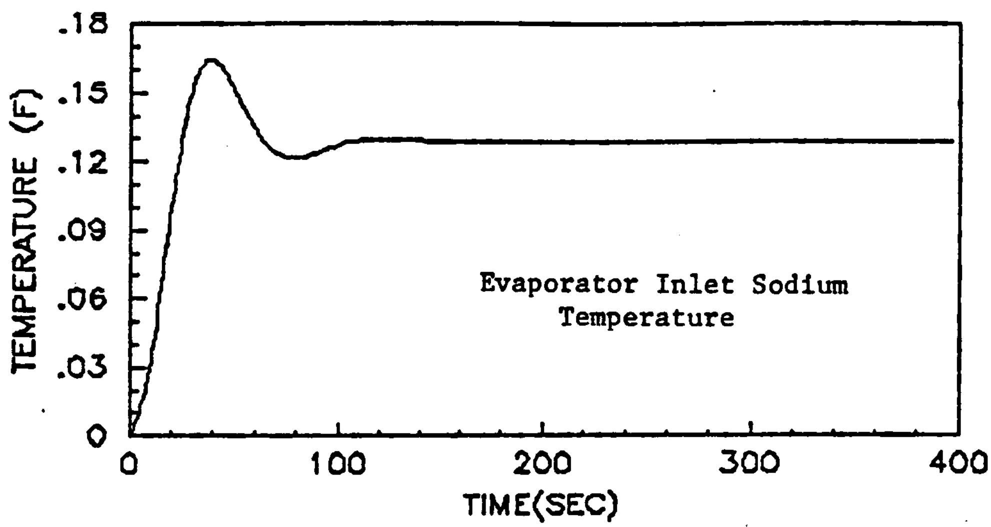

Fig. C.6 Step Responses of Open-loop Steam Generator Model to a +10 lbm/sec Feedwater Flow Perturbation.

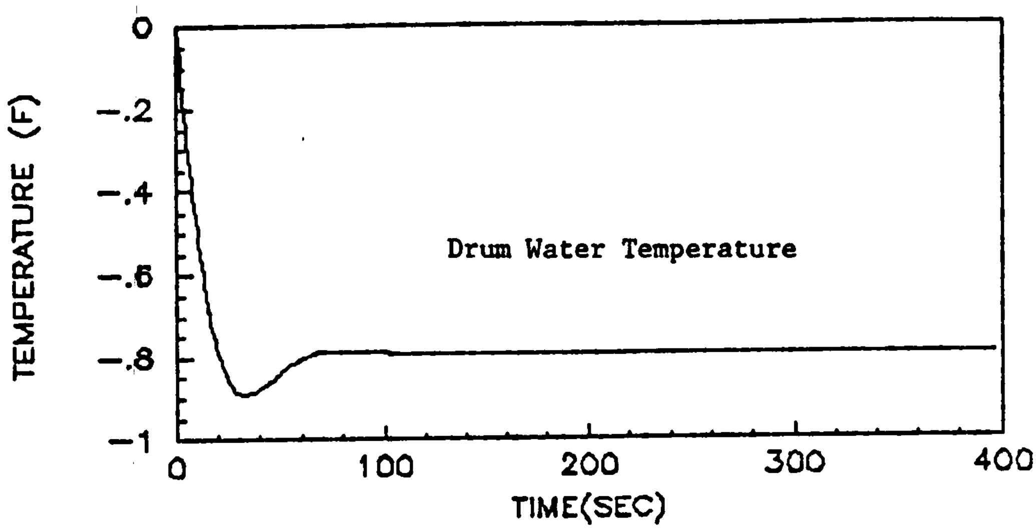

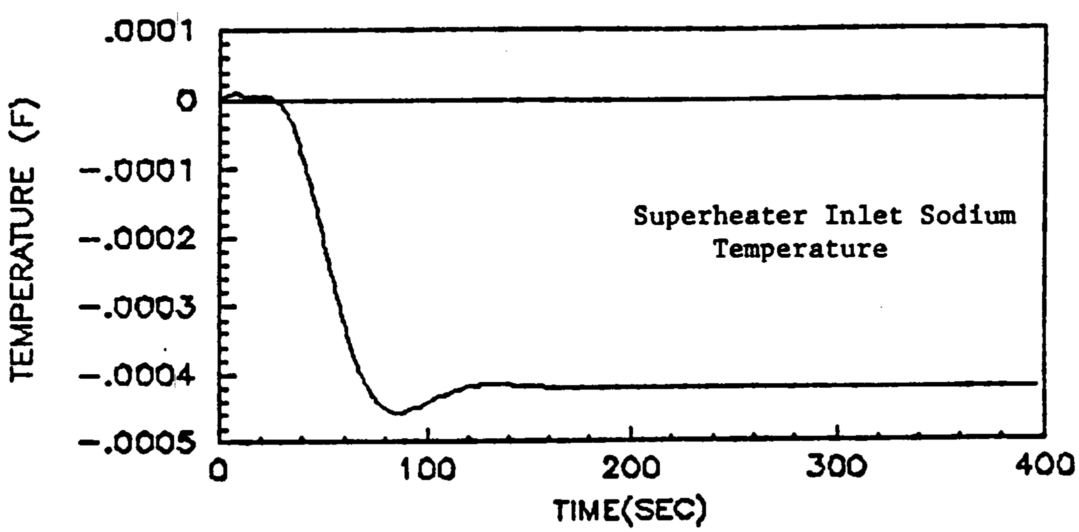

Fig. C.6 Step Responses of Open-loop Steam Generator Model to a +10 lbm/sec Feedwater Flow Perturbation.

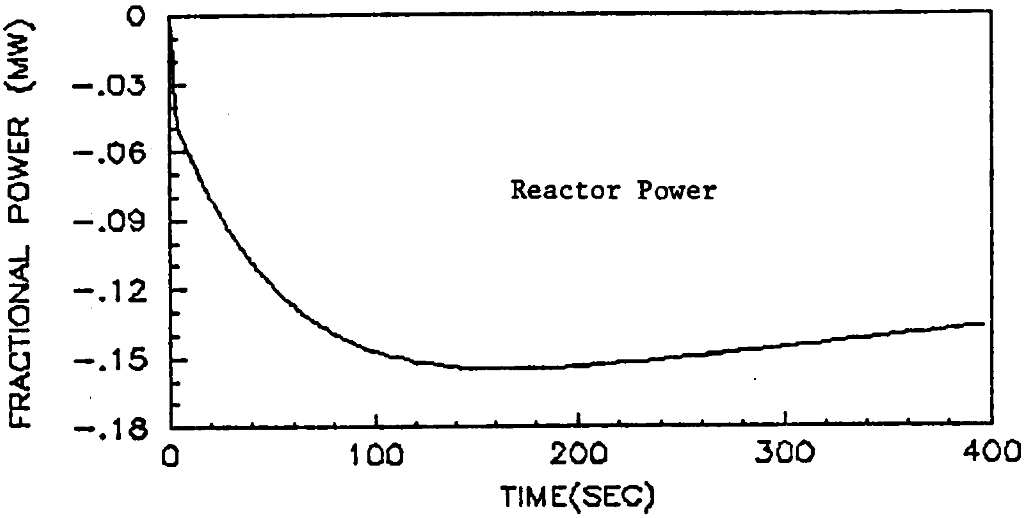

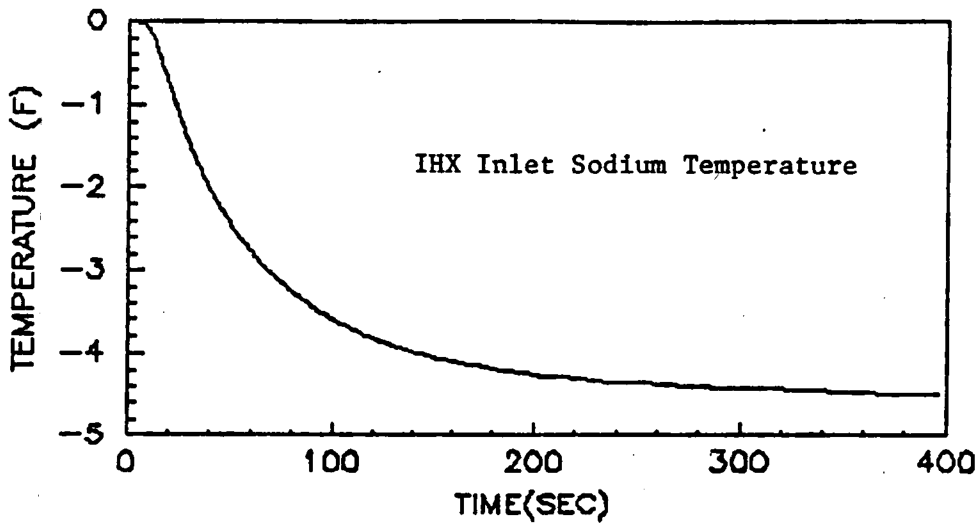

Fig. C.7 Step Responses of Open-loop Combined Model to a -5 cents Reactivity Perturbation.

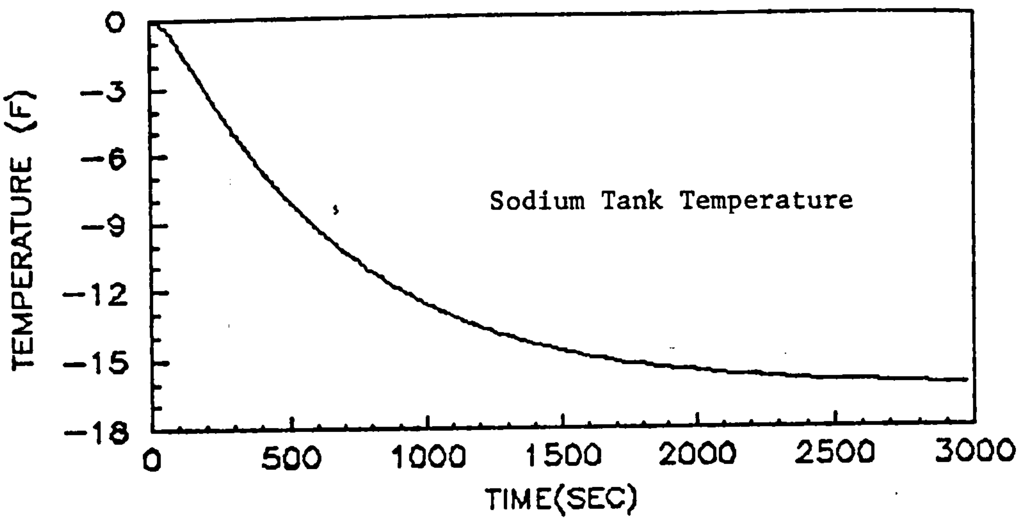

Fig. C.7 Step Responses of Open-loop Combined Model to a -5 cents Reactivity Perturbation.

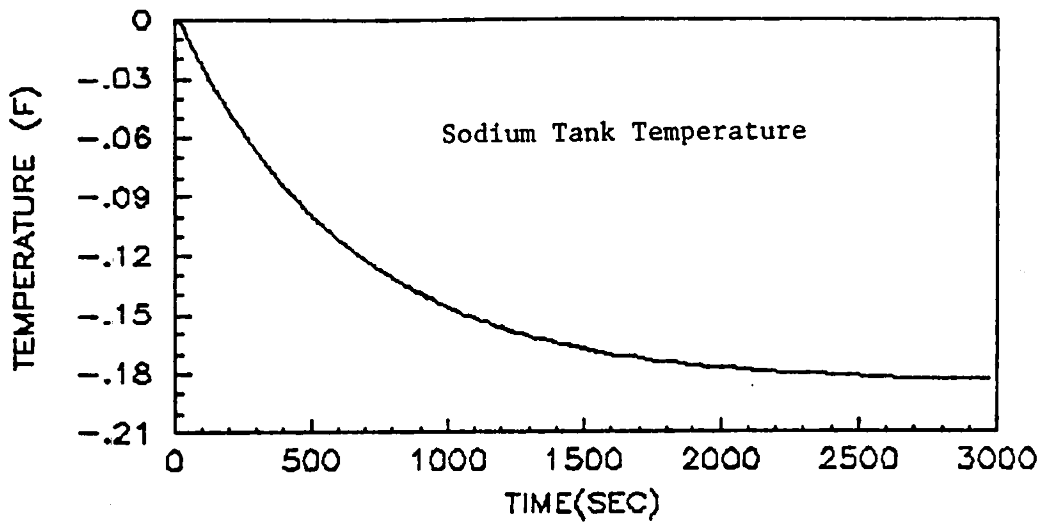

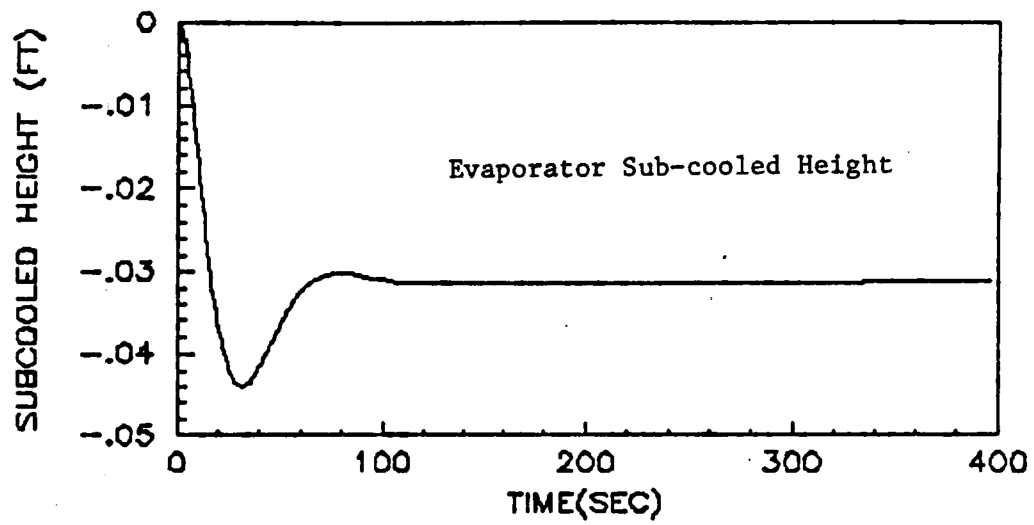

Fig. C.8 Step Responses of Open-loop Combined Model to a +10% Steam Valve Opening Perturbation.

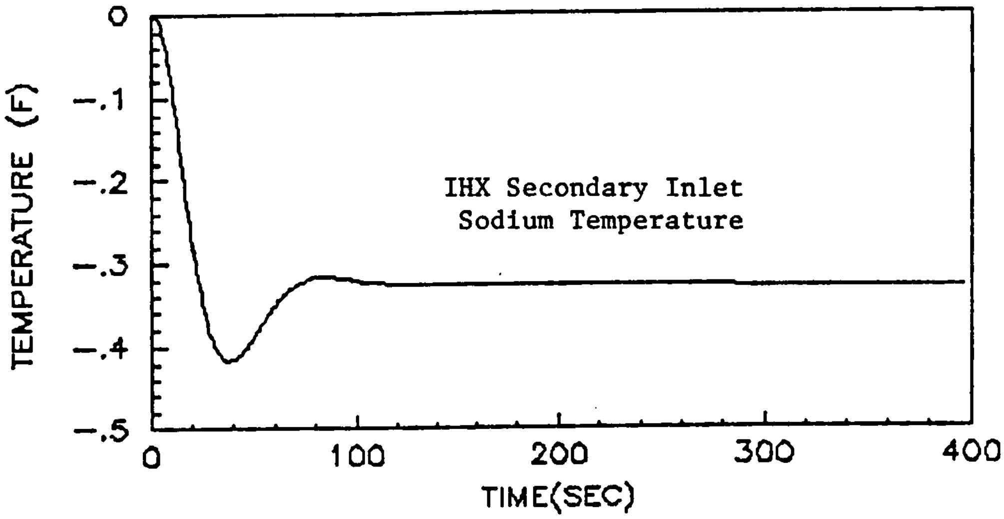

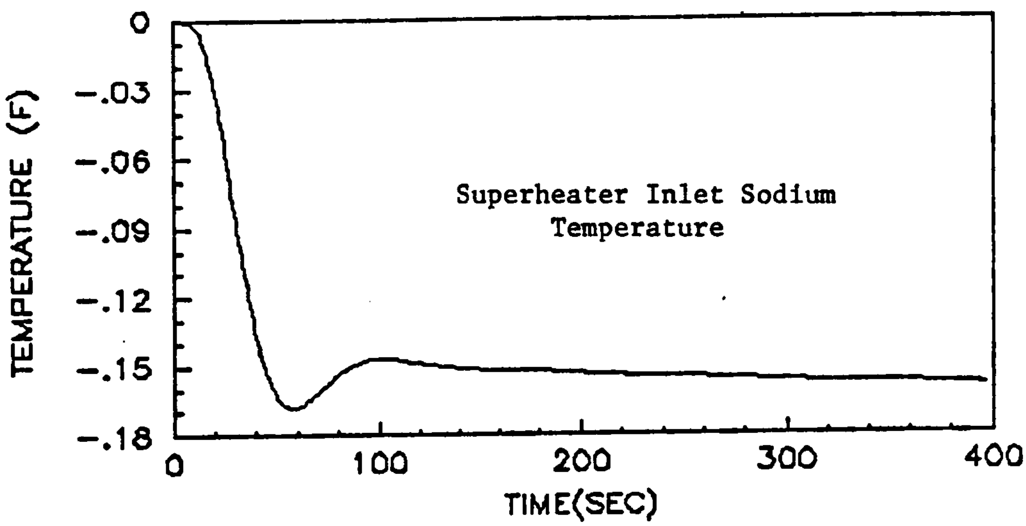

Fig. C.8 Step Responses of Open-loop Combined Model to a +10% Steam Valve Opening Perturbation.

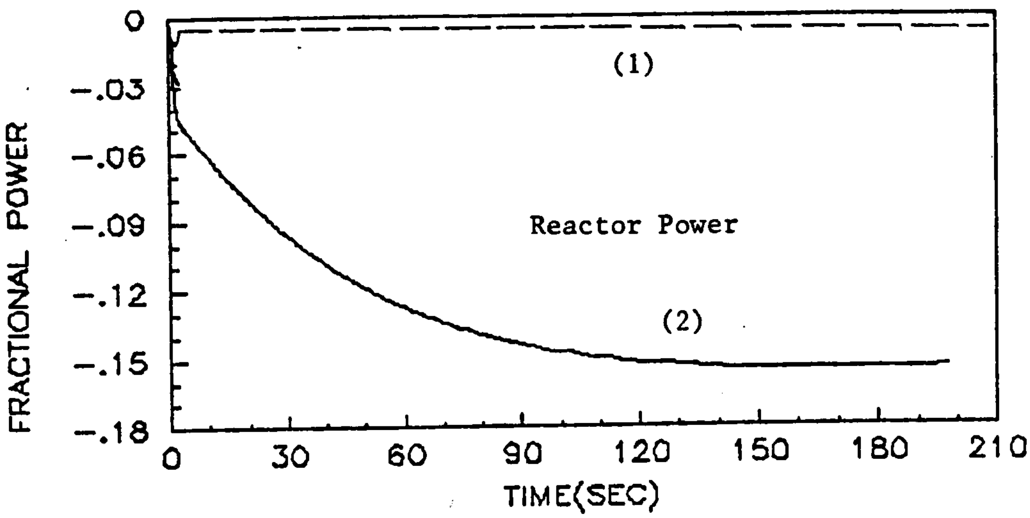

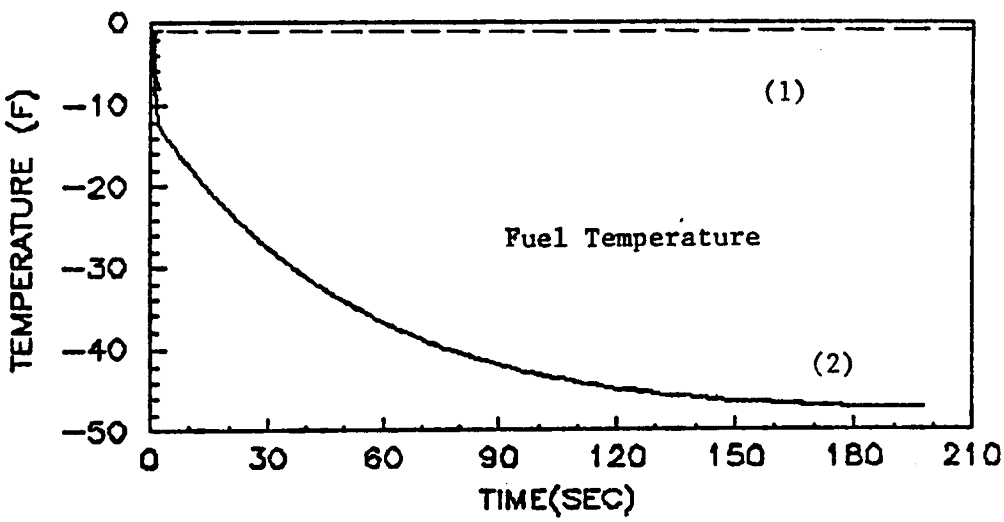

Fig. C.9 Step Responses of Closed-loop Primary Model to a -5 cents Reactivity Perturbation (1) Optimal Compensator (2) Open-loop Response.

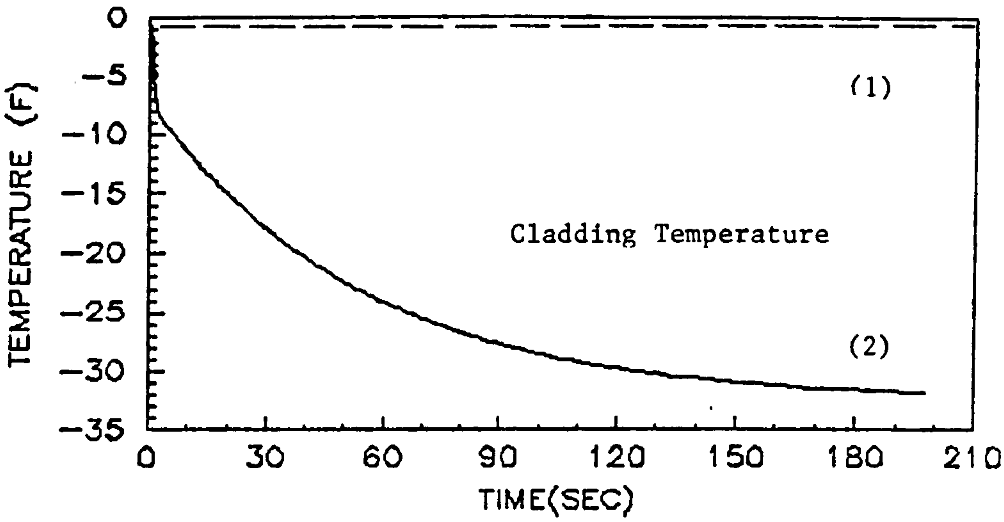

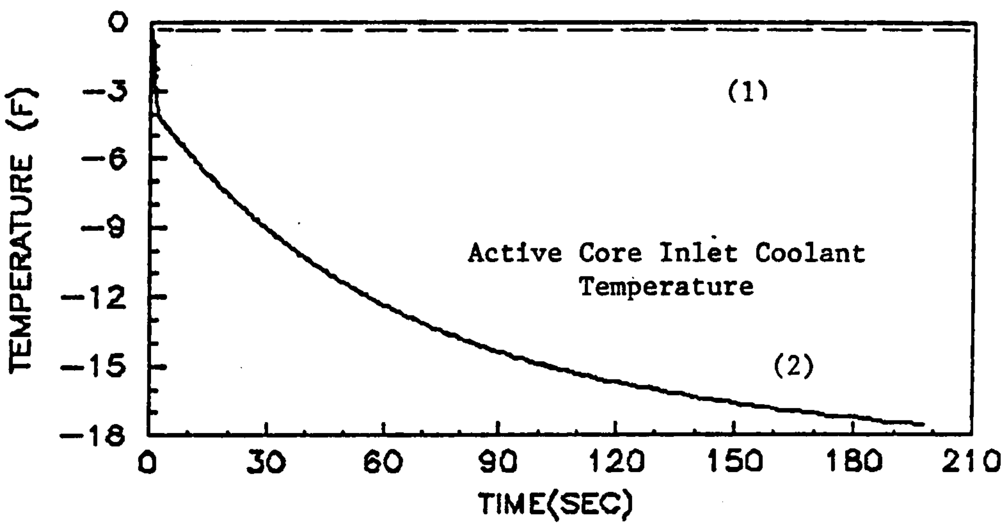

Fig. C.9 Step Responses of Closed-loop Primary Model to a -5 cents Reactivity Perturbation (1) Optimal Compensator (2) Open-loop Response.

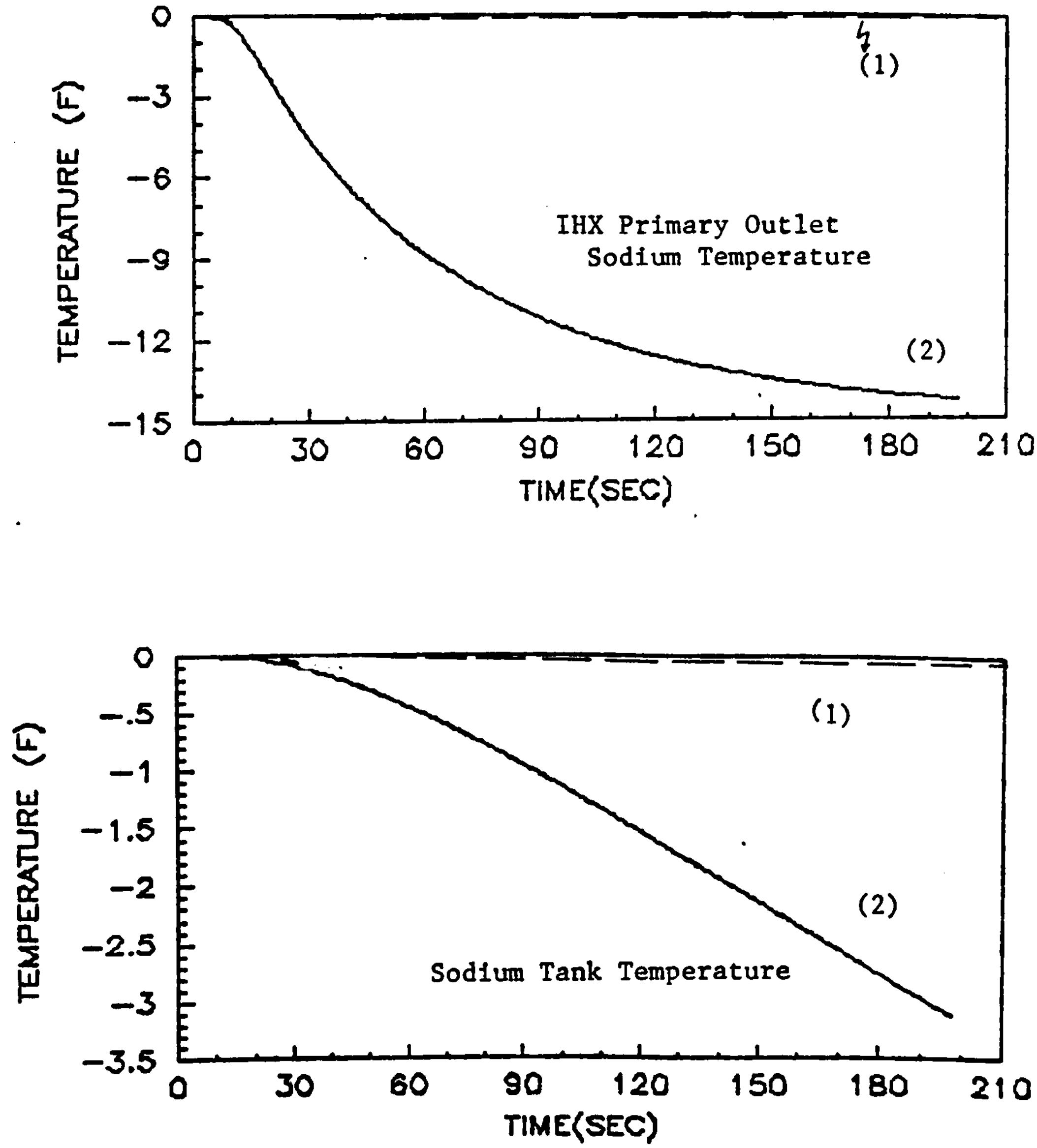

Fig. C.9 Step Responses of Closed-loop Primary Model to a -5 cents Reactivity Perturbation (1) Optimal Compensator (2) Open-loop Response.

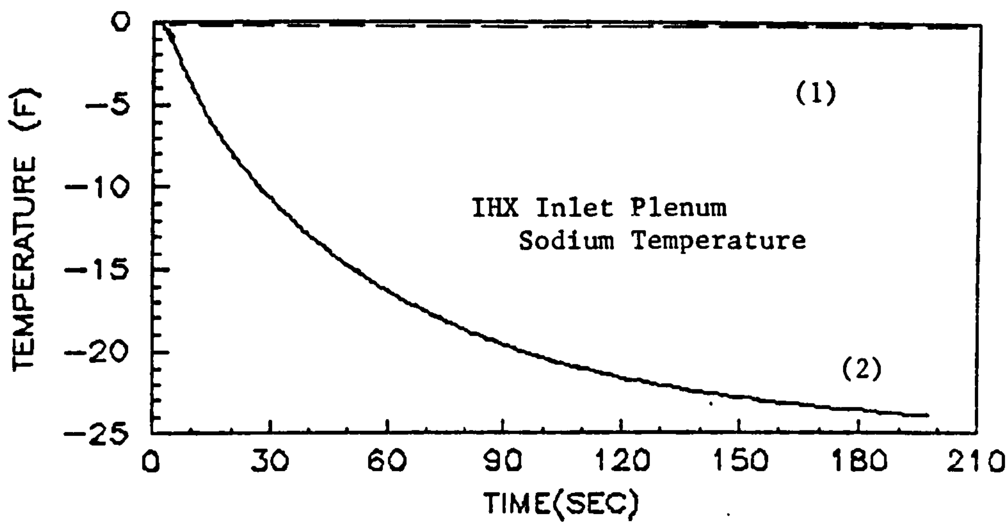

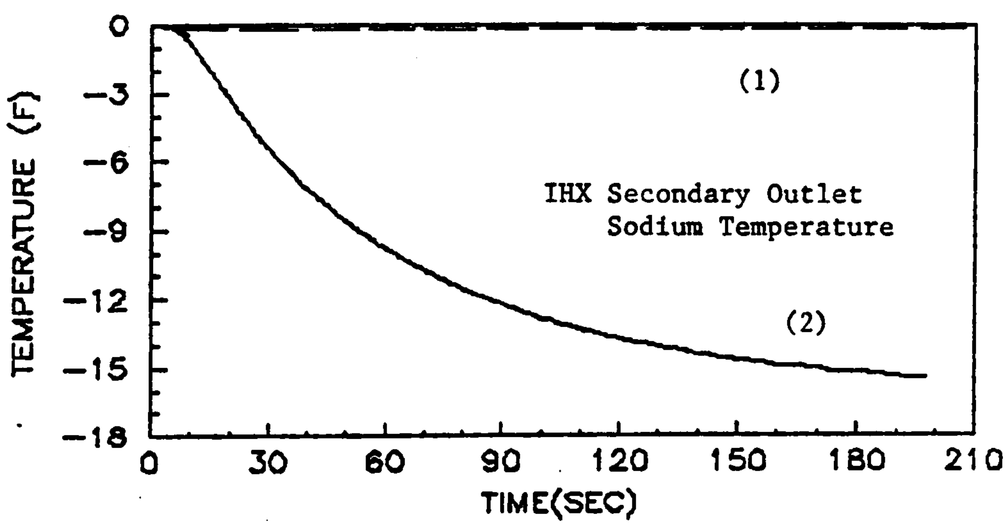

Fig. C.9 Step Responses of Closed-loop Primary Model to a -5 cents Reactivity Perturbation (1) Optimal Compensator (2) Open-loop Response.

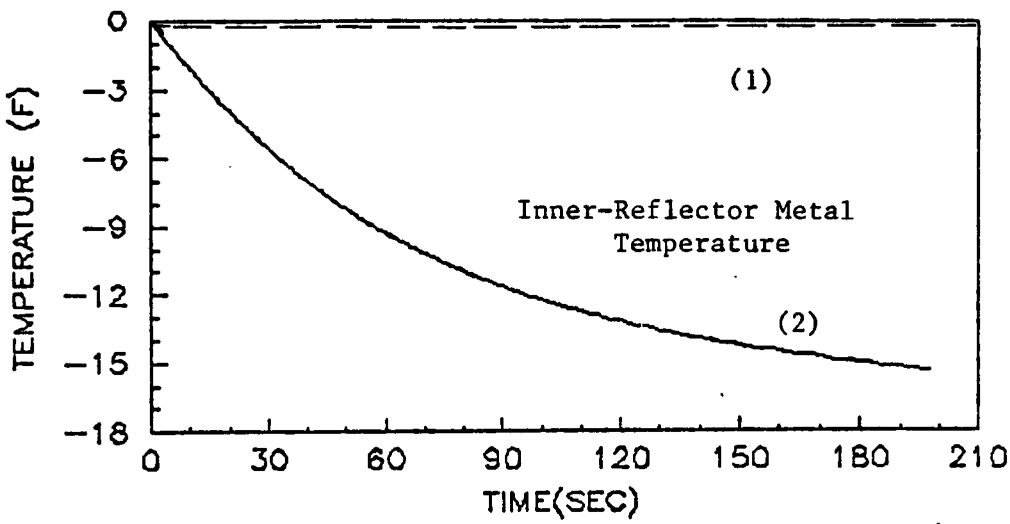

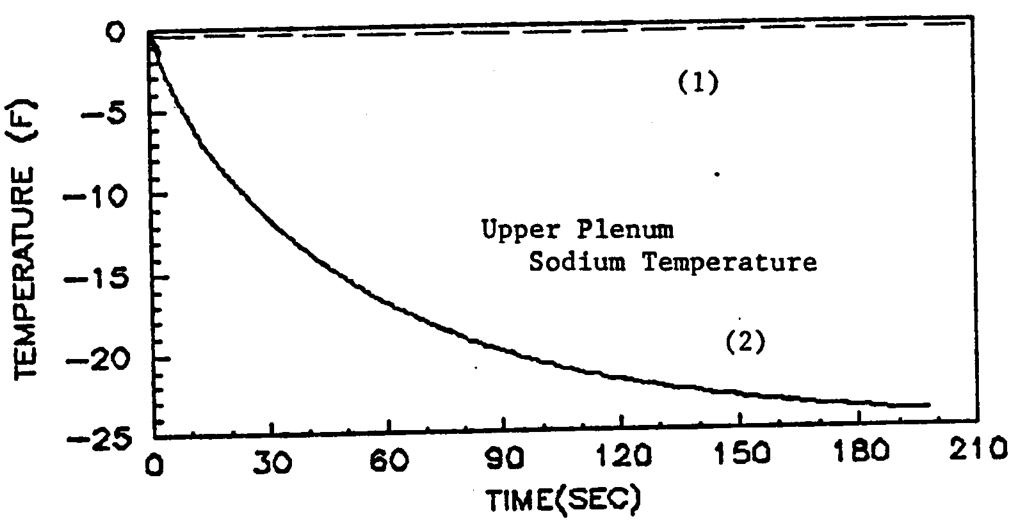

Fig. C.9 Step Responses of Closed-loop Primary Model to a -5 cents Reactivity Perturbation (1) Optimal Compensator (2) Open-loop Response.

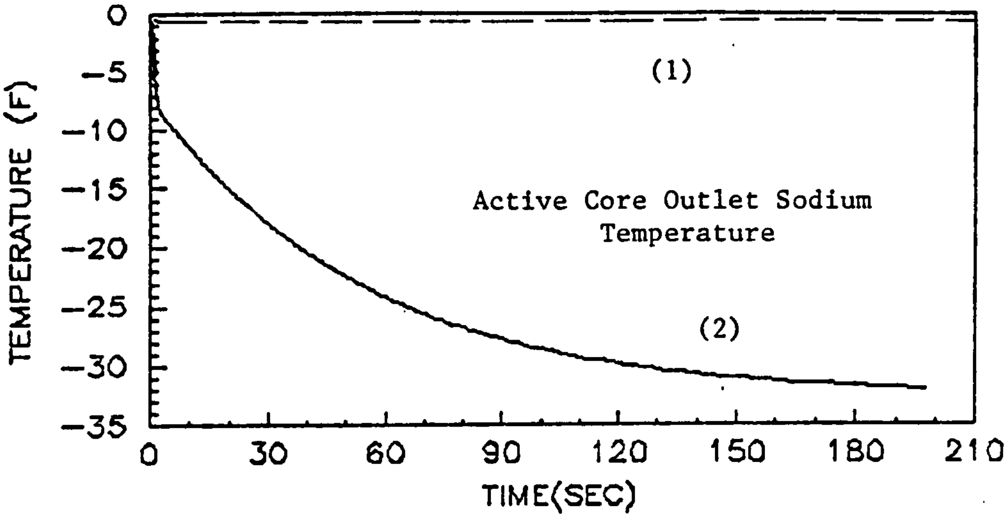

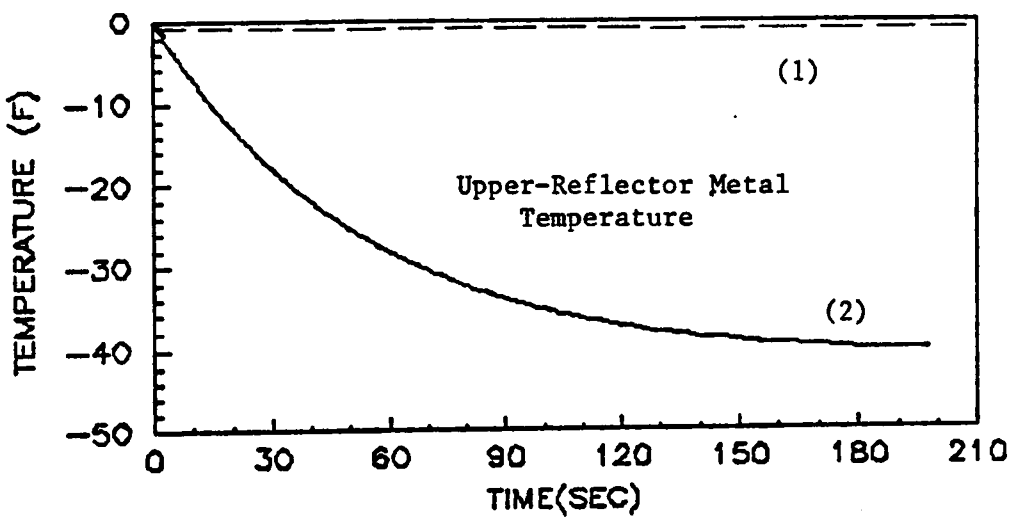

Fig. C.9 Step Responses of Closed-loop Primary Model to a -5 cents Reactivity Perturbation (1) Optimal Compensator (2) Open-loop Response.

VITA

Riza C. Berkan was born in Istanbul, Turkey, on May 4, 1961. He received his Bachelor's degree in physics from the department of Physics at the Hacettepe University in September 1984. He worked in the physical chemistry division at the Nuclear Reseach Center, Kernforshungsanlage, Julich, Germany. He attended graduate school for one year in the department of Nuclear Engineering, Istanbul Technical University, then came to the US.in September 1985. Upon his entry to the graduate program at the University of Tennessee, he obtained a research assistantship position sponsored by the Oak Ridge National Laboratory. He then received the degree of Master of Science in Nuclear Engineering in August, 1988 at The University of Tennessee in Knoxville.